Using Ground Penetrating Radar (GPR) for identifying floodplain and riverbed structural heterogeneity and implications for groundwater-surface water exchange.

by

REBWAR NASIR DARA

A thesis submitted to the University of Birmingham for the degree of
DOCTOR OF PHILOSOPHY

School of Geography, Earth and Environmental Sciences
College of Life and Environmental Sciences
University of Birmingham
November 2017

ABSTRACT

Streambed sediment heterogeneity is one of the major factors controlling variability in groundwater and surface water exchange and biogeochemical cycling. In the near-river subsurface zone (e.g. the hyporheic zone) of groundwater-fed rivers, reactive groundwater pollutants (e.g., Trichloroethylene (TCE) plume and nitrate) have threatened the lowland river. Physical and biogeochemical processes in the near-river subsurface zone controlling enrichment and attenuation processes are directly linked.

The aim of the study is to investigate the variability in riverbed permeability fields in an unprecedented spatial resolution and quantify the impacts on controlling hyporheic exchange fluxes in two different geological settings of UK lowland meandering rivers (the river Tern in Shropshire and the Hammer stream in west Sussex). Geophysical surveys were conducted deploying Ground Penetrating Radar (GPR) on the floodplain and within the river channel, in conjunction with geological information derived from core logs and bank exposures, for mapping shallow subsurface structural heterogeneity. At locations identified to be representative for the range of streambed hydrofacies identified by GPR in the investigated stream reach, multi-level mini-piezometer networks were installed in the streambed for monitoring groundwater-surface water exchange fluxes, measuring hydraulic conductivity and sampling of pore water chemistry.

The results of GPR surveys in both sites provided different radar reflections which indicated a range of different radar facies and helped to delineate the type and extent of high and low conductive materials. Vertical hydraulic gradients (VHG), distinguished at streambed piezometers, showed positive values throughout the observation period, indicating groundwater upwelling into the river. Hotspots of increased VHG were observed in piezometers installed inside and around impermeable sections. The localised high Darcy fluxes inside high conductivity piezometers indicated rapid discharge of groundwater due to

the enhanced connectivity to deeper groundwater. Low flow velocity within and around low conductivity peat and clay lenses indicated that these layers substantially inhibit groundwater upwelling, resulting in enhanced streambed residence and reaction times and a significant reduction in nitrogen and dissolved oxygen concentrations. The increase in residence time and the related depletion in the volume of dissolved oxygen facilitated the development of conditions necessary for nitrate reduction. In contrast, preferential flow paths and short residence times in highly conductive drift deposits resulted in no significant changes in nitrate concentrations along hyporheic flow paths. The revealed impact of strongly heterogeneous physical streambed properties on hotspots of enhanced residence time and biogeochemical turnover highlights the value of GPR-based of high-resolution streambed characterisation.

Dedication

To my parents and family who taught me to try my best no matter how difficult the task or great the risk of failure,

To my lovely wife, for your love, patience and support,

And to my lovely son (Lawand) and my lovely daughter (Lava), you are my inspiration.

Acknowledgements

This thesis is the result of the research work of the last four years, which represented to me a very interesting work and life experience.

I wish to express gratitude to higher committee for education development in Iraq (HCED) who provided the funding to make this research possible. I would like to kindly thank my supervisors Professor Stefan Krause, Dr Michael Rivett and Dr Nick Kettridge for their helpful guidance, support and enthusiasm throughout the project. I am very grateful to Dr Greg Sambrook Smith for his great support to provide Ground Penetrating Radar (GPR) equipment, training and advising on GPR techniques. I must thank to Richard Johnson for the all the advice on equipment design and lab work. I thank Jamie Peart for their assistance to printing out posters for conferences. I thank Eimear Orgill for her assistance with the Ion Chromatography and TOC analysis. I am very grateful to the land owners at Helshaw Grange and Heathbrook Farm for allowing me to install equipment on their property and permitting access to the River Tern at all times. I would like to thank Leica Geosystems for their help to provide software and advice for post processing GPS data.

For taking the time out to come to the River Tern and Hammer stream help install infrastructure or collect data, grateful thanks go to Paul Romeijin, Megan Klaar, Silvia Folegot, and Philip Blaen. Special thanks for Kurdish students at the University of Birmingham Mr Habib, Reber, and Hawre who helped me to collect GPR data in river Tern site.

I thank master students Warren Vokes and Christopher Grange who collected data for their dissertations at the Hammer stream field site. I acknowledge Hypotrain for allowing me to attend experimental training session conducting in Hammer stream.

Lastly, I wish to express appreciation and love to my parents and family. I thank my lovely wife Dilan, and son Lawand and daughter Lava for their patience and support. Dilan, you

have always been there during the hard times and understood what this dissertation has meant to me.

Without the encouragement and help of these people, the completion of this PhD research would not have been possible. My deepest thanks to you all.

This thesis was copy edited for conventions of language, spelling and grammar partly by Janet's Proofreading Service.

CONTENTS

LIST OF FIGURES

LIST OF TABLES

APPENDICES

APPENDIX 1 – NE-SW orientation profiles collected in the river Tern west bank site (profiles 94-14).

APPENDIX 2 – NW-SE orientation profiles collected in the river Tern west bank site, longer profiles (profiles 15-20).

APPENDIX 3 – Locations details of all mini-piezometers used in this study.

APPENDIX 4 – GRADISTAT printout for the floodplain core samples (Hammer stream, UK), (A) Floodplain core 1 (B) Floodplain core 2. (C) Floodplain core 3. (D) Floodplain core 4.

APPENDIX 5 – GRADISTAT printout for the riverbed core samples (Hammer stream, UK), (A) Riverbed core 1 (B) Riverbed core 2. (C) Riverbed core 3. (D) Riverbed core 4. (E) Riverbed core 5.

APPENDIX 6 – More GPR profiles of the floodplain Hammer stream.

1 INTRODUCTION

1.1 Overview

The Water Framework Directive (EC, 2000) demands that the EU adopt a cohesive management plan for surface water and groundwater resources. For member states to apply the plan whilst maintaining a 'good ecological status' of surface water, a deeper understanding is needed of the processes involved in pollutant exchange between the two resources (groundwater and surface water) (Smith and Lerner, 2008; McKnight et al., 2010). In streams, the subsurface transition zone that is the groundwater–surface water (GW-SW) interface is typified by considerable fluctuation in hydrological exchange pathways and sediment characteristics (Brunke and Gonser, 1997; Woessner, 2000; Fleckenstein et al., 2006). This variability challenges the reliability of predicting the dispersal of groundwater contaminants, transformation and fate in the near-river fluvial sediments (Conant et al., 2004; Milosevic et al., 2012; Weatherill et al., 2014). Niche environments inside the transition zone arise from the combination of layers of sediment texture, unstable organic materials, and a limited supply of electron acceptors. Within these niches, superior microbial biogeochemical turnover may enable the breakdown of persistent chlorinated organic pollutants at a faster rate than occurs in the neighbouring groundwater (Conant et al., 2004; Schmidt et al., 2011).

This PhD project concentrates on the importance of small scale variability in riverbed physical characteristics in controlling groundwater-surface water (GW-SE) exchanges, residence time and biogeochemical processes. Central to the study is the hyporheic zone, a saturated subsurface composition of major temperate fluvial networks. The hyporheic zone forms as a result of the mixing between surface (river) water and shallow subsurface water (Brunke and Gonser, 1997; Krause et al., 2011b).This zone is made up of the sediment beneath and around the stream water through which water from the channel flows and finally returns to the channel (Sawyer and Cardenas, 2009). This mixing brings significant changes in water quality for both groundwater and surface water (Harvey and Bencala, 1993). The

degrees of connections between aquifer and river have implications for hydrogeological and biogeochemical processes (Covino, 2017).

Subsurface structural heterogeneity and stream morphology are the main drivers for groundwater and surface water exchange (Crispell and Endreny, 2009; Ward et al., 2010). Researchers have for two decades focused on how in-stream geomorphologic features affect groundwater and surface water exchange fluxes (Harvey and Bencala, 1993; Gooseff et al., 2006; Boano et al., 2007). Hydraulic conductivity or subsurface structural heterogeneity exerts main control on exchange flow patterns, and now has become an attention for many researchers (Salehin et al., 2004; Fleckenstein et al., 2006; Cardenas and Jiang, 2010; Krause et al., 2012b).

It has been known for a long time that the dynamic processes of degradation and aggradations of sediments result in complex sediment structure within riverbeds and adjacent floodplains (Leopold et al., 1964). As a result of these dynamic processes, the complex sediment structures may differ between one river catchment to another (Miall, 1996). Buffington and Montgomery (1999) stated that streambeds normally display textural patches (grain-size facies) that differ vertically and horizontally, and this is likely to result in the hydraulic conductivity within the streambed being distributed in spatial patterns (Genereux et al., 2008), effectively influencing the amount as well as location of hyporheic exchange fluxes (Landon et al., 2001) and biogeochemical processes (Krause et al., 2013; Naranjo et al., 2015). However, the spatial distribution of sediment structural heterogeneity (e.g., small-scale variability) which is common in riverbed sediments in lowland meandering rivers and their extensions into the hyporheic and riparian zone in different fluvial systems is not well understood.

The main goal of this PhD study was to use hydrogeophysical techniques to characterise the subsurface lithostratigraphy beneath, and adjacent to, two example stream sections of UK

lowland meandering river. The selected field study sites were two stream reaches, the river Tern in Shropshire and Hammer stream in West Sussex. The river Tern and Hammer stream study site are fed by groundwater from the highly permeable underlying Permo-Triassic Sandstone (PTS) and lower Green sandstone aquifer, respectively. Both the groundwater and the river flows provide primary private and public water supplies. Therefore, both field sites have been studied by several water researchers and the Environmental Agency.

The Tern and Hammer stream reach were chosen as exemplary case studies. The river Tern is characterised by many interesting features which are dominant in many other lowland meandering settings. First, it has good connection with underlying important groundwater aquifer (the Permo-Triassic sandstone bedrock) (Weatherill et al., 2014). Second, the river Tern cut down through shallow ideal permeable (clastic deposits) lowland catchment, heterogeneous, complex glacio-fluvial drift deposits of interbedded clay, silt, fine to coarse sand, pebbles, cobbles and organic material with some low conductivity spots being present in the riverbed (Krause et al., 2012b). Third, the river Tern is at risk from groundwater resident contaminants (e.g., TCE and nitrate) (Weatherill, 2015) and hence of failing to achieve 'good water' status (WFD) due to diffuse agricultural contamination (Rivett et al., 2007). Whereas, the Hammer stream is characterised by different geological setting compared to the river Tern. The Hammer stream traverses a typical low permeable lowland catchment. Clastic materials also encompass the Hammer stream study reach is completely differently organised in which it is characterised by high amounts of low conductivity materials with few high conductivity holes. Figure 1.1 shows the conceptual model illustrating the geological settings between the two-investigated stream reaches.

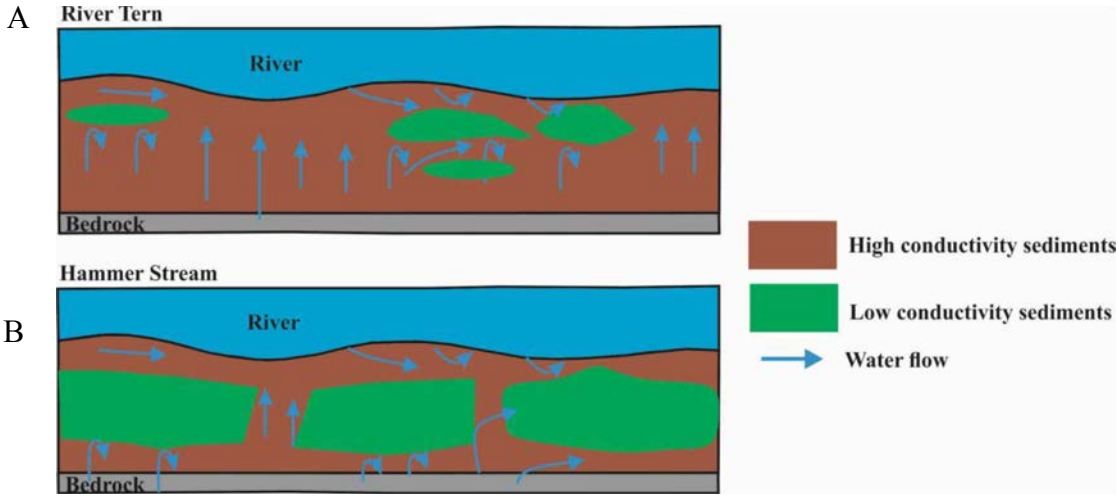

Figure 1.1 Conceptual schematic model shows different geological setting of riverbed hydrofacies and their impact on groundwater upwelling and hyporheic flow of surface water (A) River Tern and (B) Hammer stream.

1.2 Research questions and hypotheses

This research will answer the following questions:

1. What are typical streambed permeability structures of meandering lowland rivers (using two different geological settings) and what are the mechanisms of deposition that controls their development and how can they be found by GPR? (Chapters 3 and 6).
2. What is the small-scale heterogeneity in streambed physical properties and how do they extend into the hyporheic and riparian zone? (Chapters 3 and 6).
3. How does streambed permeability structure control groundwater-surface water exchange flow patterns, biogeochemical processes and residence time distributions? (Chapters 4 and 5).

   Hypothesis 1: It is hypothesized that low conductivity structures (clay and silt) and organic matter are deposited in streambed environments. These structures are

distributed in different depths which will control exchange flow patterns and residence times.

Hypothesis 2: Residence times will be short in areas where high permeable layers are present (good aquifer to river connectivity) and flow through low permeability streambed strata will be slow resulting in longer residences times. That is, lower permeable layers will "inhibit" groundwater upwelling.

Hypothesis 3: Subchannel low permeable sediments (long residence times) will responsible for the strong attenuation of reactive groundwater nitrates (denitrification) and highly conductive lithologies (short residence times) will responsible for the rapid discharge of groundwater to the river.

1.3 Aim of the study

The overarching goal of the PhD is to quantify the importance of small scale variability in riverbed physical properties (e.g. spatial heterogeneity of the permeability field) in controlling exchange fluxes and cycling of nutrients and/or contaminants.

Objectives are:

1. To develop and demonstrate the suitability of ground penetrating radar (GPR) to detect structural heterogeneity in floodplains and in-stream channels.
2. To develop an integrated three-dimensional geology and permeability field model based on the GPR and validated by core data.
3. To determine the importance of preferential exchange flows and residence time distributions through permeable bed sections and the bypassing of low permeability (often high attenuation) zones.
4. To quantify the importance of preferential and bypass flows on nutrient / contaminant exchange across the hyporheic zone for selected pollutants natural attenuation.

5. Compare between the Permo-Triassic sandstone and Cretaceous Lower Green sandstone deposited under different geological environments.

1.4 Dissertation outline

This PhD research is presented in the format of four self-contained research paper-type chapters (Chapters 3-6) followed by a synthesis (Chapter 7) in which the key findings are summarised, and future research recommended. The research strategy (workflow) and format of the thesis is presented in Figure 1.2. Within each Chapter, the relevant literature is reviewed, and descriptions of data acquisition and detailed methodologies are provided. For brevity and to avoid repetition, where the same data are employed or methods are adopted in more than one Chapter, then the Reader is referred to the relevant location in which these data or methods are first described. Chapter 2 reviews the groundwater and surface water exchanges, governing the processes of hyporheic exchange fluxes and application of near-surface geophysics at aquifer-river interfaces. Chapter 3 applies Ground Penetrating Radar (GPR) method in combination with ground truth data for mapping structural/sedimentological heterogeneity of river channel and floodplain drift deposits in an example of a UK meandering stream, the River Tern in Shropshire. Also, the potential implications for groundwater and surface water exchange fluxes stream section are described. Chapter 4 investigates the variability of hydrophysical controls of groundwater and surface water exchange fluxes through the riverbed and extended riparian zone in river Tern. The data were obtained through archive data (floodplain data) and field investigations through installing piezometers. Chapter 5 investigates spatial variability of chemical signatures (nitrate and dissolved oxygen) in contrast to riverbed lithology using multilevel minipeizometers. Chapter 6 uses GPR in combination with core samples in different geological settings, for example, in the Hammer stream in west Sussex for mapping riverbed and riparian zone. Moreover, some hydrological parameters were measured through installation of piezometers in the riverbed

for characterising aquifer-to-river connectivity. Chapter 7 synthesises the summary key findings from the research and provide recommendations for future research directions.

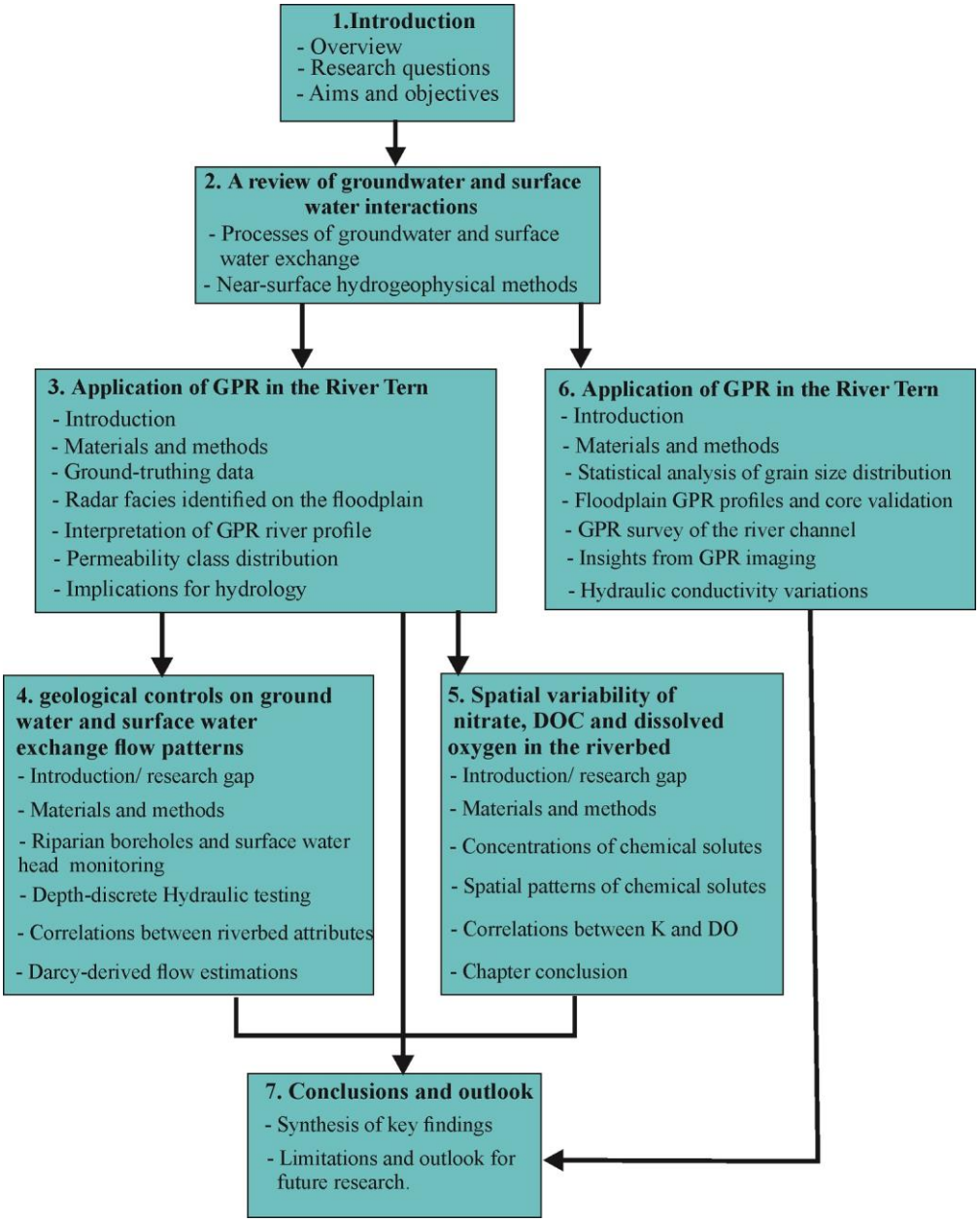

Figure 1.2 Flow diagram outlining the strategy for the research program and structure of the thesis.

2 A review of groundwater and surface water interactions

2.1 Processes of groundwater and surface water exchange

The hyporheic zones forms as a result of the mixing between groundwater and surface water in space and time (Figure 2.1) (Harvey and Bencala, 1993; White, 1993; Krause et al., 2011b) which have been identified as significant locations of macroinvertebrates habitats (Williams and Hynes, 1974; Stanford and Ward, 1988), biogeochemical processes (Triska et al., 1989; Baker et al., 1999; Byrne et al., 2014) and buffers for both various pollutants (D'Angelo et al., 1993; Fuller and Harvey, 2000) and stream water temperatures (Arrigoni et al., 2008; Burkholder et al., 2008). This zone is made up of the sediment beneath the stream water but can also extend into the riparian and parafluvial zones through which water from the channel flows and finally returns to the channel (Sawyer and Cardenas, 2009).

However, the hyporheic zone may be viewed from a hydrological, ecological, and hydrogeological perspective. A conceptual model of the hyporheic zone functioning for hydrological, ecological and hydrogeological processes can be seen in Figure 2.2.

Much of the present literature has been provided by ecologists, whose focus has been on the function of the hyporheic zone both as a site for the development of salmonid eggs and as a refuge and habitat for freshwater invertebrate fauna (Figure 2.2 A) (Malcolm et al., 2003). The current literature on hydrology takes into account the procedures that control the flow of water within the hyporheic zone, with regard to water exchange between adjoining hyporheic sediments and the river channel (Harvey and Bencala, 1993; Käser et al., 2009; Binley et al., 2013) (Figure 2.2 B). Hydrogeology is also concerned with the study of the hyporheic zone as part of the groundwater system. It also takes into account vital elements of the high Total Organic Carbon (TOC) content, and the different microbial community in the hyporheic deposit as depicted by Figure 2.2 C (Smith, 2005). Therefore, an appreciation of all processes (hydrological, biogeochemical, hydrological, and ecological) and their drivers are essential to precisely demonstrating and determining an impact of such exchanges that happen in

hyporheic zone over space and time and its implications at different spatial scales (Bardini et al., 2013).

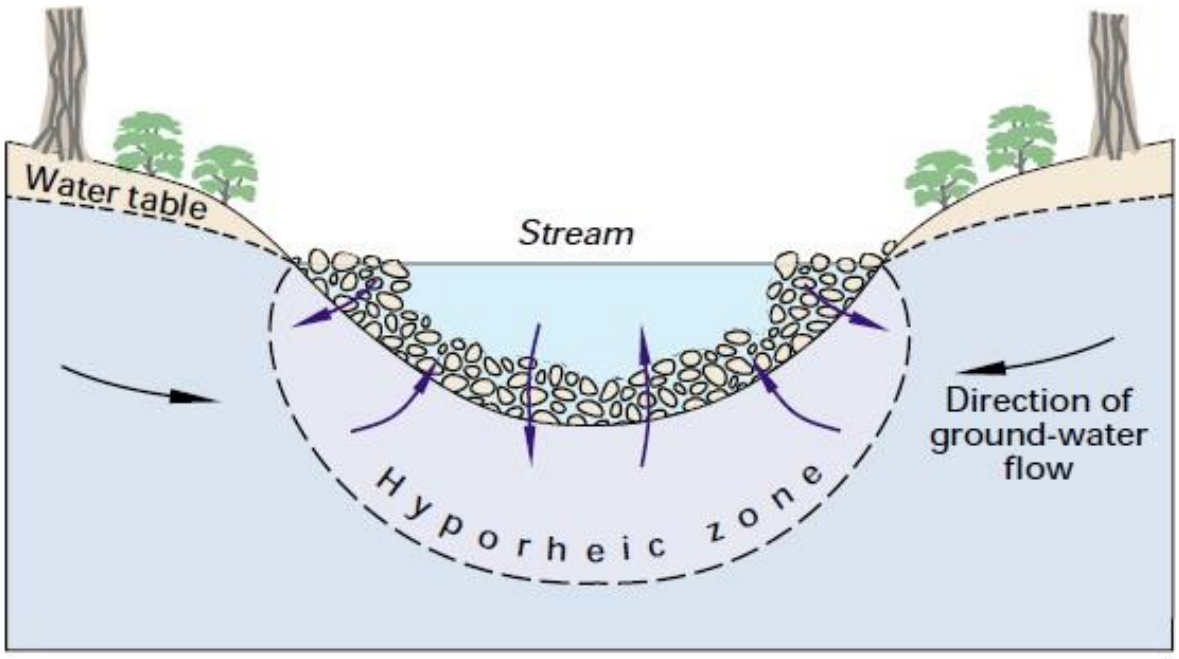

Figure 2.1 Illustrative representation of the hyporheic zone (from Alley et al., 2002)

Brunke and Gonser (1997) underlined that, in spite of the direct connection with the surface water, the hyporheic zone manages to maintain reduced oxygen concentrations in comparison with the saturation value. In addition, the hyporheic zone maintains reduced flow velocities, permanent darkness conditions, as well as smaller annual and day-to-day temperature changes. In their studies, Lautz and Fanelli (2008) and Hatch et al. (2010) discovered elevated temperature fluctuations, elevated flow velocities, steeper chemical and physical gradients as well as elevated productivity and habitat diversity in the hyporheic zone relative to the groundwater environment. As such, the HZ offers an interface and unique ecotone with abiotic conditions in between true groundwater and surface water (Stubbington et al., 2009; Boulton et al., 2010) (see Table 2.1).

Table 2.1 Summary of comparative physical and biological characteristics of groundwater, hyporheic and surface water environments (from Krause et al., 2011b).

	Descriptive characteristic of environment		
	Groundwater	Hyporheic	Surface water
Physical Characteristics			
Light	Constant darkness	Constant darkness	Daylight fluctuations
Current velocity	Low	Intermediate	High
Annual and daily temperature range	Very low	Low	High
Substrate characteristics	High	Intermediate	Low
Gradient of physico-chemical parameters	Low	Steep	Steep
Biological characteristics			
Habitat diversity	Low	Intermediate	High
Food-webs	Simple and short	Intermediate	Complex and long
Productivity	Low	Intermediate	High

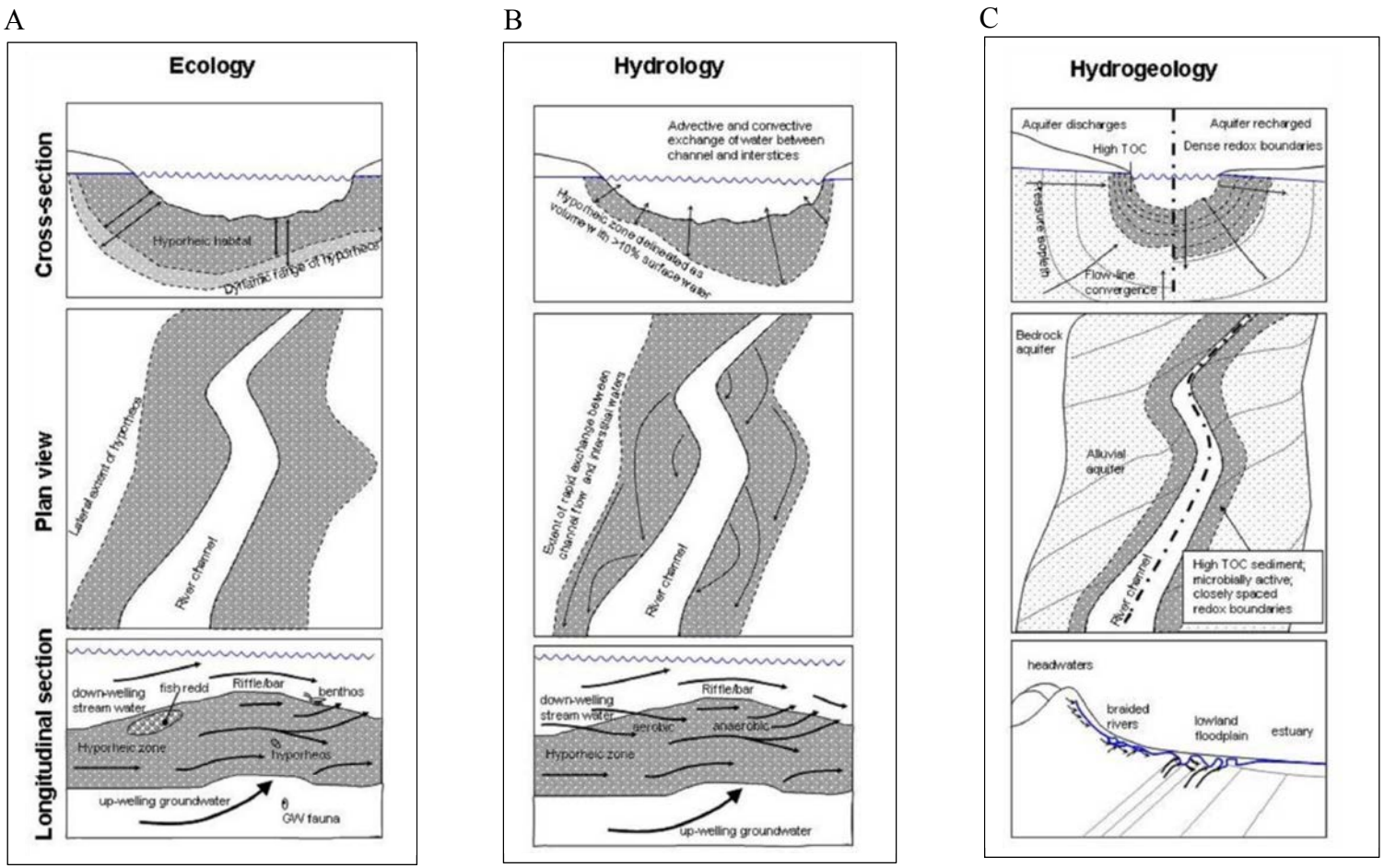

Figure 2.2 Conceptual models of the hyporheic zone for ecology, hydrology and hydrogeology disciplines (from Smith, 2005).

2.1.1 Hyporheic exchange hydrology

The mixing of river water at the sediment-water interface with shallow subsurface water is called hyporheic exchange and is driven by spatial and temporal variations of streams characteristics (e.g. hydraulic conductivity, streambed pressure, bed mobility and alluvial volume) (Malard et al., 2002; Tonina and Buffington, 2009; Krause et al., 2011b). Several factors can influence the hyporheic exchange and the size of it, for instance, topography, groundwater levels, sediment characteristics and flora (Cardenas et al., 2004; Fleckenstein et al., 2006; Boano et al., 2009). In some conditions the extension of the hyporheic zone may take place over tens of meters horizontally from the channel stream and a meter or more vertically (Wondzell and Swanson, 1996; Tonina and Buffington, 2007). Short flow paths and small residence times (e.g. a few minutes) are induced by small streambed geomorphic features, such as dunes, pools, ripples, steps and riffles (Harvey and Bencala, 1993; Elliott and Brooks, 1997a; Cardenas and Wilson, 2007), while longer pathways and bigger residence times (for instance, days by Kasahara and Wondzell (2003), or up to years) are caused by larger geomorphological features, like pool-riffle pairs (Boano et al., 2006; Tonina and Buffington, 2007; Revelli et al., 2008), step-pool sequences (Harvey and Bencala, 1993) or meander bends (Boano et al., 2006; Cardenas, 2008).

2.1.2 Mechanisms of exchange

Hyporheic exchange flow is a three dimensional phenomenon, occurring laterally, longitudinally and vertically (Jones and Holmes, 1996; Binley et al., 2013). Lateral flow can be observed in meandering streams, in which, compared to surface water that travels between meander crests, hyporheic water can take a direct path flowing laterally beneath channel bars. Whether water moves from the hyporheic zone to the stream (upwelling) or from the stream to the hyporheic zone (downwelling), is determined by the vertical component of the hyporheic flow. The direction of flow pattern can be calculated by measuring the vertical head gradient (VHG). Whereas riffle tails are most often upwelling sites, riffle heads are

inclined to be down-welling zones (Harvey and Bencala, 1993; Valett et al., 1994). Longitudinal flow is characterised as the exchange of water between the surface and subsurface, with net downstream travel. Figure 2.3 depicts examples of hyporheic exchange patterns.

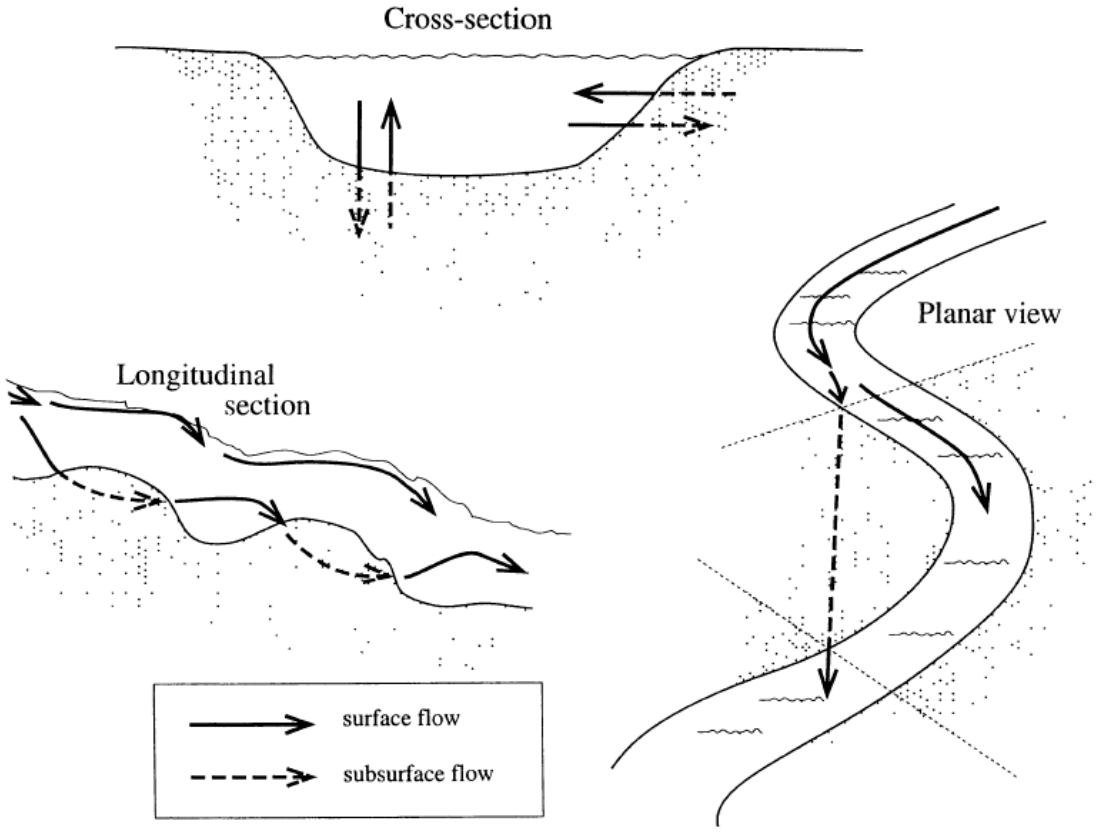

Figure 2.3 Common vertical, lateral and longitudinal patterns of hyporheic exchange; shaded area is the hyporheic zone (from Findlay, 1995).

2.1.3 Channel geomorphology governing groundwater and surface water exchange

The level of surface water in streams can be controlled by geomorphic features of channels as well as channel and valley floor within stream reaches (Wondzell and Gooseff, 2013). Many factors act to control groundwater and surface water exchange rates and residence times; the most important driver is abrupt changes in channel gradients (Wondzell and Gooseff, 2013). Significant head gradients created through valley floors which, in turn, drive groundwater and

surface exchange fluxes (Harvey and Bencala, 1993). In streams with high gradient, geomorphic features, such as pool-riffle pairs or step-pool sequences, can induce very steep hydrostatic pressure head gradients (Elliott and Brooks, 1997b). Other geomorphic factors influencing groundwater and surface water exchange include the presence of secondary channels, the degree of channel constraint (Kasahara and Wondzell, 2003), channel sinuosity (Wroblicky et al., 1998; Kasahara and Wondzell, 2003) and stream size and discharge (D'Angelo et al., 1993).

Experimental field studies (Lautz et al., 2010; Endreny et al., 2011) and model-based examinations (Boano et al., 2007) revealed that spatial patterns of groundwater and surface water exchange flow paths were highly impacted by advective pumping and hydrodynamic pressure head fields related to riverbed geomorphology and surface water turbulence (Elliott and Brooks, 1997b; Wondzell and Gooseff, 2013).

2.1.4 Spatial heterogeneity in hydraulic conductivity

Spatial variations in hydraulic conductivity can also cause groundwater and surface water exchange flow paths (Tonina and Buffington, 2009). This exchange can arise from special variances in the hydraulic conductivity. A drop in the level of hydraulic conductivity will obstruct subsurface flow, resulting in the discharge of the excess water into the stream (upwelling). However, an improvement in the permeability of sediments (higher K) will trigger an increase in the speed of the subsurface flow and draws water into the sediment in a process referred to as downwelling (Vaux, 1962).

The value of saturated hydraulic conductivity in fluvial environments depends on connectivity of pores and sediment porosity, which are functions of the sediment type (grain particle distribution and percentage of fine grain materials) as well as condition (presence of organic material and degree of consolidation (Freeze and and Cherry, 1979).

The depositional environment, sometimes also referred to as sedimentary environment, on the riverbed and along the floodplain is regulated by fluvial processes, producing a spatial heterogeneity in the sediment grain size (textural patches) of the accumulated and reworked sediments all along the riverbed and covering the whole floodplain (Wondzell and Gooseff, 2013). Moreover, riverbeds normally display textural patches (grain-size facies) that differ vertically and horizontally (Dietrich et al., 1989; Lisle et al., 1993; Buffington and Montgomery, 1999; Tonina and Buffington, 2009), resulting in a spike in the unevenness of the hydraulic channel conductivity and the subsequent hyporheic exchange (Malard et al., 2002; Genereux et al., 2008; Käser et al., 2009).

Sediment layering can also influence spatial patterns in hydraulic conductivity across the floodplain and stream channel (Wondzell and Gooseff, 2013). Chen (2004) argues that strong vertical anisotropy is likely to develop due to layering of sediments. This not only promotes lateral flows via the floodplain and streambed, but it also hinders vertical exchange (Packman et al., 2006; Angermann et al., 2012; Krause et al., 2012b; Naranjo et al., 2012). Investigations made by Krause et al. (2012b) and Angermann et al. (2012) at UK lowland rivers using different approaches and they revealed that the spatial variability in streambeds (disconnected lenses of clay and peat) play an important role in the physical properties of aquifer-river exchange fluxes, and dissolved oxygen rates in pore water sediment. Moreover, such variability contributes to controlling spatial patterns of groundwater discharge, promoting fluxes at shallow subsurface heterogeneity, and streambed residence time. Cardenas et al. (2004) showed that heterogeneity causes meaningful additional hyporheic zone flow patterns. The existence of streambed heterogeneity can either increase or decrease residence times in the hyporheic zone (Cardenas and Jiang, 2010). Salehin et al. (2004) revealed that spatial variability of streambed sediment and size of hyporheic exchange are increased by sediment heterogeneity in sandy-bed channels with dune-like or planar

topography. Weatherill (2015) reported that the low permeability alluvial cap over the sandstone aquifer on the west bank site of the River Tern is likely to impact groundwater flow paths along the river channel where the TCE plume discharges.

2.1.4 a) Measuring hydraulic conductivity

Several studies have demonstrated the measurement of hydraulic conductivity of the shallow streambed sediment utilizing slug tests (Cardenas and Zlotnik, 2003; Binley et al., 2013; Sebok et al., 2015), permeameter testing (Landon et al., 2001; Genereux et al., 2008; Chen, 2011), and pumping tests (Kelly and Murdoch, 2003).

The majority of the above studies primarily concentrated on the shallow streambed sediment at the depth of 0 m to 1.0 m underneath the channel surface, originally due to the difficulties of measuring hydraulic conductivity in the field (Cardenas and Zlotnik, 2003). The lithological sequences of deep streambed sediments are rarely demonstrated, despite the significant content of the vertical profile of streambed sediments in analysing the interactions between the streambed and neighbouring aquifers (Cheng et al., 2013).

Landon et al. (2001) used four various tests for determining hydraulic conductivity. For instance, using Hvorslev and Bouwer and Rice formulas, pumping and slug tests, grain size analysis adequate experimental relationships, as well as permeameter and seepage meter tests utilizing the Darcy law. The results of these tests showed that higher hydraulic conductivity values were produced by slug and pump tests are greater compared to sediment grain size analysis. Because of the empirical relationships disregard the fact that hydraulic conductivity is the function of sorting, packing, sediment pattern, heterogeneity and other important factors which led to those differences in value. Consequently, results indicated that pumping tests is more precise. Moreover, the values of hydraulic conductivity which derived from permeameter tests that used Darcy equation provided variable results. Due to the relatively high rate flow of stream with dynamic beds, measurements using seepage meters can lead to

fail in data measurements frequency. Thus, this technique should be considered as an inappropriate technique for determining hydraulic conductivity at stream scales.

Song et al. (2007) examined the stream vertical hydraulic conductivity with two linked depths in three major rivers in Nebraska (USA). Their findings showed that the upper part of the sediment layer (50-60 cm below the channel surface) is substantially higher than the lower part of the sediment layering (60-90 cm below the channel surface). These differences are attributed to three factors. (1) the upper layer is often subjected to larger pore spaces and unconsolidated patterns of sediment, due to the water exchange through the upward and downward zones. Consequently, high vertical hydraulic conductivity is formed in the upper layer of sediment. (2) pore spaces may grow as a result of the upper movement of gas, which in turn can loosen the upper part of the sediment. This gas is formed by redox processes. (3) microorganismal activity, such as that of invertebrates, can infer large pore spaces into the upper part of streambed, which subsequently lead to an increase in permeability. Similarly, Ryan and Packman (2006) utilized a conservative tracer, sodium bromide (NaBr), in Indian Creek, an urban stream in Philadelphia, US. The main aims were to study the solute exchange within the hyporheic zone. They found that higher tracer concentrations were observed in the shallow depth streambed (7-10 cm below the channel surface). This showed that higher hydraulic conductivity values existed in the shallow depth (7-10 cm) when compared to the values of the deeper sediments (10-12.5 cm).

Cardenas and Zlotnik (2003) used multi-level slug tests, combined with supporting techniques like core sampling and GPR in eastern Nebraska-USA, for analysing three-dimension spatial variability of the streambed. Their findings showed that streambed have differing spatial variability, with hydraulic gradient, driving the spatial distribution of upwelling and downwelling water. Also they proposed that there is a difference in the depositional mechanisms between shallow sediments and deep sediments, each of them

having their own depositional mechanisms. Additionally, the up and down water flow and seepage is suggested to occur in the hyporheic zone (Packman et al., 2004; Song et al., 2007; Sebok et al., 2015). Therefore, higher streambed hydraulic conductivity (K) can exist in the hyporheic zone when compared to the deeper sediment.

Rosenburry and Pitlick (2009) demonstrated that the "K values of shallow streambed sediments can increase with upward seepage and decrease with downward seepage, and K value may increase for both upward and downward seepage with the increasing surface water velocity when the bed is fully mobile". According to Nogaro and Mermillod-Blondin (2009), one of the invertebrate examples (turbid worms) can decrease sediment clogging and lead to higher streambed hydraulic conductivity, thereby enhancing water-sediment interplay. Furthermore, Leek et al. (2009) used an in-stream slug test at two test sites (upper and lower side) in order to determine the hydraulic conductivity of a streambed in the Touchet River in Washington (USA). Results showed that the mean and median values of the K for the depth interval of 0.3-0.45 m were significantly higher than those values for the depth intervals of 0.6-0.75m, 0.9-1.05m and 1.2-1.35m at the lower site.

2.1.5 Biogeochemical perspectives of aquifer-river interface

The heterogeneous sediment distribution results in hyporheic flow occurring through numerous diverse subsurface flow paths; the residence times of these vary, though all exceed the length of the surface flow path through the stream's thalweg (Haggerty et al., 2002; Gooseff et al., 2003). The combined effect of the close interaction between the water and sediment biofilms, together with the longer residence time in the hyporheic zone, results in several key biogeochemical transformations taking place (Naranjo et al., 2015). These influence the hyporheic zone's ecosystem. The availability of labile organic carbon and enhanced microbial diversity in the hyporheic zone, compared to the deeper aquifer, can create favor conditions for microbial-mediated redox gradients superimposed on water flow

paths (Baker et al., 2000; Morrice et al., 2000). As a result, sediment pore water in the hyporheic zone is characterized by dominant microbial activity which leads to intense biogeochemical cycling and turnover rates. Therefore, steep physico-chemical gradients over short spatial (sub-meter) scales could occur (Storey et al., 1999). The hyporheic zone can then serve as either a sink or source of nutrients in the stream ecosystem (Greenwald, 2007; Briggs et al., 2014; Naranjo et al., 2015).

2.1.5 a) Nutrient attenuation

There is a general acceptance that the hyporheic zone's capacity to function as a buffer zone that attenuates nutrients and contaminants is significant (Smith, 2005). Nonetheless, the scale of attenuation of nutrients in the hyporheic zone can vary from one region to another. In locations with appropriate conditions, the nutrient attenuation process will be substantial, but in other regions the attenuation can be minimal. The effectiveness of most of the transformation processes is also heavily dependent on the existence of sloping gradients (including complex sequences of aerobic and anaerobic conditions) and the presence of organic matter and microbial activity within the hyporheic zones (Fisher et al., 1998). Moreover, many researchers have highlighted the fact that fine grained sediments play an important role in contaminant attenuations, fluxes, and residence times (Krause et al., 2013; Naranjo et al., 2015). Smith et al. (2008) discovered that the attenuation potential increased in those areas corresponding with decreased mean grain size, this is occurring as a result of subsequent decreasing in hyporheic fluxes and increasing in contaminant residence time. Krause et al. (2013) demonstrated how the transportation of solutes and redox processes in the hyporheic zone can cause effective nutrient/contaminant attenuation, e.g. by denitrification. Ullah et al. (2014) found enhanced nitrate attenuation in riverine sediment deposits under emergent vegetation compared to adjacent un-vegetated sediments.

2.1.5 b) Nitrogen cycling

The bioavailability of nitrogen (N) in aquatic systems can be transformed and regulated by variety of microbial metabolic pathways and interacting abiotic reactions. This including nitrification, ammonification, N fixation, denitrification, anaerobic ammonium oxidation (anammox), N fixation, dissimilatory reduction of NO3 to NH_4 (DNRA), inorganic N assimilation into plant or microbial biomass (immobilization), NH_4 adsorption and desorption, NH3 volatilization (Reddy and DeLaune, 2008; Trimmer et al. 2012). Some of these microbial processes are supported by the reduction of the oxidised species of N, such as nitrate, in anoxic sediments and waterlogged soils, whilst others derive energy from the aerobic oxidation of reduced species such as ammonium (Shapleigh, 2006).

Denitrification processes are a key mechanism for conversion of nitrate to nitrogen gas, nitric oxide or nitrous oxide which is mediated by denitrifying aerobic autotrophs or heterotrophs bacteria that can switch to anaerobic growth when nitrate is utilized as an electron acceptor (Bitton and Gerba, 1994) (Bitton, 1994). In low oxygen environment (ideally < 0.5 mg/l) the rate of the denitrification reaction would be relatively fast. In addition, other factors – for example, pH, nutrient availability, temperature distribution, nitrate rates, existence of toxins and microbial acclimation – can play a significant role in denitrification (Rivett et al., 2008b). Hyporheic zones have been found to not only act as a sink, where nitrite influxes are attenuated as a result of denitrification, but also act as a potential source of nitrate, where nitrate rates can be strongly increased by main processes (e.g., nitrification and ammonification) (Briggs et al., 2014; Naranjo et al., 2015). Even as nitrification corresponds to reduced residence times up to a point where sufficient reduction on dissolved oxygen (DO) levels had been attained, the denitrification rates increased owing to increased residence times in the hyporheic environment that was depleted of oxygen (Zarnetske et al., 2011a). Further research studies also point at reduced carbon levels in microbial denitrification in

both hyporheic and riparian environments (Holmes et al., 1996; Pinay et al., 2002; Zarnetske et al., 2011b).

Discovery of anammox as an alternative pathway of N2 gas production in estuarine and marine sediment deposits by which ammonium is oxidised by nitrate, and even the anaerobic oxidation of methane (Trimmer et al. 2012). Nevertheless, denitrification process is commonly a heterotrophic route, relating to a supply of dissolved organic carbon (DOC), and, contrary, anammox is chemoautotrophic (Trimmer et al., 2012). The regulate production of N2 through denitrification and anammox remained poorly understood (Thamdrup and Dalsgaard, 2008). These metabolic processes have altered our perception of the N cycle in all aquatic ecosystems (Trimmer at al. 2012).

Various studies indicate that although there is a general agreement that subterranean water represents an important source of nitrogen for most low-lying streams in regions where there is a heavy reliance on agriculture, there is very little appreciation of the significance of the riverbed passage on the fate of nitrogen in the upwelling underground water (Foster, 2000; Krause et al., 2009b; Krause et al., 2013).

Duff and Triska (2000) reviewed the occurrence of denitrification in the hyporheic zone and discovered that it is not only related to DOC and NO_3 availability, but it is also takes the form of a very complex process. In their study, Duff and Triska (2000) also discovered that denitrification along hyporheic flow paths is also a function of three important processes: firstly, it is the function of the concentration of DO across the hyporheic zone, which is controlled by biochemical oxygen demand and advected supply; secondly, it is the function of hyporheic water temperature because it controls microbial activity and DO saturation in water; and, thirdly, it is the function of the hydraulics that drive the physical transport and residence time of water such as the head gradient, hydraulic conductivity, advection, and dispersion. Of these three factors, the biogeochemical conditions that facilitate the regulation

of hyporheic denitrification vary primarily on the basis of the volume of NO_3 and quantity and quality of DOC that was available in the system during the denitrification process (Findlay and Sobczak, 1996; Kaplan and Newbold, 2000). Several studies indicate that denitrification rates will be significant in circumstances where there is a profusion of NO_3 and labile DOC (Holmes et al., 1996; Storey et al., 2004). Pinay et al. (2009) conducted a study on the link between the nature of solutes utilized in the denitrification process and hyporheic water residence for two meandering sites in Alaska, USA. The results of Pinay et al.'s (2009) study suggested that the relationship between concentration of solutes utilized in the denitrification process and the hyporheic water residence for the two meandering sites in Alaska was significant. During the study, Pinay et al.'s (2009) observed a strong correlation between the removal of nitrate N and the travel time through the HZ. In another study, Zarnetske et al. (2011a) assessed the dynamics in the rate of nitrate production and elimination in a gravel bar in Oregon, USA. The results of their study suggested that the transition from nitrification to denitrification not only demonstrates a threshold behavior, but it is also a function of hyporheic residence time.

2.2 Near-surface hydrogeophysical methods to explore the interface between groundwater and surface water

The study of textural patches of the subsurface and processes that take place within it remains a big challenge in many scientific branches (Binley et al., 2015). In hydrological study, the transformation and transport of fluids in the shallow subsurface are mainly controlled by interaction processes (e.g., biological, physical and geochemical processes) that occur in highly heterogeneous subsurface sediment deposits (Figure 2.4). Table 2.2 lists the geophysical properties that geophysical methods provide.

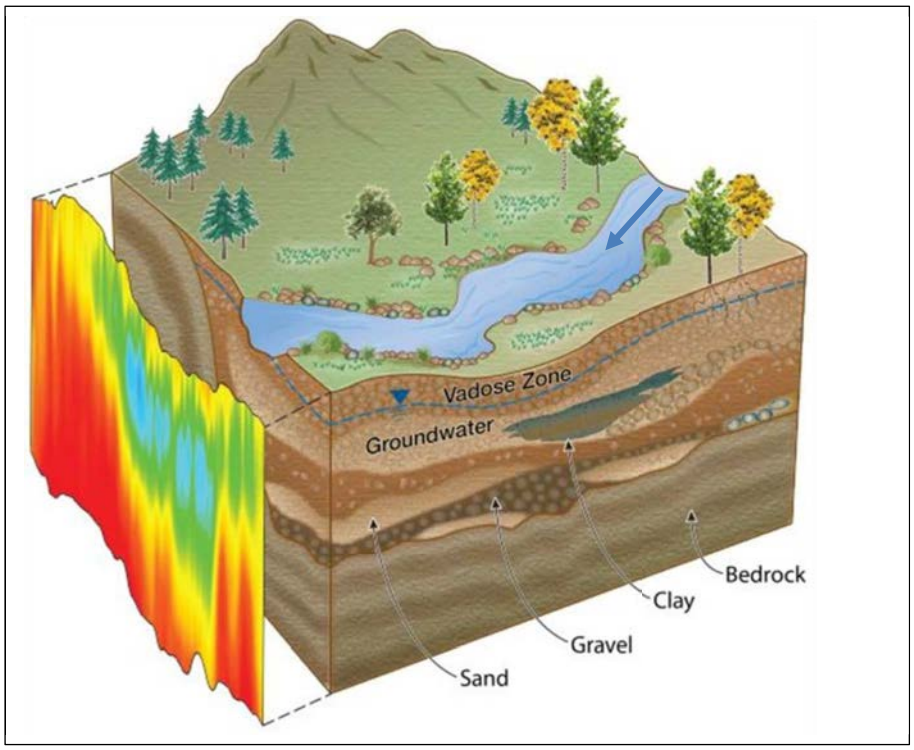

Figure 2.4 Scheme of a terrestrial environment, illustrating hydrogeological heterogeneity and how geophysical methods are often used to characterize the ‘‘hidden’’ subsurface. Geophysical data sets provide information about geophysical properties, such as electrical conductivity (shown here), which can potentially be related to hydrogeological properties as shown in Table 1 (From Binley et al., 2015).

Table 2.2 List of commonly used geophysical methods in hydrology and the geophysical properties they sense (from Binley et al., 2015)

Geophysical Method	Geophysical properties	Examples of Derived Properties and States
DC resistivity	Electrical conductivity	Water content, clay content, pore water conductivity
Induced polarization	Electrical conductivity, chargeability	Water content, clay content, pore water conductivity, surface area, permeability
Spectral induced polarization	As above but with frequency dependence	Water content, clay content, pore water conductivity, surface area, permeability ,geochemocal transformations
Self-potential	Electrical sources, electrical conductivity	Water flux, permeability
Electromagnetic induction	Electrical conductivity	Water content, clay content, salinity
Ground penetrating radar	Permittivity, electrical conductivity	Water content, porosity, stratigraphy
Seismic	Elastic moduli and bulk density	Lithology, ice content, cementation state, pore fluid substitution
Seismoelectrics	Electrical current density	Water content, permeability
Nuclear magnetic resonance	Proton density	Water content, permeability
Gravity	Bulk density	Water content, porosity

2.2.1 Near-river zone geophysical applications

Geophysical 'imaging' of the structure of riverbeds and adjacent river banks (riparian zones) is a non-destructive technique to assist in conceptualising aquifer-river exchanges at reach scales (Weatherill, 2015). Binley et al. (2015) posits that the investigative method of geophysics has transformed our capability to view of the fabric the subsurface environment. Different geophysical imaging methods have been developed within the field of 'hydrogeophysics'. Binley et al. (2010) review the emerging discipline of 'hydrogeophysics' in the context of subsurface hydrological investigations and indicates the potential of such techniques at aquifer-river interfaces. Specifically, electrical resistivity tomography (ERT), ground penetrating radar (GPR) and electromagnetic (EM) methods are most suitable in outlining important near-river lithostratigraphy controls on discharge of groundwater, for instance, the thickness and lateral continuity of hydrofacies and the depth to bedrock (Cardenas and Zlotnik, 2003; Binley et al., 2015). The measurement density realised with these methods cannot be achieved via direct observations from cores (Crook et al., 2008). Despite such advantages, only a few studies have used geophysical methods to characterise aquifer-river interfaces. Weatherill (2015) acquired ERI profiles on bank-parallel traverses along the River Tern floodplain. Based on the variations in subsurface resistivity with limited numbers of core samples, Weatherill (2015) was able to delineate the geometry and spatial extent of the alluvial aquitard, which caps the sandstone bedrock at the site. Naden (2011) showed the connectivity between the floodplain and riverbed stratigraphy in a survey conducted in the river Tern by conducting four ERT profile surveys, connecting the floodplain and river channel together. A study conducted by Crook et al. (2008) sought to reveal the ERT (electrical resistivity imaging) potential of alluvial groundwater systems. They are of the view that ERI could be applied in establishing the extent and thickness of alluvial gravel aquifer lie on top of a chalk aquifer. Crook et al. (2008) also used cross-

borehole measurements to envision the lateral continuity of the alluvial aquifer located beneath the River Lambourne channel in Berkshire, UK. Cardenas and Zlotnik (2003) have examined the role of ground penetrating radar (GPR) as a value-added tool in the classification of heterogenous modern channel bend deposits in near river zone (hyphoreic) studies. Conant et al. (2004) have also used GPR along a reach of the Pine River (Ontario, CA). They deployed GPR in-stream from an inflatable boat to successfully delineate potential preferential pathways of sandy channel infill deposits and semi-confining units that controls the rates and distribution of PCE tetrachloroethene discharge into a river channel through the hyphoriec zone. Elsewhere, Lyford et al. (1999) employed GPR profiles along the bank-side of the Royal River in Maine, USA to record images of continuity and thickness of glacial deposits. A TCE plume was identified as discharging on the riverbed under investigation. Naegeli et al. (1996) used GPR to investigate the sediment structures in the hyporheic zone of a prealpine river, Switzerland. Bradford et al. (2005) reported that GPR is a powerful technique for estimating thaw bulb depths below peat streams in arctic Alaska. Brosten et al. (2006) utilised GPR in streams of contrasting geomorphology in order to compare seasonal thaw bulb development patterns. They found that lower-energy, peat-lined streams responded less quickly to temperature changes than high-energy, cobble-lined streams. In a separate research study, Husband et al. (2009) revealed that ERT can be quite effective when used in conjunction with GPR in the categorisation and detection of near surface hydrological pathways that characterises a saturated carbonate setting.

The direct observation of exchange fluxes between aquifers and rivers at stream reach to catchment scale remains a challenge. Nitrates and chlorinated solvents as examples of reactive groundwater contaminants have been found to both enhance or reduce in the near-stream zone (hyporheic zone) (Naden, 2011; Weatherill et al., 2014), in response to hydraulic, sedimentology and biogeochemical heterogeneity (Duff and Triska, 2000; Conant

et al., 2004; Weatherill et al., 2014). At reach scale, the distribution and extent of sediment structural heterogeneity, biogeochemical gradients and hydraulic conductivity is not well understood (Claret and Boulton, 2009). A detailed understanding of the spatially complex nature of the subsurface hydrology is important. Thus, there is a real opportunity and an urgent need to address these important challenges.

3 Using Ground Penetrating Radar (GPR) for identifying floodplain and riverbed structural heterogeneity in a UK lowland meandering stream, the River Tern in Shropshire

3.1 Abstract

Ground penetrating radar (GPR) measurements have been carried out to survey floodplain and river channel in a lowland meandering river, the River Tern in Shropshire, UK. The aim was to characterize reflection patterns and delineate the type and extent of complicated spatial heterogeneity textural patches (grain size facies) of high and low conductive materials and implications for hydrology. A pulseEKKO Pro instrument equipped with shielded 250 MHz antennas were used in this study. To obtain a reliable interpretation, the radargrams have been calibrated using geological information coming from core samples and outer bank deposits. In GPR data from the floodplain, eight radar facies were identified. Most GPR profiles were dominated by trough-shaped depositional elements with erosional, curved, concave upward bounding surfaces. This could be correlated to an abandoned and chute channel that are filled by suspension fall-out fine-grained deposits (mud with O.M. and interbedded clay) which are characterised by signal attenuations. This unit is likely to be extended into the riverbed especially at the south-eastern part of the floodplain. The sub-channel organic peat and clay (extended layers from the floodplain) are also attenuated GPR signals and observed in patches in the riverbed environment. Therefore, GPR can be very helpful and appropriate method for study in fluvial deposits. This study allowed insight about the relationship between sediment structure heterogeneity with groundwater flow paths.

3.2 Introduction

The deposition of fine particles (clay and silt) and organic matter in alluvial sediments can substantially reduce the permeability of riverbed sediments and extend towards the wider floodplain (Tonina and Buffington, 2009; Wondzell and Gooseff, 2013). The resulting spatial patterns of hydraulic conductivities within streambed and floodplain have been shown to control both location as well as intensity of hyporheic exchange (Krause et al., 2009b; Krause et al., 2012b; Gomez-Velez et al., 2014) as well as larger scale groundwater and surface water interactions (including substantial bank storage) in many lowland rivers (Naranjo et al., 2012; Binley et al., 2013). Alluvial valleys are characterised by the existence of complex spatial patterns of hydraulic conductivities, resulting from their history of erosion and deposition in the valley that operated in different palaeo-geomorphic environments (Kostic and Aigner, 2007a; Tonina and Buffington, 2009). Alluvial sediments usually range from decimetre-to-metre scale, spanning several orders of magnitude in hydraulic conductivity (K) (Miall, 1996). Detailed knowledge of sediment property distributions and specifically spatial heterogeneity of the permeability field in streambed and riparian sediments are crucial for better understanding and predicted shallow groundwater flow and recharge in floodplains as well as groundwater – surface water exchange flow patterns across multiple spatial scales (Beres and Haeni, 1991; Huggenberger, 1993; Beres et al., 1995; Conant, 2004; Krause et al., 2012b).

Invasive approaches to determine information of sediment permeability and potential patterns of groundwater and surface water exchange fluxes, such as core drillings or the sampling and analysis of bank exposures for estimating hydrological parameters are expensive and time-consuming (Binley et al., 2015). These more traditional methods provide spatially limited information of hydrological properties and their distributions, often unsuitable to make adequate assumptions about the spatial complexity of alluvial sediment systems required to

support a comprehensive hydrogeological characterisation (Clifford and Binley, 2010). Furthermore, invasive approaches prevent or at least limit re-occurring analysis since they modify the subject of investigation, which is of particular importance for temporally less stationary structures such as riverbed sediments (Krause et al., 2012b).

The development of near-surface geophysical analysis tools over the last decades has opened unprecedented opportunities for larger scale, high resolution characterisation of subsurface structural complexity and hydrological functioning units (hydrofacies) in order to better understand the geological and geomorphological controls on riparian flow systems and groundwater and surface water exchange flow patterns (Salehin et al., 2004; Fleckenstein et al., 2006; Krause et al., 2012b). A wide range of geophysical methods (e.g. electrical method, electromagnetic induction (EM), and ground penetrating radar (GPR)) have been trialled and applied to investigate the spatial complexity of alluvial deposits (Conant et al., 2004; Crook et al., 2008; Binley et al., 2015). Near surface geoelectrical methods such as vertical electrical soundings (VES) and electrical resistivity tomography (ERT) have been regularly applied for hydrogeological applications (Daily and Ramirez, 2000; Reynolds, 2011). However, due to their limitation with accurately resolving lithological boundaries between hydrofacies (Bersezio et al., 2007) and strategic difficulties for setting up larger scale in-stream surveys in particular, they have not been applied frequently for characterising complex hydrofacies distributions in riparian zones and streambed environments (Naden, 2011).

Ground penetrating radar (GPR) refers to a non-invasive method which is designed mainly for subsurface investigations (Neal, 2004; Cassidy and Jol, 2009). A GPR method can detect changes in dielectric properties of the shallow subsurface using high frequency electromagnetic (EM) waves in the range of 10-1000 MHz (Neal, 2004). The spatial resolution being rather high as well as the radar velocity and moisture content being directly interconnected can be the reason why GPR is widely used in hydrogeophysics (Topp et al.,

1980). However, it is widely acknowledged that low conductivity layers can excessively attenuate GPR signals, while reducing the depth of penetration (Theimer et al., 1994; Heteren et al., 1998; Bristow and Jol, 2003). Nevertheless, it can be constructive as a means of assessing the alluvial fill thickness (Leclerc and Hickin, 1997). Compared with EM-based techniques, including resistivity surveying, GPR is a significantly better choice, given its relative insensitivity to changes in pore water chemistry, and its provision of high resolution images which makes the GPR results less equivocal (Binley et al., 2001).

Numerous studies using GPR have been carried out in floodplain fluvial settings (Gourry et al., 2003; Kostic and Aigner, 2007b; Słowik, 2013b) whilst studies using GPR in streams is generally a challenge and has only been done few times. Naegeli et al. (1996) used GPR in river channels to investigate the sediment structures in a floodprone gravel-bed River. Conant et al. (2004) have also used GPR successfully to delineate potential preferential pathways of sandy channel infill deposits and semi-confining units that control the rates and distribution of PCE tetrachloroethene discharge into a river channel through the hyporheic zone.

Geophysical surveys will focus on a UK lowland river (River Tern), where previous investigations have revealed substantial complexity of spatial patterns in sediment hydraulic conductivities and groundwater and surface water exchange fluxes (Angermann et al., 2012; Krause et al., 2012b). In particular, the spatial patterns of streambed peat and clay lenses that extend into the riparian zone have been shown to play an important role in the physical properties of aquifer-river exchange fluxes, and dissolved oxygen rates in pore water sediment (Krause et al., 2013). Furthermore, recent modelling studies evidence that knowledge of the location and spatial extent of contrasting hydrofacies is essential to understanding and predicting patterns and intensities of groundwater and surface water exchange and in particular hyporheic exchange fluxes (Gomez-Velez et al., 2014).

In this study, investigations using a combination of novel in-stream GPR with riparian surveys in conjunction with a limited number of point observations of local lithology from core logs suggest that aquifer-to-river hydraulic connectivity and residence times are governed by near-river zone substratum characteristics. Hence, the knowledge of architecture and spatial distribution of sediments in the hyporheic zone is extremely important for understanding the biotransformation and transport of discharging groundwater contaminants.

The main objective of the study was to verify the effectiveness of GPR imaging for sedimentological studies of river channel and floodplain drift deposits. In this study, ground truthed GPR surveys are carried out to: (1) Characterise the sedimentary architecture of the streambed and riparian zone; (2) Identify radar facies representative of lowland meandering fluvial architectural elements observed in drift deposits; (3) Reconstruct the quasi-three-dimensional GPR profiles from closely spaced grids of two-dimensional GPR data for the subsurface floodplain sediment deposits; (4) Delineate low conductivity layers across heterogeneous streambed and riparian sediments and (5) Discuss potential implications for the groundwater and surface water interactions.

3.3 Materials and methods

3.3.1 Study area

The study area (River Tern) is a tributary of the River Severn which is located in central England, UK (Figure 3.1). The investigated field site (2◦ 53'W, 52◦ 86'N) covers an approximately 240 m long section, 4–8 m wide and extending into the extensive, predominantly agricultural floodplain on the west side of the river (Figure 3.1).

Under the lowland catchment research (LOCAR) thematic programme, the investigated stream reach was selected by the UK's Natural Environment Research Council (NERC) as a typical lowland groundwater-fed river section in the UK. The field site geology along the alluvial corridor is dominated by heterogeneous alluvial drift deposits of Pleistocene to Recent age forming variable thickness across the Tern catchment (Adams et al., 2003;

Angermann et al., 2012). These deposits overlie the highly permeable Permo-Triassic Sherwood Sandstone (PTS) formation (Wheater and Peach, 2004), which is considered one of the regionally significant aquifers in the UK and is also the main source of water in the Tern River (Weatherill et al., 2014). In local terms, the investigation region is based upon the Permian Bridgnorth sandstone (Figure 3.1), and forms the principle aquifer (Streetly and Shepley, 2005; Weatherill et al., 2014).

In the study area, the river channel corridor incised through shallow, heterogeneous fluvioglacial sediments (Adams et al., 2003) which are typically composed of silt, clay, various sizes of sands, gravels as well as organic materials (Naden, 2011; Krause et al., 2012b). Floodplain core logs in the west bank site displays high spatial variability in textural facies and stratification as a result of the postglacial depositional history and are characterized by a wide range of hydraulic conductivities (Krause et al., 2012b; Weatherill, 2015). Unconsolidated streambed core sediments of the high permeable layer, for instance sand and gravel, are characterised by hydraulic conductivity between 10^{-3} and $10^{-5}ms^{-1}$ (Angermann et al., 2012; Krause et al., 2012b). The streambed also contains low permeability layers such as organic peat and clay lenses (Krause et al., 2012b). Krause et al. (2012b) presented substantially lower hydraulic conductivities ranging between 10^{-8} and 10^{-9} for the clay and peat heterogeneities deposited in the streambed of the Tern River.

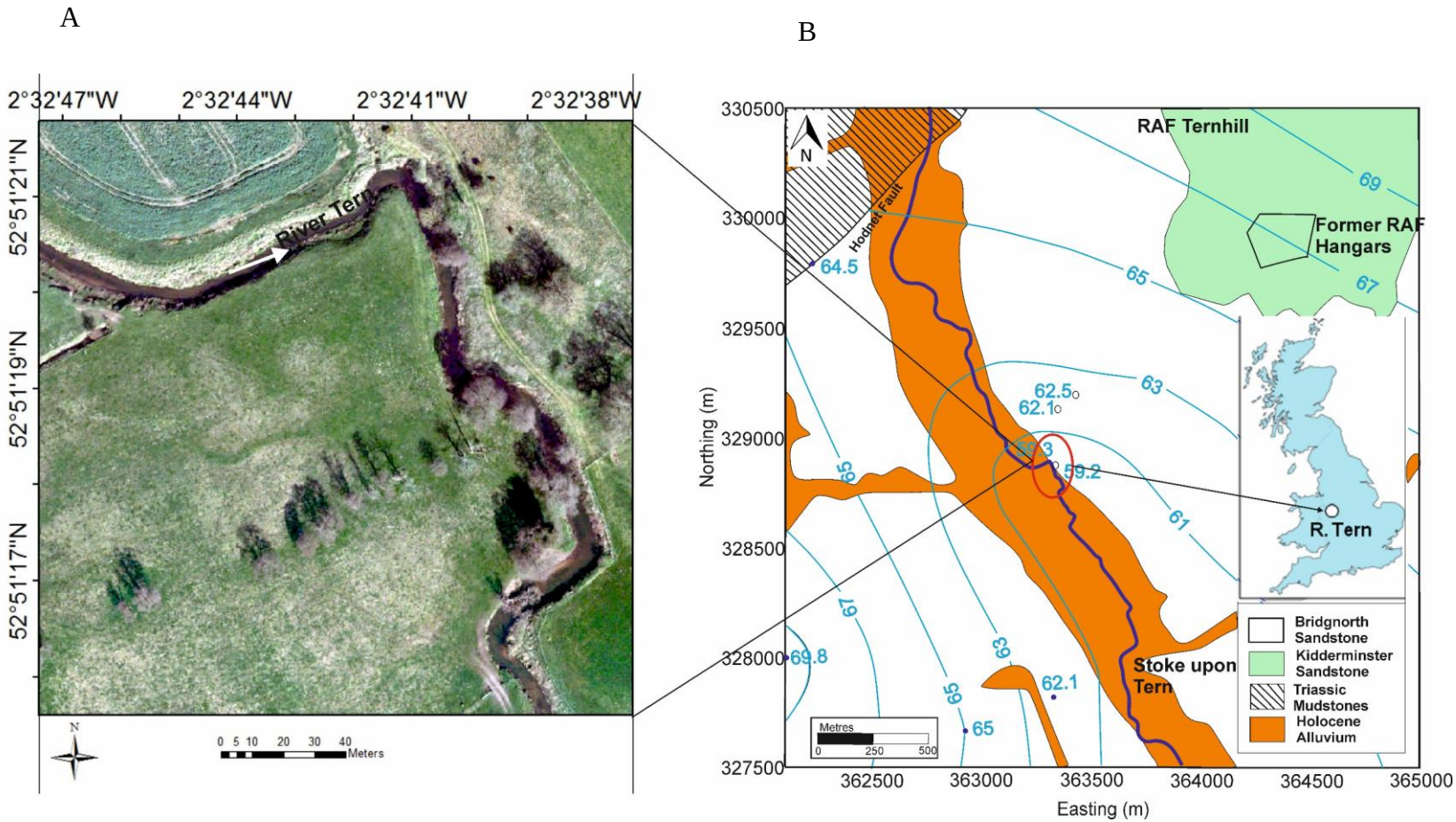

Figure 3.1 (A) Overview of floodplain and river channel investigation area (GetMapping Plc; copyright). (B) Regional geology and location of the study area at the River Tern, UK. Contours of hydraulic heads based on mean monthly groundwater levels measured at Environment Agency regional observation boreholes (2007–2010).

3.3.2 Ground-truthing method

Sediment coring was used to verify features present in the GPR profiles. Floodplain core sediments were retrieved using an extendable hand-driven gouge auger set (Eijkelkamp, The Netherlands) with a blade 6.5 cm in diameter and 50 cm long (Figure 3.2A). The auger has shaft extensions and is usually used after 50 cm of subsurface depth. The auger could reach approximately 300cm depth depends on the subsurface sediment type. However, due to the subsurface sediment heterogeneity in the floodplain study area as well as difficulty disconnecting shaft extensions in the field, this reduced to 170 cm to 250 cm depth for most cores. Sediment core logs were dug to the required depth using a hammer. After extraction, the cores were photographed (Figure 3.2B) and analysed visually in the site and then placed in a long plastic tray for further analyses (e.g., grain size analysis).

In contrast, riverbed core sediments were retrieved using 2 m long plastic uPVC tubes (unplasticised polyvinyl chloride) (Figure 3.2C). The ends of the plastic tube were sealed and large rubber bungs were used to secure the plastic sheeting. The tube was driven into the riverbed; a hammer was used where needed to facilitate digging into the riverbed.

The locations of the floodplain and riverbed core sediments are shown in Figure 3.3.

A

B

C

Figure 3.2 (A) Extendable Dutch auger used for retrieving floodplain sediments. (B) An example of the floodplain sediment core after extraction using Dutch auger. (C) An example of retrieved riverbed sediment core using plastic tube (For core locations see Figure 3.3).

3.3.3 Ground penetrating radar (GPR): principles

Ground penetrating radar (GPR) refers to a non-invasive and rapid method for the characterization and detection of the shallow subsurface (Davis and Annan, 1989; Neal, 2004). The transmitting antenna of the GPR system releases short pulses of electromagnetic energy. The energy passes via the material and then is reflected at an interface between materials characterised by various dielectric properties (Jol and Smith, 1991; Neal, 2004). Abrupt changes in dielectric properties lead to strong reflections from lithological boundaries (Jol and Smith, 1991). Several factors, for instance, groundwater level, differences in sediment moisture, diffractions resulting from subsurface and surface infrastructure could all

make measurements and interpretation of GPR survey results difficult (Bano et al., 2000; Neal, 2004).

Two-way travel time (TWT) is refer to the time between signal transmission, reflection and reception, and commonly measured in nanoseconds (10^{-9} second). This is a function of reflector depth and the propagation of electromagnetic (EM) velocity (Jol and Smith, 1991; Neal, 2004). GPR provides a continuous profile of the shallow subsurface, displaying horizontal survey distance against vertical TWT. Vertical TWT is converted to depth with knowledge of the propagation velocity, expressed as:

$$d = v*t/2$$

In which d is depth, v is velocity, and t is TWT.

The permittivity (dielectric coefficient, e) and the electrical conductivity (σ) of the subsurface have a strong impact on resolution and depth penetration (Jol and Smith, 1991; Cassidy, 2009) (Table 3.1). A higher water content (high e) causes diminishing in propagation velocity, whereas for instance saline water, clay or the differing degree of decay of the peat increases the electrical conductivity and leads to the development of rapid signal attenuation (Theimer et al., 1994; Heteren et al., 1998; Comas et al., 2004; Sass et al., 2010). Typical dielectric constant, electrical conductivity, velocity and attenuation values of common subsurface materials are shown in Table 3.1.

Table 3.1 Typical dielectric constant, electrical conductivity, velocity and attenuation values of common subsurface materials (from Annan, 2005).

Material	Dielectric constant (e)	Electrical Conductivity (σ)	Velocity	Attenuation
		(mSm-1)	(m ns-1)	(dB m-1)
Air	1	0	0.3	0
Salt water	80	3000	0.033	600
Fresh water	80	0.5	0.033	0.1
Ice	3-4	0.01	0.16	0.01
Granite, dry	5	0.01	0.13	0.01
Limestone*	4-8	0.5-2	0.12	0.4-1
Shales*	5-15	1-100	0.09	1-100
Sand,dry	5	0.01	0.13	0.01
Sand, wet*	20-30	0.1-1.0	0.06	0.03-0.3
Clay, wet	10	500	0.095	300
Soils:				
sandy,dry	2.6	1.4	0.19	1
sandy, wet	25	69	0.06	23
clayey, dry	2.5	2.7	0.19	3
clayey, wet	19	500	0.07	200
frozen	6	0.1	0.12	0.1

3.3.3 a) GPR survey on floodplain and river channel sediments

Ground penetrating radar (GPR) measurements were conducted to characterize reflection patterns and delineate the type and extent of complicated spatial heterogeneity textural patches (grain size facies) of high and low conductive materials. The floodplain GPR surveys were conducted in 19th of August 2014 along a 240-m section of the river channel and the west bank site of River Tern, a UK lowland meandering stream. The PulseEKKO PRO radar system from Sensors and Software Inc., Canada, was used to conduct the measurements. A lightweight 250 MHz center frequency bistatic shielded square transducers (0.3 m x 0.3m in dimension) antennas have been used in this study. The antennas are separated by 0.4 m and with 165 pulser voltage and were attached to the smart cart. These were then dragged along the floodplain profile lines, thereby generating a large number of 2-D profiles. An odometer wheel was used to trigger the measurement. In choosing the 250 MHz antenna, it was

necessary to consider an ideal compromise between the resolution and the desired penetration depth. The maximum depth range of the 250 MHz antenna in soils with high electrical conductivity like clay could reach to 2-4 m while in sandy soils it could reach to more than 10 m depth (Jol and Bristow, 2003).

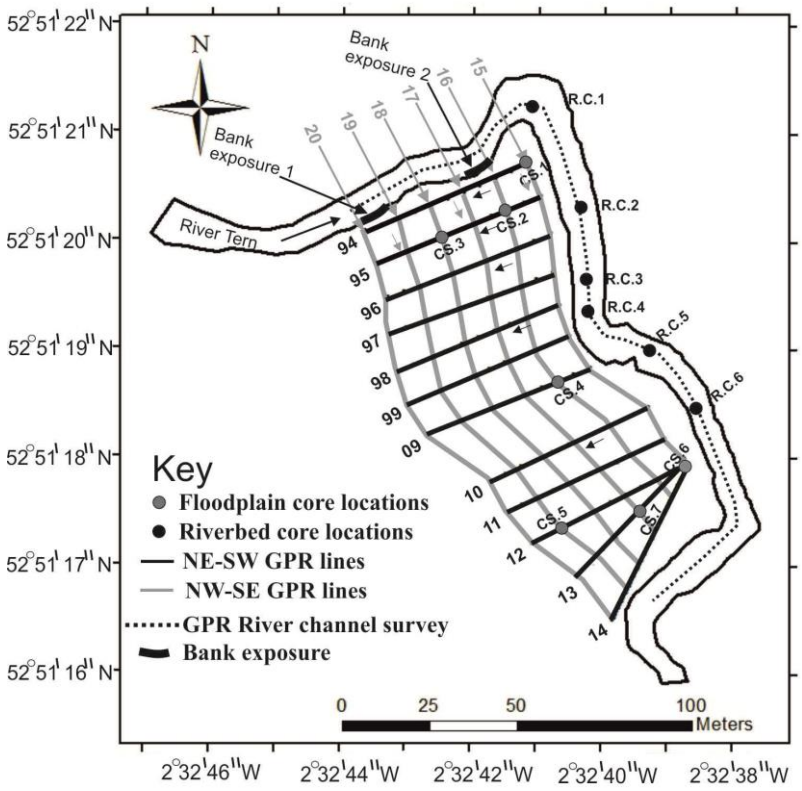

Figure 3.3 Study area with floodplain GPR profiles, in-channel GPR survey, and location of core logs and bank exposures. Floodplain Profiles 94–14, NE-SW orientations (solid black lines) are 50 m long and Profiles 15–20, NW-SE orientations (light grey lines) are varied between 100-132 m. In-stream GPR survey is 240 m. Grey and black dots represent floodplain and riverbed core logs, respectively.

For the floodplain GPR surveys, in order to conduct an accurate measurement, 12 NE-SW and 6 NW- SE orientated profiles were taken creating a raster of approximately 10 m (Figure 3.3). The NE-SW orientated profiles consisted of 50 m and ran from NE (close to the active river channel) towards SW (away from the river channel), while NW-SE profiles consisted of between 100 and 132 m. The non-equal lengths in NW-SE GPR line profiles are caused by

the meandering of the modern river channel (Figure 3.3). Parameters setting during the GPR measurements for all floodplain GPR profiles are shown in Table 3.2.

Table 3.2 Parameters setting during GPR measurements on floodplain (west bank site) river Tern site.

GPR parameters	Values
Frequency (MHz)	250
Survey type	Reflection
Time window (ns)	100
Units	m
Step size (m)	0.050
Antenna separation (m)	0.40
Odometer Cal (ticks/m)	1082.483
Stacks	8
Time sampling interval (ps)	400.000
Pulser voltage (V)	165

The riparian terrestrial GPR surveys were accompanied by a longitudinal in channel GPR survey (Figure 3.3) for which the antenna was deployed on a floating device. The antennas and battery (with 165 pulser voltage) were mounted on the surface water inside the bottom of plastic boat by keeping it firmly.

A rope was attached to both sides of the boat to facilitate pulling. Alongside the river's west banks, 22 ranging poles were positioned with a distance of 10m separating them. The ranging poles acted as land markers to aid in the identification of distinct places alongside the river channel.

The survey starts from the upstream section down to the downstream section (Figure 3.3) in which approximately 240m of the stream reach was surveyed.

3.3.3 b) GPR data processing

The GPR profiles were processed using Radpro 3.2 software and involved the following processes.

1) Dewow: is designed to remove unwanted low frequency while preserving the high frequency signal. The removal of this wow in the data is also called the "signal saturation correction" (Cassidy and Jol, 2009). For the data collected data in the study area, residual median filtering with windows length 20 nsec has been applied for all GPR lines.
2) Automatic gain control (AGC): the Automatic Gain Control (AGC) gain attempts to equalize the amplitudes of all GPR signals by applying a gain which is inversely proportional to the signal strength (Sensor and Software, 2005). In areas of weak signal, a gain is large and in areas of strong signal, the gain is small (Jol and Bristow, 2003). This type of gain is most useful for defining continuity of reflection events (Cassidy and Jol, 2009), but obliterate all amplitude information (Jol and Bristow, 2003). AGC start time zero nsec and window size 30 ns have been used for floodplain and riverbed GPR profiles.
3) Band-pass (frequency domain filters): Low cut filter (50-100 MHz) and high cut filter (300-450 MHz) was applied to cut the unwanted noise at the low and high ends of amplitude spectrum (Best et al., 2006; Cassidy and Jol, 2009).
4) Time zero shift correction: this was done to correct zero time of the first wave arrival. This correction is necessary for the proper position of the GPR reflections on the vertical scale (Lejzerowicz et al., 2014).
5) Topographic Adjustment: This can be adjusted by lowering or increasing traces, by a suitable TWT, in relation to a common datum. It must be in accordance with data on velocity which was 0.1 m/ns and the depth makeup of the uppermost section of the

radar profile (Sensors and Software, 1996). To achieve this, survey line topography needs to be sufficiently defined.

3.3.4 Digital elevation model (DEM)

A DEM was created to provide a precise spatial framework in which to locate the measuring data collected in the field site. A roaming survey was carried in the study site using a Leica 1200 differential GPS system. The main aim of the survey was for accurately surveying the heights and locations of GPR profiles, core logs, riparian groundwater boreholes and installed riverbed piezometers (Chapter 4). The GPS point locations for floodplain GPR profiles are listed in Appendix 3. The GPS base reference station was established in the west bank site of the river channel and close to an Environment Agency borehole (Figure 3.4). Also, the base station was always placed far from potential sources of interferences such as metal fences and tress.

Figure 3.4 Construction of the differential GPS base reference station on the west bank site of the river Tern river channel. The base reference station was set up around 20 minutes before a roaming GPS survey was due to begin. Time was needed for the reference station to locate itself both vertically and laterally through the exchange of signals with at least ten different satellites to ensure the highest accuracy.

A dGPS Rover unit was then put together and performed the survey by the user (Figure 3.5). The collected data were processed utilising Rinex Continuously Operating Reference Station (CORS) data supplied by the British Isles continuous GNSS Facility (BIGF), www.bigf.ac.uk, and Leica Geo Office. The Leica GPS 1200 generated measurements which were accurate only to within 10m. Therefore, these were corrected using Rinex CORS data from five CORS observation stations: located at Droitwich, Leek, Shobdon, Lichfield and Shrewsbury - along with GPS satellite navigation data. Observation and navigation data were supplied by the BIGF (British Isles continuous GNSS Facility). This correction refined the accuracy of latitude, longitude and elevation data to within an average of 0.008m.

The integrated GPS dataset was used to create a DEM in the Arcmap (version 10.2) program by applying the Inverse Distance Weighted (IDW) interpolation method to create a digital contoured surface.

Figure 3.5 Before each dGPS survey, initial checks were carried out to make sure that the Rover unit was transmitting on the same channel as the base station. Next, the Rover unit had to be configured for survey ID and the acquisition of the coordinate data points within a limited margin of error for quality control.

3.4 Results and discussion

3.4.1 Ground-truthing data

In order to accurately interpret GPR result profiles, ground truth data is imperative. Therefore, on a number of the NE-SW and NW-SE intersection lines and some distinct locations in the river channel, several ground truthing from bank exposures and corings from auger holes were done (Figure 3.3) to facilitate the recognition of the size and composition of alluvial deposits on the floodplain and riverbed, in addition to aiding in the determination of the interfaces of the sediments that the GPR images identify as distinct reflectors (Bridge et al., 1995; Sambrook Smith et al., 2006). Before the execution of the GPR surveys, two geological bank exposures were examined (Figure 3.9 A and B), which in turn facilitated obtaining some initial information about preserved lithology in the study section. These outcropped banks are extensive and naturally formed from collapse and erosion of the recent bank side (Figure 3.9 A and B). The description of ground-truthing data include bank exposures, floodplain sediment cores, and riverbed sediment cores (shown in Table 3.3). Grain size analysis were carried out for selected floodplain and riverbed sediments. The proportions of sediment were shown in Figure 3.8.

Table 3.3 Ground truth data presentation and relation to GPR profiles of the study area.

Ground-Truth data	Location and relation to the GPR profiles	Main characteristics
Bank exposure 1	Located at the north of Heathbrook farm at the west bank. This exposure was correlated with GPR profile 94.	The top 75 cm of the outcrop is composed of fine to medium sand with clay fractions and organic fragments. Below this, 122 cm (76 cm to 205 cm) has characterised by a slight dip towards the active channel and is composed of pale yellow medium sand, interbedded with thin layers of dark grey to black silt including organic debris. This overlies a very thin (3cm) layer of gravel (205-208 cm). A layer of soft black peat approximately 12 cm thick from 208 to 220 cm was observed to be underlain by gravel layer. From 220 cm to 240 cm, a clay layer was encountered at the bottom of the outcrop (Figure 3.9 B).
Bank	Located at the north of	The top 20 cm is composed of medium brown sand,

exposure 2	Heathbrook farm at the west bank close to the meander bend. This exposure was correlated with GPR profile 94 as well.	sandy topsoil. Below this, pebbles and cobbles supported within a peaty clay matrix was encountered to a depth of approximately 160 cm of the exposure (Figure 3.9 A).
Floodplain (C.S.1)	Retrieved at the intersection between GPR profile 94 and 15 at the start position.	Poorly consolidated, fining upward sequences of dark brown muddy sand containing occasional gravel, and rich in plant roots in the top 40 cm. This was underlain by sand deposits (Figure 3.6).
Floodplain (C.S.2)	Retrieved at the intersection between 10 m position of GPR profile 16 and 95.	Medium sand is predominant in this sample (Figure 3.8). 13% of sediment proportion was mud. Muddy sand with scattered gravel were dominant at the top 50 cm. Below this, 30 cm of muddy sand rich in organic matter was observed which was underlain by medium sand interbedded with dark silt which was further underlain by high permeable bedrock PTS sandstone (Figure 3.6).
Floodplain (C.S.3)	Retrieved at the intersection between 30 m position of GPR profile 95 and 10 m of GPR profile 18.	Mud was relatively higher in this sample compared to C.S.2 (Figure 3.8). Muddy sand with scattered gravel of overbank deposits was encountered at the top 60 cm of the core. Below this, clay nodules, sandy mud rich in organic matter, and peat of approximately 30 cm thick was found. Approximately 40 cm of medium sand lies underneath the channel fill deposits. This was underlain by a layer of approximately 70 cm (130–200 cm) of mud rich in organic matter and wood fragments. From 200 to 250 cm of the core a layer of saturated sand was encountered (Figure 3.6).
Floodplain (C.S.4)	Retrieved at the intersection of 10 m of GPR profile 09 and GPR profile 16, position 60-62 m.	The upper 60 cm of the core was found to be dominated by reddish brown muddy sand interbedded with sandy mud rich in organic matter in which plant roots are abundant at the top of the core. Below this, a layer of saturated sand was noticed from depth 60 to 120 cm of the core which was underlain by 35 cm of grey to blue soft clay. This was observed to be underlain by a layer of soft black peat (Figure 3.6). The mud proportion was 35%. (Figure 3.8).
Floodplain (C.S.5)	Retrieved at the intersection of 90 m position of GPR profile 19 and 40 m position of GPR line 12.	This sample is characterized by high proportions of clay and peat layers (Figure 3.8). The top 80 cm was composed of unsaturated fine-grained sandy mud rich in organic matter with occasional peat layer; a clay component and organic content are present in patches. Below this, more heterogeneous saturated muddy sand rich in organic matter, peat, and clay layers with rising water levels were observed at a depth of 80 cm to 200 cm during coring (Figure

		3.6).
Floodplain (C.S.6)	Retrieved at the intersection of the start position of GPR profiles 12,13,14 and end position of GPR survey 15.	The top 75 cm was interbedded between muddy sand and sandy mud rich in organic matter. Below this, interbedded pale yellow sand with thin layers of dark grey to black silt was encountered from 75 to 205 cm of the core log profile (Figure 3.6).
Floodplain (C.S.7)	Retrieved at the position 20 m of GPR profile 13 and end of profile 16.	The top 120 cm was predominant with muddy sand and sandy mud rich in organic matter. Below this, a layer of saturated sand was encountered (Figure 3.6).
Riverbed (R.C.1)	Retrieved at 60 m position of GPR river profile.	Poorly sorted gravelly sand interbedded with sand layers dominated the top section of the core. The bottom section was rich in muddy sand with clay nodules which were underlain by sand layer (Figure 3.7).
Riverbed (R.C.2)	Retrieved at 90 m position of GPR river profile.	Fining-down succession was observed in which the top gravelly sand layer was thicker in this core (about 40 cm thick) with including 5 cm of peat. This was underlain by sandy clay layer (Figure 3.7).
Riverbed (R.C.3)	Retrieved at the 110 m position of the longitudinal GPR profile.	Sand is predominant in this sample and R.C.4 (Figure 3.8). A mixture of poorly sorted gravelly sand interbedded with medium-fine sand including a small organic matter fraction. The bottom sand layer has stringers of grey-to-brown organic silt. A layer of sandy or silty peat was encountered at the base of the core (Figure 3.7).
Riverbed (R.C.4)	Retrieved at 125 m position of GPR profile.	A similar mixture of R.C.3. Below this unit, the competent red-to-orange Permo-Triassic sandstone was observed at the base of the core at approximately 95 cm below the riverbed level (Figure 3.7).
Riverbed (R.C.5)	At 150 m of GPR profile ("hotspot") location.	A 60cm layer of fine muddy sand containing clay and organic fragments has been preserved on the top of the core logs (Figure 3.7).
Riverbed (R.C.6)	At 155 m of the GPR profile.	Generally, fine grained sediment (clay particles) is predominate in this sample (Figure 3.8). A fining-down succession is observed in the upper metre of the core. Gravelly sands are in the first 25 cms below the riverbed, underlain by a medium sand including stringers of grey- to-brown organic silt which was further underlain by sandy or silty peat, rich in wood fragments (Figure 3.7).
Riverbed (R.C.7)	Around 170 m of the GPR profile.	A similar fining-down succession of R.C.6 observed here in which the thickness of the gravelly sand reduced to 15 cm (Figure 3.7). Clay proportion was very high in this core sediment (50%) (Figure 3.8).

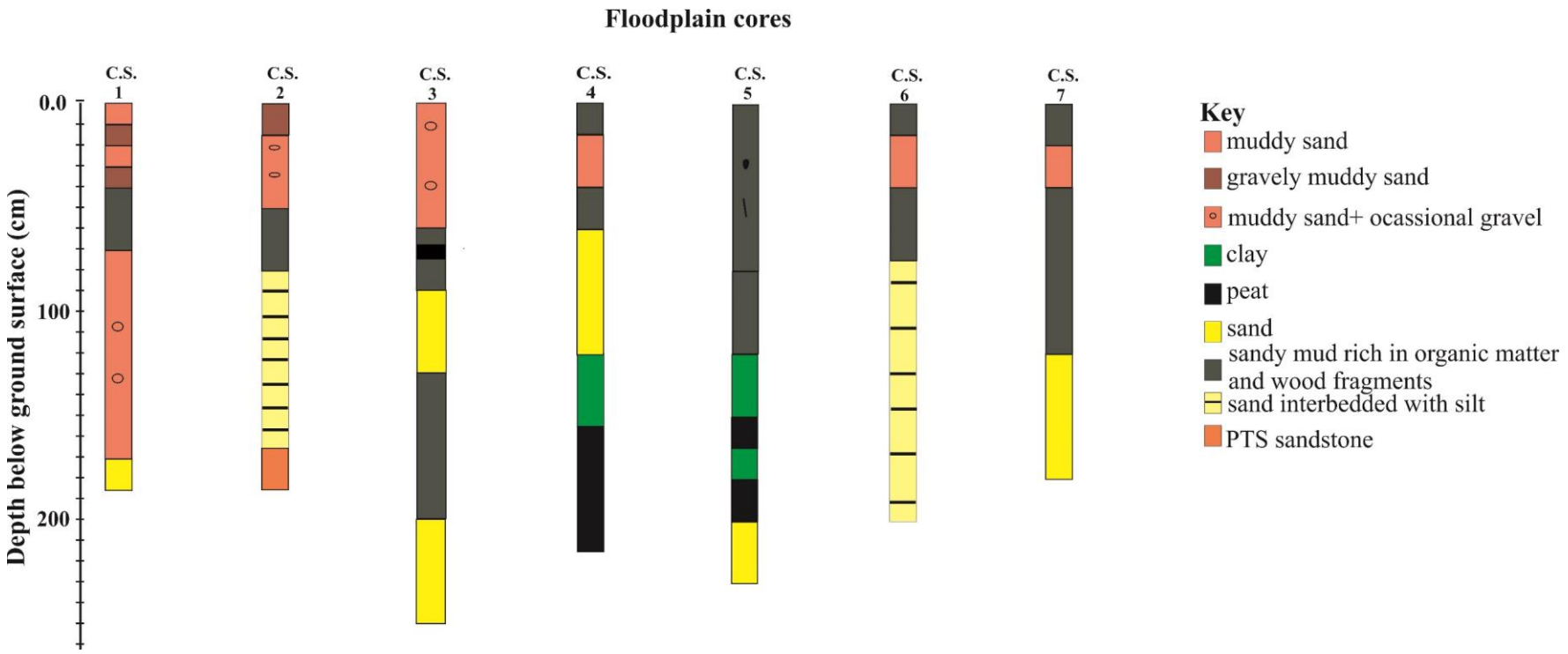

Figure 3.6 Geological logs for auger holes retrieved from the floodplain (west bank site) during the GPR survey (see figure 2 and table 1 for coring locations).

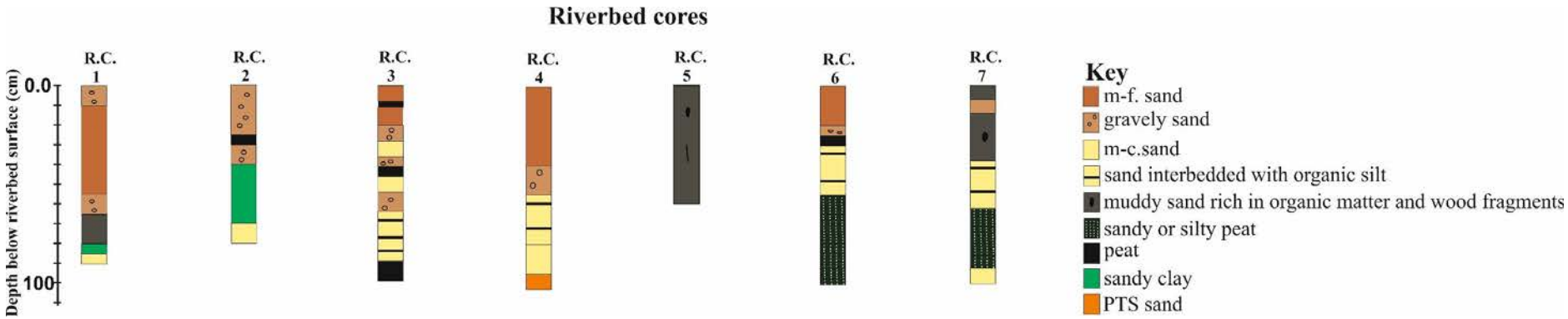

Figure 3.7 Riverbed lithology determined from core logs along the investigated study reach.

A

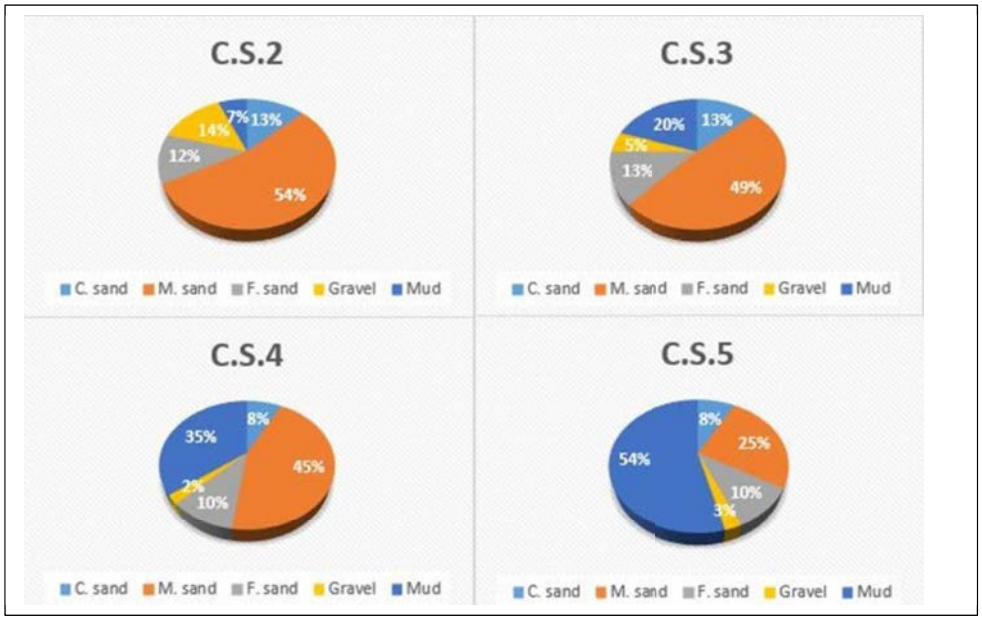

B

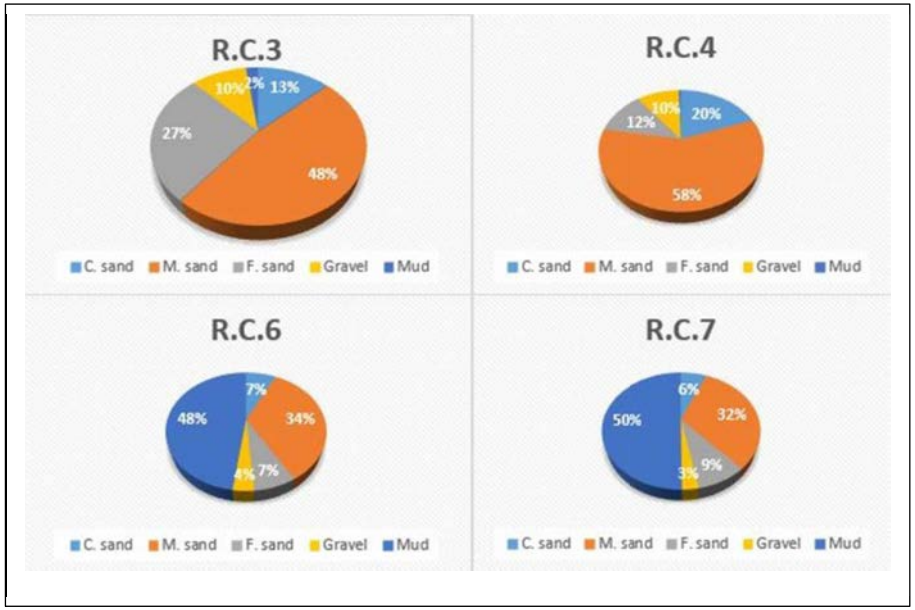

Figure 3.8 Sediment proportions in the river Tern study reach (A) Floodplain cores (B) Riverbed cores.

3.4.2 Radar facies identified on the west bank (floodplain) study site

Twelve NE-SW orientated GPR profiles, with six intersecting NW-SE orientated profiles, were collected on a west bank site of the River Tern at Heathbrook Farm (see Figure 3.3). The interpreted forms for each NE-SW and NW-SE orientated profiles are presented in Appendix 1 and Appendix 2, respectively. Based on distinct GPR signal reflections, eight different radar facies were identified in the study area (as illustrated in Figure 3.12). Characterization of these radar facies was performed according to the principles of radar stratigraphy (Beres and Haeni, 1991), which are derived from seismic stratigraphy (Mitchum et al., 1977). Radar facies refer to the sum of all the characteristics of a reflection configuration induced by a sedimentary sequence or distinct rock formation (Van Overmeeren, 1998). They are defined as mappable 2-D units, comprising reflections with an internal reflection pattern, continuity, amplitude, shape, and external 2-D form that differs from adjacent units using the approach applied by Beres and Haeni (1991), Heteren et al. (1998); Ekes and Hickin (2001). Neal (2004) highlighted the terminology used to describe radar facies and radar packages. These descriptions are shown in Figure 3.10.

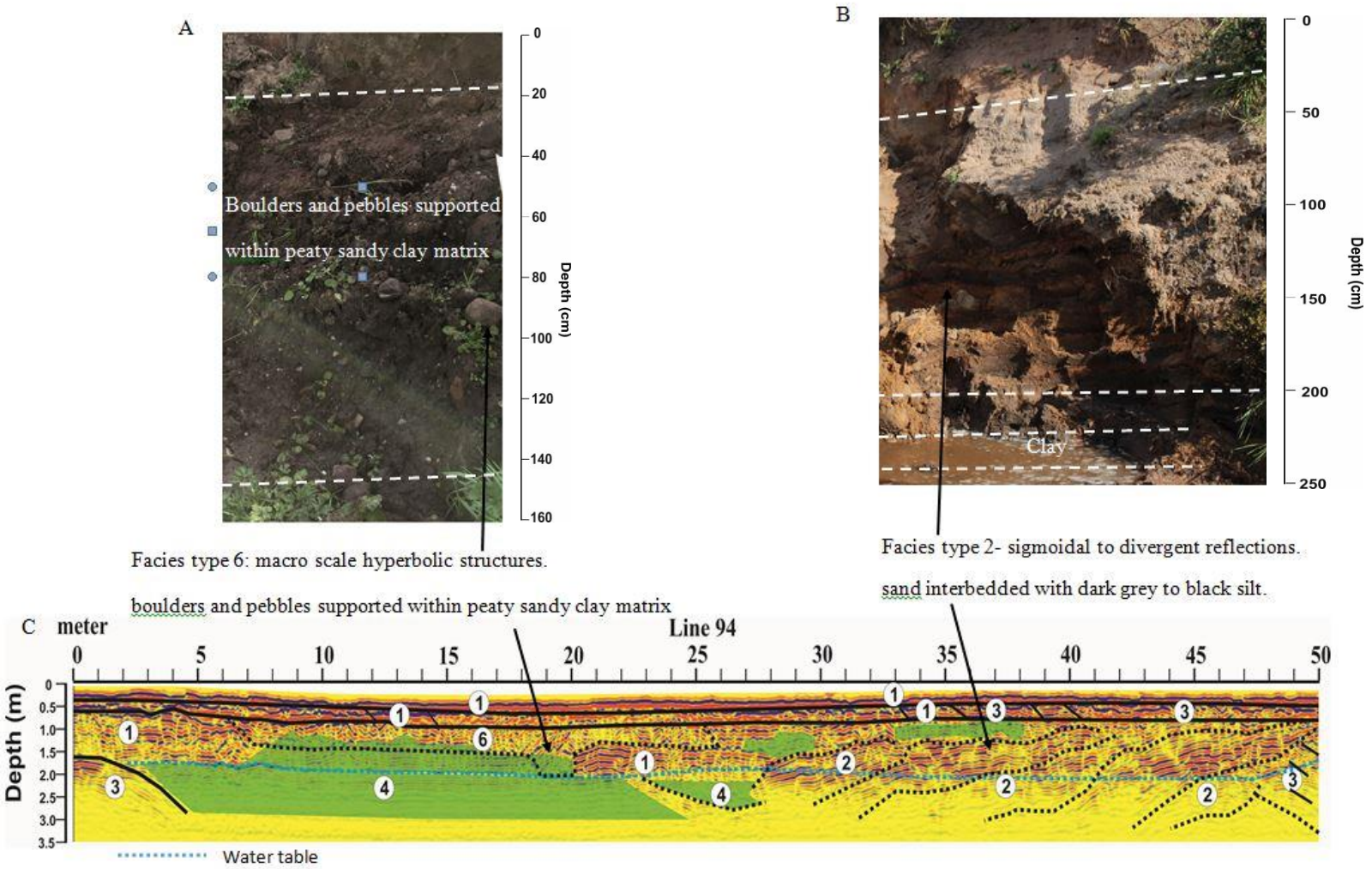

Figure 3.9 (A) and (B) Sections of the ground truth (Bank exposure) control the profile. (C) GPR line 94 surveys collected close to the river bank, illustrating radar facies and ground truth validation with exposures.

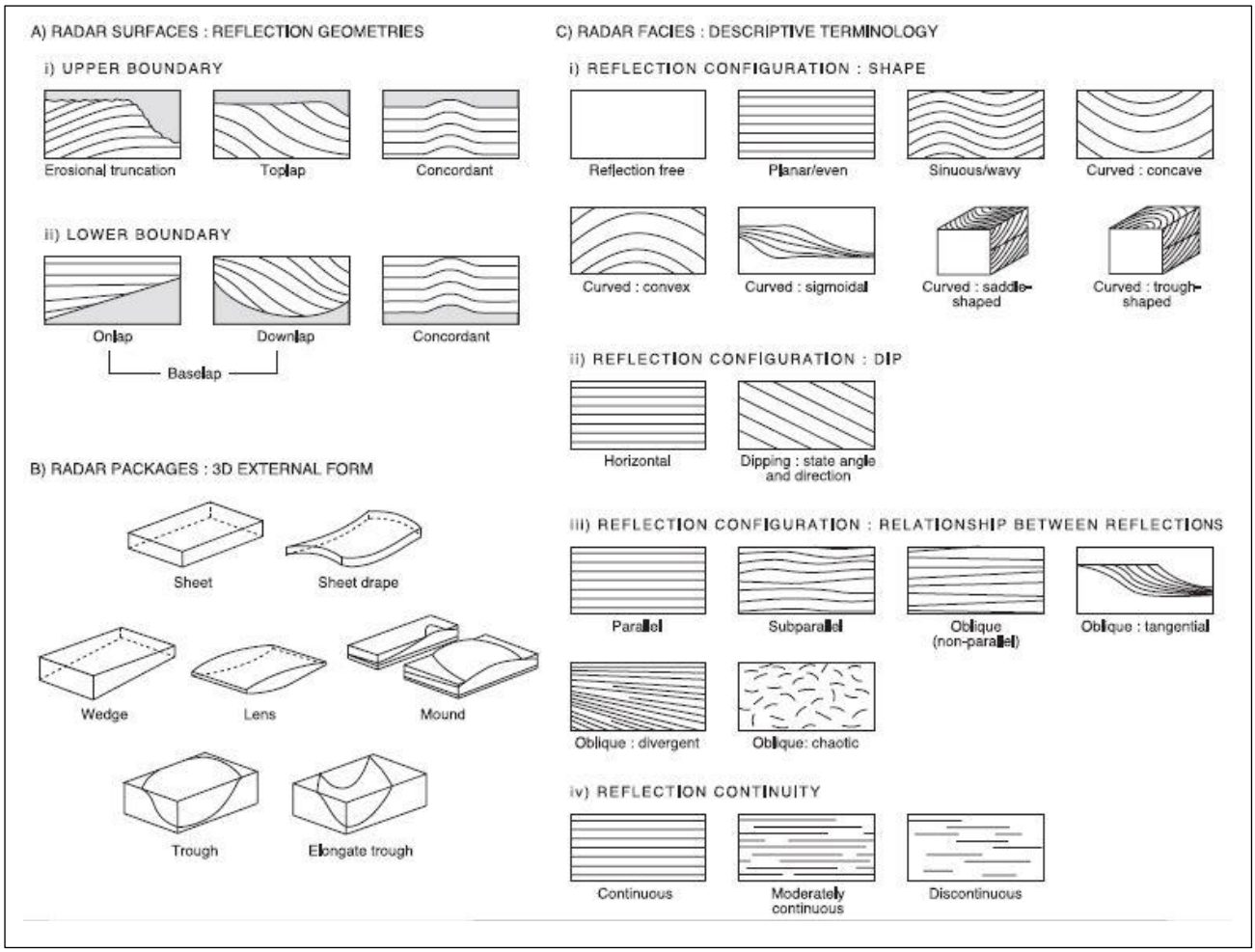

Figure 3.10 Descriptive terms of radargram images (after Neal, 2004).

3.4.2 a) Radar facies type 1: horizontal-to-sub-horizontal reflections (Floodplain fines)

Description

This radar unit is characterized by very strong amplitudes; wavy and even horizontal-to-subhorizontal reflections with localised sparse reflections (Figure 3.11, Figure 3.12 and Figure 3.13). This facies dominate the upper parts of all floodplain GPR profiles, and with a perfect lateral continuity (Figure 3.13).

Interpretation

Core logs and bank exposures match this reflection configuration (Figure 3.6, Figure 3.7 and Figure 3.9 A, B). The uppermost wavy horizontal to subhorizontal with small hyperbolic

(sparse) reflections agree well with muddy sand, gravel, plant remains, clay nodules, as well as some scattered gravel (C.S. 1, 2, and 3, Figure 3.6). This unit is abundant in proximal areas of the active river channel in particular in the northern part of the floodplain and can be seen up to 1.7 m depth (Figure 3.15). Locally, hyperbolic (sparse) reflections indicate texturally coarse grain materials (gravel) within a fine matrix element (Heteren et al., 1998). The existence of few scattered pebbles indicated that flooding of the adjacent areas was of sufficient vigour, at least initially, to deposit coarser-grade material before standing water conditions and deposition of fine-grained from settling took place (Wakefield et al., 2015).

Even-horizontal reflections are generally distinguished by the limited apparent thickness and can be seen within a depth range of 0–0.75 m. This correlates with stratified muddy sand rich in organic matter and occasional peat (C.R. 4, 5, 6, and 7; Figure 3.6). This feature is abundant in distal areas of the river channel, especially in the south and southwest part of the floodplain (Figure 3.15). In spite of having strong dielectric contrasts between sand and peat layers, there is no distinct reflection which would mark the peat to sand interfaces in the top part of GPR profiles (e.g. line 19). The reason may be peat deposits include mineral admixtures. Sass et al. (2010) pointed out that dielectric properties of peat can be influenced by the allochthonous minerogenic material. Weatherill (2015) found low resistivity values (40–120 Ω.m) at the top part of ERT profile surveys conducted for the same region of the investigated floodplain section. Weatherill (2015) interpreted this layer as alluvial cover deposits containing a main fraction of fine-grained, conductive materials.

Generally, these reflections might represent the bottom of fine-grained floodplain (overbank vertical accretion) deposits which form the youngest stratigraphy unit in the study area. This unit of deposits formed by settling of fine-grained sediment from suspension or by flood events when the floodplain was inundated (Miall, 1996; Słowik, 2014b). The presence of

minor interbedded gravel deposits indicates variations in river flow discharge and local channelized bedload transport on the river bank (Kostic and Aigner, 2007b).

Such interpretations coincide with findings of those of Asprion and Aigner (1999), Ekes and Hickin (2001) and Hickin et al., (2009) where they interpreted horizontal reflections as stratified sheet floods or vertically accreted bed-load sheets. In several of Slowik's research papers (2012a, 2013a, 2014a) carried out for the lowland meandering Obra river in Poland, horizontal reflections were abundant in the top part of the GPR sections and were interpreted as the traces of horizontal bedding in sand deposits that might have been accumulated by a series of flood events.

A prominent alteration in GPR reflections from sigmoidal to divergent clinoform (facies 2) to horizontal (facies 1) led to the deposition of heterogeneous layers. This feature was observed clearly in south-western part of GPR line 94 (Figure 3.9 C). Possible powerful sheet-floods may have eroded the floodplain deposits (Figure 3.9 C). The resulting deposited horizontal sheet layers are recognized by very low and high amplitude horizontal reflections (Line 94, Figure 3.9 C). Sheet-like deposition may have resulted in the formation of homogenous bodies of sands (Huisink, 2000b).

3.4.2 b) Radar facies type 2: Sigmoidal to divergent clinoform reflections (modern floodplain)

Description

This radar facies is recognised by sets of sigmoidal to divergent reflections, high-to-low amplitude reflectors, slightly inclined (1°-10°) towards the main channel river, downlapping (striding) onto a slightly undulatory reflector and good penetration (Figure 3.9 B, Figure 3.12 and Figure 3.13). This facies can be seen exclusively in a few 2D profiles in NE-SW and NW-SE directions, close to the modern river channel. For example, these occurred between 27.1–48 m as multiple sets of deposition in profile 94 at a mean depth of about 0.7–3.5 m

b.l.s., 2–7 m of profile 19 at a mean depth 0.7–2.5 m, 40–46 m of profile 95 at 2–3.5 m depth, 20–26 m, and 34.5–40 m of the profile 96 (see Appendix 1 and 2 for details).

Interpretation

This facies correlates well with low angle and streamward-dipping interlaminated sand with dark grey to black silt occurring between 0.75 m and 2 m over an extensive bank exposure 1 (Figure 3.6 and Figure 3.12). The lower part of this reflection is characterised by low-intensity signals which attribute to the presence of clay laminae with localised concentrations of black, organic remains (Figure 3.6). This unit was also observed in core sample 2 and 6 (Figure 3.6) which mainly located at the head of the meander. A complicated sigmoidal reflection configuration coincides with a variety of internal structures; for example, epsilon cross stratification (ECS) and longitudinal bar foresets, which in turn are an indication of point bar deposits as well as river channel and bar migration (Ekes and Hickin, 2001). Based on these characteristics as a whole, this radar facies can be interpreted as floodplain sediments. This interpretation is supported by the fact that the GPR line 94 was surveyed in the vicinity of the modern active channel (Figure 3.3).

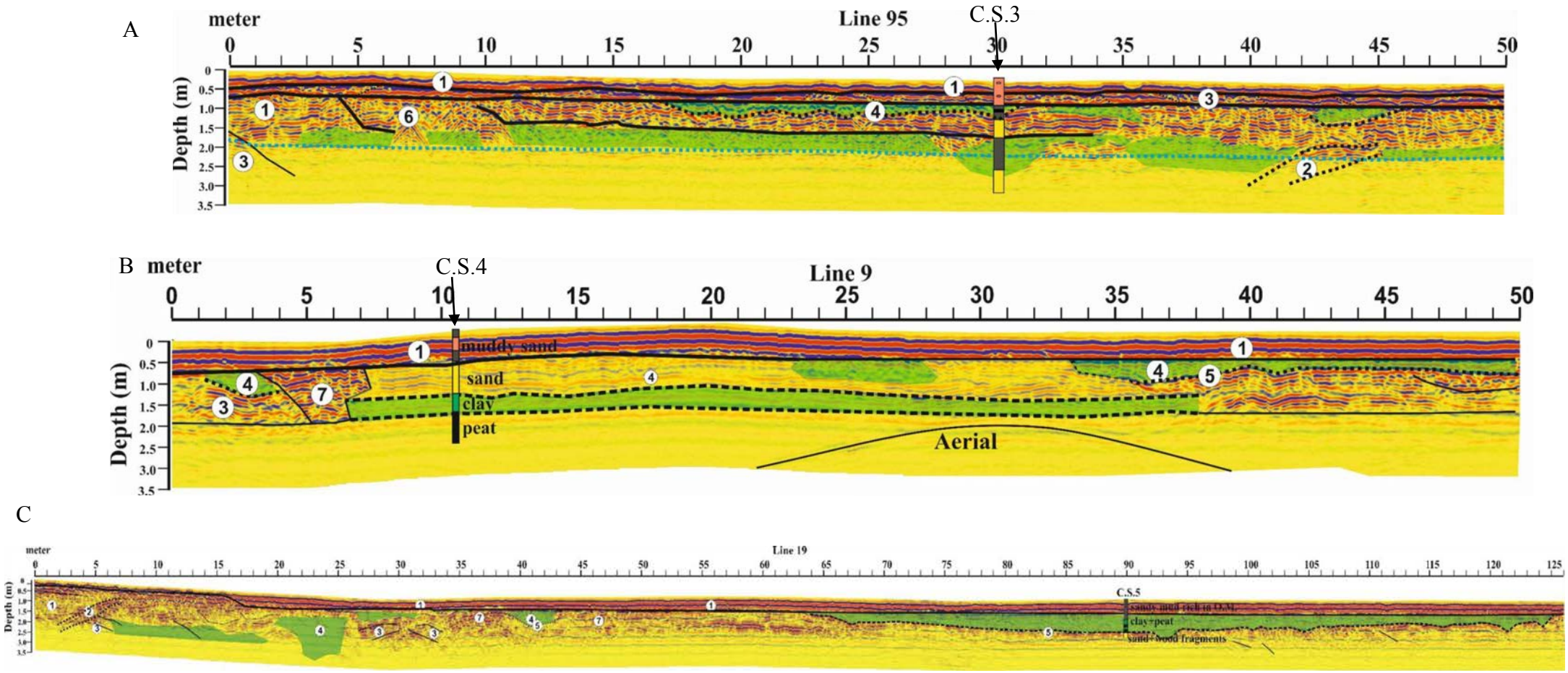

Figure 3.11 Two examples (50 m long) (A) line 09 and (B) line 95 of NE-SW orientation GPR floodplain surveys, and (C) one example (126 m long) of NW-SE) orientation, illustrating numbered radar facies and calibration with core logs along the profile.

Radar facies	GPR example image	Core section	Lithology	Interpretation	Permeability class
Radar facies type 1 Horizontal-to-subhorizontal reflections	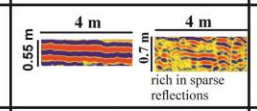	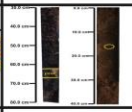	Fine muddy sand, plant remains, clay nodules, as well as some isolated pebbles	Overbank vertical accretion deposits	Intermediate
Radar facies type 2 Sigmoidal to divergent clinoform reflections	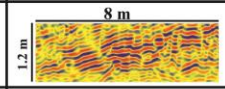		Sand layers interbedded with dark silt	Overbank flooding (modern floodplain)	High
Radar facies type 3 Wavy and Inclined reflections	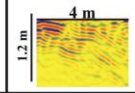		Sand sediment	Lateral or downstream accretion and lateral migration of the river	High
Radar facies type 4 Faint subhorizontal, undular,variable dip, and structureless reflections	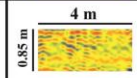		Muddy sand rich in organic matter, peat, and clay	Channel fill elements	Low
Radar facies type 5 Curved, concave-upward reflections associated with dipping and small hyperbolic reflections	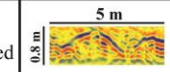		Sand with organic fragments	Erosional surface	High
Radar facies type 6 Discontinuous, chaotic or irregular rich in macro scale abundant stacked hyperbolic reflections	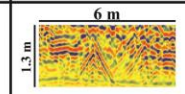		Big boulders or baedrock surface	Deposits of submerged palaeomeander or bedrock	Low-High
Radar facies type 7 Hummocky,dipping and chaotic reflections including micro-scale hyperbolic diffractions.	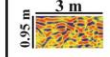		Small boulders within sand deposits	Surrounding the older channels represent point bar sediment.	High
Radar facies type 8 Structureless, reflection free zone.	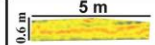		Clay layers	May correspond to swamp deposits	Low

Figure 3.12 Types of GPR reflections, their connection with ground truth data and interpretation, identified in the west bank (floodplain) river Tern study site.

3.4.2 c) Radar facies type 3: Wavy and inclined reflections (Lateral or downstream accretion elements)

Description

This radar facies 3 is characterized by variable orientation and dip of reflectors, medium-to-low amplitudes. It is bounded by a lower erosion surface and an irregular upper surface and is the most common facies in the study area and can be seen in different depths (Figure 3.12).

Interpretation

This facies mark layers of sand deposits which are exhibiting fining upward sequences. This facies can be interpreted as the lateral migration of river channel (Kostic and Aigner, 2007b; Słowik, 2013a) in which indicating the development of point bars deposits (Vandenberghe and Van Overmeeren, 1999; Słowik, 2015) or may represent downstream accretion elements as well (Hickin et al. 2009). It can be seen from profile 19 (Figure 3.11 and Figure 3.13) at 26—39 m that the orientation of reflectors is variable, suggesting frequent changes in migration direction of the channel. A similar feature was identified by Slowik (2013a) in a study on the Obra River floodplain in Poland.

3.4.2 d) Radar facies type 4: Faint sub-horizontal, undular, variable dip and structureless reflections (channel-fill facies) with (abandoned channel elements)

Description

This facies is presented in GPR as a very weak amplitude, faint sub-horizontal, undular, variable dip and structureless reflections. As well as very irregular geometry that is undulating and disturbed, with a total absence of lateral continuity (Figure 3.11 and Figure 3.13). This unit is bordered by horizontal reflections at the top and curved, concave up reflections at the bottom. The penetration of GPR within this unit is contingent upon the quantity of low permeability layers representing channel fill sediments. Typically, these

reflectors were prevalent across the majority of the floodplain GPR profiles at variable depths.

Interpretation

This facies exhibits an important attenuation that is comprised of peat, clay and/or saturated alternate combinations of low conductivity materials (Figure 3.12), evidenced by a low-energy depositional setting characterised by uneven sedimentation (Heteren et al., 1998). It is widely acknowledged that low conductivity layers can excessively attenuate GPR signals, while reducing the depth of penetration (Theimer et al., 1994; Heteren et al., 1998; Bristow and Jol, 2003). Nevertheless, it can be constructive as a means of assessing the alluvial fill thickness, as observed by Leclerc and Hickin (1997) as well as Froese et al. (2005). Boisson et al. (2011) determined that heterogeneities within silt sediments produced electromagnetic energy losses of a GPR signal. However, Bristow et al. (1999) had observed that an antenna resolution that was low in respect to the sediment's internal architecture may consequently produce free GPR signal reflections. In the instance of this study, for both the floodplain and river channel GPR survey the attenuation was a consequence of the presence of low permeability layers, for example, the peat and clay deposits that were detected by the core logs (C.S. 3, 4, and 5 in Figure 3.6).

The core sample 5 (C.S.5) was overlapping to the GPR image profile 19 at position 90 m (Figure 3.11 C). Using the lithological information, some boundaries between units characterised by similar reflections were outlined. For example, saturated layers of muddy sand rich in organic matter, peat and clay (C.S. 5, Figure 3.6) detected from 80 cm to 200 cm depth correlates well with this facies. This radar facies was predominantly seen in the floodplain's south and southwestern areas (Figure 3.15) that are characterised by low topography, particularly below facies 1 unit. This radar unit (low conductivity channel fill sediments) propagated through GPR lines 09, 10, 11, 12 and 13 in a NE-SW orientation

profile, as well as lines 17, 18, 19 and 20 in a NW-SE orientation profile within the depth range of 0.8–2.5 m (Figure 3.13). Furthermore, it has been observed that this facies cannot delineate all along the profiles but it seems to laterally disappear corresponding to a body of finite length (Figure 3.13). The resulting shape is similar to a lenticular body, with a flat uppermost boundary and a concave upwards bottom, which eventually tapers thinner at both of the sides approaching the adjacent point-bar sediment deposits (Figure 3.11 C and Figure 3.13). Considering this characteristic, it may correlate to the infilling of an abandoned channel filled by low conductivity layers. This unit's maximum lateral extent was 66 m and can be observed in the GPR section 20 (NW-SE orientation), analogous to the direction of river flow (Figure 3.13). In addition, there are some small channels observed in north west section of the floodplain and filled by low permeability layers (GPR line 96-99) (Appendix 1). Those channels observed in GPR profiles 99,09, 10, 11, 12, 15 and 16 (Figure 3.13), situated in the south-eastern region of the study area in close proximity to the hot spot section of the active channel can be called chute channels. Here, the channel's internal EM signal gradually weakened with greater depth. This is likely to be a consequence of the high water level, alongside the higher electrical conductivity apparent within the clayey peat infill that contributed to significantly attenuated radar waves. This attenuation obstructed the base of the channel from being observable due to rather large thickness of low conductivity layers. Furthermore, the channel fill was also comprised of a number of small hyperbolic reflections of facies 6 at the top of the channel, which was likely to correspond to some buried boulders (Figure 3.13). The filling submerged channel in the NE part of the west bank site expressed irregular reflections that were filled with stacked hyperbolic reflections (facies 6), typically associated with signal attenuation that indicates high groundwater water level. Moreover, the material infilling the channel in the central region of the floodplain (coloured white in Figure 3.13) displays more vigorous and continuous subhorizontal reflections in GPR sections, while

being dissimilar from infillings of the channels (green colour in Figure 3.13). The almost wholly saturated sand recovered at 60–120 cm depth of floodplain core sample 4 (C.S. 4, Figure 3.6), at position 10 m of GPR profile 09, corresponds largely to the features of its reflections. The location of white channels mainly relates to the positions of the formerly active river channel that, following its abandonment, was infilled with sand layers.

Similar GPR reflections and interpretation were found in several other studies (Leclerc and Hickin, 1997; Vandenberghe and Van Overmeeren, 1999; Slowik, 2012b).

The existence of peaty channel-fill in this floodplain area may indicate that the abandoned channel has not received clastic material over a considerable period. Consequently, this may suggest that the active channel was not in close proximity during the infilling process. A sand layer topping may be connected to a reactivation of the depression. As abandoned channel features remain as topographical depressions in the floodplain over a considerable duration of time, running into centuries, they are commonly disposed to channel reactivation or crevasse splay formation, both of which can explain the presence of sandy deposits close to the surface. Miall (1996) and Kostic and Aigner (2007b) stated that during the process of cut-off from the main flow, the abandoned channels were gradually packed with fine grains from suspensions.

3.4.2 e) Radar facies type 5: Curved, concave-upward reflections (erosional surface)

Description

This facies is characterised by high amplitude, curved, and concave upward reflections associated with dipping and small hyperbolic reflections (Figure 3.12). Generally, this type of reflection is abundant in the study area and can be found below channel fill facies 4 elements (Figure 3.11 C and Figure 3.13). The occurrence of this configuration provides significant information concerning formerly functioning riverbeds in the study site.

Interpretation

It should be noted that in GPR image results, this reflection is characterized by strong intensity due to the strong contrast in dielectric properties with channel fill elements of facies 4. This pattern is consistent with sand deposits rich in wood fragments which were detected at the base of the core sample 5 (C.S.5, Figure 3.6). Local hyperbolic reflections mark wood fragments inside sand deposits. This unit might represent the pre-existing deposits on top of which the abandoned channel has developed. Many studies identified similar characteristics in their study areas (see, e.g., Vandenberghe and Van Overmeeren, 1999; Lunt et al., 2004; Słowik, 2014a).

3.4.2 f) Radar facies type 6: Discontinuous, chaotic or irregular rich in macro scale abundant stacked hyperbolic reflections (buried boulders or bedrock surface)

Description

This facies was identified on many GPR profiles (in both orientations) at a range depth 0.8–2 m, most of which were collected in areas nearby the head of the meander bend. Their stacked hyperbolas reflections resemble inverted chevron shapes (Figure 3.11).

Interpretation

Hyperbolic reflections appear as a consequence of the response of the divergent radar beam to extremely uneven boundary (Heteren et al., 1998). The antenna receiver obtaining electromagnetic waves not only via reflection on the near-horizontal boundary but also via reflection of that part of the peripheral GPR beam that forms a fresnel zone on subhorizontal to sharply inclined boundary surfaces (Heteren et al., 1998). When compared bank exposure 2 (Figure 3.9) to the GPR profile 94 (position 6 to 20 m), at the range depth 0.5–1 m, different gravel sizes supported within a peaty sandy clay matrix could match this facies. This can be considered as a part of paleo-meander channel fill sediments. Another interpretation

could be representing the top of the irregular surface of Permo-Triassic sandstone bedrock (C.S.2, Figure 3.6).

3.4.2 g) Radar facies type 7: High amplitude, discontinuous hummocky and chaotic reflections including micro-scale hyperbolic diffractions (alluvial deposits with pebbles).

Description

Facies 7 is observed in most of the NE-SW and NW-SE oriented GPR 2D profiles within the depth range 0.7-2 m, observed around channel fill elements (Figure 3.11).

Interpretation

Unfortunately, there is no ground truth data for validating this facies. This unit exhibits several small-scale hyperbolic diffractions which should correspond to point objects buried at different depths, probably being large clasts (e.g. small boulders) within sand deposits. Moreover, their geometry fit well with 0.08-0.1 m/ns electromagnetic (EM) velocity value.

These configurations suggest the existence of a heterogeneous lithological unit of high conductive materials which surround older channels and indicate sediments of bar deposits. This facies was also present in Zuk (2011).

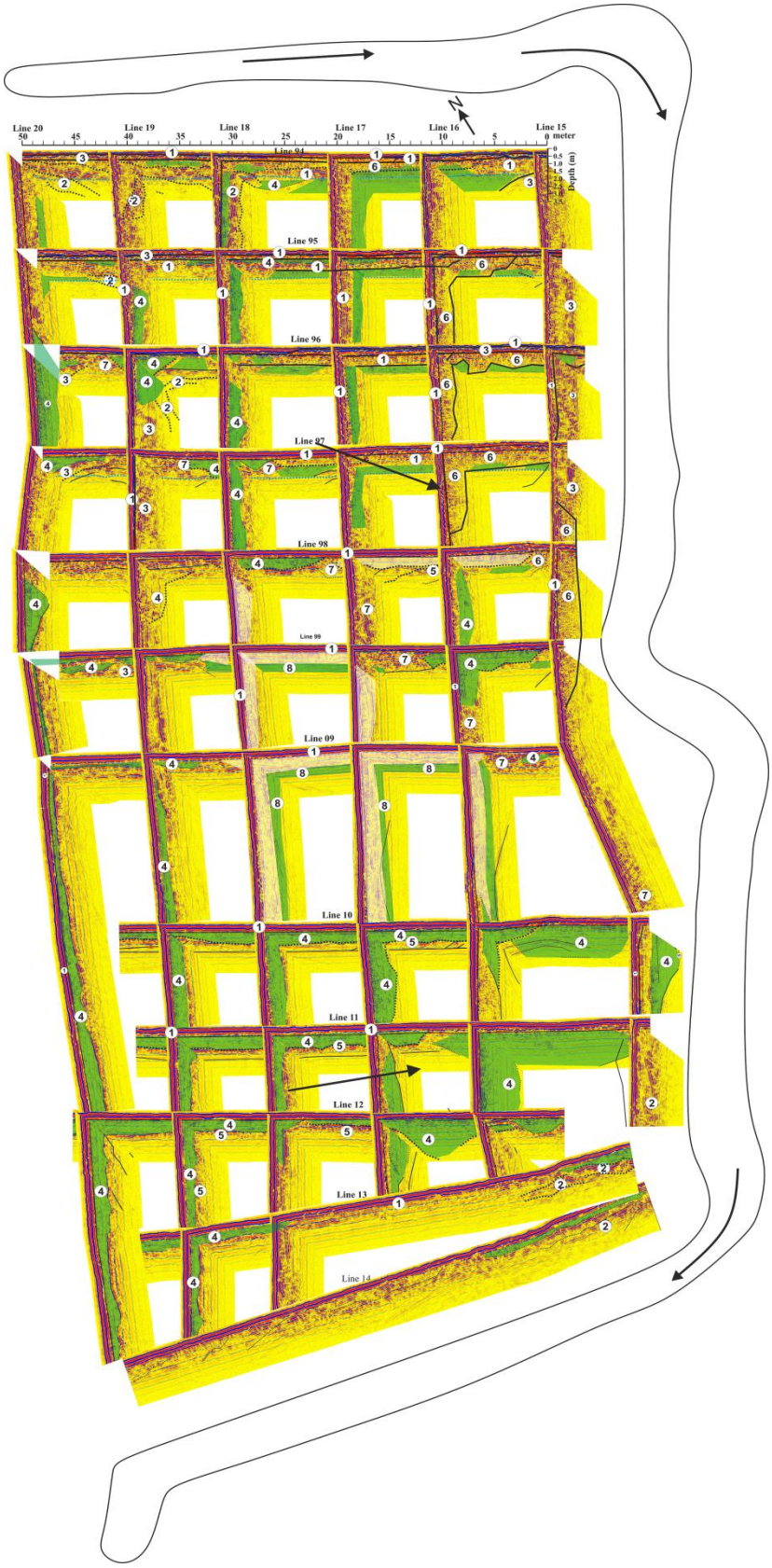

Figure 3.13 Quasi three-dimensional GPR profiles illustrating permeability class and radar facies distribution along west bank site of the river Tern. Green colours represent spatial distribution of channel elements filled by low permeability layers (low permeability field), while white colours represent channels filled by high permeability layers.

3.4.2 h) Radar facies type 8: Structureless, reflection free zone

Description

This facies can be identified in the middle part of the floodplain section, specifically in the area of low topography close to the second meander bend. They have been imaged in both NE-SW profiles (profile 99 and 09) and NW-SE profiles (profiles 16, 17, and 18), below subhorizontal reflection patterns of sandy channel fill deposits (Figure 3.13).

Interpretation

Structureless facies may indicate the presence of large thickness highly conductive materials (Ekes and Hickin, 2001). In the study site, this facies seems to disappear laterally in both GPR direction profiles, corresponding to a body of finite length (Figure 3.11 C and 8). These structureless signals correlate well with the retrieved clay layer (~ 35 cm thick) observed at a depth of ~ 120 cm, extending up to 155 cm in depth in core sample 4 (Figure 3.6). Clay has dramatically attenuated the GPR signal, because it is comprised of charged particles.

3.4.3 Interpretation of GPR river profile

The longitudinal GPR image survey was performed to investigate the detailed internal structure of alluvial valley fill deposits. It revealed geomorphological features that included former channel fills and the lateral accretion of point bars (Figure 3.14). However, horizontal, wavy, dipped, curved, concave-up, attenuation, and multiple reflections can all be discerned in the GPR image. The first strong undulating reflection represents the bottom of the river (the sediment-water interface). Subsequent reflections are from the sediment structure on the sub-bottom of the river. The strong reflection obtained from the bottom also produced some multiples (Figure 3.14). The signal reflected from the bottom, traveled up to the surface, was reflected from the water-air interface and then traveled back down to be reflected from the bottom a second time before traveling again to the surface. Such results are easily interpreted,

because they take double the travel time of a bottom only reflector. The clearest example is visible between 140 m and 190 m; however, there are other examples throughout the data.

From 0 m to ~ 57 m of the river profile corresponds to E-W river orientation, and the upper reflections from the top 20 to 50 cm of the riverbed are characterized by high and low amplitude subhorizontal signals, associated with chaotic and disturbed reflections. Below this level, there are a set of dipping reflections, associated with low amplitude disturbed reflections from ~ 17 m to ~ 30 m, which reveal greater thickness than in other regions. These reflections correlate with sandy silt that is rich in deposits of organic matter, and the dipping reflections can be interpreted as constituting lateral accretion.

The river makes a right turn towards the south at about 60 m along the profile, after which point, water flows toward the N-S direction, until 200 m of the profile into the study site. Where the surface water flow impinges the outer banks of the meander, the water level rises as a result of the pressure against the bank and the erosion of the active cutbank (Miall, 1996). The water flow then turns downward, developing a helical overturn pattern. The return flow, which occurs at depth, passes obliquely up the bed of the inner bank (Miall, 1996). The uplift area observed between 57m and 62 m represents the inner bank of the meander. It is composed of fining-upward sequences of point bar deposits of gravely sand and muddy sand sediments (R.C.1, Figure 3.7). From ~ 62 m to ~ 98m of the longitudinal profile, different GPR signal reflections were identified, for example, dipping, subhorizontal and dipping reflections, which may represent sediments created by the erosion of the cutbank. In the radargram, the reflections arise from high amplitude reflectors, which correspond with the highly permeable sand and gravel deposits identified in core samples 2–4 (Figure 3.7). A lens of sandy clay layer was identified at 77 m–88 m, at a range depth of 40–80 cm, and recognised by a trough-shaped reflection in the GPR image (Figure 3.14). This finding was confirmed during the installation of minipiezometers in the riverbed.

At ~ 100 m to ~130 m along the profile, the upper reflections are characterized by medium to strong subhorizontal reflectors, which are associated with small hyperbolic reflections, with good lateral continuity. These reflections indicate high permeability layers such as gravel and sand with minimal organic matter content, in accordance with the river core sample 1 (R.C.3, R.C.4 , Figure 3.7). Below this level, the GPR result shows signal attenuation is associated with disturbed and weak amplitude, and wavy to subhorizontal reflections. The underlying reflections correlate with the sandy or silty peat layers identified at the bottom of the core sample (R.C.3). It has been noted that from 125 m to ~ 135 m of the profile the signal shows a lens comprising disturbed and attenuated features, which might denote sediments rich in organic matter or peat. The longitudinal GPR survey result covering this section (~ 98 m to ~130 m) reveals the predominant high permeability layers in this region have a greater thickness comparative to the other parts of the profile (Figure 3.14). Regarding the geological characteristics, R.C.3 and RC.4 were retrieved at positions 100 m and 125 m of the GPR profile respectively. An ERT survey for this section by (Naden, 2011), found high resistivity values in the subchannel section, which was interpreted as layers of superficial sand and diamict deposits.

The area 140 m to ~ 192 m along the profile is characterized by low surface water level (Figure 3.14). Geophysically, the first strong reflections were diagnosed by disturbed subhorizontal reflections. This agrees well with the presence of a gravelly sand top unit rich in organic matter, as identified in riverbed core samples 5-7 (Figure 3.7). Below this, the area is characterized by a strong GPR signal, including disturbed and attenuated alternates showing multiple reflections from surface water (Figure 3.14). This is corresponding with peat and clay layers identified in riverbed core samples 5-7. This area is corresponding with south east section of the floodplain which also was rich in low permeability layers. Previously, Krause et al. (2012) also identified these layers in this section. The presence of

subchannel low conductivity layers, such as clay, peat, and sediments rich in organic matter content resulted in GPR free signal reflections, due to the absorption of the majority of the electromagnetic waves (Davis and Annan, 1989).

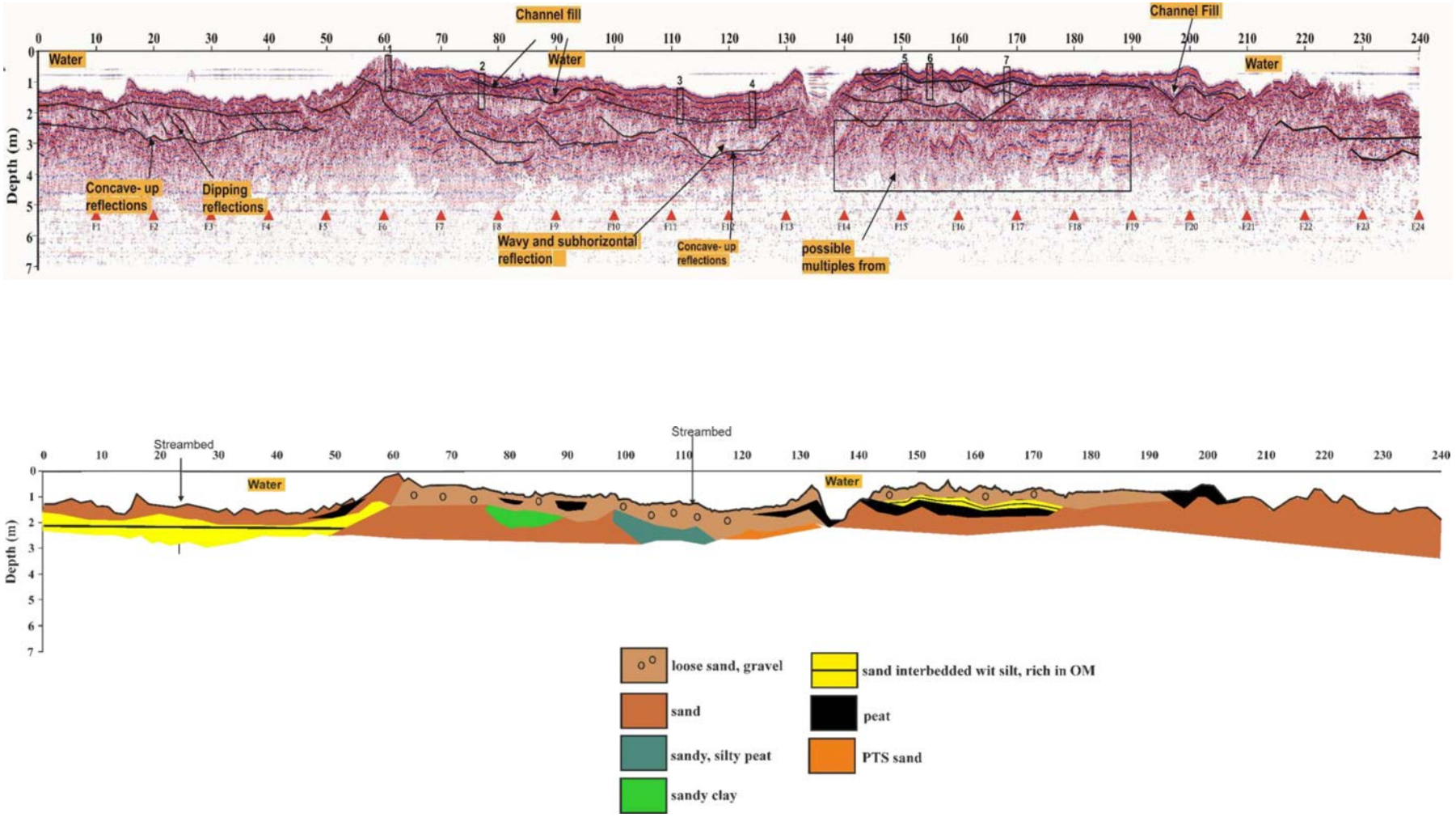

Figure 3.14 Longitudinal in-channel survey (240m) showed GPR reflections, bathymetry, streambed topography, core locations, lithology and structures of the riverbed.

3.4.4 Permeability class distribution

Figure 3.13 shows the permeability class distribution in the west bank river site (riparian zone, outlined in green). The results of quasi three-dimensional GPR images (Figure 3.13) revealed that the low permeability layers are distributed in different places with various thicknesses and extensions. Fence diagram were created using Rockwork software (version15). Types of geologic and numeric data were represented in interpolated fence diagram such as lithology distribution, stratigraphic layers, geophysical data and colours. Geophysical data was entered at depth points with optional dates. Three-dimensional geological fence diagram for floodplain deposits showed that the northern part of the floodplain is rich in high permeable materials with some patches of low permeability materials (Figure 3.15), whereas it is clear that the low permeability deposits are abundant in the south and southwestern part of the floodplain. The top unit of floodplain deposits are composed of muddy sand with peat. Below this, the alluvial aquitard (peat and clay) is laterally continuous representing channel fill sediments (Facies 4) (Figure 3.15). The resulting shape of low permeability structures is similar to a lenticular body, with a flat top boundary and a concave upward bottom. Taking this into account, it would correspond to part of the infilling of an abandoned channel filled by peat and clay. The mapped low permeability deposits (e.g. clay and peat) (Figure 2.12 and (Figure 3.15), which are observed on the south-eastern part of the bank, near the river, between GPR profiles 9-12, coincide with attenuated section of the river channel GPR profile (140-192 m). This is likely to be the riverward extension of low permeability layers underlying the floodplain across the active river channel (Figure 3.13). The highly permeable materials in the northern part of the west bank river site correspond to non-attenuated area of river channel survey. Hence, three-dimensional geological model helped to better our understanding of the spatial variability and sediment heterogeneity in the study area.

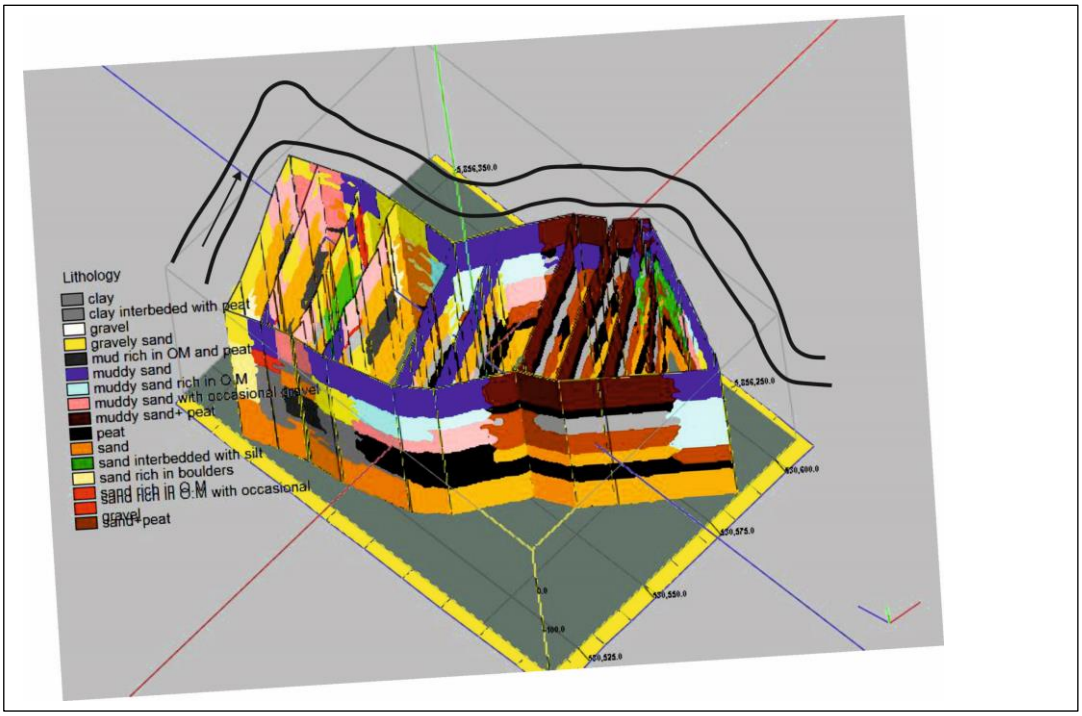

Figure 3.15 Three-dimensional fence diagram for west bank floodplain sediment deposits.

3.4.5 Implications for hydrogeology

Knowledge of the sedimentary structure of the glaciofluvial deposits and their internal heterogeneities facilitate a better understanding of groundwater flow and transportation of groundwater resident contaminants (Huggenberger, 1993; Kostic and Aigner, 2007b). Hydraulic characteristics are strongly controlled by sediment texture and grain size distribution. Individual lithofacies can create interconnected, hydrogeological related regions that display relatively homogeneous hydraulic characteristics defining discrete hydrostratigraphic and hydrofacies units (Poeter and Gaylord, 1990; Heinz and Aigner, 2003b; Kostic et al., 2005).

Generally, various sizes of the sedimentary units in the streambed and riparian zones may form a complex three-dimensional mosaic which is thought to induce complex subsurface flow patterns (Naegeli et al., 1996). The sediment grain size influences subsurface flow paths

(Steel and Thompson, 1983) which in turn affects oxygen transformation, dissolved organic carbon and the cycling of nutrients.

From a hydrogeological viewpoint, in the riparian zone of the investigated field site, the components concerned with lateral accretion elements form extensive but heterogeneous elements that are essential in the composition of the hydraulic system (Kostic and Aigner, 2007b). Such components are typified by a highly conductive, sheet-like geometry with slightly dipping layers. Characteristic interfingering occurring within variable dip lateral accretions implies that a complex general flow system exists. This system is generally determined by the orientation of dipping, highly permeable layers (Kostic and Aigner, 2007b). However, the presence of highly conductive elements of point bar lateral accretion, shallow bedrock depth in this area, as well as high amplitude irregular reflections associated with stacking hyperbolic structures of different gravel sizes, creates good floodplain-to-subchannel hydraulic continuity in the north-eastern subsurface of the field site. The sub-channel region associated with this part of the floodplain is made up of shallow sand and diamictic layers. These layers exhibit a fairly high degree of hydraulic conductivity (Chapter 4), which in turn allows for the reasonably rapid discharge of groundwater into the river channel. The residence time of water would be therefore low in this section.

The low topographical area in the south and south-western part of the floodplain, low permeability dominated layers representing channel fill elements, plays a pivotal role on the hydrology of fluvial system as their presence influences the groundwater flow patterns. These sediments are also considered to be part of the drift deposits that caps the Permo-Triassic sandstone at the study area and characterized by low resistivity values, as well as very low hydraulic conductivity (Ks) magnitude (e.g., < 0.005 md-1) as identified by Weatherill (2015). The presence of high amounts of shallow peat and clay layers representative of channel fill deposits can control the location of the water table (Gómez-Ortiz et al., 2010). It

is worthwhile to mention that the core log that exist within this channel-fill deposit unit (for example, C.S.5) correspond with the lowest hydraulic head area in the floodplain groundwater system (Figure 3.16). This head pattern, which this log intercepts, can potentially be construed through a hydraulic isolation of the groundwater by the in-fill deposits produced by the regional upwelling pressure from the bedrock system in other places in the floodplain (Figure 3.16).

Channels can be buried by vertical overbank deposits producing “paleochannels” where coarse particle riverbed alluvium is buried underneath fine grain floodplain deposits (Stanford and Ward, 1993). In case the water table is intercepted by the paleochannels, the paleochannels effectively act as large preferential-flow conduits capable of directing water the entire distance of a floodplain (Wondzell and Gooseff, 2013).

Figure 3.16 C.S. 5 core shows saturated area (high water level) which is caused by channel fill low conductivity materials in the study area (see Figure 3.3 for core locations).

3.4.6 Conclusion

The local underground sedimentology preserved at the River Tern study site is very complex and heterogeneous at very small-scales (e.g. centimetre). Hence, quasi three-dimensional geological reconstruction of the lowland river section was undertaken to better understand the spatial distribution of sediment heterogeneity of the fluvial environments. This study shows that GPR, in conjunction with ground truth data, provides sufficient information on the sediment stratigraphy and the geometry of the sediment texture in fluvioglacial deposits in a lowland meandering river. It is a recommended method for structural and lithological studies of deposits in an alluvial valley fills, for example, the hyporheic zone and the adjacent floodplain, due to the relatively high spatial resolution and the possibility to image large areas.

Eight major radar facies were recognized in the west bank river site. Radar facies 4 and 8 marks low conductivity layers in the study area which represents channel fill sediment deposits. Lenses of clay and peat (channel fill sediments) structures were delineated in the study area based on the GPR signal attenuation in relation to the adjacent area. These structures are predominantly deposits in the south and south-eastern part of the floodplain and distributed laterally with different thicknesses and extensions.

Sedimentary units of different grain size are thought to create a complex pattern of subsurface flow paths. Moreover, the distribution of low conductivity layers controls the geometry and location of a local water table.

4 Geological controls on groundwater-surface water exchange flow patterns

4.1 Abstract

Sediment heterogeneities in the riverbed can control groundwater and surface water exchange flow patterns, influencing biogeochemical cycles and stream ecosystem functioning. Detailed geology including small-scale variability in riverbed physical properties controlling exchange flow patterns is still poorly understood. This study investigates how geophysical information of the riverbed sediment structural heterogeneity explains more of the exchange flow paths. Experimental studies were conducted in varying riverbed lithology in a lowland meandering river, the river Tern. The conjunctive use of detailed geophysical data, vertical hydraulic gradients (VHG), hydraulic conductivity, and vertical fluxes, quantified using Darcy's law, was employed to investigate the spatial variability of sediment heterogeneity on exchange flow patterns across the investigated stream reach. In the midstream section (site 2) (highly conductive area), good connectivity to the underlying groundwater aquifer was identified. Low and temporally less variable VHG were observed in this region. In the downstream section (site 3) around low conductivity layers, poor aquifer-to-river connectivity was identified. High and temporally variable VHG were observed in this region due to flow confinements at depths in the riverbed. The geological and hydrological conceptualisation for the investigated reach is fundamental for future studies and successful managements of water resources in most watersheds.

4.2 Introduction

The hyporheic zones forms as a result of the mixing between groundwater and surface water in space and time (Harvey and Bencala, 1993; White, 1993; Boulton et al., 1998) which have been identified as significant locations of habitats macroinvertebrates (Williams and Hynes, 1974; Stanford and Ward, 1988), biogeochemical processes (Triska et al., 1989; Baker et al., 1999) and buffers for both various pollutants (D'Angelo et al., 1993; Fuller and Harvey, 2000) and stream water temperatures (Arrigoni et al., 2008; Burkholder et al., 2008). Interest in measuring water exchange at the riverbed in fluvial environments has increased significantly in recent years, driven mainly by the necessary to better understanding chemical and physical processes that influence ecological functioning in the hyporheic zone (Brunke and Gonser, 1997; Duff and Triska, 2000; Binley et al., 2013).

Lithostratigraphy characteristics of riverbeds, such as textural patches and organic matter content, are normally determined by water flow dynamics and channel morphology (Pretty et al., 2006). Buffington and Montgomery (1999) stated that streambeds normally display textural patches (grain-size facies) that differ vertically and horizontally, and this is likely to result in the hydraulic conductivity within the streambed being distributed in spatial patterns (Genereux et al., 2008), effectively affecting the amount as well as location of hyporheic exchange fluxes (Landon et al., 2001). In places where fine sediments clog the streambed, this will undoubtedly restrict hyporheic exchange fluxes (Rosenshein, 1998; Krause et al., 2012b). Riverbed strata type may play a significant role in groundwater-surface water fluxes, nutrient/contaminant cycling and streambed residence times (Genereux et al., 2008; Krause et al., 2012b) because different patches differ in their hydraulic conductivity (Malard et al., 2002; Pretty et al., 2006).

Many studies on the stream reach scale have highlighted aquifer- river exchange fluxes as being driven by variability in hydraulic head distributions in relation to riverbed

geomorphology (Boano et al., 2006; Cardenas and Wilson, 2007). Experimental field studies (Lautz et al., 2010; Endreny et al., 2011) and model-based examinations (Boano et al., 2007) revealed that spatial patterns of such exchanges were highly controlled by advective pumping and hydrodynamic pressure head fields related to riverbed geomorphology and surface water turbulence (Elliott and Brooks, 1997b).

Former research into hydrogeological heterogeneity in lowland riverbeds discovered that one factor which influences groundwater-surface water exchange and chemical species through the aquifer-river interface is the lithostratigraphy characteristics of the riverbed (Fleckenstein et al., 2006; Angermann et al., 2012; Krause et al., 2012b; Krause et al., 2013). At the River Tern (Figure 1), an example of a groundwater-fed river in the UK, by placing heat tracing technology at several points over a pool-riffle-pool sequence (Krause et al., 2011a), as well as along a 250m long stretch of the river (Krause et al., 2012a), researchers established that both streambed topography and streambed hydraulic conductivity impact on the spatially heterogeneous patterns in exchange fluxes between aquifer and river. At the same stream reach, heat pulse sensor (HPS) was applied by Angermann et al. (2012) for identifying shallow hyporheic flow paths at three locations illustrating for low versus high riverbed connectivity. Furthermore, by using vertical hydraulic gradient (VHG) observations and fiber-optic distributed temperature sensors (FO-DTS) on the streambed (Krause et al., 2012b), researchers found evidence that groundwater up-welling patterns are substantially influenced by low conductivity organic-rich peat and clay structures in the streambed. This leads on the one hand to up-welling inhibition in places with flow-confining layers, and on the other hand to preferential groundwater discharge in locations where the low-conductivity strata were disrupted.

Investigating how groundwater and surface water interact can now be accomplished in a cost-effective and simple way using piezometers (Rivett et al., 2008a). Installing piezometers into

riverbeds facilitates the computation of water quality determinants and the vertical flux of water. Baxter et al. (2003) further contend that installing of such piezometers aids in the approximation of hydraulic conductivity. According to Rosenberry et al. (2008), besides piezometers, the other two commonly utilized tools for calculating the exchange between surface water and groundwater are seepage meters and water level measurements. With seepage water, these are often installed in the body of surface water, while water level measurements make use of groundwater wells system. Piezometers have successfully been utilised in numerous studies, usually alongside other methods, to assess the interactions between groundwater and surface water (for example, (Rivett et al., 2008a; Käser et al., 2009; Krause et al., 2013; Dudley-Southern and Binley, 2015).

Previous works on near-river subsurface zone have been driven without a detailed understanding of the spatially complex nature of the subsurface hydrology. In this study, the previous GPR result chapter has provided a unique opportunity to direct sampling based on geophysical knowledge. Installing piezometers inside known streambed lithostratigraphy provides a better understanding of exchange flow patterns.

The overarching goal of this study is to establish the importance of small-scale variability in streambed physical properties (e.g. spatial heterogeneity of the permeability field) in controlling exchange fluxes. The objectives are: (1) Investigate the spatial patterns of upwelling groundwater based on observation of VHG patterns and temporal variability to distinguish between riverbed locations with highly conductive materials versus locations with confining riverbed structures; (2) Estimate riverbed hydraulic conductivity using falling head test; (3) Determine the importance of preferential exchange flows and residence time distributions through permeable bed sections and the bypassing of low permeability (often high attenuation) zones using Darcy law and (4) Investigate the correlation between riverbed attributes (K, VHG, and Darcy fluxes) in piezometers.

4.3 Field site and methods

4.3.1 Study area description

The study focuses on a meander reach (approximately 240 m long by 5–8 m wide) of the River Tern, a tributary of the River Severn in North Shropshire, UK (see Figure 3.1, chapter 3). The River Tern has a surface water catchment of 852 km2 (Keery et al., 2007). An extensive and predominantly agricultural floodplain surrounds the river channel. Pool–riffle–pool sequences and steep riverbanks dominate the channel morphology, as well as partially vegetated channel bars (Krause et al., 2013). This reach section has previously featured in many experimental field studies; consequently, the present study benefits from an extensive existing monitoring network (Weatherill, 2015). Average annual precipitation at the river source varies from 583 mm to 740 mm. The flow rate, measured at streams 2 km from the headwaters, has a daily average of 0.8 m^3s^{-1} and a 95th exceedance percentile flow (Q95) of 0.4 m^3s^{-1} (Hannah et al., 2009).

In local terms, the investigated region is based upon the Permian Bridgnorth Sandstone (Lower Mottled Sandstone) and narrowly topped in the east by Kidderminster Sandstone (Bunter Pebble Beds) (see Figure 3.1, Chapter 3). It creates the foundation of the Triassic Sherwood Sandstone Group (Papatolios and Lerner, 1993) that is present in the region. Heterogeneous drift deposits of Pleistocene to Recent age have dominated the field-site geology along the alluvial corridor (Adams et al., 2003; Angermann et al., 2012). These deposits overlie the highly permeable Permo-Triassic Sherwood Sandstone (PTS) formation (Wheater and Peach, 2004), which is considered a regionally significant aquifer in the UK and is also the main source of water for the River Tern (Krause et al., 2012b; Weatherill, 2015).

The investigated reach was originally selected by the UK's Natural Environment Research Council (NERC) as part of their Lowland Catchment Research (LOCAR) thematic programme (http://catchments.nerc.ac.uk/about/), due to the known connectivity with the

sandstone aquifer (Wheater and Peach, 2004). As part of that programme, a borehole configuration was drilled on the western river bank in 2000 (Adams et al., 2003). According to Shepley and Streetly (2007), the dominant control over groundwater–surface water exchanges at the investigated reach section is the regional groundwater upwelling derived from the Bridgnorth Sandstone. Nevertheless, at sub-reach scale, Krause et al. (2012b) observed substantial inhibition of groundwater upwelling due to the presence of impermeable layers (e.g., heterogeneous peat and clay) deposited at depth in the riverbed.

Geophysical surveys (e.g., (GPR) and (ERT)) and limited point observations from core logs at the site reveal significant variations in textural patches and stratifications as a consequence of the postglacial depositional history, which is characterised by a wide range of hydraulic conductivities (Weatherill, 2015). Within the streambed, Krause et al. (2012b) identified hydraulic conductivity values for high-conductivity streambed core materials (range 10^{-3} to 10^{-5} ms^{-1}) and low-conductivity (range 10^{-8} to 10^{-9} ms^{-1}) clay and peat layers.

4.3.2 Topographic survey

A Leica 1200 differential GPS system was employed for accurately surveying the heights and locations of installed riverbed piezometers, GPR profiles, core logs and riparian groundwater boreholes. High-resolution digital elevation models (DEM) of riverbed and floodplain topography have been provided, with a vertical precision of 1 cm and horizontal precision of 25 cm (for details of data collection and processing, please see section 3.3.4 in chapter 3).

4.3.3 Piezometer design and installation

At locations identified to be representative for the range of riverbed hydrofacies identified by GPR and core samples in investigated stream reach (Chapter 3), multi-level mini-piezometer networks were installed in the streambed for monitoring groundwater-surface water exchange fluxes, water sampling, and measuring hydraulic conductivity at the aquifer-river interface.

In total, networks of 18 multilevel mini-piezometers (P1–P18) were installed during April 2015 within the Tern site riverbed sediments at depths of 100 cm to 115 cm below the sediment–water interface (Figure 4.1). Three cluster piezometer network locations were chosen based on riverbed strata characteristics (Figure 4.1). This study made use of a design similar to those used by Krause et al. (2013) and Rivett et al. (2008a). In this case, the design consisted of a central, rigid cross-linked polyethylene (PEX) tube. The tube (Piezometer), in turn, consisted of screened intervals of 6 cm with 5 mm perforations, beginning at 10 cm from the bottom of the tube. The screened section was wrapped with mesh to prevent fine sediments entering the piezometer. Multiple polytetrafluoroethylene (PTFE) tubes (outer diameter 3.2 mm, internal diameter 1.6 mm) were fitted alongside the tube wall, on the outer side. Various piezometer sampling points (PTFE tube) (see Table 4.1 for details) were made for piezometers (within the PEX tubes) for the purpose of sampling pore water from different riverbed strata and depths below the sediment–water interface. This was done prior to installation piezometers inside the riverbed.

A polyester mesh of 105 µm diameter was used to wrap the ends of sampling tubes. This was to ensure that there was no blockage from particles when undertaking water sampling. Tight fitting brass panel pins were also used to close the tubes at the top ends except during tracer injection and pore water sampling. To install each mini-piezometer, use was made of a sledgehammer to hold the prefabricated unit to a 1.2 m depth, and by advancing a steel drive tube. A sacrificial nut/washer assembly was also installed at the steel drive tube's lower end, to overcome the likely invasion of sediment into the tube. This was then secured tightly at the bottom of the piezometer tube, as shown in Figure 4.1 C.

Once the required depth had been attained and it had been ascertained that the piezometer was secure at the target depth in the riverbed, the drive tube was removed. A re-collapse of the riverbed deposits was then enabled, and the annular space around the piezometer filled up

deposits. In this study, the failure in pore water extraction, at the various 1.6 mm sampling points, offers more support for the presence of the sub-channel semi-confining and confining constraining units.

In May 2016, additional piezometers were added to the existing network (Figure 4.1D) for performing falling head tests. These piezometers were constructed from uPVC (unplasticised polyvinyl chloride) of 38 mm outer diameter. Each has a screen length of 12 cm with approximately 60 perforations of 3 mm diameter and covered with a tight mesh. Then, piezometers were installed to the desired depth below the riverbed, downstream of the existing multilevel piezometers (clusters) in order to conduct falling head tests to determine saturated hydraulic conductivity.

4.3.4 Riparian groundwater level monitoring

Seven 3m deep groundwater boreholes were installed in 2008 at the west bank field site for observing of the shallow riparian groundwater levels within the floodplain fluvioglacial drift sediments. During the observation period, hydraulic head (i.e. water depth) in four groundwater boreholes (GW1, GW2, GW3, GW7, Figure 4.1A) and surface water levels (SW3) at a downstream located stream gauge (Figure 4.1A) were automatically recorded by pressure transducers at 5-15 min intervals. Monitored groundwater and surface water pressure heads were corrected for barometric pressure fluctuations using an atmospheric pressure sensor located at groundwater borehole site GW 7. For validating water levels recorded automatically, manual head measurements were carried out at all boreholes during each sampling dates.

Table 4.1 Details of all piezometers sampling depths installed in the riverbed Tern site (for locations see Figure 4.1).

Piezometers	Sampling depths (cm)
P1	10, 20,40,60,80,115
P2	10, 20,40,60,80,115
P3	10, 20,40,60,80,115
P4	10, 20,40,70,115
P5	10, 20,40,70,115
P6	10, 20,40,70,115
P7	10, 20,40,70,115
P8	10, 20,40,70,115
P9	10, 20,40,70,115
P10	10, 20,40,70,115
P11	10, 20,40,70,115
P12	10, 20,40,70,115
P13	10, 20,50, 100
P14	10, 20,50, 100
P15	10, 20,50, 100
P16	10, 20,30,70,115
P17	10, 20,30,70,115
P18	10, 20,30,70,115

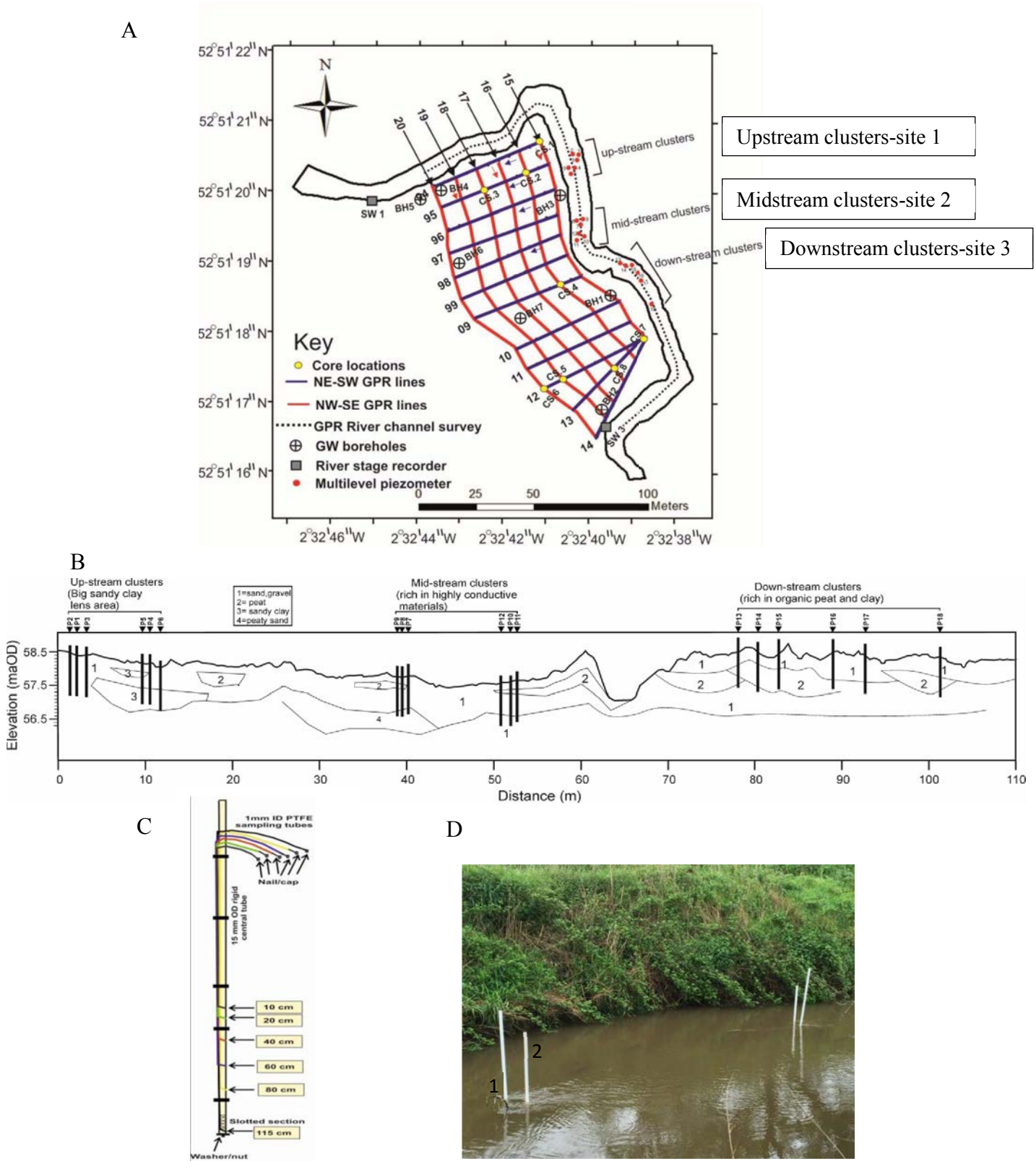

Figure 4.1 (A) Study area shows locations of floodplain and in-stream GPR profiles, stream stage and groundwater observation boreholes, multilevel piezometer network and core samples. (B) Longitudinal GPR survey shows streambed topography, riverbed stratigraphy, and piezometer network locations. (C) An example of experimental design of multilevel piezometers. (D) Installed multilevel (1) and big diameter (2) (OD=38mm) piezometers in riverbed.

4.3.5 Hydraulic head measurements

During each fieldwork campaign, riverbed piezometers were set up vertically to allow heads to stabilize for 30 minutes; then water levels were measured in the piezometers using a graduated mini water level meter (Solinst Model 102 M; Canada). The device has a probe attached to a narrow coaxial graduated cable, fitted on a robust reel. When the probe is in contact with surface water, the electrical circuit is completed, sending a signal back to the reel where light and visibly audible buzzers are activated. The water level inside the piezometer is then determined by taking a reading directly from the cable at the top of the piezometer. The stream water level was also measured adjacent to each piezometer allowing for the calculation of vertical hydraulic gradients. The dipmeter-based hydraulic head observations were around ±3 mm in terms of their accuracy. This allows for ambiguous measurements, which can be caused by turbulent flow conditions around the piezometers and can affect or slightly alter the outside head estimates (Käser et al., 2009).

4.3.6 Vertical hydraulic gradient (VHG) calculation

At each piezometer, the direction and magnitude of exchange fluxes were deduced by measuring the vertical hydraulic gradient (VHG). The VHG is a dimensionless parameter which represents a potential gradient direction (Naranjo et al., 2015). It is calculated by $\Delta h/\Delta l$, with Δh given by the difference between distances from the top of the piezometer to the water level outside (stream stage) and inside (pore water) the piezometer, and Δl given by the distance from the sediment-water interface to mid-point of the screen on the piezometer. Negative values indicate a downwelling (downward) flow direction, and positive values indicate an upwelling (upward) flow direction (Figure 4.2). If no gradient is present, this means that hydraulic gradient at the piezometer equal to the hydrostatic gradient of the river (Kalbus et al., 2006; Krause et al., 2012b). The bulk of the VHG can imply the degree of aquifer-river connectivity (Naranjo et al., 2015). Generally, hydraulic conductivity is inversely proportional to the hydraulic head gradients, and subsequently, high values (VHG >

-1.0) indicate low-permeable material that obstructs vertical flow and potentially enhances horizontal flow (Naranjo et al., 2012). Also, horizontal flow predominates in regions where VHG is near zero (Lautz and Fanelli, 2008; Naranjo et al., 2012). However, as Rosenberry and Pitlick (2009) pointed out, a positive (or negative) VHG does not necessarily indicate a hydrological connectivity is existing, as a low conductivity layer may be present between the screened interval of the piezometer and the streambed. The positive VHG value can be caused by regional groundwater upwelling through Permo-Triassic sandstone bedrock and local upwelling inhibition by streambed low conductivity structures above the piezometer screen section (Angermann et al., 2012; Krause et al., 2012b).

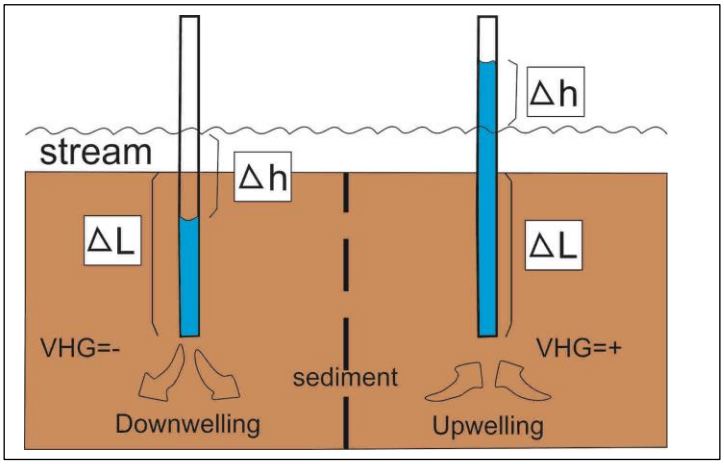

Figure 4.2 Conceptual model of vertical hydraulic gradient (VHG) in an upwelling and downwelling region of the hyporheic zone.

4.3.7 Saturated hydraulic conductivity

Due to the low cost and ease of installation, a large number of measurements can be done at various locations to assess the riverbed heterogeneity. Saturated hydraulic conductivity was estimated through falling slug tests for the piezometers added downstream of the nested piezometers (Figure 4.1D). These additional piezometers were installed within a 1 m radius of the three cluster piezometers at multi-point depths. This test was conducted from the 11th to the 13th of May 2016, during a baseflow period in which steady-state conditions could be

assumed. Automatic pressure transducers (Solinst Levelogger Junior LT or LTC Model 3001, Waterra, UK) were suspended inside the piezometer at the midscreen section using nylon cord. The tests were carried out by releasing a shot of water from a bailer (capacity 1 L), which significantly raised the head in the piezometers.

4.3.8 Slug test analyses

Data for a particular falling head test was isolated, the original head is then subtracted from each value of the test to obtain the effective additional head during the test. For each test the data was plotted as h/h0 on the Y logarithmic scale axis with time on the x-axis and an exponential trend line is fitted to the data.

h/h0 refers to the ratio of the water level at any particular time to the water level at the time zero.

From the trend line an exponential equation is produced of the form:

$Y=ae^{-bx}$

The Hvorslev method (Hvorslev, 1951) was used to calculate the saturated hydraulic conductivity derived from falling head tests performed on the riverbed piezometers using the following variant of the Hvorslev equation for a partially penetrating well (Freeze and Cherry, 1979).

$$Ks = \frac{r^2 \ln(\frac{L}{R})}{2\,L\,T0}$$

Ks = Saturated hydraulic conductivity cm s^{-1}

r = radius of well casing

R= radius of well screen (same as r^2)

Le =length of well screen

T0 =Time for water level to fall to 37% of the initial level

Where T0 can be calculated from the equation of the exponential trend line of the falling head test as follows:

$$T_0 = \frac{Log\ (0.37/a)}{-b}$$

According to Binley et al. (2013), the estimation of saturated hydraulic conductivity will include both vertical and horizontal compositions, with a bias towards horizontal permeability in an anisotropic setting. Falling head test data were discarded when only two or three head measurements were recorded before the water level returned to the steady-state conditions (e.g., in some of the highly responsive deposit sediments).

4.3.9 Determination of flow using Darcy's law

The obtained hydraulic conductivity values can be used in combination with piezometer head differences and surface water head to derive a general estimate flow to the river using the Darcian Law (Ellis, 2003) as:

$q = k_s \frac{dh}{dl}$

Where:

q = the specific discharge (m/d)

ks = the saturated hydraulic conductivity derived from the slug tests (m/d)

dh = the head difference between the river and the piezometer (m)

dl = vertical distance between riverbed and midscreen of the piezometer (m)

4.3.10 Statistical analysis

Descriptive statistical analyses of the hydraulic data of this chapter were conducted in SPSS v22 (IBM, USA). The data was tested for normality assumptions using the Shapiro-Wilk test using a significance level of 0.05 (Schuenemeyer and Drew, 2011). One-way analysis of variance (ANOVA) was undertaken to test for differences among three or more groups with a 0.05 significance level. Whereas, paired T-test analysis was undertaken to test differences in mean between two groups. Pearson's correlation coefficients were employed to depict the direction and strength of relationships between hydraulic data variables (Pallant, 2005). Only significant correlations are reported ($p = <0.05$).

4.4 Results and discussion

4.4.1 Hydraulic head patterns in riparian groundwater and surface water

The large-scale exchange between aquifer and river in a landscape is driven by the magnitude and distribution of hydraulic conductivities, both within the alluvial plain and river channel, the location and geometry of the channel within the alluvium planform (Woessner, 2000), and head gradient relationship between stream water level to the adjacent groundwater level (Sophocleous, 2002).

It has been stated that the general orientation of regional groundwater flow pattern is towards the River Tern, north east of the site (Figure 4.1A). A close examination of the hydraulic head distribution in the alluvial groundwater system, points to the fact that the flow of the lateral groundwater is an approximate reflection of the subdued replica of the local land surface topography, which has a remarkable gradient that is lateral from NE to SW, and equivalent to the hydraulic gradient in the Permo-Triassic aquifer, placed within the broader drainage basin (Weatherill, 2015).

Throughout most of the monitoring period, riparian groundwater heads (GW1, GW2, GW3, and GW7) exceeded surface water heads (Figure 4.3). This suggests that groundwater is discharging into the investigated stream reach. Inverse head gradients were observed when surface water heads recorded higher than groundwater heads during rainfall storm events (Figure 4.3). During these events surface water recharges into the riparian groundwater system, as a result of the groundwater level increasing at a slower rate than the surface water level. The observation of spatial variability in riparian head gradients could be caused by heterogeneity in the hydraulic conductivities of alluvial materials. Krause et al., (2009) attributed changes in riparian groundwater heads to changes in local groundwater variability or in spatial heterogeneity in the hydraulic conductivities of riparian sediment deposits, which is varied by five orders of magnitude from low conductive clay to highly conductive sands (Krause et al., 2012b). Although the riparian groundwater observation borehole GW2 was

installed nearby the active river channel, measured groundwater heads in GW2 were consistently higher than the adjacent river level (SW3) and other monitoring riparian groundwater boreholes (GW1, GW3, GW7). Also, groundwater level at observation boreholes (GW7) in the central floodplain also remained above surface water levels for most of the time except during two short storm events (< 2 days) in November 2009 and January 2010 (Figure 4.3).

In this study, low permeability sediments (alluvial aquitards) as outlined by GPR surveys (see chapter 3) were representing channel fill elements and characterised by variable thickness and dimensions. The geometry and spatial extent of the alluvial aquitards play a significant role in controlling the distribution of water heads in the floodplain western bank site. For example, it has been shown that GW2 and GW7 were continuously recorded the highest head values throughout the monitoring period (07/2009-07/2010) (Figure 4.3) suggesting that low conductivity layers are abundant in the shallow subsurface and their screen sections might be positioned between two confined layers. Therefore, shallow peat and clay layers could be responsible for the accumulation of water close to the surface and the formation of a perched water table (for example GW2 and GW7) (Figure 4.3). Some installed monitoring wells by a previous researcher (e.g., Weatherill, 2015) revealed that slow refill characteristics of many of the wells, together with distinct examinations of the hydraulic conductivity made from slug tests, point to the possibility of alluvial cover acting in the form of a local aquitard at reach-scale, thereby resulting in the formation of a low-permeability cap. Furthermore, Weatherill (2015), measured hydraulic conductivity in this area and the value was within the range of 0.001–0.006 m/d with geometric mean 0.0035 m/d for the majority of monitoring wells which were mostly dominated by silt or clay materials. The repressed highly permeable bedrock flow system is confined by the cap over the floodplain's low-lying area, west of the terrace, making the river corridor's eastern edge conspicuous (Weatherill, 2015).

Channels could also be buried by overbank depositions, leading to the formation of "paleochannels" in places where burying of coarse streambed alluvium has taken place beneath finer floodplain soils (Stanford and Ward, 1993; Poole et al., 2004).

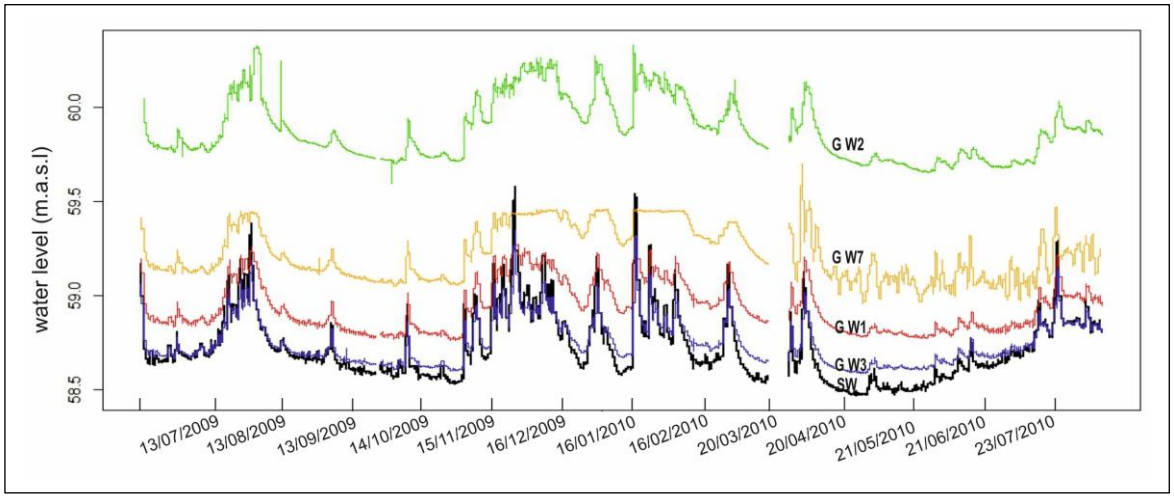

Figure 4.3 Groundwater levels (GW1, GW2, GW3, and GW7) in four exemplary shallow riparian observation boreholes and surface water stage (at SW3) (locations indicated in (Figure 4.1) for the period from 12 June 2009 to 30 June 2010.

4.4.2 Spatial patterns of vertical hydraulic gradient (VHG)

Two VHGs selected measurement dates (June 2015 and September 2015) and summary statistics (maximum, minimum, mean, and standard deviation) for each site are provided in Table 4.2. The range in VHG in the upstream cluster piezometers (site 1, around big sandy clay lens) was 0.19 recorded in P5 on September 2015 to 0.42 recorded in P4 on June 2015, in the midstream cluster piezometers (site 2, in highly conductive area) the range was 0.13 recorded in P10 on June 2015 to 0.38 recorded in P12 on September 2015, and in the downstream cluster piezometers (site 3, areas with evidence of low conductive peat and clay layers) the range was 0.02 recorded in P13 on June 2015 to 0.55 recorded in P14 on June 2015 (Table 4.2).

Table 4.2 Statistical Summary (Minimum (Min), Maximum (Max), Mean, and Standard Deviation (SD)) of observed vertical hydraulic gradient (VHG) across the riverbed piezometers for two selected measurement dates.

VHG			
Locations	MP	23/06/2015	28/09/2015
Site 1	P1	0.28	0.29
	P2	0.32	0.36
	P3	0.40	0.34
	P4	0.42	0.27
	P5	0.31	0.19
	P6	0.32	0.20
	Min	**0.28**	**0.19**
	Max	**0.42**	**0.36**
	Mean	**0.34**	**0.27**
	SD	**0.06**	**0.07**
Site 2	P7	0.32	0.26
	P8	0.21	0.29
	P9	0.22	0.20
	P10	0.13	0.15
	P11	0.21	0.26
	P12	0.38	0.24
	Min	**0.13**	**0.15**
	Max	**0.38**	**0.29**
	Mean	**0.24**	**0.23**
	SD	**0.09**	**0.05**
Site 3	P13	0.02	0.02
	P14	0.55	0.41
	P15	0.08	0.15
	P16	0.44	0.15
	P17	0.38	0.26
	P18	0.08	0.04
	Min	**0.02**	**0.02**
	Max	**0.55**	**0.41**
	Mean	**0.26**	**0.17**
	SD	**0.19**	**0.15**

Results indicate that the degree of spatial and temporal variation in VHG was greatest among piezometers installed at site 3; specifically, in piezometer P14 recorded the highest value throughout the monitoring period (Table 4.2) (Figure 4.4). A comparison of means from the different locations using one-way ANOVA indicated no statistically significant differences were present ($p > 0.05$). It has been observed that during base flow conditions (e.g., the June measurement), VHGs data recorded relatively higher values for different piezometer locations compared to the data recorded in September.

The depth of piezometer screened sections was between 85 cm and 105 cm below the sediment-water interface. Generally, all measured vertical hydraulic gradients using riverbed piezometers were recording positive values throughout the observation period (June 2015 and September-2015). This indicates that there was a constant up-welling of groundwater flowing into the reach of the stream which was being investigated. Although absolute magnitude of VHG at riverbed piezometers in three different locations varied at the monitoring dates, spatial patterns stayed steady throughout the observation period (Figure 4.4).

Based on VHG observations during the monitoring periods (June and September data) at the finer scale (85 cm-105 cm), VHGs within the research area were found to be extremely spatially variable (Figure 4.4). However, as in riverbeds with spatially highly variable K, it is not sensible to directly deduce water fluxes from VHGs measurements; VHGs have been found to be poor signals of surface water-groundwater exchange (Kaser et al., 2009).

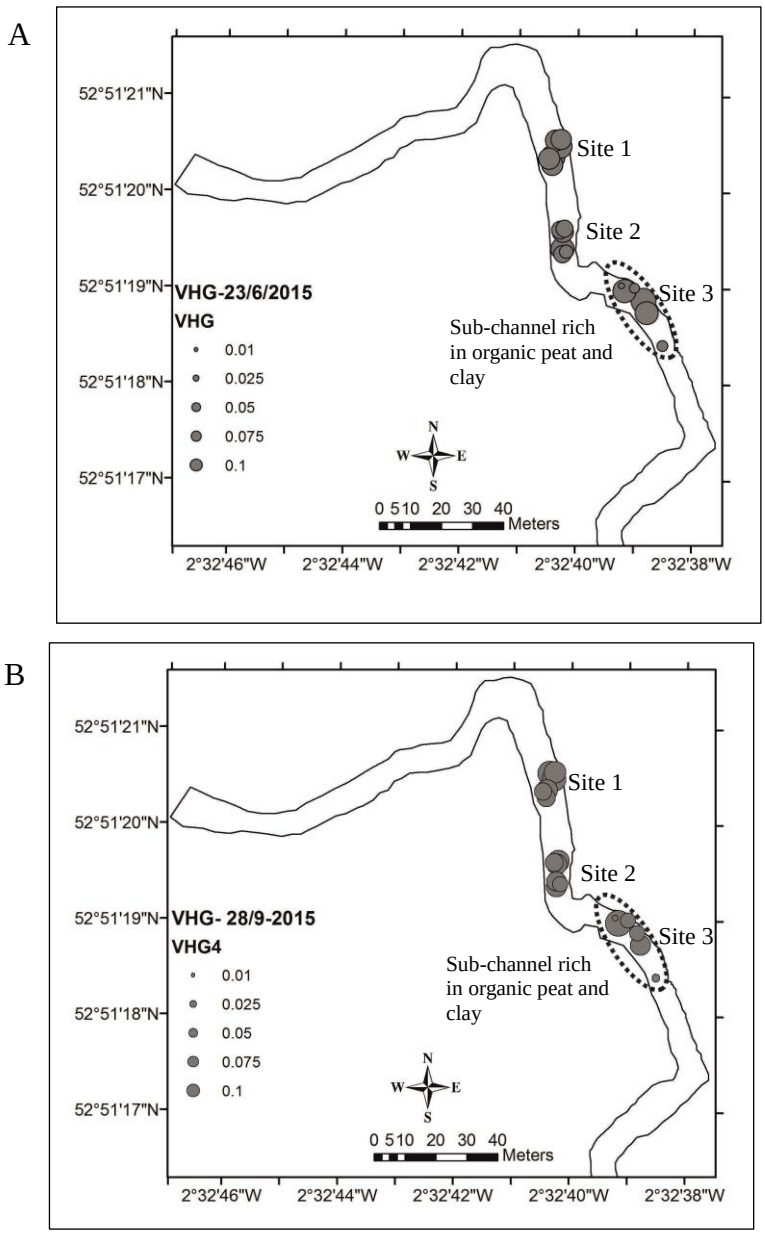

Figure 4.4 Spatial patterns of vertical hydraulic gradients (VHG) in the river Tern streambed for two selected sampling dates. (A) June measurements and (B) September measurements, with subchannel area marked.

The complex spatial patterns observed in monitored vertical hydraulic gradients (VHG) are likely to result from the extensive range and high level of spatial variability in the hydraulic conductivities of the drift deposits that formed the riverbed stratigraphy within the research area. The sediment properties of the non-fractured Permo-Triassic sandstone aquifer are spatially homogeneous at the investigation scale (Angermann et al., 2012). This means that the observed VHG patterns likely relates to the variable material properties of the drift sediments rather than resulting from local or regional groundwater flow variability. Considering the above, the VHG observations of spatially isolated, high values (up to 0.42 and 0.55, as seen at sites 1 and 3 respectively) were taken to indicate local inhibition of groundwater upwelling by flow-confining riverbed peat and clay structures. This suggests that the massive, low-permeable clay layer at site 1, and organic-rich riverbed peat and clay layers around site 3, which were identified in longitudinal in-stream GPR profiles (Figure 3.14, chapter 3) as well as riverbed core samples (Figure 3.7, chapter 3), can significantly separate pressure gradients within the study area. The in-stream GPR survey indicated that the semi-confining or confined layers were absent from most areas of the mid-stream section (site 2), and that preferential paths (e.g., geological windows with high hydraulic conductivities) occurred between the river and the underlying Permo-Triassic sandstone aquifer. Therefore, upwelling inhibition was considered to be less likely at locations with lower, more spatially homogeneous VHGs (as, for example, at site 2, P7–P12) in which free groundwater upwelling through this 'geological window' was most possible. Some piezometers in highly conductive areas (site 2) recorded relatively high VHG values (e.g., P12), this could be caused by strong direct connectivity between sandstone aquifer and highly conductive riverbed drift deposits in this section of the river based on the stratigraphic and piezometric evidence (e.g., riverbed core 4 (R.C.4), Figure 3.7). The lowest VHG (0.01) was recorded in P13 at site 3, indicating neutral conditions (Figure 4.4). This is potentially

attributed to the close coupling of hydraulic head inside the piezometer and the surface water head. This suggests the piezometers (P13) did not fully penetrate the semi-confining layer. Due to the depth of the piezometer screening sections (85 cm–105 cm below the surface of the streambed), it is unlikely that a relevant impact involving streambed topography-induced advective pumping would be found on the observed head gradients.

Krause et al. (2012b) and Angermann et al. (2012) carried out a study to establish the spatial patterns of VHGs (vertical hydraulic gradients) along the same investigated study reach. In their study, a network of piezometers (27 piezometers) were deployed along 250 m of the study reach by conceptualising their knowledge of temporal changes in pressure gradient and stratigraphic heterogeneity along the riverbed. Where the researchers identified peat and clay structures, large VHGs were also evident, with near magnitudes of 0.8. A further revelation from the study by Krause et al. (2012b) and Angermann et al. (2012) was that unconfined mode, characterised by a less temporal variability and a much weaker pressure gradient of between 0.1-0.4, was also evident, which contrasted with the semi-confined or confined mode. They posited that the mode could be a sign of the upwelling of "free" groundwater from the bedrock aquifer that lacked a flow-confining structure in its fluvial sediment sequence. In addition, Weatherill (2015) measured VHG's for the same stream reach but at multiple depths within the nested piezometers. VHG's observation data at all locations were increased with depth suggesting that steeper pressure gradients driven by groundwater upwelling from the underlying sandstone bedrock resulted from local groundwater upwelling flow confinements. Elsewhere, Naranjo et al. (2012) found that, VHG in the riffle were less susceptible to change during the observation period of their study. They also revealed pronounced differences in VHG in pool area relative to the riffle areas. The variation identified was attributed to control of low permeability deposits in the subsurface as established by integrating hydraulic gradients; temperature envelops, and model calibration.

Wang et al. (2017) observed highest VHG values close to the depositional bank at the two different sites. They stated that the riverbed vertical hydraulic conductivity in these areas were the lowest, possibly due to low permeability fine grained deposits inhibited the water interchange between surface water and groundwater.

4.4.3 Spatial pattern of hydraulic conductivity (K)

Channel sediments generally show larger K value relative to a silty-clay floodplain deposit or paleosol (Niswonger and Fogg, 2008). The effective K of a riverbed sediment has a wide range of magnitudes, depending on several processes such as the shape of the streamflow hydrograph, source material, and other processes (Niswonger and Fogg, 2008). The hydraulic conductivity (K) of riverbeds is an essential variable controlling groundwater and surface water exchanges (Naranjo et al., 2012; Burnette et al., 2016). The magnitude and spatial patterns of chemical solutes and water fluxes through riverbeds related to the magnitude and spatial pattern of riverbed K (Kennedy et al., 2009b; Naranjo et al., 2012; Gilmore et al., 2016). Riverbed K may also be varying temporary in association with time-varying controls such as erosion, deposition, or temporal variation in biogenic gases in riverbed deposits (Genereux et al., 2008; Cuthbert et al., 2010).

Table 4.3 shows the saturated hydraulic conductivity data measured at different depth horizons. Saturated hydraulic conductivity measurements within the top meter of the riverbed over the study reach revealed significant spatial variability (Figure 4.5). Overall, saturated hydraulic conductivity recorded at two depth ranges (e.g. shallower depth= 15 cm–20 cm and deeper depths= 50 cm–115 cm) exhibited a normally distributed data, based on Shapiro-Wilk test of normality ($p = 0.094$), which is compatible with previous studies reported for other fluvial sediment sequences (Ellis, 2003; Binley et al., 2013; Weatherill, 2015). However, when log transformed hydraulic conductivity at shallow layers (15 cm–20 cm) and deep layers (50 cm–115 cm) were compared using independent t-test (two sample assuming

unequal variances), a statistical significant difference was found ($P > 0.05$), showing that the hydraulic conductivity at deeper sediments were significantly lower than at shallower depths. The average saturated hydraulic conductivity of the riverbed was 7.16 m/d with an overall observed range of 0.06–14 m/d. This distribution indicates a large degree of heterogeneity in hydraulic conductivity was present across the area.

In this study, the riverbed lithostratigraphy distribution varies remarkably at different locations, even at the same test site, and this could lead to the different distribution of riverbed hydraulic conductivity, and further impact the distribution of water exchange at the sediment-water interface. The hydraulic conductivity observed in the shallow range depths (15-20 cm depth) for all three clusters revealed quick responds in water levels inside piezometers except for piezometer 14 (20 cm) in downstream section. This depth mainly corresponds to a mixture of gravel and coarse to medium loose sands deposited during large flood events. Sand layers component can be considered as a part of drift deposits and bank erosion materials which formed the most part of the riverbed in the investigated study reach. The relatively lower K value recorded at depth 20 cm in piezometer (P14), compared to other piezometers, could be attributed to the predominant fine silty sand layer rich in organic matter and wood fragments deposited in localized shallow depth in downstream section as identified in river core sample 6 (Figure 3.7, chapter 3). The hydraulic conductivity distribution at the site 2 is generally highest (Figure 4.5) which contain a larger grain size compared to other sites. However, in this area, K value becomes lower towards the deeper part of the riverbed. This could be due to the compaction of sediments in further deep riverbed. The recorded high K value deeper depth (e.g., 115 cm) at P12 could be attributed to the presence of highly permeable Permo-Triassic sandstone as observed in core sample 4 (Figure 3.7, chapter 3). The lowest value of K was recorded at downstream cluster piezometers (site 2) (Figure 4.5), specifically in deeper sediments. These locations are

characterised by evidence of low conductivity layers which are possibly an extension of the alluvial aquitard in the floodplain as observed in GPR surveys (chapter 3). The hydrogeological understanding demonstrates the aquifer-to-river connectivity as being fairly low in site 3, because of the presence of sub-channel low conductivity structures (e.g., peat and clay deposits) as observed in GPR and core samples (R.C. 5, 6 and 7) (chapter 3). The peat accumulations are distinct from the mineral ones, in the way that the connections between the capillary plant fibres and their various radiuses determine the hydraulic conductance (Schlotzhauer and Price, 1999). Also, the hydraulic conductivity of the peat is significantly lowered after it has been compacted. Therefore, in response to overburden forces, a greater number of capillary channels, with the power to move water, become obstructed and turn into unhealthy, useless cells (Hoag and Price, 1997).

Table 4.3 Saturated hydraulic conductivity values determined from the slug tests across the riverbed stream reach (for locations see Figure 4.1 A).

Piezometers	Riverbed depths (cm)	Hydraulic conductivity (K) (m/d)
P4	20	11
P6	20	11.23
P7	20	12.23
P10	20	13.2
P12	20	13.78
P14	20	1.8
P15	20	7.46
P16	20	8.4
P17	20	8
P18	20	9.78
P6	70	3.23
P7	115	7.2
P12	50	5.3
P12	115	14
P14	50	1.1
P14	100	8.2
P16	70	0.06
P17	115	0.09
P18	70	0.08

GPR surveys on the floodplain and in-stream channel also provide strong evidence of contrasting geological information across the investigated study reach (Chapter 3). It may be interpreted that the variation in GPR radar reflections could be as a consequence of contrasts in the sediment texture (dielectric permittivity) of the riverbed sediment deposits. Nevertheless, within the variability of all falling head test measurements, spatial variability in hydraulic conductivity may not be resolved, although differences in sediment texture characteristics were observed in riverbed core samples (Binley et al., 2013) (Figure 3.7).

A

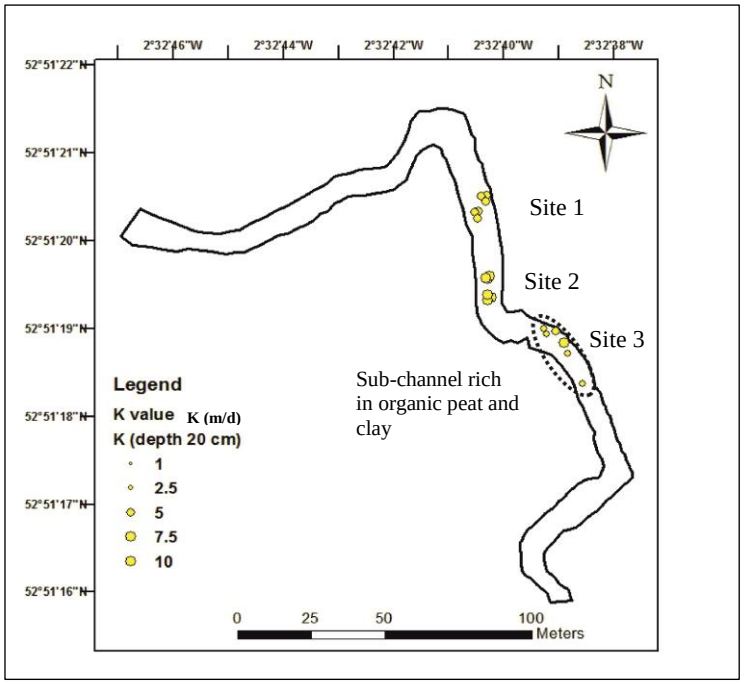

B

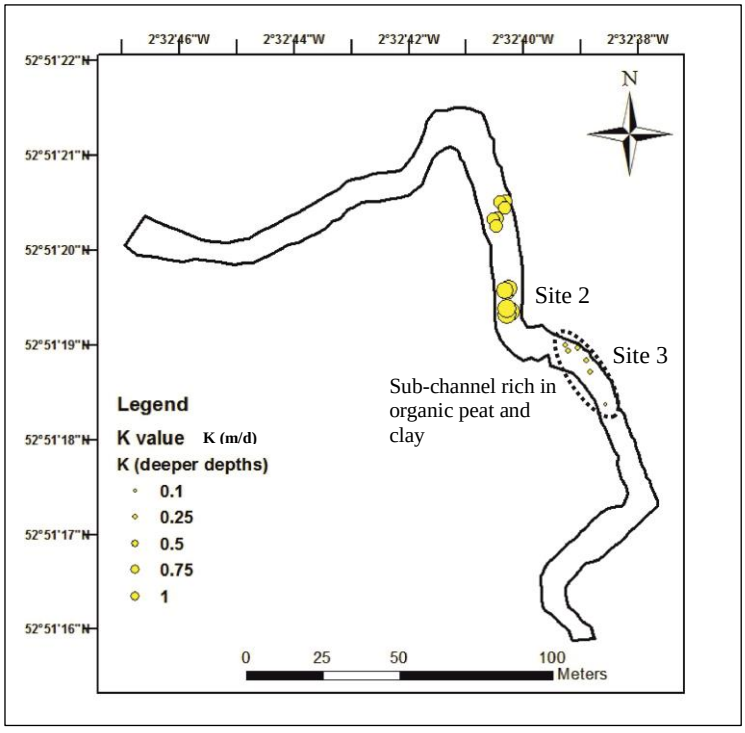

Figure 4.5 Spatial distribution of saturated hydraulic conductivity across three sites of the investigated river Tern stream section (A) for shallower depths (15-20 cm) and (B) for deeper depths (50-100 cm), with subchannel area marked.

In general, this decreasing trend in hydraulic conductivity with depth in riverbed deposits have also been reported in works of Song et al. (2007); Chen (2011); and Binley et al. (2013). Similarly, Weatherill (2015) found considerable changes in riverbed sediment hydraulic conductivity with depth in which more conductive and homogeneous sediments (deeper materials) are overlain by low but variable conductivity sediments (shallow materials). In a study conducted by Binley et al. (2013), it was stated that the hydraulic conductivity across channels may vary as a consequence of localized deposition of fine grain sediment. This variation was proved to be accurate when the geometric mean of the hydraulic conductivity at 20 cm depth was almost two times higher in mid-channel piezometers as compared to the channel margin piezometers. Genereux et al. (2008) conjectured that the relatively higher conductivities in mid-channel locations can be attributed to the fine particles which are deposited near the channel margins as compared to mid-channel margins. Furthermore, Wu et al. (2016) found that in the centre of the channel, larger vertical hydraulic conductivity (Kv) for the upper sediment deposit more likely occurred, but found various spatial patterns for the lower sediment deposits. Käser et al. (2009) experimented on the gravelly alluvium of the River Leith during erosion and found the river bank sediments slumping on the eroding side of the river while fine sediment deposition was taking place on the opposite bank; which is possibly the reason for the lower hydraulic conductivities in channel margin piezometers as compared to mid-channel area.

4.4.4 Calculations of water flux based on Darcy's equation

1-D vertical riverbed water fluxes passing through the top meter of the riverbed were calculated by Darcy's law. For this purpose, distinct measurements of vertical hydraulic gradient (VHG) and the hydraulic conductivity obtained by slug tests were used (Table 4.3) to calculate the flux. Based on stratigraphy evidence, it is suggested that hydraulic conductivity value is close within each cluster. Thus, for piezometers that did not have

hydraulic conductivity measurements, the nearest piezometer with known hydraulic conductivity has been counted for measuring Darcy fluxes in the site. For example, for piezometers 1–5, hydraulic conductivity values measured in piezometer 6 was used.

Figure 4.6 and Figure 4.7 show the variability of fluxes in all piezometers (all three clusters) for shallower (upper layers) (15–20 cm) and deeper (lower layers) (50–115 cm) depths, respectively. In upper layers, both in site 1 (P1–P6) and site 2 (P7–P12) the vertical flux values were high (Figure 4.6), whereas in site 3 (P13–P18) only P16 and P17 recorded high vertical fluxes during measuring period. In lower layers, the vertical fluxes in site 2 were higher than site 1 and site 2 (Figure 4.7).

The results of Darcy fluxes (VHG-derived fluxes) show spatial variability at three sites (Figure 4.8 and Figure 4.9). In general, the high Darcy flux values (vertical flow components) are associated with locations where high conductivity layers exist in the riverbed. The low Darcy flux values are associated with locations where low conductivity layers exist (site 3) (Figure 4.8 and Figure 4.9). The flux values at midstream section (P7-P12) are higher for both shallower and deeper depths and in both seasons than those at up-stream and downstream sections (Figure 4.6-4.9). In-stream GPR survey result for this section is characterised by medium to strong subhorizontal to wavy reflections associated with hyperbolic structures. These indicate that laterally continuous subchannel with high conductivity layers such as sand and gravel with less organic matter content (as identified in R.C. 4 and 5) (Figure 3.7), formed this section of the riverbed. The substantial sub-channel region of increased hydraulic conductivity is accommodating of rapid groundwater discharge to the surface water. Thus, good aquifer to river connectivity is likely to be present in this section. The observed Permo-Triassic sandstone at about (1m) depth in riverbed core 4 (R.C. 4, chapter 3) (Figure 3.7) have also confirmed the direct connection with underlying aquifer. Krause et al. (2012b) identified it was also in line with low riverbed temperatures using FO-

DTS and high upwelling fluxes. Binley et al. (2013) measured horizontal and vertical fluxes, combined with a survey of riverbed electrical conductivity of the River Leith, UK. They identified the zone's likelihood as a 'preferential discharge location' (Conant, 2004) in the upstream section and is seemingly typified by directly connecting with the sandstone aquifer where elevated vertical upwelling fluxes restrict hyporheic exchange flows. Datry et al. (2015) reported similar outcomes, which suggested hydraulic conductivity was higher in upwelling regions than in downwelling regions. Song et al. (2016) reported that mostly upwelling fluxes are compatible with the result that vertical hydraulic conductivity has a decreasing trend from upper layer to lower layer.

In contrast, the downstream area (site 3) is characterised by low vertical fluxes, GPR signal attenuation and highly complex VHG pattern. This leads to the conclusion that in this area there are largely heterogeneous riverbed materials, as well as a mosaic of highly conductive sediments combined with flow-confining clay or peat structures as identified in GPR and core logs (chapter 3). The few recorded cases of vertical flow in some upper layer piezometers and generally low flow in this region corroborates the idea that increases in horizontal flow and surface water infiltration above flow-confining riverbed strata which hinders or at least diminished the pressure of groundwater upwelling in the uppermost riverbed materials which overlay low conductivity structures. Angermann et al. (2012) used heat pulse sense combined with VHG data in the same stream reach. They showed that the low conductivity streambed strata may infer increasing in downward surface water and horizontal hyporheic advective flow into shallow streambed sediment in those areas which are located above low conductivity streambed layers. Various former studies have stressed the effects of dynamic pressure fields caused by riverbed morphology and advective pumping on hyporheic exchange fluxes (Boano et al., 2007; Endreny and Lautz, 2012). However, the combined geophysical information with multi scale hydrology measurements of this research provide

evidence that at this particular site, spatial patterns of low versus high conductivity riverbed layer, especially the extent and size of clay and organic peat, can significantly influence the near surface groundwater and surface water exchange flow paths in the riverbed, and can even in some cases overrule the effects of streambed topography on hyporheic exchange fluxes (Angermann et al., 2012). The results of this study extend former mechanistic process by highlighting a detailed understanding of the spatially complex nature of the subsurface hydrology.

A

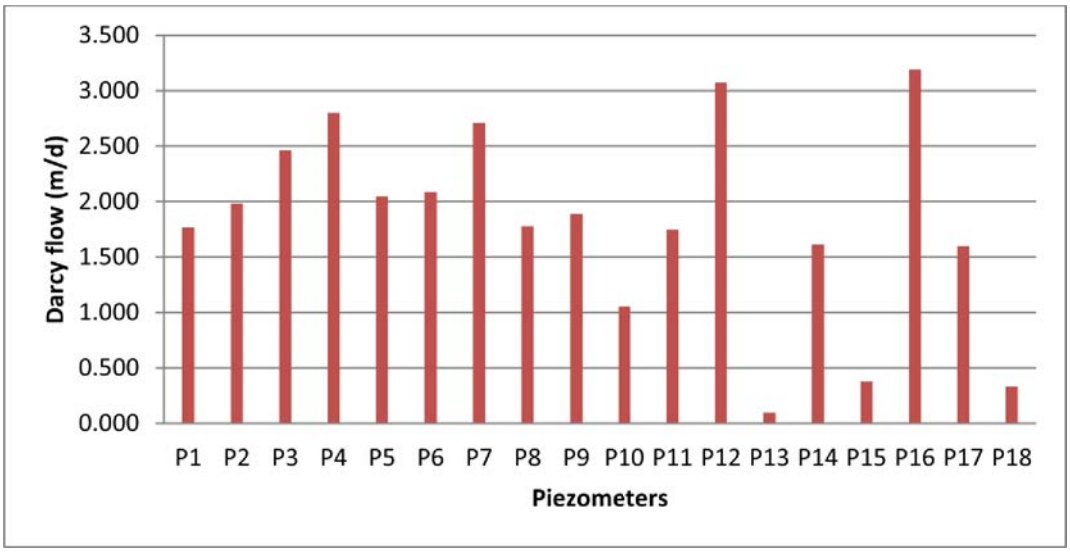

B

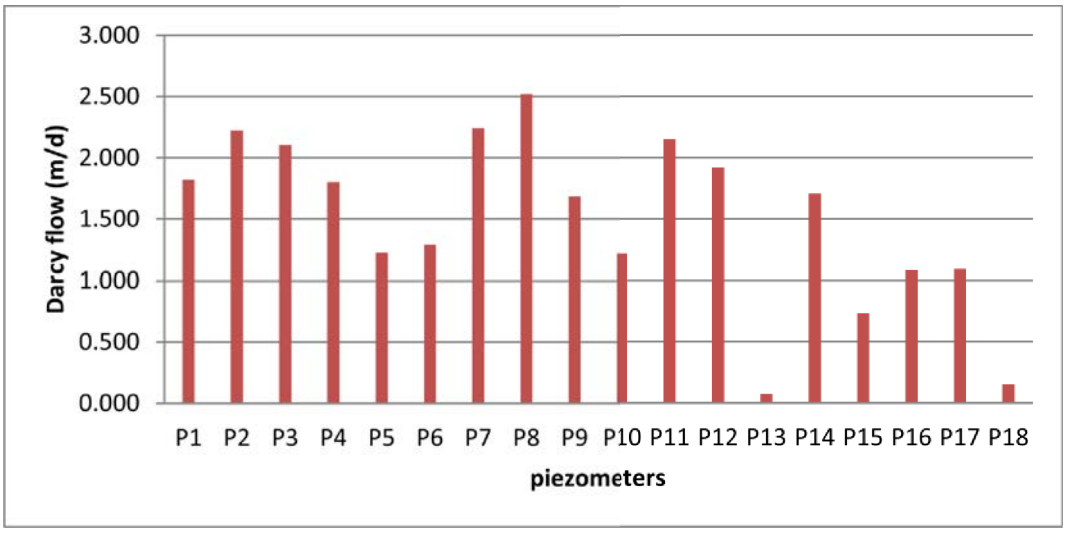

Figure 4.6 Variability of Darcy fluxes in each piezometer measured for shallow (15 cm-20 cm) depths in (A) June and (B) September repeat surveys.

A

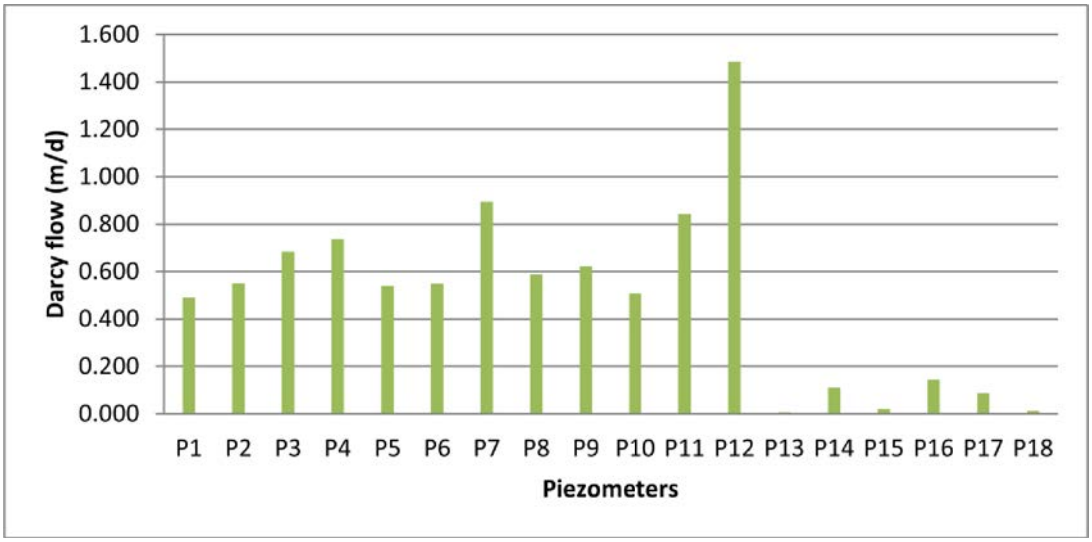

B

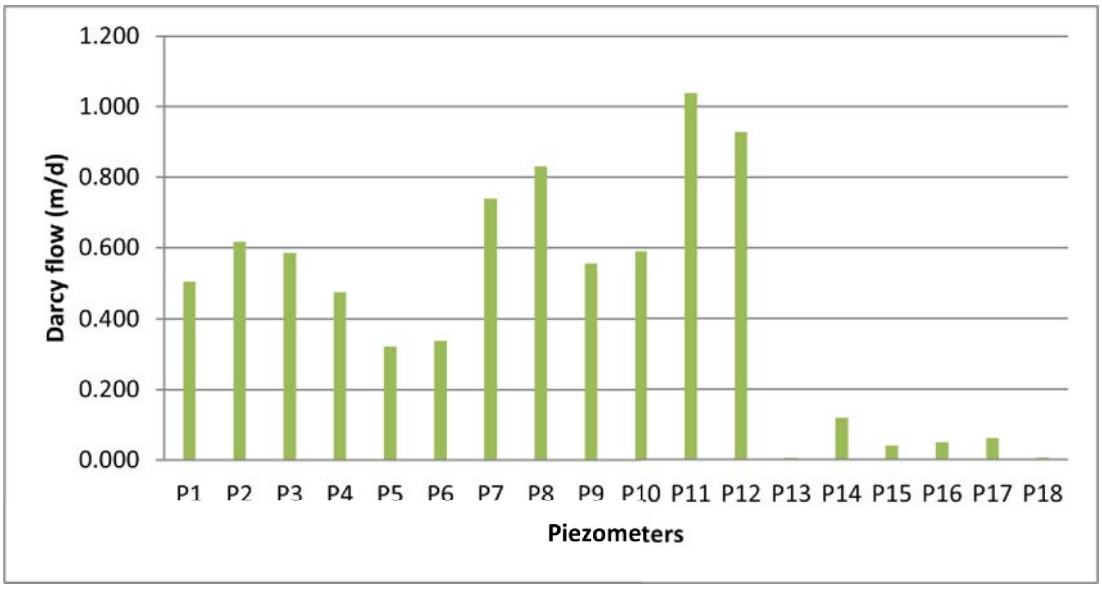

Figure 4.7 Variability of Darcy fluxes in each piezometer measured for deeper (50 cm-115 cm) depths in (A) June and (B) September repeat surveys.

A

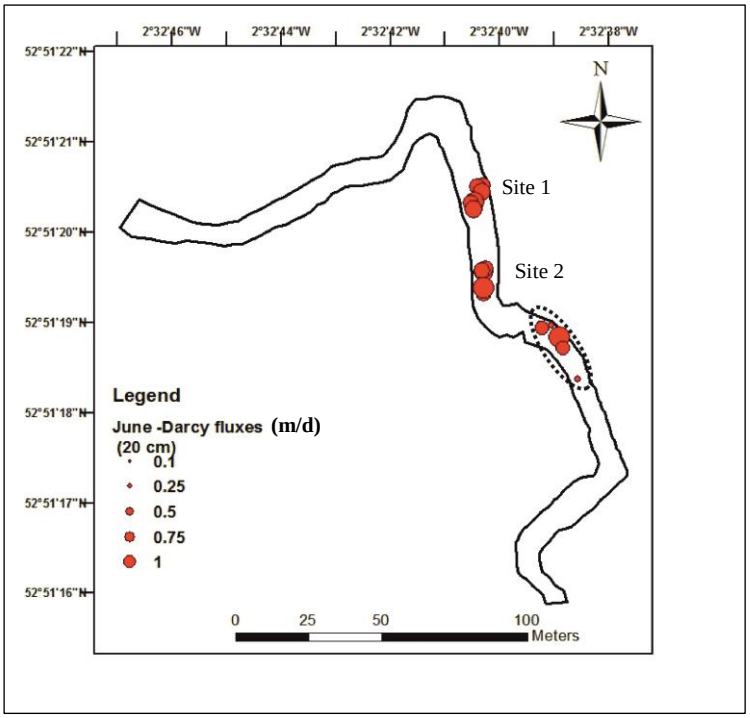

B

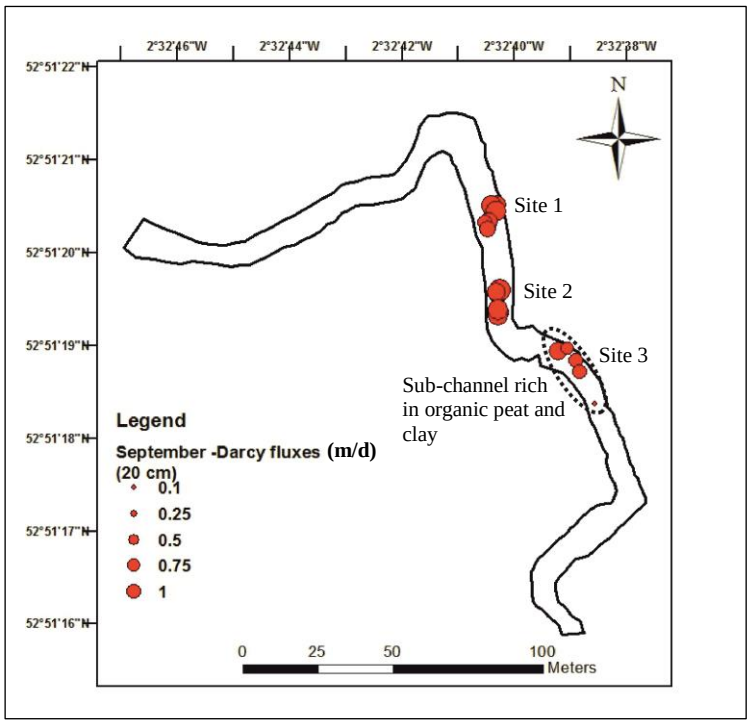

Figure 4.8 Spatial distribution of Darcy fluxes for shallower (15 cm-20 cm) depths in the study site on (A) June and (B) September repeat surveys, with subchannel area marked.

A

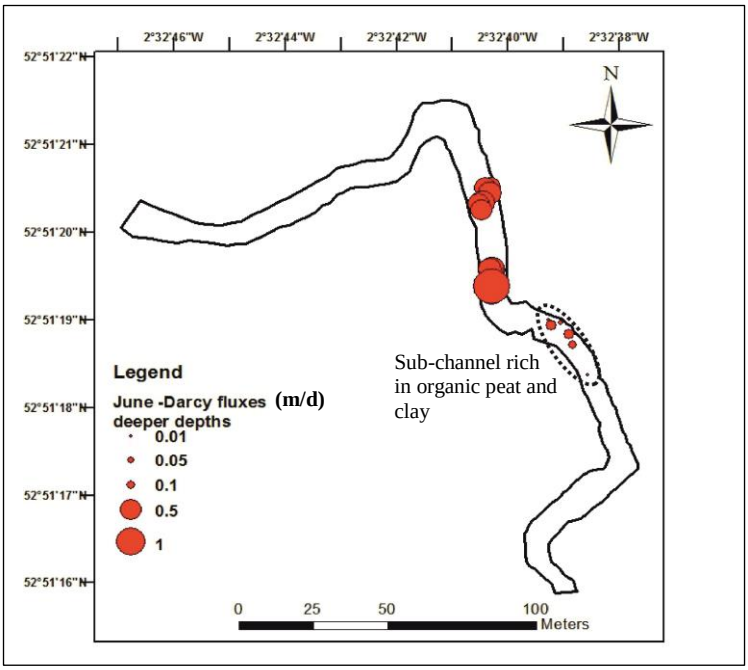

B

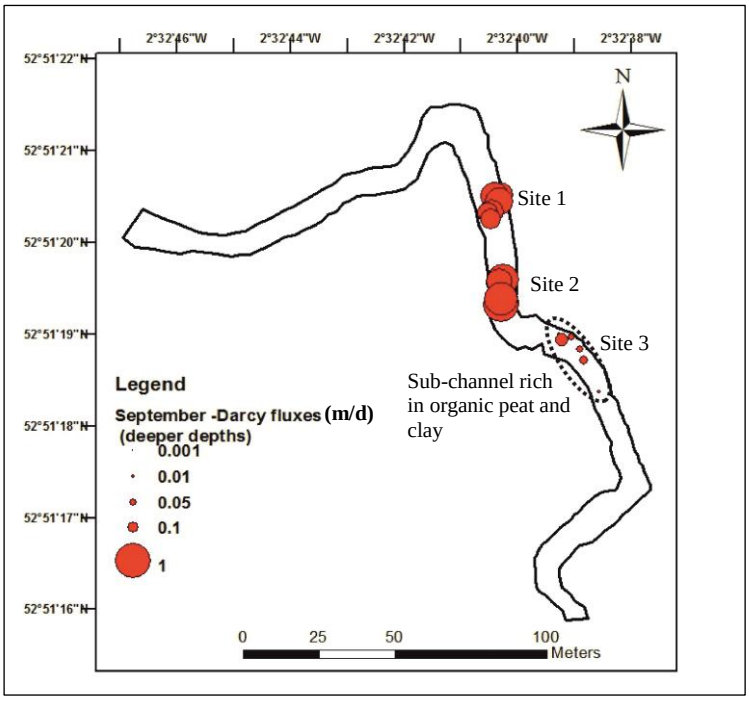

Figure 4.9 Spatial distribution of Darcy fluxes for deeper (50 cm-115 cm) depths in the study site on (A) June and (B) September repeat surveys, with subchannel area marked.

4.4.5 Correlations between fluxes, VHG, and hydraulic conductivity values

As expected, there were significant correlation between saturated hydraulic conductivity (R^2= 0.696, $p < 0.05$) with fluxes derived from the Darcy equation (Figure 4.10 A), indicating that saturated hydraulic conductivity may represent a reliable measure of riverbed pore water fluxes, at least at some locations. Such a result is in accordance with previous results reported for other groundwater and surface water exchange settings (e.g., Anibas et al., 2011; Hyun et al., 2011; Binley et al., 2013; Wang et al., 2017). Wroblicky et al. (1998), Binley et al. (2013) and Wang et al. (2017) also reported similar finding and outlined that hydraulic conductivity has a crucial influence on the spatial distribution and magnitude of vertical fluxes in the hyporheic zone. Anibas et al. (2011) demonstrated that changes in water fluxes across the channel could be attributed to changes in local-scale riverbed hydraulic conductivity and groundwater discharge. There are no significant correlations between VHG and hydraulic conductivity across the riverbed (Figure 4.10 B). This observing no correlation between VHG and hydraulic conductivity suggest that the homogeneity of groundwater discharge in the riverbed appears to be controlled by riverbeds' permeability distribution, which result in an increase of VHG in low hydraulic conductivity areas. Such interpretations are coherent with findings of others (Käser et al., 2009; Sebok et al., 2015). Chen et al. (2013) emphasized that, in groundwater-fed stream reaches, hydraulic conductivity decreases with depth; in addition, vertical hydraulic gradient values vary from −0.19 to 0.18 and show an inverse distribution to vertical hydraulic conductivity values. At some stream sites, pressure head gradients can be considered as an indicator of water exchange fluxes; nevertheless, head gradients cannot serve as a simple indicator for heterogeneous riverbeds (Kennedy et al., 2009b; Wang et al., 2017). In addition, Käser et al. (2009) suggested that vertical hydraulic gradient (VHG) can be a misleading indicator of the intensity of pore water flow. VHG and Darcy fluxes revealed low positive correlations (Figure 4.10 C).

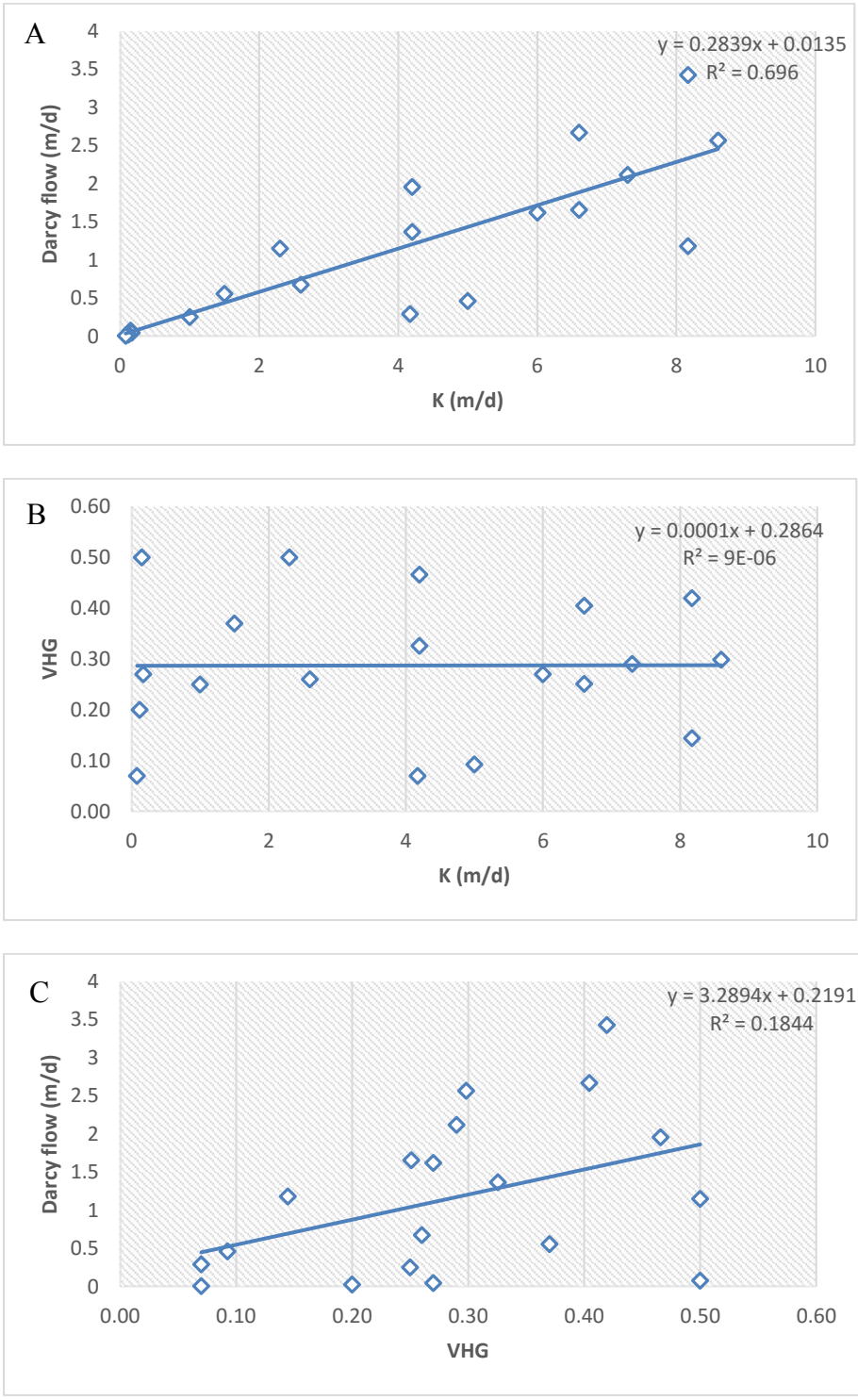

Figure 4.10 Correlation between riverbed physical properties (A) Hydraulic conductivity (K) versus Darcy flow (B) Hydraulic conductivity (K) versus vertical hydraulic gradient (VHG) (C) Vertical hydraulic gradients (VHG) versus Darcy flow.

4.5 Conclusion

Riverbed attributes of vertical hydraulic gradient (VHG), hydraulic conductivity, and Darcy fluxes were observed at three piezometer cluster sites. These piezometers were installed in riverbeds with different lithostratigraphy along approximately 110m of investigated stream reach. All riverbed attributes showed significant spatial variability related to riverbed sediment heterogeneity. VHG in riverbeds are controlled by patterns of clay and peat structures, this in particular can be seen at site 3 (locations with evidence of clay and peat). The high hydraulic conductivity was generally observed in site 2 (locations with high conductive materials, see chapter 3 for results of GPR survey in stream channel). The high hydraulic conductivity values in these areas are related to high vertical fluxes and sediment materials and thus preferential discharge from groundwater is predominant. The low hydraulic conductivity values were observed in site 3, especially at deeper horizons. The low conductivity values are related to the presence of flow confining layers (e.g., peat and clay) in these areas thus hindering groundwater upward flow.

The results of this chapter show that streambed material properties as identified in GPR survey (chapter 3), in particular the presence of organic peat and clay extended from the floodplain into the river channel, have a large impact on hydraulic conductivity and consequently on groundwater discharge into the stream. These layers suggest the possibility of shallow hyporheic zone with lateral flow below the low-permeability layers.

5 Spatial variability of nitrate, DOC and dissolved oxygen in the riverbed

5.1 Abstract

Residence time distribution and exchange flow patterns at the sediment-water interface can drive biogeochemical processes, such as denitrification, in riverbeds. This study examined the effect of structural heterogeneity within riverbed sediments on the fate of dissolved oxygen and nitrate in upwelling groundwater flow paths, through the riverbed of a lowland, meandering river (River Tern, UK). Depth-dependent patterns of nutrients were analysed within multilevel minipiezometer networks, which were spatially distributed across the reach at depths of 10 cm-115 cm below the sediment surface. Overall, good aquifer-to-river connectivity is believed to predominate at site 2 (midstream minipiezometers). Preferential discharge from upwelling groundwater was associated with high nitrate and dissolved oxygen (oxic conditions). In site 3 (downstream minipiezometers), patterns of clay and peat heterogeneities at depth in the riverbed, that produced locally confined conditions, controlled the spatial heterogeneity of upwelling groundwater flow. This action was an indication that there was an increase in riverbed residence times in this section of the river. Significant reduction of nitrate concentrations were found around site 3 (reducing conditions). The correspondence of confined groundwater discharge and diminished oxygen concentrations at site 3 indicate that enhanced residence times facilitate the development of conditions necessary for nitrate reduction. Findings elucidate the substantial control of riverbed physical properties and water fluxes flow paths on patterns of redox-sensitive chemical solutes in the riverbed.

5.2 Introduction

Rivers and aquifers were managed independently for a long time and treated as separate lotic systems. Recently, researchers identified that these two systems are interrelated and exchange with each other (Bencala, 1993; Wojnar, 2008; Krause et al., 2009a). Understanding the degree of hydraulic connection between an aquifer and adjacent river water is essential because of the increasing demand for clean drinking-water supplies (Wojnar, 2008). A significant gap in our knowledge still exists in understanding the spatial variability of permeability fields and the importance of water fluxes in hydrochemistry of the riverbed and in controlling its capability to attenuate the potential chemical reactive nutrients, e.g., nitrogen (Binley et al., 2013). Research studies indicate that aquifer to river retention times, hydrological fluxes and redox gradients are under the control of internal characteristics, near river zone sediment structure, and spatial configuration (Vervier et al., 1992; Naden, 2011; Krause et al., 2013). Duff and Triska (2000), Conant et al. (2004) and Weatherill et al. (2014) also indicate that such redox sensitive contaminants, as chlorinated solvents and nitrates, undergo biotransformation and either reduction or substantial enrichment owing to the availability of the sediment heterogeneity evident at the aquifer to river interface. On the other hand, Claret and Boulton (2009) highlight the difficulty in understanding the link between the geometry of impermeable and permeable layers to biogeochemical gradient and hydraulic conductivity in biogeochemistry and microbial activity at 3-D reach scales.

Generally, the enhanced chemical reaction efficiency found in hyporheic deposits is controlled by: (1) steep redox-gradients (from high oxygen to low oxygen) as well as high profusions of microbial activity and organic matter (Duff and Triska, 1990; Jones et al., 1995; Chafiq et al., 1999; Hill and Cardaci, 2004; Zarnetske et al., 2011a; Heppell et al., 2014; Pinay et al., 2015), and (2) hyporheic residence times and hyporheic flow patterns (Jones et al., 1995; Duff and Triska, 2000; Zarnetske et al., 2011a; Briggs et al., 2013; Krause et al.,

2013; Briggs et al., 2014; Naranjo et al., 2015). Therefore, in order to undertake a quantitative evaluation of the biogeochemical cycling located at the river-aquifer interface, there is a need for a comprehensive understanding of the exchange flow patterns of the surface water and groundwater flow patterns (White, 1993; Krause et al., 2011b; Angermann et al., 2012).

Hyporheic exchange is driven by the heterogeneity of streambed sediment which, in turn, deflects the flow down into the sediment, or it upwells into the stream channel. Subsequently, the heterogeneity of the permeability plays an important role in altering the hyporheic exchange flow pathways, and the time of residence in the channel forms and planforms (Sawyer and Cardenas, 2009; Cardenas and Jiang, 2010; Krause et al., 2012b). For instance, coarse-grained sediments (e.g. gravels) could be characterised by short hyporheic residence times and elevated hydraulic conductivity in comparison with finer grained sediments (Packman and Salehin, 2003). In finer grained sediments with low hydraulic conductivity characteristics and longer hyporheic water residence times, aerobic respiration may deplete oxygen, resulting in the utilisation of substitute terminal electron acceptors such as nitrate (NO_3), CO_3 and sulphate (SO_4) (Baker et al., 2000). As a result, aerobic processes could end up dominating the hyporheic zone in those catchment areas characterised by high hydraulic conductivity (e.g. short residence times), whereas anaerobic processes dominated hyporheic zones with low hydraulic conductivity (e.g. longer residence times) (Valett et al., 1996; Grimaldi and Chaplot, 2000). Consequently, water residence times in hyporheic zone is a key element in establishing the main bio-geochemical processes that happen within the riverbed sediment and hence the availability of such essential nutrients as phosphorus (P) and nitrogen (N) to riverbiota.

Recent field studies in groundwater-fed settings have focused on the importance of the groundwater upwelling flow paths for nitrate transport and fluxes in a riverbed (Flewelling et

al., 2012; Stelzer and Bartsch, 2012; Heppell et al., 2014). Other study has focussed on other mechanisms of exchange, for example through meander bends (Zarnetske et al., 2011a) or through hyporheic exchange flow patterns (Kasahara and Hill, 2006). Few studies, however, have taken into account the impact of small-scale structural heterogeneity of sediments on fate and transformation of chemical solutes (e.g. nitrate) (Bardini et al., 2013; Krause et al., 2013; Naranjo et al., 2015). Krause et al. (2013) revealed that spatial structure of low-conductive riverbed peat and clay layers can significantly affect groundwater and surface water flow paths, residence time and nutrient cycling such as nitrate and dissolved oxygen rates in the riverbed pore water. Given the abundance of low permeable deposits in Truckee River sediments, it is likely that low-permeable anoxic sediments are generated by internal colmation processes (Naranjo et al., 2012).

The groundwater is the source of nitrate in the study area. Denitrification process in the hyporheic zone has been shown to be the predominant route for the nitrate reduction (Baker and Vervier, 2004, Sgouridis et al. 2012) and is pervasive because it is related to the presence of organic carbon supply and nitrate. Moreover, Dissimilatory nitrate reduction to ammonium (DNRA) is another potentially significant component of the nitrogen cycle in temperate re-connected floodplain environments (Burt et al., 2010). The conditions enhancing DNRA and denitrification and are similar (available nitrate, organic carbon substances, and absence of oxygen), denitrification process represents a permanent nitrogen removal route, while DNRA is a nitrogen-conserving mechanism that transforms nitrate to another more bio-available inorganic-N form, ammonium (NH4). In temperate freshwater environments, for example, wetlands and riparian fens, DNRA accounts for only 5-15% of nitrate reduction (Ambus et al., 1992; Scott et al., 2008) with denitrification process responsible for the majority of nitrate removal through the production of N2 gas. Hence, the DNRA routes of nitrate removal have

rarely been measured directly in freshwater sediments, and the existing evidence is equivocal (Trimmer et al. 2012).

The work explained in this chapter uses interpretation of nitrate (NO_3), dissolved oxygen (DO) and dissolved organic carbon (DOC) in the detailed information of the riverbed sediment complexity from samples collected in April 2015. The sampling time reflects emphasis on investigations of pore water chemical patterns in the riverbed under base flow conditions as well as the desire to intensively cover the spatial distribution of different riverbed stratigraphy encompassing the river channel with multiple depth measurements of pore water chemistry. Samples for chemical analysis were collected in combination with measurements of hydraulic head data to show the crucial spatial controls on dissolved oxygen and nitrate concentrations.

The aim of this chapter are to; (1) quantify nitrate concentrations and changes in nitrate concentrations in a typical UK lowland meandering river (River Tern); (2) identify the fate of dissolved oxygen, dissolved organic carbon and nitrate in groundwater upwelling flow paths and the relationship to residence time across the investigated stream reach (approximately 110 m long) along network piezometer profiles at riverbed depths ranging from 10 cm to 115 cm; (3) describe concentrations of dissolved oxygen and nitrate inside and around permeable and impermeable sediments; (4) investigate the correlation between hydraulic conductivity and dissolved oxygen and; (5) investigate the correlation between dissolved oxygen and nitrate as well as dissolved oxygen and DOC for riverbed piezometers in the Tern study site.

5.3 Methods and materials

5.3.1 Study area

The investigated field site is approximately 110 m long lowland meandering river section of the river Tern in the UK (Figure 4.1). The detailed descriptions of the study site are presented in sections 3.3.1 and 4.2.1.

5.3.2 Experimental infrastructure

A Leica 1200 differential GPS system was employed for accurately surveying the elevations and locations of installed riverbed piezometers, GPR profiles, and core logs (see details in section 3.3.4). A network of 18 multilevel mini piezometers (P1–P18) were installed in riverbed with different lithologies for observing pore water pressure head distributions and hydrochemistry concentrations at sediments depths of 10 cm–115 cm below the sediment-water interface. The locations of piezometers are shown in Figure 4.1A. The details of piezometer design and installation are presented in section 3.2.3. Moreover, the details of sampling points are shown in Table 4.1.

5.3.3 Interstitial pore water sampling

Sampling pore water took place after three weeks of the filling of the annular space. For an individual survey, first, the sample tubes were purged from trapped water to minimize gas exchange risk (Krause et al., 2013). For measuring dissolved oxygen of pore water samples, the optical-based sensor ProODO handheld dissolved oxygen meter was used (YSI, a xylem brand). All DO measurements were conducted on site. Following that, 30 ml of pore water were extracted from designated multi-level samplers (for all depths) using disposal polypropylene syringes and plastic tubing. A sample of stream water from upstream and downstream of the reach was also collected on each sampling occasion to construct whether there was any distinct variability in stream water chemistry along the investigated reach (for instance due to inserts of upwelling groundwater resident contaminants). For measuring DO,

the collected 30ml sample was then injected into the second adapted syringe holder (removed plunger) including DO sensor inside. To address the issue of the technique's sensitivity to ambient light, insulation tape (black colour) was wrapped around the barrel of the syringe, enabling DO to be measured in a limited-light environment. For each extracted sample, at respective times, hydraulic conductivity and dissolved oxygen (DO) were measured using the Hanna (HI 98129) and the YSI ProODO handheld dissolved oxygen meter, respectively. For anion and cation analysis, around 7 ml-10 ml of collected samples were filtered in the site using a surfactant-free cellulose acetate membrane of 0.45 µm diameter and stored separately in unused, factory clean plastic centrifuge tubes (Fisher Scientific, UK). Furthermore, 15 ml of samples were also filtered (as above) into acid-washed centrifuge tubes and acidified to pH<2 with HCl in the site for analysis of dissolved organic carbon (DOC). The samples for DOC were stored in 50ml plastic centrifuge tubes (Fisher Scientific, UK). All collected water samples were then stored in an ice box at 3°C until transfer to the lab and following analysis within 48h of sample collection. A Dionex ICS1100 ion chromatograph (Dionex Corporation, UK) (Figure 5.1), which has an anion exchange column and an ASDV autosampler, was used to identify the anions. The eluent bottle was filled with 4.5mM Na2CO3/1.4mM NaHCO3 solution, (18mls of 0.5M sodium carbonate and 5.6mls of 0.5M sodium bicarbonate diluted to 2L with deionised water). To identify unknowns, 10% of the samples were subjected to duplicate analysis and a 4-point calibration curves was created for serial dilutions of an approved mixed stock solution (Sigma Aldrich, UK). Between each 10 samples as well as at the start and end of the samples batches, laboratory blank samples were included. Based on replicate analysis of 1 mg/L^{-1} standard, detection limits were 0.2 mg/l for NO_3, 0.1 mg/l1 for SO_4^{-2} and 0.05 mg/l for Cl; the average precision was < 0.04.

DOC was measured using non-purgeable organic carbon (NPOC) on a Shimadzu TOC-Vcpn analyser (Shimadzu Corporation, Japan).

A

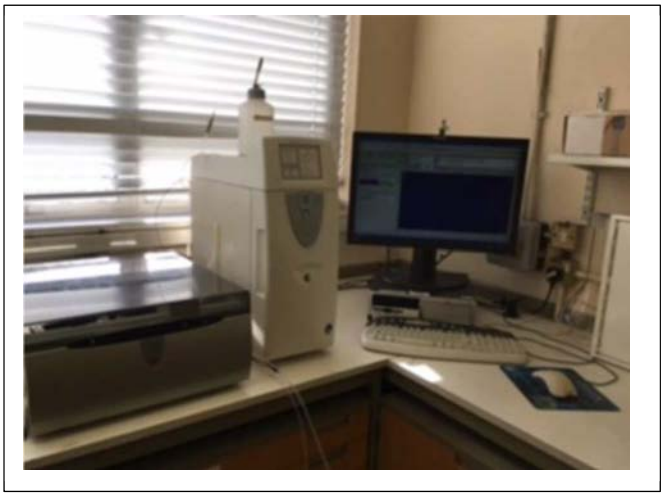

B

Figure 5.1 (A) Dionex ICS1100 ion chromatograph (Dionex Corporation, UK), (B) Shimadzu TOC-Vcpn analyser (Shimadzu Corporation, Japan).

5.3.4 Statistical analysis

Statistical analyses of the hydrochemical variables were conducted in SPSS v22 (IBM, USA). Equality of distribution were checked using the Shapiro Wilks with a significance level of 0.05 (Schuenemeyer and Drew, 2011). One-way analysis of variance (ANOVA) was undertaken to test for differences among three or more groups with a 0.05 significance level. Whereas, paired T-test analysis was undertaken to test differences in mean between two groups. Pearson's correlation coefficients were employed to depict the direction and strength of relationships between variables (Pallant, 2005). Correlation between chemical (dissolved oxygen) and physical (hydraulic conductivity) as well as between chemical variables (NO_3 and DO) was conducted. Only significant correlations are reported ($p = <0.05$).

5.4 Results

Comparison of data among piezometer positions was based on the conceptual understanding that spatial heterogeneity of the permeability field exists in streambeds which, in turn, affects flow paths and biogeochemical processes along the hyporheic zone of the study area. To evaluate this conceptualization, piezometers were grouped into three clusters along the investigated reach. Upstream piezometers (site 1) (P1-P6) were installed inside and around a massive sandy clay lens. Midstream piezometers (site 2) (P7-P12) were installed inside highly conductive materials. Finally, downstream piezometers (site 3) (P13-P18) were installed around and inside organic peat and clay strata. The summary statistics (maximum, minimum, mean and standard deviation) for nitrate (NO_3), dissolved oxygen (DO) and dissolved organic carbon (DOC) at each piezometer and surface water are provided in Table 5.1. Pore water in the riverbed is characterized by a distinct biogeochemical signature which is different than river water. Figure 5.2 shows the depth profile concentrations of NO_3, DO, and DOC observed in riverbed multi-level minipiezometer sampling points.

5.4.1 Concentrations of nitrate (NO_3)

The NO_3 concentrations varied spatially among piezometer clusters across the study area (Table 5.1 and Figure 5.2). The average NO_3 concentrations in interstitial porewater from piezometers collected in the down-stream region (areas rich in organic peat and clay, P13–P18) exhibited more variability (mean= 9.05–52.15 mg/l), compared to pore water collected in the mid-stream region (highly conductive gravely sand regions, P7–P12) (mean= 59.59–79.96 mg/l) and up-stream region (around massive sandy clay lens, P1–P6) (mean= 29.14–39.23 mg/l). Generally, nitrate concentrations along the sampling profile at upstream piezometers (site 1) (around massive clay lens) ranged from 19.14 to 48.78 mg/l (average = 34.6 mg/l), nitrate concentrations at midstream piezometers (site 2) (inside high conductive alluvial gravelly sand materials) ranged from 38.46 to 95.09 mg/l (average = 67.8 mg/l), and nitrate concentrations at downstream piezometers (site 3) (with peat and clay layers) ranged

from 1.30 to 64.84 mg/l (average = 20.41 mg/l). Overall, average NO_3 concentrations in the piezometers installed inside highly conductive materials (67.8 mg/l) exceeded the average concentrations observed at locations with massive clay lens at the upstream section (34.6 mg/l) and known floodplain origin peat and clay layers at the down-stream (20.41 mg/l) section. The highest NO_3 porewater concentration was found in mid-stream highly conductive piezometer P10 (max=95.09 mg/l) at depth of 70 cm. Whereas, the minimum NO_3 concentration was found in down-stream locations with evidence of low permeable clay and peat piezometer P14 (min=1.3 mg/l) at depth of 10 cm. The up-stream surface water NO_3 concentration was 39.1 mg/l and down-stream surface water concentration was 38.9 mg/l. A comparison of nitrate concentrations from the different locations using one-way ANOVA revealed statistically significant differences ($p = <0.05$). Post-hoc testing, using Games-Howell method for comparison among groups where homogeneity of variances cannot be assumed (Levene's test $p = >0.05$), showed that the data were statistically significant ($p = <0.05$).

Vertical changes of nitrate varied significantly along the profiles for different piezometer locations (Figure 5.2). While at some piezometers, in particular, in mid-stream highly conductive cluster piezometers, concentrations were only changed slightly along the vertical profile (e.g. P8, P10, and P11). Significant vertical changes of nitrate concentrations along the piezometer depth profile were observed in areas with known low permeable organic peat and clay lenses (downstream piezometers) which NO_3 values decreases towards deeper sampling points with exception of piezometer P14 in which the value of NO_3 increases towards deeper sampling points (Figure 5.2). Piezometers installed in this region were extremely characterised by significant volume of reduction in nitrate concentration within the boundaries of the low-conductivity riverbed strata. Slightly vertical changes of nitrate along the vertical profiles were observed at locations with predominantly highly conductive layers

(midstream piezometers) (P7–P12) (Figure 5.2B). Only minor changes in NO_3 concentrations were observed in the uppermost depth (e.g., in P7 and P9 at depth 10 cm).

5.4.2 Concentrations of DO

Patterns of DO concentrations show substantial spatial variability along the study reach (Figure 5.2). DO concentrations along the sampling profile at upstream piezometers (site 1) (around massive clay lens) ranged from 1.44-9.58 mg/l (average = 5.15 mg/l), DO concentrations at midstream piezometers (site 2) (inside high conductive alluvial gravelly sand materials) ranged from 1.65 to 7.34 mg/l (average = 4.01 mg/l), and DO concentrations at downstream piezometers (site 3) (with peat and clay layers) ranged from 0.78- 8.7 mg/l mg/l (average = 2 mg/l) (Table 5.1). The highest value recorded at depth 10 cm in P18 could contain high proportion of surface water. A comparison of means from the different locations using single-factor analysis of variance (ANOVA) indicated statistically significant differences were present ($p = < 0.05$). Post-hoc testing using the Games-Howell method where unequal variances are assumed (Field 2006), according to a significant result for the Levene's test ($p = <0.05$), DO means in areas rich in organic peat and clay (downstream piezometers) (site 3) revealed significantly lower than mid-stream and upstream clusters. Whereas there were no significant differences in mean DO between mid-stream (site 2) and upstream piezometers (site 3).

Similar to the NO_3, the lowest DO concentrations were found at locations with low conductive organic peat and clay layers (in down-stream piezometer clusters) (Figure 5.2). DO concentrations were depleted with depth in some piezometers with peat and clay structures (site 3) than in clastic alluvial subsurface (site 2). In high conductive piezometers (site 2) DO concentrations were slightly changed with depth.

5.4.3 Concentrations of DOC

Patterns of depth profile DOC concentrations show substantial spatial variability in the research area (Figure 5.2). DOC concentrations along the sampling profile at upstream piezometers (site 1) (around massive clay lens) ranged from 3.11 to 6.7 mg/l (average = 4.54 mg/l), DOC concentrations at midstream piezometers (site 2) (inside high conductive alluvial gravelly sand materials) ranged from 1.82 to 11.16 mg/l (average = 4.13 mg/l), and DOC concentrations at downstream piezometers (site 3) (with peat and clay layers) ranged from 6.62 to 59.99 mg/l (average = 20.7 mg/l) (Table 5.1). In general, downstream piezometers with evidence of low conductivity layers were recorded higher DOC concentrations compared to other sites. DOC concentrations in piezometers with evidence of organic peat and clay layers (site 3) is significantly larger than piezometers at site 1 and 2 based on one-way ANOVA.

Vertical changes of DOC varied significantly along the profiles at downstream piezometers (with known low conductivity area) (site 3). Whereas, in both site 1 and site 2, DOC concentrations were only changed slightly along the vertical profile. DOC was recorded highest concentration in some certain depths at downstream piezometers (e.g., depth 50 in P13, depth 10 cm in P14, and depth 20 cm in P16) (Figure 5.2). DOC concentration in downstream surface water was higher than upstream surface water (Table 5.1).

Table 5.1 Statistical summary **(**maximum (max), minimum (min), mean and standard deviation (SD) of nitrate (NO_3) dissolved oxygen (DO) and dissolved organic carbon (DOC) across the study area.

	Upstream piezometers (around large clay lens)						Midstream piezometers (High conductive region)						Down-stream Piezometers (Low conductive region)						Surface water	
	p1	P2	P3	P4	P5	P6	P7	P8	P9	P10	P11	P12	P13	P14	P15	P16	P17	P18	Upstream	Downstream
	NO_3 (mg/l)																			
Max	45.29	48.78	40.06	30.66	39.41	41.88	72.01	83.49	80.33	95.09	64.62	83.94	31.90	29.98	20.71	64.84	21.10	28.02	39.1	38.9
Min	23.78	19.14	20.06	27.62	29.40	26.38	40.09	59.15	38.46	70.49	61.80	57.92	7.18	1.30	1.36	28.45	1.51	4.62		
Mean	37.16	39.23	31.66	29.14	34.93	31.78	59.69	70.50	60.77	79.96	63.37	72.60	18.80	9.24	9.05	52.16	14.17	16.18		
SD	8.57	12.09	7.89	2.15	5.08	6.98	12.92	10.53	15.95	9.46	1.26	11.08	12.06	13.88	10.27	16.56	8.66	9.57		
	DO (mg/l)																			
Max	8.82	6.42	9.58	9.58	5.31	9.45	5.83	6.99	3.53	5.04	7.34	5.20	3.36	2.28	2.09	1.61	1.96	8.70	9.8	9.6
Min	3.64	2.15	2.38	1.89	2.62	1.44	1.76	1.65	1.74	3.43	3.75	3.01	1.15	1.14	0.90	1.30	0.78	1.13		
Mean	6.55	4.53	5.48	5.74	3.52	4.69	3.66	4.00	2.77	4.15	5.50	4.37	2.06	1.68	1.32	1.44	1.39	3.96		
SD	1.99	1.54	3.02	5.44	1.55	3.64	1.51	2.07	0.74	0.69	1.48	0.76	0.94	0.62	0.67	0.15	0.58	3.59		
	DOC (mg/l)																			
Max	4.69	6.70	6.28	5.64	4.74	5.03	3.13	3.42	3.69	9.75	11.16	6.87	39.64	46.27	17.64	50.99	26.28	17.47	19	29.14
Min	3.11	4.18	4.14	5.17	3.72	3.49	1.82	1.89	2.25	3.17	2.89	4.49	13.69	6.62	10.46	9.63	19.37	12.96		
Mean	3.56	4.99	4.93	5.41	4.17	4.15	2.39	2.65	2.91	4.88	6.65	5.30	27.35	23.92	13.08	22.04	23.31	14.47		
SD	0.65	1.05	0.85	0.33	0.52	0.70	0.49	0.55	0.58	2.77	3.43	1.10	11.90	16.53	3.96	19.42	2.88	2.04		

A

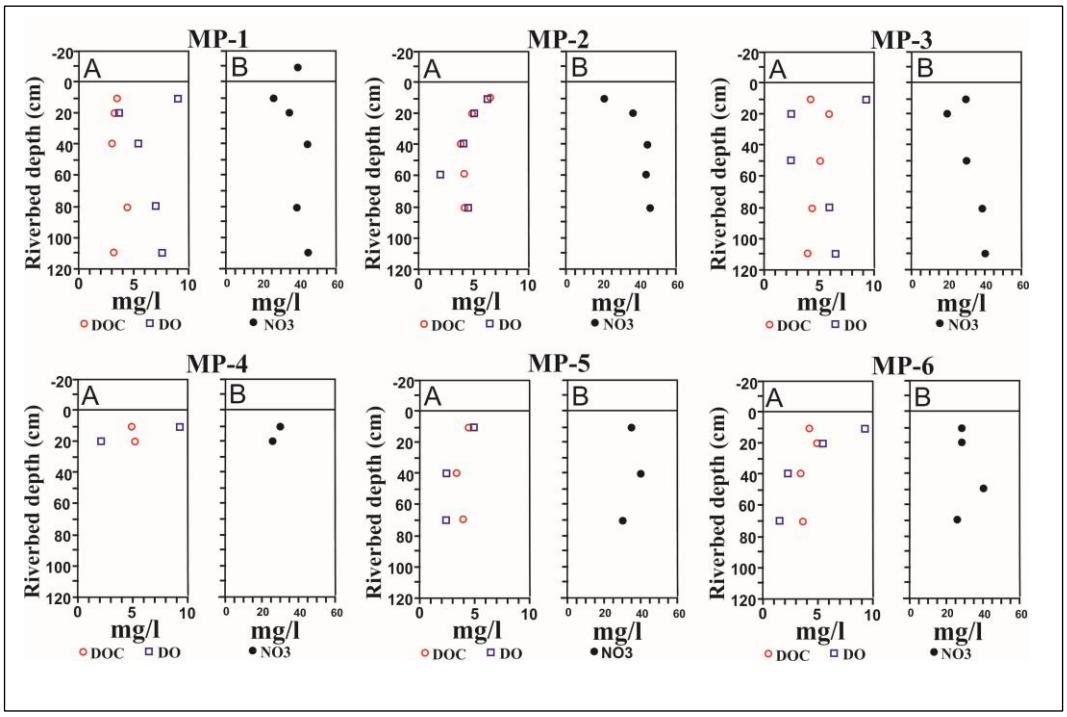
MP-1
MP-2
MP-3
MP-4
MP-5
MP-6
A
B
Riverbed depth (cm)
mg/l
DOC
DO
NO3

B

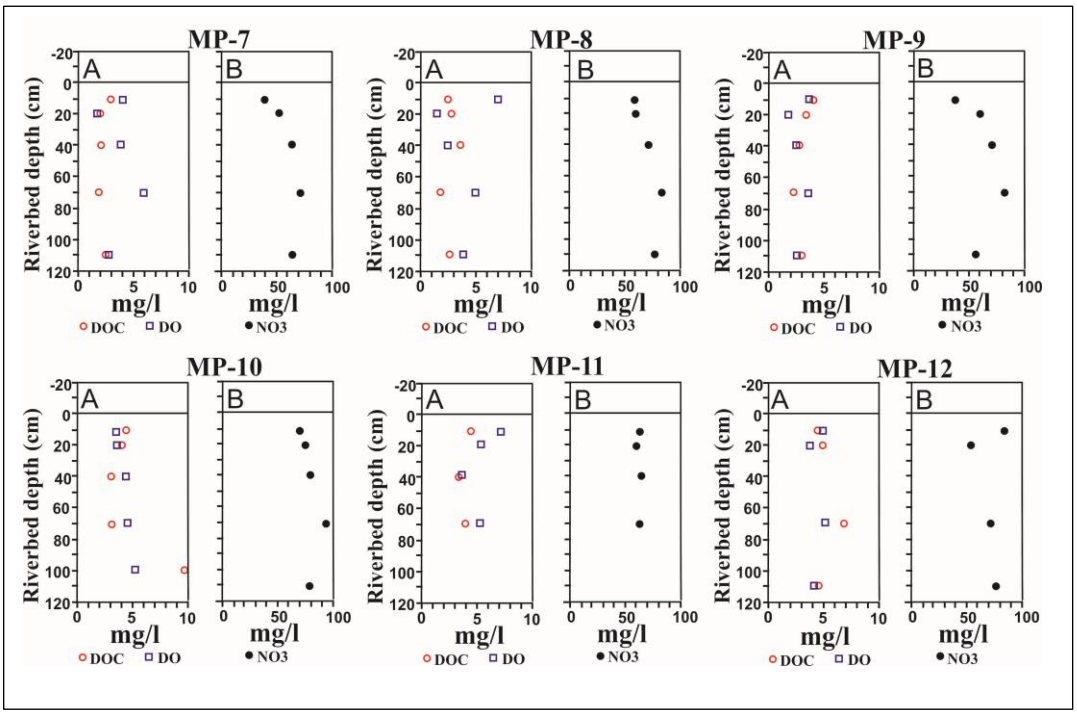
MP-7
MP-8
MP-9
MP-10
MP-11
MP-12
A
B
Riverbed depth (cm)
mg/l
DOC
DO
NO3

C

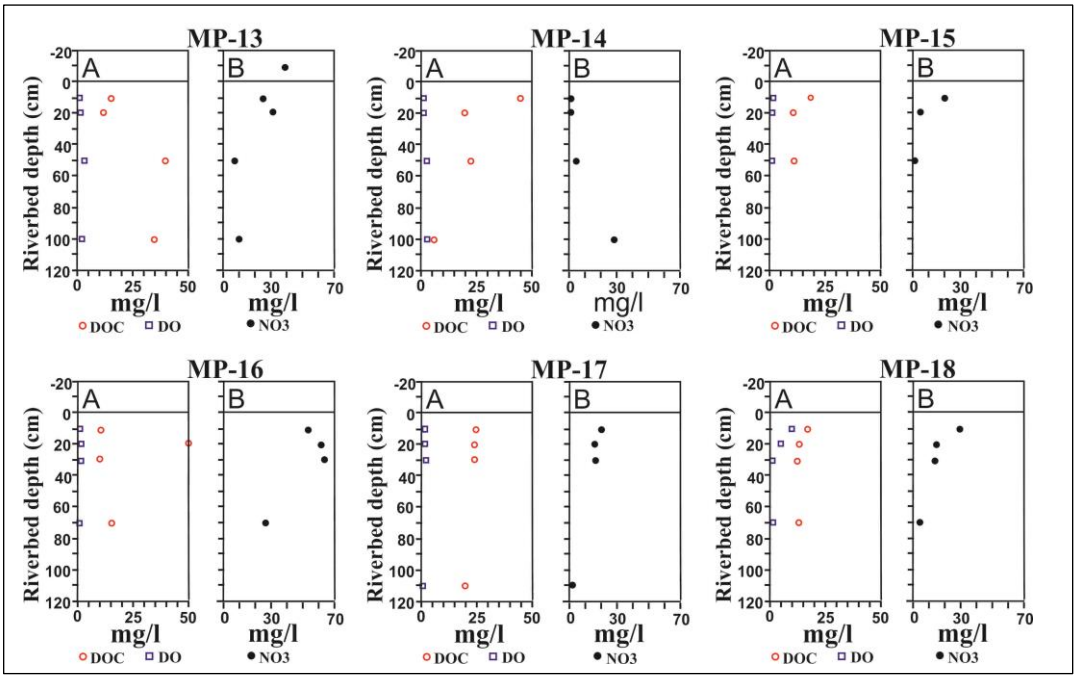

Figure 5.2 Riverbed solute profiles exhibiting the depth distribution of NO_3, DO, and DOC observed in the multi-level profiles. (A) for upstream piezometers (P1-P6), (B) for midstream piezometers (P7-P12) and (C) downstream piezometers (P13-P18). See Figure 4.1 A for the location of these mini-piezometers. Upstream surface water was plotted with MP-1 and downstream surface water was plotted with MP-13.

5.5 Discussion

The biogeochemistry of water flow patterns within the investigated stream reach can be controlled by sediment structural heterogeneity (distribution of permeability fields) in the riverbed. The results of this study suggest that both denitrification and nitrification occurs as evidenced by low concentrations in NO_3 in low conductivity piezometers (site 3) where DO concentrations were low and DOC were high, and high concentrations in NO_3 in high conductive piezometers (site 2) where DO concentrations were high and DOC were low (Figure 5.2). Several studies have described nitrogen transports in both hyporheic and riparian environments (Holmes et al., 1994; Jones Jr et al., 1995; Zarnetske et al., 2011a; Marzadri et al., 2012; Naranjo et al., 2015). However, this study shows the exchange between groundwater and surface water flow patterns within spatial complexity of riverbed lithology of the active channel and reveals a more complex biogeochemistry that comprises distribution of flow patterns (groundwater upwelling) and residence times.

Figure 5.3 shows the positive correlation between nitrates and DO (R^2= 0.2666) in riverbed piezometers. High nitrate concentrations were found at locations with high DO (Figure 5.3). Similar nitrate concentrations patterns in Tern site were found in previous work by Krause et al., (2013). This indicates nitrification or simply a lack of denitrifying the nitrate that was present in the upwelling groundwater region. Krause et al. (2013) found strong correlation (R2=0.73) between DO and nitrate for samples from deeper piezometer levels (150 cm depth), where there was evidence for lacking surface water downwelling to deeper depths than shallower depths (15 cm).

Threshold value seems to be present around DO=2.5mg/l (Figure 5.4). The patterns of DO in this study were comparable to the threshold behaviour reported by Zarnetske et al. (2011a), who observed nitrification along horizontal exchange flow patterns in the hyporheic zone to be corresponded with enhanced water residence time up to a point where sufficient reduction

of dissolved oxygen (DO) levels based residence-time dependant caused nitrate reduction. Thus, hot spots of nitrate and DO concentration changes can be regulated by spatial heterogeneity of the permeability filed across 115 cm of the riverbed depths with upwelling groundwater.

The link between DOC and DO is less strong in riverbed piezometers (Figure 5.4), however, slightly higher DOC concentrations were found in areas of low oxygen. Two outliers (piezometer 14-10cm and 16-20) can be explained by high DOC because it is more or less inside a peat lens with a low K value.

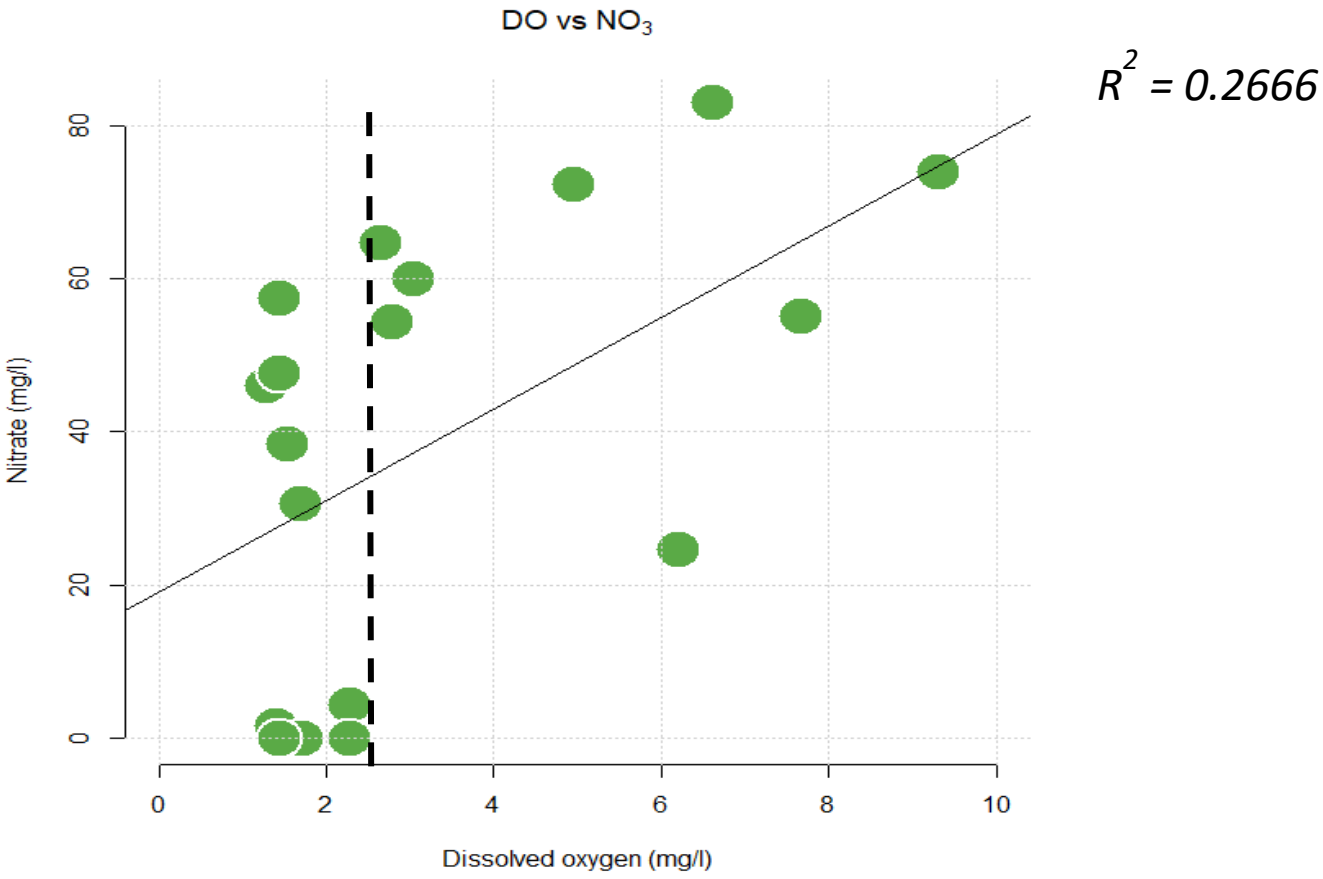

Figure 5.3 Relationship between DO and nitrate in riverbed piezometers of the Tern river study site.

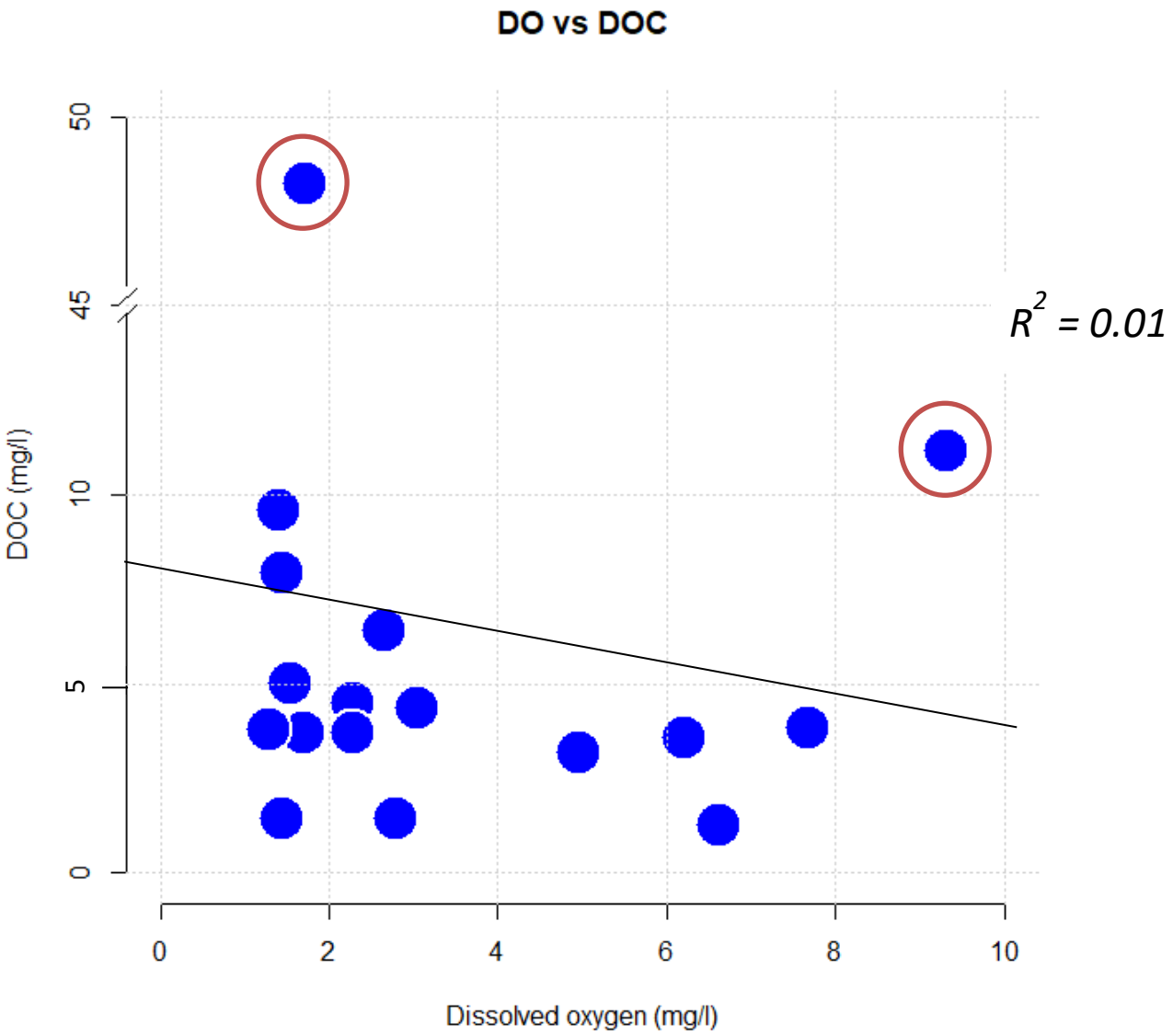

Figure 5.4 Relationship between DO and DOC in riverbed piezometers of the Tern river study site.

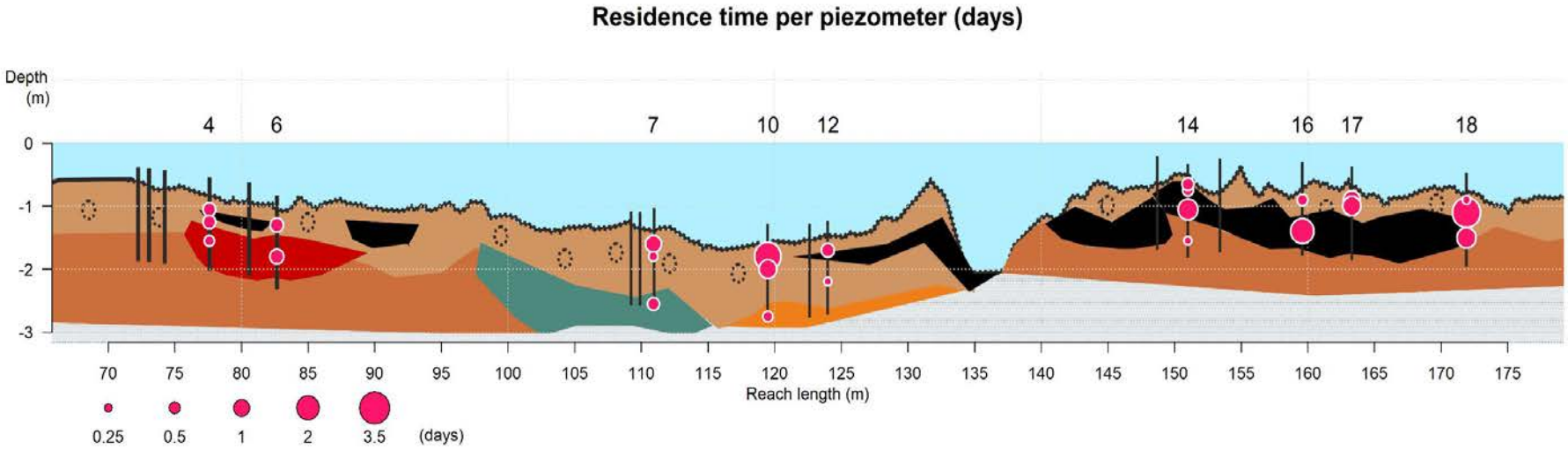

Figure 5.5 Residence time distribution across the study reach.

5.5.1 Spatial patterns of NO_3, DO, and DOC and the relationship to residence time

Variability in nitrate (NO_3), dissolved oxygen (DO), and dissolved organic carbon (DOC) concentrations in interstitial pore water, among various piezometer networks in the investigated stream reach section, were determined by spatial heterogeneity in riverbed sediments (e.g., the presence of high versus low conductivity layers beneath the water-sediment interface), the direction of flow as well as surface water infiltration.

Riverbed sedimentary layered deposits are characterised by more pronounced residence time (Figure 5.3) and water flow paths and these may, in turn, relate to spatial variability in chemical solutes concentration. Krause et al. (2009, 2013) sampled interstitial pore water in piezometers at high spatial resolution, which reveals high spatial variability in groundwater and surface water exchange patterns being strongly determined by riverbed sedimentary layers. Krause et al. (2013) observed low DO and NO_3 concentrations in interstitial pore water samples taken from piezometers around high conductive organic peat and clay layer in comparison with profiles where these layers were absent. Gomez-Velez et al. (2014) demonstrate the influence that low conductivity deposits continuation have over DO concentrations and hyporheic flow patterns, and this could be an explanation to the substantial contrasts in observed solute concentrations among three piezometer clusters along the study reach.

The degree of aquifer-river connection drives the measured biogeochemical patterns seen in the study site. Generally, good aquifer-to-river connectivity is thought to be most prevalent at site 2 (midstream piezometers, P7–P12). Based on stratigraphic, piezometric and in-stream GPR survey evidence (from 100m to 130m of the profile) at site 2, the sub-channel region is composed of mixtures of sandy gravel layers. These layers exhibit a high degree of hydraulic conductivity (see chapter 4). Piezometers (P7–P12) are associated with low and temporally less VHG. Figure 4.5–4.9, in chapter 4 highlights the high Darcy (vertical) flux and

associated short residence times (Figure 5.5) measured in this area of the riverbed in comparison with the rest of the investigated stream reach. The results of vertical flux in piezometers (P7–P12) indicated that site 2 corresponded to a location of rapid groundwater discharge with enhanced connectivity to regional or local groundwater body.

The groundwater is a source of nitrate in the study reach. The analysis of pore water nitrate for piezometers installed inside high conductivity layers (sandy area) (P7–P12) (site 2) found that this region revealed little variation (from bottom to top) in nitrate with depth during sampling time, or in rare cases revealed some clue of dilution with stream water especially in the upper most sampling point (10 cm depth) as seen in P7 and P9. DO concentrations were relatively higher in this area (site 2) compared to other areas. Thus, it is postulated that the riverbed at site 2 is a region of upwelling groundwater and short residence times (Figure 5.3) with a discrete hydrochemical signature, within which the strong upwelling groundwater provides little opportunity for mixing with riparian or surface water origin. Moreover, Heppell et al. (2014) identified that the distribution of horizontal and vertical water fluxes in the riverbed of River Leith reach had influenced the chemical signatures in the riverbed. They found reducing conditions associated with lateral and longitudinal fluxes of water and oxic conditions associated with localised upwelling groundwater discharge. The oxic subsurface environment at site 2 (in piezometers with highly conductivity materials) supports the production of nitrate via nitrification. Nitrate concentrations are significantly higher at this site and this indicates that oxygenated water associated with vertical flow paths inside highly conductive drift deposits in this region.

In peaty/clayey sediment, areas with high residence time (site 3) (P13-P18), nitrate decreases with decreasing DO (Figure 5.2). It is expected that denitrification takes place in this region. This was observed in some piezometers, that the nitrate concentrations are higher at deeper points, but declines towards the streambed in locations where there is long residence time.

This suggests that subsurface hydrology (e.g. water residence time) largely impacts the biogeochemical properties that develop there. For instance, the oxygen depletion and nitrate reduction along upwelling groundwater in downstream reach study section (site 3) are compatible with the locations of low conductivity structures (e.g., clay and peat) (Figure 5.5) and associated enhanced residence times and also due to a lack of connection to the stream water. Generally, water moves much more slowly through this section. If the flow path is slow, then water becomes anoxic. The longer it takes for the water to pass through, the more time it gives the bacteria in the biofilms that coat the substrate sediments to remove the pollutants. Sgouridis et al. (2012) demonstrated that, the significant factor controlling denitrification in an N-rich riparian environment is the liability of the organic carbon. They also demonstrated that, the dissimilatory nitrate reduction to ammonium (DNRA) operates at considerably lower rates than denitrification in temperate N-rich riparian soils, and is compatible with fine grained soils subject to frequent saturation which would result in fluctuating oxygen conditions. Hence, the majority of nitrate in floodwaters infiltrating the soil is reduced to nitrogen gas and is removed rather than maintained in the system as NH_4.

In addition, Peat and clay lenses are an important source of organic carbon and, as such, they are responsible for the spike in the level of the electron donor that is normally utilized in denitrification. Such interpretations are coherent with findings of those (Hedin et al., 1998; Sobczak et al., 1998; Zarnetske et al., 2011b) where they indicated denitrification rates and nitrate concentrations are associated with the availability of oxidisable labile organic carbon. The very low (< 2 mg/l) of DO concentrations in piezometers with evidence of organic peat and clay structures, especially in the lower layers, indicates that DO is not normally renewed by incoming surface water and that any oxygen that may reach in lower layers is quickly consumed by heterotrophic metabolism. The very low nitrate at the lower layers (site 3) indicated that any nitrate that might be present there is rapidly being consumed by

denitrification. Such interpretation is coherent with outcomes of Heppel et al., 2013 and Ramon et al., 2015. Zarnetske et al. 2011a assessed the dynamics in the rate of nitrate production and elimination in a gravel bar in Oregon, USA. The results of their study suggested that the transition from nitrification to denitrification not only demonstrates a threshold behavior, but it is also a function of hyporheic residence time. The observed high DOC in some certain depths in piezometers installed in peaty area (e.g., depth 50 in P13, depth 10 cm in P14, and depth 20 cm in P16) suggesting a source of DOC supply in this area of the reach. Figure 5.6 shows a sketch (longitudinal and plain view) conceptualization of subsurface flow and measured chemical variables (NO_3, DO and DOC) within the reach.

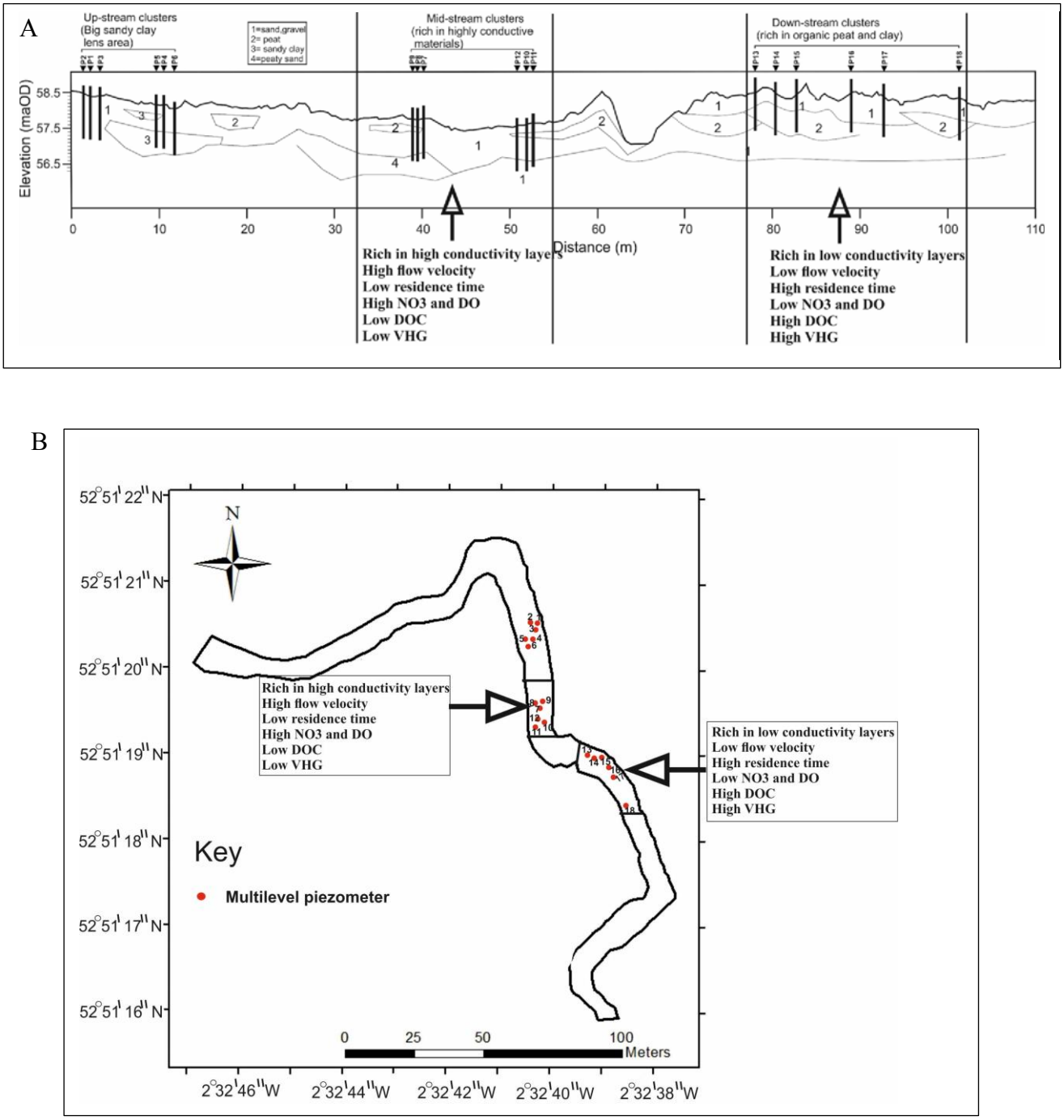

Figure 5.6 Sketch of conceptualization of subsurface flow velocity and measured biogeochemical data within the reach. (A) Longitudinal profile and (B) Plan view.

5.5.2 Correlations between hydraulic conductivity and DO concentration

The correlation coefficient (R) of riverbed hydraulic conductivity (Ks) and dissolved oxygen (DO) at the 0.01 level (2-tailed) was 0.43 (p = 0.067), indicating significant positive correlation between riverbed hydraulic conductivity and dissolved oxygen at the investigated site (Figure 5.7). Decrease in the subsurface sediments hydraulic conductivity and an increase in hyporheic residence time have an effect on the development of pore water dissolved oxygen concentration gradients in hydraulic conductivity. Silt and clay on account of their smaller particle sizes are characterised by comparatively low hydraulic conductivities, causing longer residence times of water through sediments, and this could result in DO depletion (Baker et al. 2000). The predominant mixture of high conductivity gravely sands in site 2 provides less opportunity for pore water to stay for long time. Therefore, short residence times with high DO concentration have observed during the investigated period. In several stream reaches, Kennedy et al. (2009a and 2009b) and (2009b) showed correlation between riverbed K and fluxes of water on residence time distributions and following nitrate transport rates. The results of this study highlight the particular influence of small scale variability of riverbed physical properties (low permeability structures) on upwelling groundwater and nitrate, DO and DOC concentration changes.

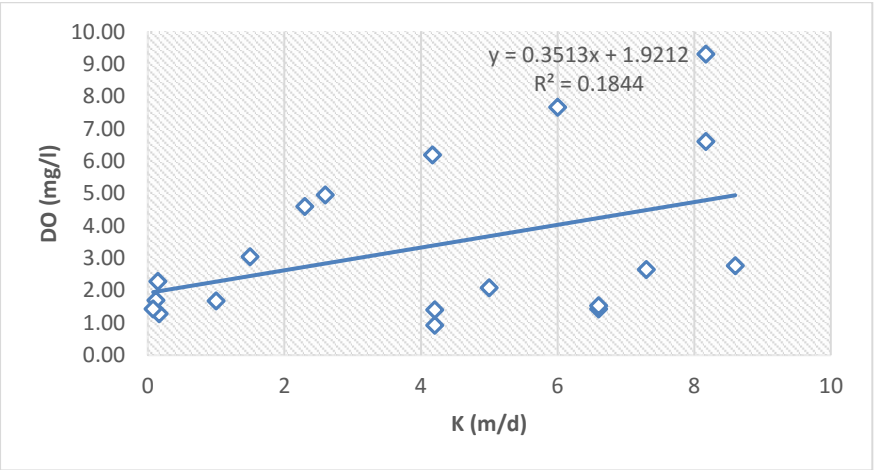

Figure 5.7 Correlation coefficient between riverbed hydraulic conductivity and corresponds DO value.

5.6 Conclusion

This study shows the transformations of nitrate, DO and DOC at sediment-water interfaces at multiple scales including riverbed depths (10-115 cm) with piezometers installed in different riverbed lithostratigraphy. This study also shows very detailed geophysical information of the spatial heterogeneity of the permeability field explains much more of the biogeochemical processes. Also, this study shows nitrate and dissolved oxygen concentrations is lower by up to an order of magnitude in areas with evidence of peat and clay structures (site 3) (downstream piezometers).

Lower DO and nitrate with high DOC concentrations at downstream piezometers (site 3) (areas rich in peat and clay lenses) is interpreted as a consequence of enhanced residence times around low permeability structures. The subchannel clay and peat heterogeneities create an anoxic environment associated with poor water transmission volume, which is favourable for the strong attenuation of the groundwater pollutants. The anoxic conditions that arise after this depletion are highly conducive for denitrification. As expected, DO was strongly positively correlated with hydraulic conductivity based on Pearson's parametric correlation. Furthermore, positive correlation was also observed between nitrate and oxygen in streambed piezometers with the threshold value seems to be present around DO=2.5mg/l.

6 Geophysical and hydrological characteristics of the Hammer stream in West Sussex-UK

6.1 Abstract

Ground penetrating radar (GPR) surveys in combination with sedimentological data (e.g., sediment core samples, grain size analysis, and hydraulic conductivity) were used to study the sedimentology of the near-river subsurface zone of the investigated Hammer stream reach in west Sussex, UK. A pulseEKKO pro equipped with a shielded 250 MHz antenna was used in this study. Several closely spaced GPR profiles in the form of grids were collected on the floodplain west bank site (riparian zone) of the river section. The riparian GPR surveys were accompanied by a longitudinal in channel GPR survey for which the antenna was deployed on a floating device. Sub-horizontal reflectors on the floodplain GPR records are interpreted as sand-grained sediments. The prominent hyperbolic reflections are interpreted as pockets of high water-content fine-grained sediment (clay sediments). Dipping reflections are interpreted as sand layering within channel bars. GPR records collected on river channel had discrete water-bottomed multiples. Weak-amplitude and disturbed reflections are interpreted as shallow sand streambed deposits. Strong reflections associated with hyperbolic reflections are interpreted as clay deposits which were absent in some areas of the river channel stratigraphy. Therefore, the GPR proved to be very appropriate and helpful in supporting hydrogeological data in near-river sedimentology and hydrology studies.

6.2 Introduction

Subsurface near-river zone characteristics such as grain size distribution, sorting, and organic matter content are defined by dynamics of flow and channel form, leading to a mosaic of various lithostratigraphy patches within the river corridor (Pretty et al., 2006). Hydrofacies type may play an important role in aquifer-river exchange because hydraulic conductivity could be differ in different patches, therefore influencing exchange fluxes, biogeochemistry and residence times (Malard et al., 2002; Krause et al., 2013).

The overarching goal of this chapter is to explore the suitability of GPR in similar sediment properties but with substantially different distributions in comparison to the river Tern. The Hammer stream traverses a lowland catchment area rich in low conductivity sediment deposits. The depositional setting in the Hammer stream site is characterised by high amounts of low conductivity layers with few high conductivity holes (see conceptual model in Figure 1.1). A key message in this work is to examine the continuity and discontinuity of low conductivity layers (e.g., clay) and implications for hydrology. However, many researchers (Fleckenstein et al., 2006; Angermann et al., 2012; Krause et al., 2012b; Naranjo et al., 2015) found local sediment heterogeneity at the aquifer-river interface. They described the effects of such heterogeneity on flow exchange and nutrient cycling.

Although traditional methods for analysing field exposures such as shallow excavations, outcrop data, and core logs are still typical, these methods are expensive and time consuming and often providing only limited information which are difficult to make connections between sampling points (Neal, 2004). In contrast, ground penetrating radar (GPR) refers to a rapid emerging non-invasive method which designed mainly for subsurface investigations (Comas et al., 2004; Neal, 2004). The GPR transmitter antenna emits high frequency (typically 100-1000 MHz) electromagnetic energy (EM) into the subsurface. The strong reflections at the lithological boundaries of the subsurface are attributed to the differences in

dielectric constant (Neal, 2004). However, the resolution and depth range of the measurement is dependent on the many factors such as antenna frequency (e.g., the higher antenna frequency produces higher resolution results and lower depth of penetration (Neal, 2004; Słowik, 2014a), hydrogeological conditions (e.g., type of shallow subsurface sediments and groundwater level) (Heteren et al., 1998; Barone et al., 2013; Słowik, 2014a) and climatic conditions (e.g., influence of precipitation and infiltration, moisture content, frost and permafrost on dielectric properties of sediments and soils) (Lunt et al., 2005; Tran et al., 2012).

GPR, in combination with geological information such as core logs and outcrops, can provide sufficient information on the sediment stratigraphy, hydrological functioning units (hydrofacies), and the geometry of the sediment texture in fluvial deposits in lowland meandering rivers (e.g., Huggenberger et al., 1994; Beres et al., 1995; Binley et al., 2015). It is recommended for structural and lithological studies of deposits in an alluvial valley fill, for instance, the hyporheic zone and the adjacent floodplain due to the relatively high spatial resolution and the possibility to image large areas (Bridge et al., 1995; Robinson et al., 2008; Clifford and Binley, 2010).

The main aim of the study is to develop and demonstrate the suitability of GPR in similar sediment characteristics but with remarkably different distributions in comparison with the river Tern. The objective was to; (1) detect shallow, unconsolidated alluvial deposits for river channel and floodplain deposits; (2) describe the connection of the GPR results with ground-truth data from vibracoring; (3) some hydrological parameters were explored to determine the potential limitations and applications of GPR techniques in fluvial environments. For example, obtaining hydraulic conductivity (K) estimates from both slug tests and grain size analysis.

6.3 Field site and methods

6.3.1 Study site descriptions

The study focuses on a meander reach of the Hammer stream, a small 4th order tributary of the Wester Rother River in west Sussex, UK (Figure 6.1). The Hammer stream has a surface water catchment of approximately 25 km^2 (Vokes, 2015). It holds significance due to its essentially cultivable feature where forests are present adjacent to the stream (Table 6.1). The topography is characterised by slightly undulating land surface with some steep valleys beside the stream. The underlying field site geology is composed of a Lower Greensand outcrop of Cretaceous age, all covered with sands including wood fragments, clays, and loamy soils; this is found to be the best area for arable cultivation (Boardman et al., 2009). Nevertheless, deforestation has caused these fertile soils to erode with the flow of the stream which carries and dumps them on the floodplains. On the left riverbank of Hammer stream, there is a floodplain, covering the area of 320 m2, comprising stream bank, swamps, and the toe of neighbouring hillslope. A huge backwater acquires the water that runs down the slope of the adjacent hill; which when induced with extended precipitation, streams along with the channel in the investigated section, before discharging back into the stream reach (Vokes, 2015).

Typical of catchments with the south of the UK, the Hammer catchment has also witnessed an alteration in the cultivation focus; which has shifted from meadows to winter and spring cereal crops. Preservation measures are being investigated but the landowners are not being encouraged to implement any of these procedures (Boardman and Vandaele, 2015). The extensive catchment is a nitrate vulnerable area, which exposes the surface and groundwater. Three wells located near the Hammer stream have been used for drinking purposes, and one of these wells is blocked because it was found to have the intensities of N that are more than the permissible 50 mg/l (Wright et al., 2013).

Table 6.1 Details of land use in the Hammer stream catchment (Wright et al., 2013).

Catchment	Area (km^2)	% Urban	% Water	% Woodland	% Rough grazing	% Arable	% Improved grazing
Hammer Stream	25.2	5.7	0.8	42.4	2.1	22.2	26.9

Cores taken from the floodplain and riverbed (Figure 6.2) generally showed different sizes of sands interbedded with clays. Clay sediments are higher in floodplain sediment deposits than in riverbed deposits. The hydraulically most significant difference in the floodplain and riverbed strata materials were represented by the continuous and discontinuous clay layers, as indicated in the retrieved core samples from the study area.

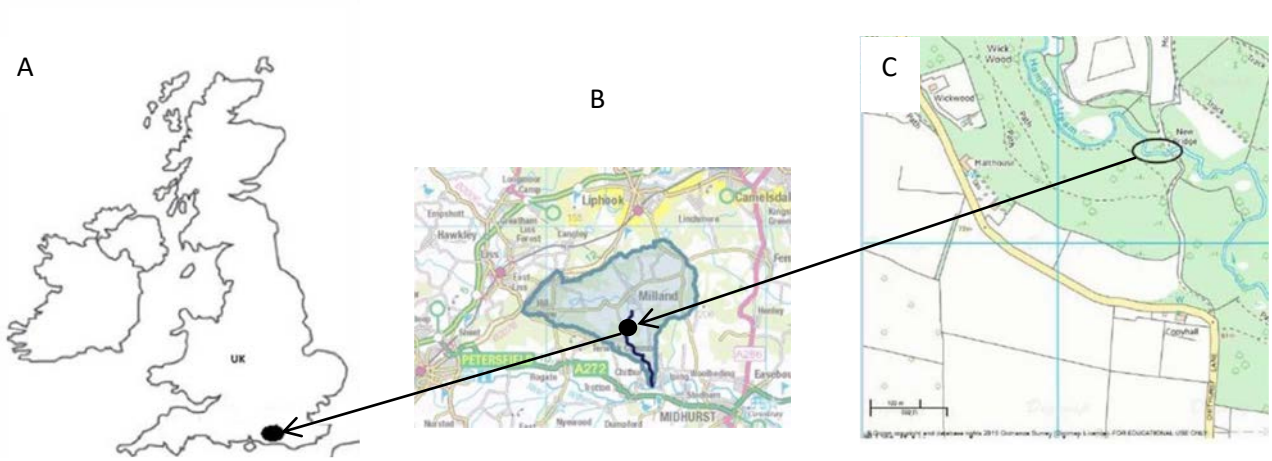

Figure 6.1 (A) Location of the Hammer stream field site (outlined in black circle) within the UK. (B) Hammer stream catchment (outlined in blue), black dot represents study stream reach (Source: Ordnance survey 2017, Environmental agency). (C) Location of study reach (Outlined in black circle) (Source: Klarr, 2016, unpublished map).

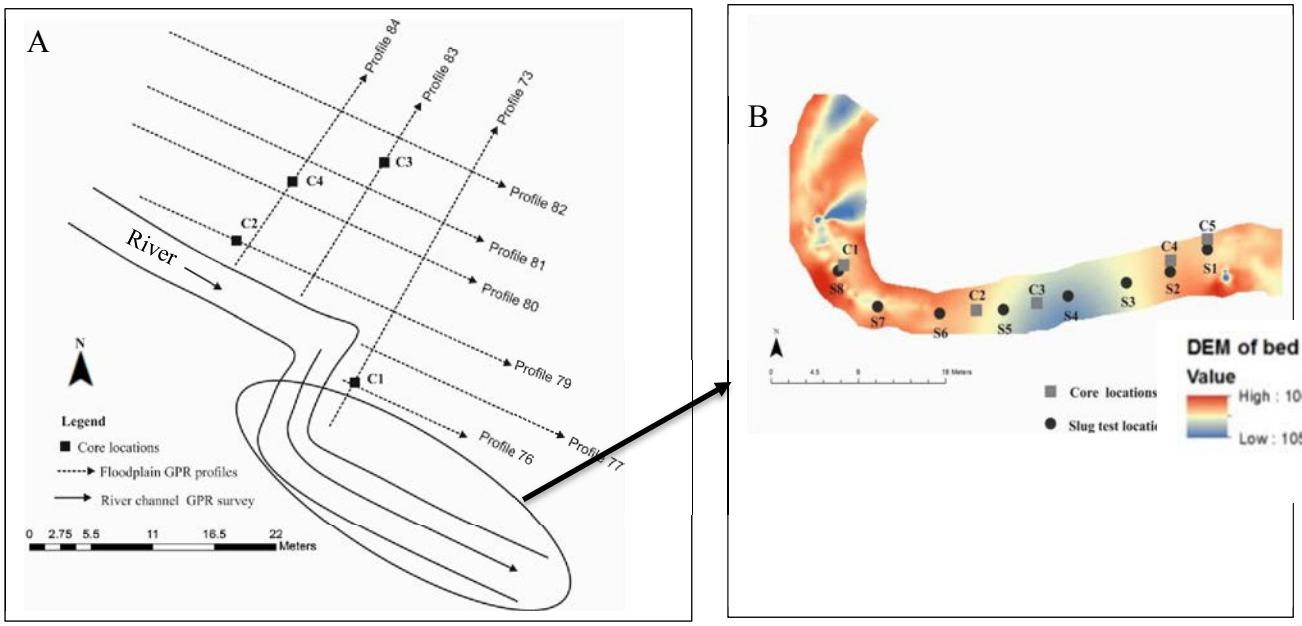

Figure 6.2 (A) Plan view schematic of the Hammer stream study section, showing locations of GPR survey profiles (floodplain and longitudinal river channel survey) and floodplain retrieved core samples. (B) Investigated stream reach shows riverbed core samples and slug test locations.

6.3.2 Characterisation of the riverbed and floodplain sediments

6.3.2 a) Ground-truthing methodology

Ground-truth data is fundamental for the true attributes of sediment stratification (Naden, 2011). A sediment coring technique was developed in order to characterise the alluvial deposit materials of the Hammer stream reach site. The Van Walt coring augers (vibracoring) which are powered by the 'Cobra Pro Atlas' (Figure 6.3) were used to retrieve local point sediments from the riverbed and floodplain in the studied reach. Vibracores were obtained to maximum depths of approximately 2 m for floodplain cores and 1 m for riverbed cores. However, vibracore drilling differed by location and often did not penetrate the whole depth imaged by GPR and varied by location. Vibracores' locations were chosen to demonstrate features of interest noticed in the GPR survey results, as well as provide core control across the investigated survey region (Figure 6.2).

Figure 6.3 (A) Cores extracted in the riverbed and floodplain using a Van Walt coring augers and powered by the 'Cobra Pro Atlas' petrol generator. (B) Levering out cores. (C) Riverbed example core. (D) Floodplain example core (for core numbers and locations see Figure 6.2).

6.3.2 b) Grain size analyses for floodplain and riverbed cores

The grain size is an essential component of the deposits as it influences their activity, movement and sedimentation. Thus, the grain size analysis offers significant evidence to the origin, transference and accumulation settings of the deposits (Folk and Ward, 1957; Friedman, 1979). A total of nine sediment cores were extracted in the study reach. Four 2 m cores were collected from the east bank site on a number of GPR profiles, locations shown in Figure 6.2. In addition, five cores were collected from the riverbed along the stream reach

and the length of the riverbed collected cores ranged from 65 cm (riverbed Core 1) to 100 cm (Figure 6.2). The floodplain and riverbed sediments of the Hammer stream comprise unconsolidated sand interbedded with different thicknesses of clay, which are relatively easily subjected to grain size analyses. Core samples were selected from the material obtained during vibracoring (Figure 6.3). All retrieved sediment samples were first analysed visually and then underwent a wet and dry grain size analysis in the laboratory using a sieve. Sieves from 2 mm to 0.063 mm sizes were employed. The particles of the floodplain and streambed sediment logs are initially dehydrated using a fan extractor under 105° C for 24 hours; these particles are then weighed, which is followed up by washing them in a fine sieve to eradicate any particles that are smaller than 0.063 mm size. These particles are then dehydrated again, and weighed, to determine the quantity of the particles that were removed. The remaining particles are then sieved again. The quantity of the particles on every sieve is weighed up and the percentage of the whole amount that goes through every sieve can be recorded into a grain size illustration. The constructions of grain size distribution are made by plotting grain size diameter against percent finer weight.

6.3.2 c) Falling head test in the riverbed piezometers

Saturated riverbed hydraulic conductivity was measured for riverbed piezometers across two depth horizons, using falling head tests (slug tests). Slug tests measure hydraulic conductivity values that include both vertical and horizontal flow. Tests were performed on 3.8-cm diameter uPVC (unplasticised polyvinyl chloride) piezometers which were installed along the river at 5 m intervals. Piezometers were driven to depths between 20 and 50 cm beneath the riverbed. Eight and three slug tests were carried out to 20 and 50 cm, respectively. An example piezometers used for slug tests in the Hammer stream riverbed is showing in Figure 6.4. The detailed experiment of falling head test is discussed in chapter 4.

Water level within the piezometer was measured using a pressure transducer logging at 1 or 5 second intervals. Pressure transducers were connected to a nylon cord. This allowed pressure transducer to be inserted into the piezometer and extended to the midscreen section at the desired depth and then pulled out after the test was completed. After the pressure transducer was installed, the water level inside the piezometer was allowed to re-equilibrate before one litre of river water was added to the piezometer.

Figure 6.4 An example of installing piezometer in the riverbed (50 cm depth) for slug test purpose (locations are shown in Figure 6.2).

6.3.2 d) Slug test analyses

Recorded falling head data were analysed using the Hvorslev method (Hvorslev, 1951). The value for the riverbed materials hydraulic conductivity was derived using the following variant of the Hvorslev equation (Section 4.3.8, chapter 4).

6.3.2 e) Estimation of floodplain sediment hydraulic conductivity through grain size analyses by Hazen method

The hydraulic conductivity of unconsolidated sediments is directly related to the packing of the particles and the void spaces between them which are a function of the grain size distribution (Ellis, 2003). Hydraulic conductivity of sands can be estimated using grain-size distribution curves where the effective grain size is between approximately 0.1 to 3.0 mm (Fetter, 2000) by adopting the Hazen approach (Hazen, 1911). The effective grain size, D10, is the grain size diameter for which 10% (by weight) of sediment distribution is finer. These values from the generated grain-size distribution curves were applied to the Hazen method for hydraulic conductivity as follows:

$K= C *(D10)^2$

K= Hydraulic conductivity (cm/s)

D10= is the particle size for which 10% of the material distribution is finer (cm).

C=uniformity coefficient based on grain size and sorting see Table 6.2, ($cm^{-1}s^{-1}$).

Table 6.2 Representative values of the Hazen coefficient for the different degree of sorting and grain sizes (Fetter, 1994).

Sediment character	Range of 'C' coefficient (cm^{-1} s^{-1}
Very fine sand, poorly sorted	40 – 80
Fine sand with appreciable fines	40 – 80
Medium sand, well sorted	80 – 120
Coarse sand, poorly sorted	80 – 120
Coarse sand, well sorted, clean	120 – 150

6.3.3 Statistical analysis for grain size distribution

A piece of software known as GRADISTAT has been produced to promptly examine the grain size statistics from any of the normal assessing methods, e.g., sieving and laser granulometry (Blott and Pye, 2001). The GRADISTAT program, written in Microsoft Visual Basic, is integrated into a Microsoft Excel spreadsheet, which acknowledges both tabular and graphical outcomes.

6.3.4 GPR Data collection and data presentation

The GPR surveys were carried out on December 2015 along the investigated river channel and the floodplain of the Hammer stream. The PulseEKKO PRO GPR radar system developed by Sensors and Software Inc., Canada, was used in this study. GPR data collection were made using a 250 MHz centre frequency bistatic shielded square antennas with a separation of 40 cm between transmitter and receiver, considering the compromise between the resolution and depth of penetration necessary for this survey.

For the floodplain, GPR transects were collected in a grid pattern as shown in Figure 6.2. The collected profiles on the floodplain have different lengths due to the nature of the floodplain. Parameters setting during the GPR measurements for all floodplain GPR profiles are shown in Table 3.2.

6.3.5 GPR data processing

Data processing was conducted to enhance the signal-to-noise ratio prior to analysis. Processing was conducted using Reflex2D Quick (version 2.5). The detailed GPR processing was presented in section 3.3.3b, chapter 3. Data processing involved zero-time correction of 14 ns, a subtract mean dewow filter with a time window of 4 ns, a band-pass frequency filter of 60 MHz-110-MHz-235 Mhz-380 MHz, a diffraction stack migration with a summation width of 10 traces and mean velocity of 0.05 m/ns, and an AGC gain curve of a 40-ns time window.

6.3.6 Digital elevation mapping (DEM)

Boreholes, GPR profiles, piezometers, and floodplain topography were surveyed with a Leica total station. The total station data were recorded in DXF CAD format. The data were then transferred into ARC GIS (version 10.2) and georeferenced utilising the control data. Digital elevation maps were prepared utilising the Inverse Distance Weighted (IDW) interpolation method to create a digital contour surface. This weights sample points, meaning that the influence of a point relative to another reduces over increasing distance.

6.4 Results and discussion

6.4.1 Statistical analysis of grain size distribution results

The statistical analyses (GRADISTAT printout) of the floodplain and riverbed sediment cores are presented in Appendix 4 and Appendix 5 , respectively. Table 6.3 reveals the grain size distribution parameters of the sediment deposits in the study area: the mean grain size (M) in ϕ-values, the standard deviation (degree of sorting) (σ) and the skewness (Sk).

6.4.1 a) Mean grain size (M)

The range and mean grain sizes for riverbed and floodplain cores are 2.05–2.75 ϕ (average 2.54 ϕ) and 4.0–4.94 ϕ (average 4.44 ϕ), respectively (Table 6.3). Generally, the riverbed average mean grain size suggests a prevalence of medium sand in the study area (Table 6.3). The range values of riverbed cores indicate that the sediments were transported in saltation and suspension processes (Lejzerowicz et al., 2014). The floodplain core samples range values suggest that most sediment are deposited by the settling of fine-grained sediment from suspension or may be from when the floodplain was inundated during flood events.

Table 6.3 Grain size parameters of the sediment samples (riverbed and floodplain samples) from the investigated Hammer stream reach.

Sample Number	Grain size parameters			
	Median	Mean (M)	Standard deviation (σ)	Skewness (sk)
Floodplain cores				
Floodplain core 1	3.95	4.45	1.55	-0.16
Floodplain core 2	3.64	4.00	1.51	0.28
Floodplain core 3	3.86	4.35	1.56	-0.08
Floodplain core 4	4.80	4.94	1.42	-0.80
Riverbed cores				
Riverbed core 1	2.58	2.75	1.57	1.01
Riverbed core 2	2.61	2.67	1.27	1.38
Riverbed core 3	1.88	2.70	1.79	1.04
Riverbed core 4	1.79	2.05	1.21	1.73
Riverbed core 5	1.88	2.52	1.58	1.37

6.4.1 b) Standard deviation (degree of sorting) (σ)

Sorting (standard deviation σ) is a procedure by which a given transportation environment plays a significant role in separating out specific grains depending on their size, shape or density. Table 6.4 shows the sorting value of sediments according to the Folk (1980) classification:

Table 6.4 Sediment sorting classification based on Folk (1980).

Sorting (σ)	Values (ϕ)
Very well sorted	<0.35
Well sorted	0.35–0.50
Moderately well sorted	0.50–0.70
Moderately sorted	0.70–1.00
Poorly sorted	1.00–2.00
Very Poorly sorted	2.00–4.00
Extremely poorly sorted	>4.00

The riverbed and floodplain core values of σ range from 1.21 to 1.79 ϕ (average 1.48 ϕ) and 1.42 to 1.56 ϕ (average 1.51 ϕ), respectively (Table 6.3). The riverbed value indicates poorly to very poorly sorted material including different sizes and sands and muds. The poorly sorted sediments suggest that the riverbed sediments were deposited in the channel zone with a relatively stronger current than in the floodplain. While floodplain sediments were deposited under low energy depositional environments.

6.4.1 c) Skewness (SK)

Skewness (Sk) is the measurement of the symmetry of the distribution of grains. Symmetrical curves possess Sk = 0.0; deposits with excess fine material (a tail to the right) have positive skewness and those with surplus coarse material (a tail to the left) have negative skewness (Folk, 1974; 1980). The skewness values for the riverbed and floodplain core sediments recorded fine to very fine skewness which indicating an excess of fine sediments (see Appendix 4 and Appendix 5).

6.4.2 Descriptions of the riverbed and floodplain sediment grain size distribution

Figure 6.2 shows the locations of the retrieved cores in the study area. The vertical distribution of the sediment particles such as sand, silt, peat and clay varied between all retrieved cores. The cores showed distinctive layers as well as gradual changes in the sediment texture (see core matches with GPR profiles from Figure 6.5 to 6.10.

In terms of floodplain core sediments, it was generally found that the four retrieved cores were composed of a majority of clay/silt particles (particles with less than 0.063 mm) with a high presence of sand, particularly fine sand. The particle proportion content obtained from the grain size analysis method for floodplain cores are shown in Appendix 4. In floodplain core 1, the proportion of sand and clay is relatively similar, where 51.2% and 48.8% of the core contain sand and mud, respectively. Fine sand (0.250–0.125 mm particle diameter) is the most dominant sand size. The majority of clay particles (> 0.063 mm) were measured at deeper depths (90–200 cm depth). Floodplain core 2 is more homogenous compared to other cores; this core is made up of 65.4% of sand and 34.6% of mud. Hence, the largest grain size component is over 0.063 mm in diameter. The majority of fine sand (0.250–0.125 mm particle diameter) in this core was observed in the range of 20–70 cm depth. Floodplain core 3 has the main constituents of 54.2% of sand and 45.8% of mud. However, fine sand particles (0.25–0.125 mm) appear to increase with depth, until the deepest sample at 170cm. In contrast, clay particles (>0.063 mm particles) mostly occur in the first 1 m depth. Floodplain core 4 contains the highest percentages of mud particles >0.063 mm (63.3%) and similar to core 3, are mostly seen in the first upper metre (20 – 90 cm depth) of the core. The total sand percentage in this core was 36.7% and was mostly measured from deeper depths (between 100–200 cm) during the grain size analysis test.

Regarding riverbed core sediments, typical proportions from grain size analysis can be seen in Appendix 5. It was generally found that the upstream reaches of the study area (riverbed

core 1 and 2) consisted of mixtures of various proportions of sand, silt and clay (Figure 6.11 A). Fine sand is considered to be the most predominant sediment particle in the upstream section, from which 35% in core 1 and 44% in core 2 were recorded during the grain size analysis. Clay content in riverbed core 1 (7.7%) was higher than in core 2 (4.7%). The greatest thickness was observed in riverbed core 1 and at a relatively shallow depth; however, this may be attributed to the deposition of finer sediments at the inner bend of the stream. At the downstream reach of the study area, three cores were retrieved in the riverbed (riverbed core 3, 4 and 5) and classified as muddy medium sand. Generally, it has been shown that towards the downstream section coarser particle sediments (particle diameters 500-250 micron) are prevalent. For example, riverbed core 3 was retrieved downstream of core 2 and was composed mainly of medium sand (48%). In contrast to the other cores, this core recorded the highest proportion of clay (10.4%) (particle diameter > 0.063 micron), which mostly occurred at the depth of 70 cm to the base of the core. Further downstream of the reach, riverbed core 4 is homogenous (mostly sand) throughout its sample grain size distribution. This is composed of 21.3%, 48.3% and 20.7% of coarse, medium and fine sand, respectively. Interestingly, the clay layers have remarkably disappeared in this section of the river, which clearly occurred in this core log. Hence, the lowest proportion of clay (>0.063 mm particle diameter) was measured during the grain size analysis. Moreover, riverbed core 5 was composed of the highest proportion of medium sand, 50.3 %, among the riverbed cores. The particle sizes > 0.063 micron clay sediment are relatively high (7.5 %) in this core they occur mostly at the bottom of the core in the forms of clay and peat (Figure 6.11 A).

6.4.3 Floodplain GPR profiles and core validation

This section compares the ground truth data (core logs) from the floodplain with corresponding GPR radar profiles. The main aim of this comparison is to distinguish the lithology of the alluvial drift deposits and to ground truth the GPR surveys. The GPR profiles with available core samples can be treated as a reference profile for interpreting the remaining GPR surveys (Słowik, 2014a). Each profile is presented in an interpreted form with some migrated and unmigrated applied examples in which they identify and interpret radar facies regarding their two-dimensional (2D) appearance. The location of the GPR radar profiles and sediment core samples retrieved in the study area are shown in Figure 6.2.

No core exceeded 1 m depth for the riverbed cores, due to the rapid collapse of the streambed sediment and also the inability of the vibracore to penetrate more in such a difficult environment.

6.4.3 a) Profile 73

This profile displays many hyperbolic reflections that fit well with discrete objects buried into a 0.06 m/ns velocity medium (Figure 6.5). This velocity is consistent with pockets of fine grained saturated layers such as those seen at the range depth of 80-100 cm of the floodplain core 1 (Figure 6.5). These pockets of saturated layers could be caused by clay deposits in the study area. Apart from the hyperbolic reflections; it is possible to delineate some layers, at least partially along the line, that could correspond to different fine-grained sandy layers and clay layers.

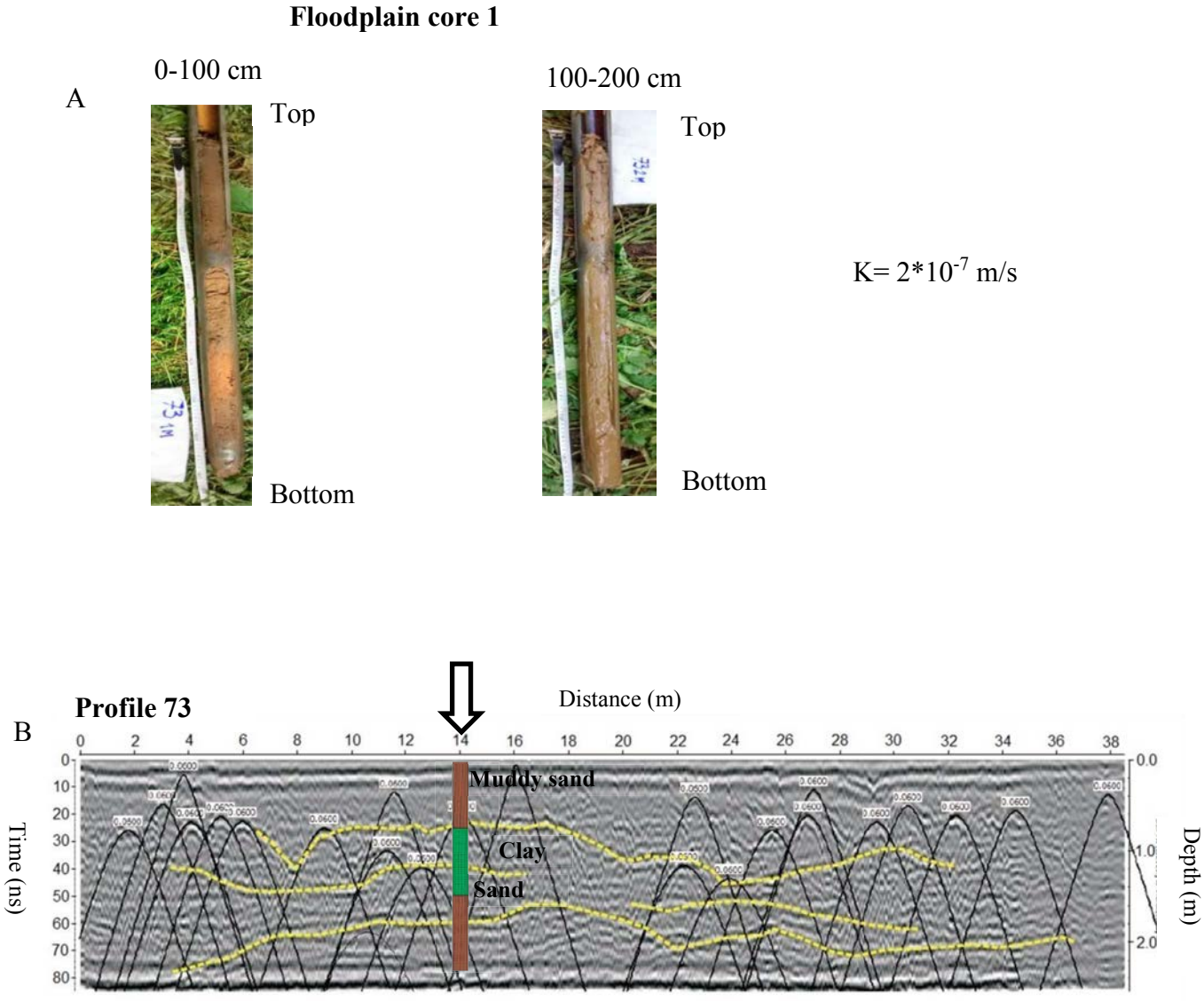

Figure 6.5 (A) photographs of the floodplain core 1 with hydraulic conductivity (K) value derived from grain size analysis. (B) GPR profile 73 shows the location of the retrieved core (at position 14 m) and their interpretation, top image shows processed unmigrated radar record and bottom image shows processed migrated radar record (for GPR profiles and sampling locations see Figure 6.2).

6.4.3 b) Profile 76

This line was collected perpendicular to the lines 73, north-south orientation (Figure 6.2). Both migrated and unmigrated radargram are presented in Figure 6.6. By comparing this line with the previous line, fewer hyperbolic reflections are apparent, but they still fit well to velocities of 0.05-0.06 m/ns and are mostly located from the 6 m location to the end of the

profile. A boundary located at ~30 ns (e.g., at ~1 m depth) can therefore be inferred. After migration, some dipping reflections towards the end of the line are clearly visible at the upper part. At depth, it looks like a lenticular shaped body can be also seen (Figure 6.6).

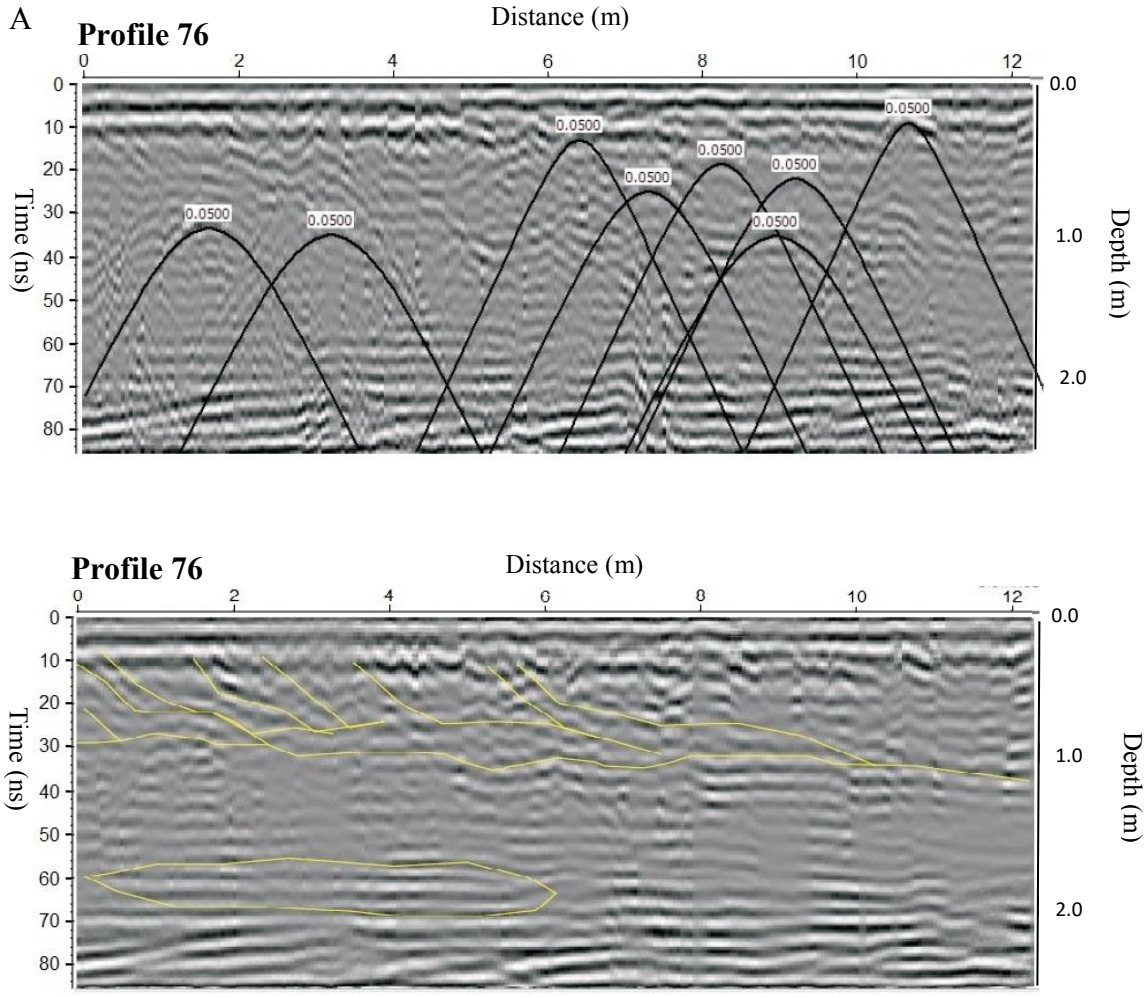

Figure 6.6 GPR profile 76, top image shows processed unmigrated radar record and bottom image shows processed migrated radar record with interpretation (for GPR profile locations see Figure 6.2).

6.4.3 c) Profile 77

Numerous hyperbolic reflections are evident through this profile, fitting well for velocities of 0.05-0.06 m/ns (Figure 6.7). After applying the migration process, most of the reflections are removed but the stratigraphy is still not so clear. Some aerial reflections are still visible at the lower part of the line along the whole profile. It reveals that a shallow layer, more or less

continuous along the line, can be drawn at about 0.3 m depth. Below, an irregular boundary can be found at about 1 m depth at the beginning of the line, but from the middle to the end, it looks like this reflection and some others dipping towards the end are dominant. It is not clear how they end, it looks like they are cut by the shallow reflector. In this case, any clear lenticular body related to an infilling channel is not obvious (Figure 6.7).

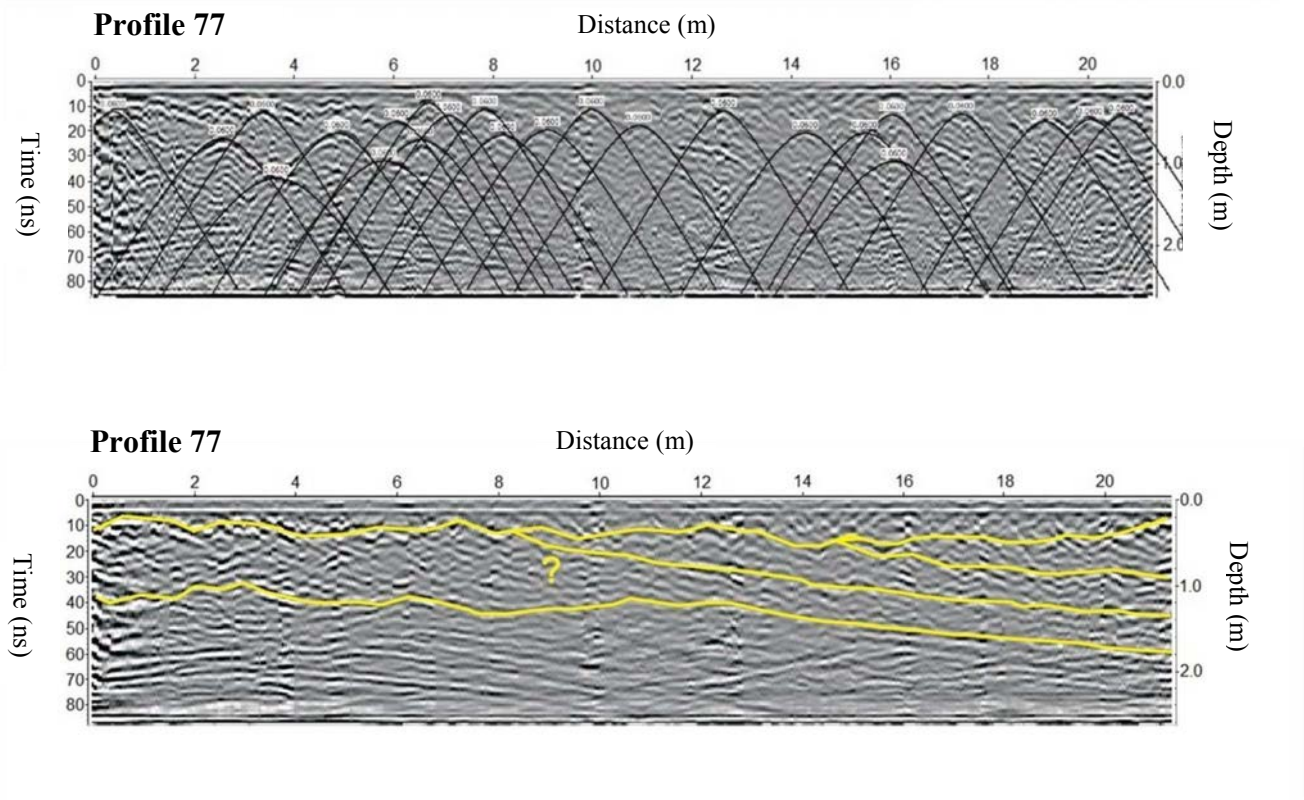

Figure 6.7 GPR profile 77, top image shows processed unmigrated radar record and bottom image shows processed migrated radar record with interpretation (for GPR profile locations see Figure 6.2).

6.4.3 d) Profile 79

This profile was collected at the upper section of the floodplain, close to the active river channel. Floodplain core 2 was retrieved at a 5-m location and was used to validate this profile survey (Figure 6.2). Although the hyperbolic reflections are not so abundant in this profile, weak to medium amplitude sub-horizontal reflections are more discontinuous and it is difficult to obtain reliable stratigraphical relationships. In order to try to improve the

visualization, a migrated process has been applied to the line to collapse the hyperbolae using the 0.05 m/ns velocity (Figure 6.8B) included both the unmigrated and migrated sections). Thus, many of the hyperbolae are totally or partially removed and then some reflections can be better displayed.

A couple of boundaries are evident ~1m and 2 m depth. It looks like two partial lenticular bodies located at both ends of the boundaries could also be defined, probably related to channel facies (Figure 6.8).

6.4.3 e) Profile 83

In this line, the hyperbolic events occurred at shallow depths and mostly can be noted between 2-8 m in this line. In this case the fit is better for a 0.05 m/ns velocity. Also, some half-hyperbolic reflections can be distinguished (red lines) as well as a sub-horizontal interface located at ~1m depth (solid yellow) (Figure 6.9). This could be related to the top boundary of the sandy clay layer observed at approximately 50 cm depth of the core log taken at the location of 5 m in the profile (Figure 6.9). Parallel reflections observed at approximately 100 cm depth mark laminar sands observed in the core sample. After migration, at the lower part of the line a couple of lenticular bodies can be drawn, which might be related to clayey channel facies.

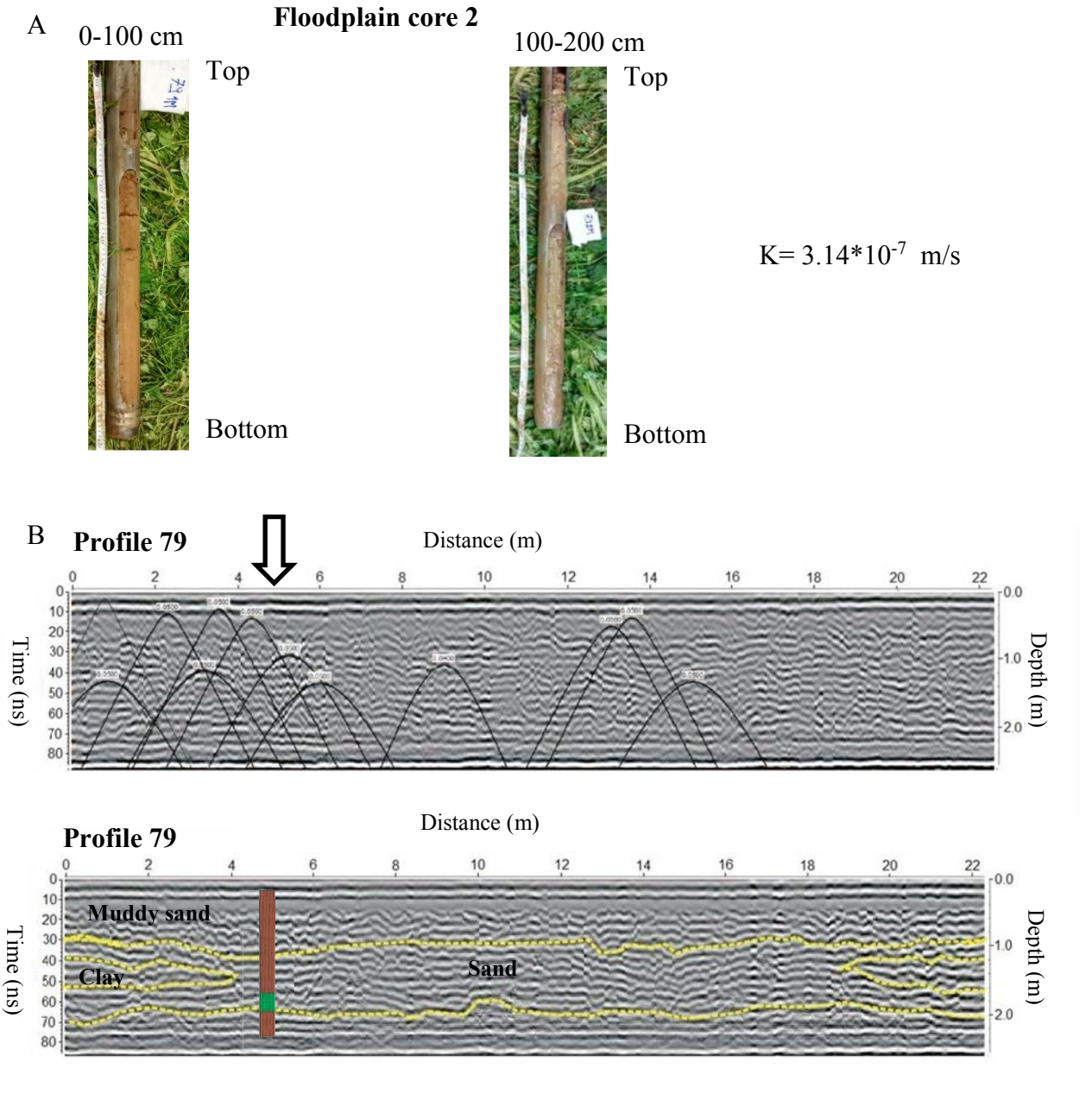

Figure 6.8 (A) Photographs of the floodplain core 2 with hydraulic conductivity (K) value derived from grain size analysis. (B) GPR profile 79 shows the location of the retrieved core (at position 5 m) and their interpretation, top image shows processed unmigrated radar record and bottom image shows processed migrated radar record (for GPR profiles and sampling locations see Figure 6.2).

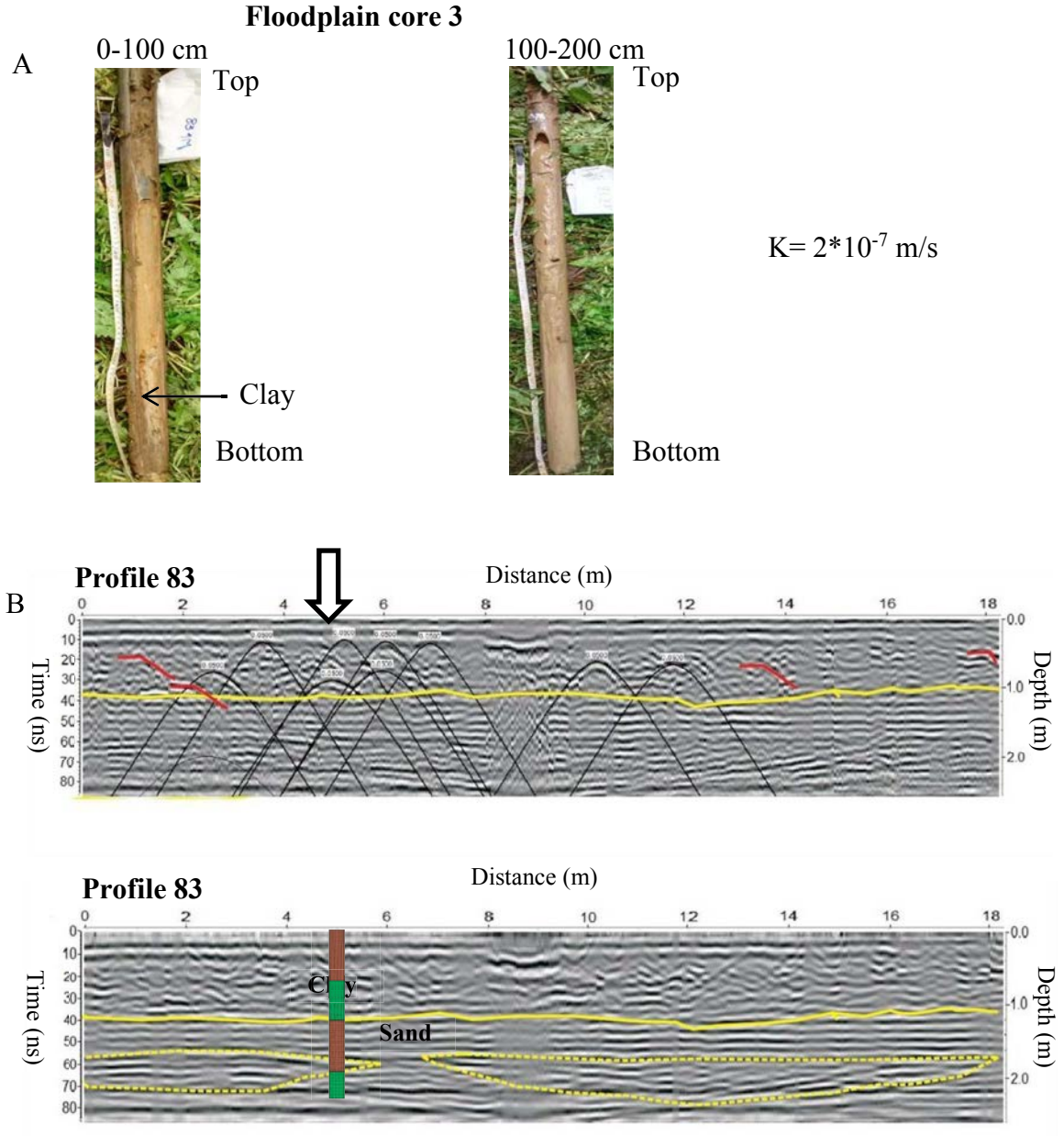

Figure 6.9 (A) photographs of the floodplain core 3 with hydraulic conductivity (K) value derived from grain size analysis. (B) GPR profile 83 shows the location of the retrieved core (at position 5 m) and their interpretation, top image shows processed unmigrated radar record and bottom image shows processed migrated radar record (for GPR profiles and sampling locations see Figure 6.2).

6.4.3 f) Profile 84

This profile was collected upstream of the profile 83. Core was taken at the 5 m location of the profile (Figure 6.2). The superposition of hyperbolic diffractions make difficult to draw the sub-horizontal reflections. The lower part of the line, from ~1.5 m depth, seems to be characterized by continuous parallel reflections dipping towards the beginning of the profile (towards the river). There is a sub-horizontal reflection at that depth that seems to cut the underlying dipping ones (may be channel base), with at least three points (meters 11, 16 and at the end of the line) where toplap relationships can be seen.

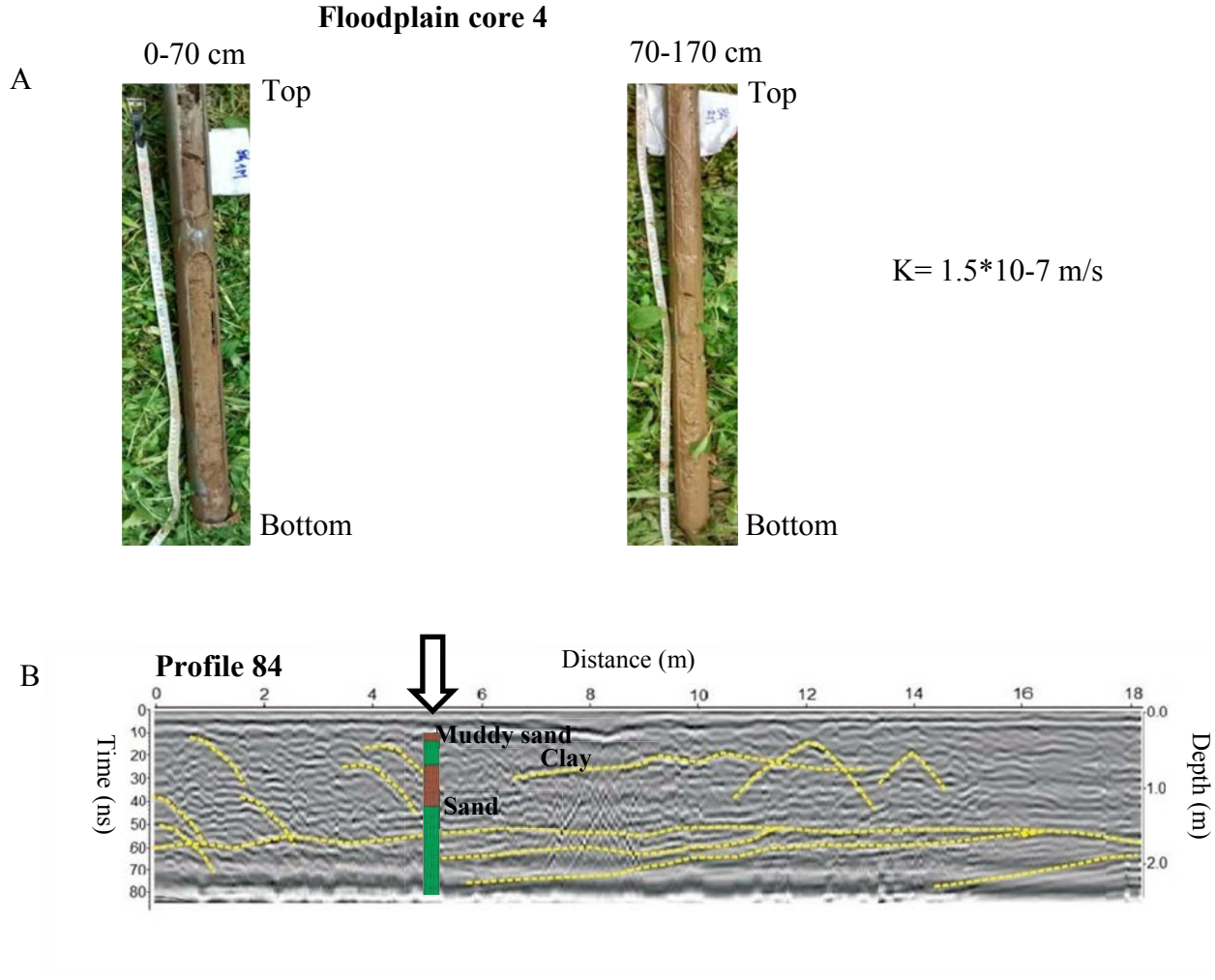

Figure 6.10 (A) Photographs of the floodplain core 4 with hydraulic conductivity (K) value derived from grain size analysis. (B) GPR profile 84 shows the location of the retrieved core (at position 5 m) and their interpretation (for GPR profiles and sampling locations see Figure 6.2).

6.4.4 GPR survey of the river channel

A longitudinal GPR profile matching with corresponding core logs of the shallow sandy bottomed Hammer stream, in West Sussex UK, is shown in Figure 6.2. The first strong reflections in the profile marked the sediment-water interface. Below, the shallow chaotic reflections can relate to saturated greyish yellow sand including wood fragments. Strong discontinuous sub-horizontal, chaotic reflections, associated with hyperbolic diffraction patterns corresponded to clay layers identified in the core logs. From 27 to ~ 35 m, the reflections are characterised by weak amplitude, chaotic and disturbed patterns as well as the disappearance of strong reflections. These configurations are interpreted as layers of sand deposits. Based on the stratigraphic evidence in this area (core sample 4), clay deposits are intermittent. Some multiple reflections caused by surface water are also present in the radar record (Figure 6.11 B).

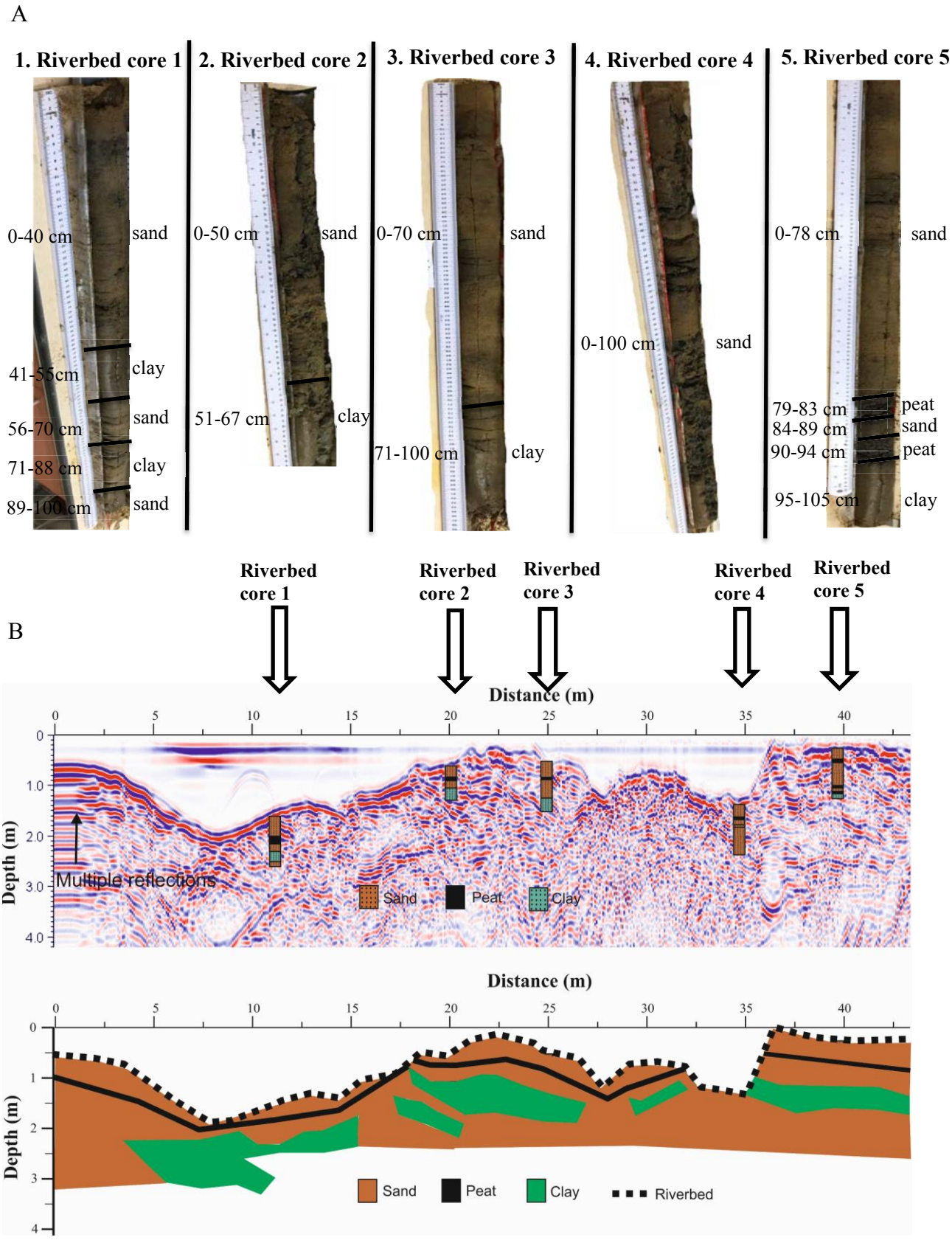

Figure 6.11 (A) photographs of the riverbed core samples with lithology outlines. (B) Longitudinal in-stream GPR survey and locations of the retrieved cores (Top) and geological interpretations (Bottom).

6.4.5 Insights from GPR imaging

With the use of 2-D GPR imaging as non-invasive technique, in conjunction with limited number of local point stratigraphy observed in core samples, it is possible to understand the lateral continuity of hydrostratigraphic units alluvial-scale with measurement densities deemed impractical with intrusive examination approaches alone (Binley et al., 2010). Figure 6.12 shows quasi three-dimensional profile which illustrates the detailed spatial distributions of low conductivity layers. Generally, the geology of the floodplain is comprised of fine particles such as clay, silt and different sizes of sand, based on stratigraphic evidence of core samples and grain size distribution (Appendix 4). Hence, the strong dielectric permittivity between sand and clay are thought to provide distinct reflections in radar images. The first continuous strong reflection which occurs in all GPR profiles is referred to as the ground wave. Below this, the top weak amplitude sub-horizontal reflections on the radargram agree well with the thickness of the sandy mud top unit. When comparing core samples to the GPR transects, the dominantly silt and clay sediments are compatible with prominent hyperbolic reflections (Figure 6.12). The hyperbolic reflections for all profiles are better fitted to a discrete object inside a 0.05–0.06 m/ns velocity medium. This velocity is compatible with pockets of high water-content fine grained sediment. All floodplain GPR profiles are characterised by a remarkable presence of clay structures dispersed within saturated regions. Saturated sediment deposits usually attenuate the GPR EM waves (Heteren et al., 1998) and thus the GPR reflections are weaker in amplitude in these regions. The sub-horizontal reflections that illustrate the most part of the floodplain GPR profiles indicate overbank vertical accretion deposits originating from the active river (e.g. fine sand, as observed in floodplain core samples) accumulated during flood stages. Several researchers (Asprion and Aigner, 1999; Huisink, 2000a; Słowik, 2013b) interpreted such GPR signals as stratified sheet flood deposits or vertically accreted bed-load sheets. The dipping GPR reflection

pattern as apparently see in Profile 76 indicates sand and silt sediment layering within channel bars. The sediment architecture suggests developments of point bar sediments and lateral migration of the channel bars.

At the bottom of some GPR profiles (e.g., line 80, 81, 82) (Appendix 6), geometry is observed in the form of a hyperbolic parallel (velocity 0.3 m/ns) reflection several metres wide (dome shape). Considering the geometry, it can correspond to aerial reflections due to the presence of a large tree canopy available predominantly in the study area.

In GPR line 79 (Figure 6.12), high conductive sediment (sand deposits) appeared in the form of a "conductive hole"; which is distinguished by sub-horizontal reflection in the radar record. This "conductive window hole" can clearly be seen in the middle part of the profile. Furthermore, the grain size analysis result for floodplain core 2 also indicated a high proportion of sand sediment measured in the core (Appendix 4). This is likely the floodplain received clastic materials from channel especially during flood events. Although the profile 80 was collected next to the profile 79 (5 m apart), hyperbolic reflections are predominant all along the profile 80 and with higher amount of it (Appendix 6). This result indicated that clay layers are abundant in this area of the floodplain (areas away from the active river channel). This was also confirmed through the stratigraphic evidence observed from floodplain core 3 and 4 (Figure 6.9A and Figure 6.10 A). The spatial distribution of clay across the study area can substantially affects groundwater flow pattern and consequently nutrient cycling processes such as oxygen and dissolved organic carbon (Naegeli et al., 1996). Smith et al. (2008) discovered that the attenuation potential increased in that areas corresponding with decreased mean grain size, this is occurring as a result of subsequent decreasing in hyporheic fluxes and increasing in contaminant residence time.

In profile 76, towards the river channel, hyperbolic structures are less frequent. This is likely due to the disruption of low conductivity layer (clay) towards the river channel (riverbed) in

this section of the study area. Profiles 77 correspond with strong sub-horizontal associated with hyperbolic reflections observed below the pool section in the river channel GPR survey. The extension of clay deposits from floodplain towards the river channel is more likely exist in this section of the study reach.

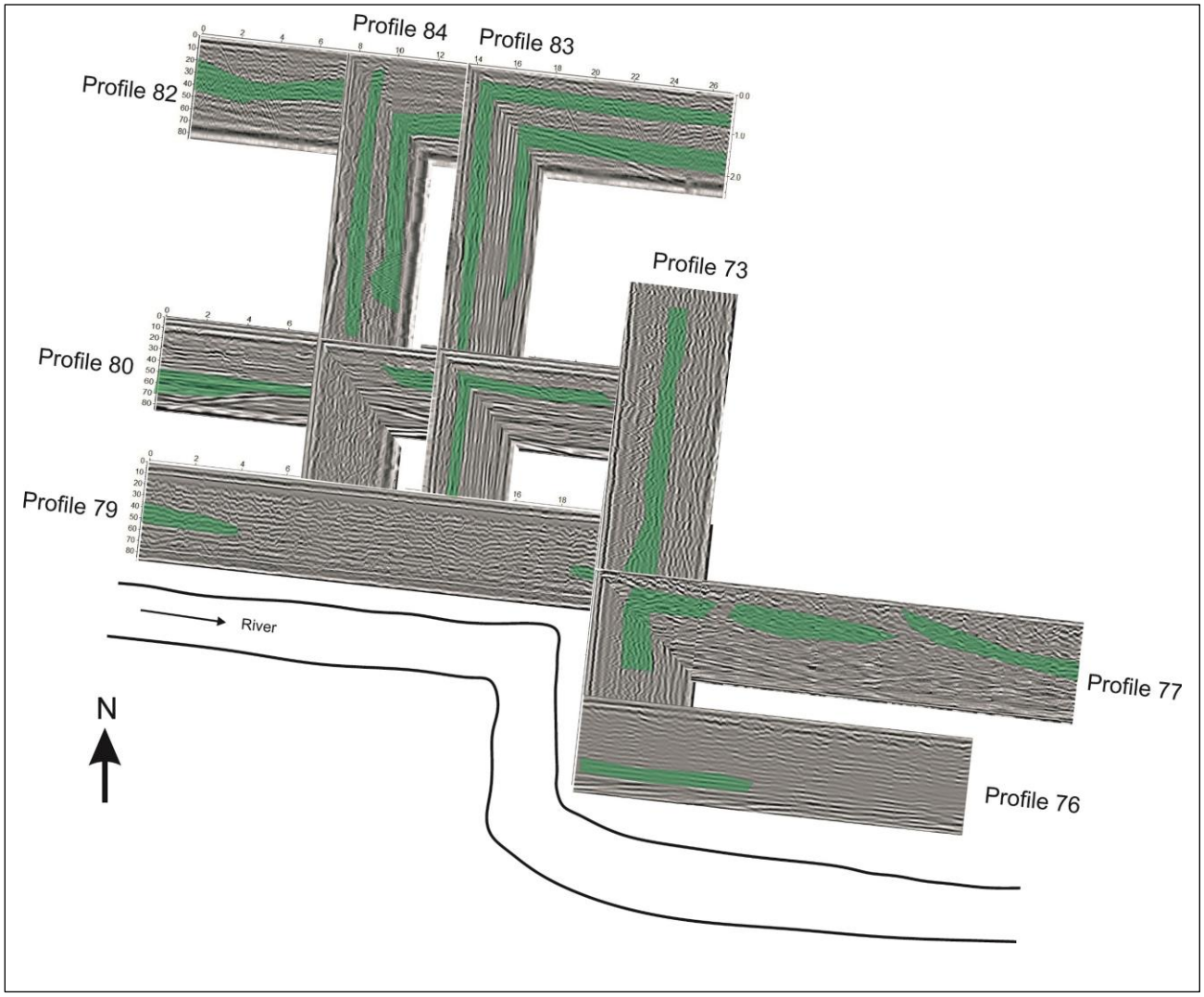

Figure 6.12 Quasi three-dimensional GPR profiles illustrating distribution and continuity of low conductivity layers (clay) in the Hammer stream floodplain.

6.4.6 Hydraulic conductivity variations

There is a strong link between sediment grain size and hydraulic conductivity, decrease in mean sediment grain size typically leads to decrease in hydraulic conductivity. Many researchers have highlighted the fact that fine grain sediments play an important role in contaminant attenuations, fluxes, residence times and temporary storage (Smith, 2005). Table 6.5 contains the hydraulic conductivity data for floodplain cores. The lowest value of K was measured in riverbed core 4 as the clay proportion in this core was the highest among them (Appendix 5).

Table 6.5 Hydraulic conductivity value determined from the floodplain cores based on the grain size analysis distribution (Hazen, 1911) method (for locations see Figure 6.2).

Core samples	(K (m/s)
Floodplain core 1	1.98E-07
Floodplain core 2	3.14E-07
Floodplain core 3	2.13E-07
Floodplain core 4	1.53E-07
Average	2.19E-07

Table 6.6 shows the saturated hydraulic conductivity data measured at two depth horizons. The results of the Hammer stream riverbed hydraulic conductivity using slug tests shows high and relatively low hydraulic conductivity values for shallow (20 cm) and deeper (50 cm), depths respectively. Eleven falling head tests in the riverbed piezometers were analysed using the (Hvorslev, 1951) method and gave conductivity ranging between 0.58 m/d and 7.22 m/d with an average of 3.76 m/d. For the shallow piezometer level (e.g. 20 cm) the water level inside the piezometers responded too quickly in all locations. This depth corresponded to the loose sand deposits associated with wood fragments which constitute most parts of the shallow riverbed (Figure 6.11 A).

Table 6.6 Saturated hydraulic conductivity values determined from the slug tests across the riverbed stream reach (for slug test locations see Figure 6.2 B).

Hvorslev (1951) method			
Slug test	Depth (cm)	K (m/d)	comments
S1	20	2.5	
S2	20	2.48	
S3	20	4.73	
S4	20	4.05	
S5	20	5.54	
S6	20	3.72	
S7	20	7.22	
S8	20	7.12	
S2-2	50	2.42	50 cm depth of slug test 2
S6-2	50	0.58	50 cm depth of slug test 6
S8-2	50	1.04	50 cm depth of slug test 8
Average		**3.76**	
Min		**0.58**	
Max		**7.22**	

The result of this study is consistent with the findings of Song et al. (2007), Chen (2011) and Binley et al. (2013). They have reported a decreasing trend in hydraulic conductivity with riverbed sediment depths. The highest value of hydraulic conductivity was observed at the upstream part of the meandering section (slug 7) (Figure 6.2B) at the thalweg of the stream reach. The outcomes generated by Genereux et al. (2008) credited the alterations in the vertical hydraulic conductivity throughout the river channel to the variations in the riverbed grain size texture, making it inversely proportional to the velocity of the water. Furthermore, they connected decline and increase in hydraulic conductivity to the erosion and deposition of sediments, respectively. The grain size distribution in the riverbed study site varies remarkably at different locations (Appendix 4 and Appendix 5) this could cause a different distribution of riverbed hydraulic conductivity and further impact on the distribution of water exchange fluxes. Wang et al. (2017) used Spearman's rank correlation test. They revealed

significant negative correlation between fine grained alluvial deposits (silt-clay content of the riverbed sediment) and riverbed hydraulic conductivity and VHG. This was inconsistent with the outcomes of Roque and Didier (2006), who found a negative exponential relationship between the weight of clay and silt and the hydraulic conductivity; therefore, sediment grain size can be one of major controlling factors of riverbed hydraulic conductivity and water fluxes at the study reach.

The range of saturated hydraulic conductivity values calculated in the Hammer stream riverbed (0.58–7.22 m/d) coincide with values defined by Freeze and and Cherry (1979) for clean sand, as also seen in the grain size distribution analysis. Conductivity measures of 0.01–8.37 m/d may be as low as those observed for low permeability clay sediments of 0.6–2.5m/d (Chen, 2004). These measures were also substantially lower than the mean values for sand as recorded in other research. Chen (2000) recorded 18.8–43 m/d, Chen (2011) reported 17–45 m/d, while Dong et al. (2012) observed 16.6 m/d for slightly silty sand. The low hydraulic conductivity values recorded for the greatest depths (50 cm) (Table 6.6) and their considerable variation possibly could be attributed to the presence of the low conductivity sediment layer, revealed in most of the sediment core samples (Figure 6.11 A). Hydraulic conductivity could be reduced significantly by merely a narrow layer of low conductivity material (Sebok et al., 2015). Exceptionally, relatively high hydraulic conductivity value was observed at the greatest depth in certain test sites, such as a slug test S2-2, at a depth of 50 cm (Table 6.6). This is likely to be lower clay layers being non-existent or interrupted, as illustrated in riverbed core 4 (Figure 6.11 A).

Other complicating aspects such as clogging processes (Brunke and Gonser, 1997; Blaschke et al., 2003), sedimentary structures (Packman et al., 2006; Leek et al., 2009), and hyporheic hydrologic processes (Song et al., 2007; Chen et al., 2013) could also be linked to the spatial distribution of riverbed hydraulic conductivity and groundwater-surface water exchange

fluxes. The formation of a clogging stratum in the riverbed can cause the dropping of the pore water volume, as well as a reduction of riverbed hydraulic conductivity; therefore it decreases the hydrological connections between groundwater and surface water at the sediment-water interface (Brunke and Gonser, 1997). The structural attributes of the riverbed sediment deposits can substantially affect hyporheic exchange flow (Leek et al., 2009); for example, with the high permeability gravel; the flow was much more rapid than with the sand-gravel mixtures (Packman et al., 2006). Hydrological processes, for instance groundwater upwelling flow pattern in riverbeds, can likely broaden pore space within riverbed sediments and result in an increase in riverbed hydraulic conductivity; thereby enhanced hyporheic exchange will likely occur (Song et al., 2007). On the other hand, downwelling flow patterns in riverbeds can decrease hydraulic conductivity (Rosenberry and Pitlick, 2009).

6.4.7 Perspectives on GPR reflections with low conductivity layers

It is difficult to distinguish low conductivity layers (peat and clay) on the GPR images, as the response of the low conductivity layers to the electromagnetic waves can be various. Thus, the interpretations of the GPR results are difficult if there is no geological information such as core logs and good outcrops. Moreover, in order to try to distinguish the lithology causing attenuation, it is important to compare the intensity of the reflections before applying the gain increase. If the GPR raw data shows an area with high attenuation, this might be related to the occurrence of clay, peat and sediment rich in organic matter. Whereas if we strongly increase the gain in order to see a better image of the stratigraphy, the differences in intensity may be removed and then it is more difficult to make lithological interpretation (Bristow and Jol, 2003).

It is widely recognised that low conductivity layers can excessively attenuate GPR signals and reduce its depth of penetration (Theimer et al., 1994; Heteren et al., 1998; Bristow and Jol, 2003). Boisson et al. (2011) found that heterogeneities inside silt sediments induced

electromagnetic energy losses from a GPR signal. If it is assumed that clay and peat attenuate GPR signal, the interpretation would vary depending on the material that is interbedded with the clay or peat, and the thickness of the clay or peat layers. For example, if the clay layer is very thin, it would provide a strong reflection due to the strong contrast in dielectric permittivity with other materials but wouldn't attenuate the GPR signal much (Ulriksen, 1982; Gómez-Ortiz et al., 2010), and with increasing thicknesses, a stronger attenuation of the GPR signal would occur (Jol and Smith, 1995). For example, Gómez-Ortiz et al. (2010) were able to delineate two distinctive clay layers in the Doñana National Park area in Spain, where clay layers were only a few cm in thickness and were bounded by aeolian sands. Consequently, the strongest reflections were corresponded to the clay layers in their study.

Another factor is the type of material that is found at the top and the bottom of the clay layers. Depending on the lithology and the water content, it is possible that there would not be a strong contrast in dielectric permittivity between the clay and its surrounding materials, and the reflection of the clay layer would be weak.

6.5 Conclusion

In this study, the local subsurface sedimentology preserved at the Hammer stream study site (west Sussex, UK) has been characterised by GPR. From the analysis of the GPR survey results and point sampling from core logs, hydrostratigraphic units in the floodplain and the river channel could be delineated. Grain-size distribution analyses revealed that mainly sand and clay grains are present with significantly high amounts of clay in floodplain cores. GPR reflection pattern were consequently distinguished based on differences in textural and structural characteristics of the sediment deposits. Unmigrated and migrated forms of some floodplain GPR forms were presented. The unsaturated top muddy sand observed at the top of floodplain GPR profiles and core samples have been interpreted as overbank deposits. The top sand layer in river channel profile was characterised by chaotic and disturbed reflections. The saturated clay mostly dominates the saturated zone along the river banks in the study area with different thicknesses and extensions. When comparing core samples to the GPR transects, the dominantly saturated clay sediments are compatible with prominent hyperbolic reflections which fit well to the velocity of 0.05-0.06 m/ns medium. These prominent reflections were used to define the upper part of the infinite clay layers throughout the profiles. These clay layers form an aquitard in the study area and characterised by low hydraulic conductivity (average = $2.2*10^{-7}$ m/s for floodplain sediments). In some places of the floodplain, these clay layers are extended towards the river channel. Nevertheless, some permeable zone exists in the form of “conductive hole” which might be an evidence of preferential flow in the study reach. the presence of low permeability clay structures which disperse within saturated region are likely to impact groundwater flow pattern along the bank and river corridor.

7 Discussion

7.1 Sedimentological/geophysical comparison between river Tern and Hammer stream sites

The interpretations of the GPR profiles were carried out based on the selection of areas with different GPR patterns of reflections. Therefore, based on the stratigraphic evidence observed in the core logs from both sites and correlating with radar reflection patterns, the low conductivity layers showed different reflection patterns in each site. For example, in the Tern river site (e.g. profile 9), the clay and peat (organic matter) layers produce a certain degree of GPR signal attenuation (e.g., radar facies 4 and 8, chapter 4) which can be interpreted as channel fill deposits based on the overall morphology and attenuation degree. In the Tern site, the attenuated unit is characterised by irregular geometry, undulating and disturbed, with a total absence of lateral continuity across the investigated reach, as well as not being delineated all along the profiles (Figure 7.1). Whereas, in the Hammer stream, based on the stratigraphic context forming the area, the strong dielectric contrast between clay and sand provides strong reflections. It has been observed that clay sediments are abundant in floodplain deposits. GPR profiles collected in the Hammer stream study site shows a large amount of hyperbolic structures at shallow depths, which fit well with 0.06 m/ns velocity medium. This velocity is compatible with pockets of fine-grained saturated layers (clay deposits) such as those seen in the floodplain 2. After core calibration with GPR profiles, especially at the lower part of some GPR profiles, a strong GPR reflection can correspond to a clayey or sandy clay layer (Figure 7.1). This layer appeared to be disconnected and shows in the form of lenticular bodies. This result indicated that in the Hammer site, the subsurface clay is laterally continuous with some local interruptions in which forming a ‘geological window’ of high conductivity layer in the study reach area (Figure 7.1).

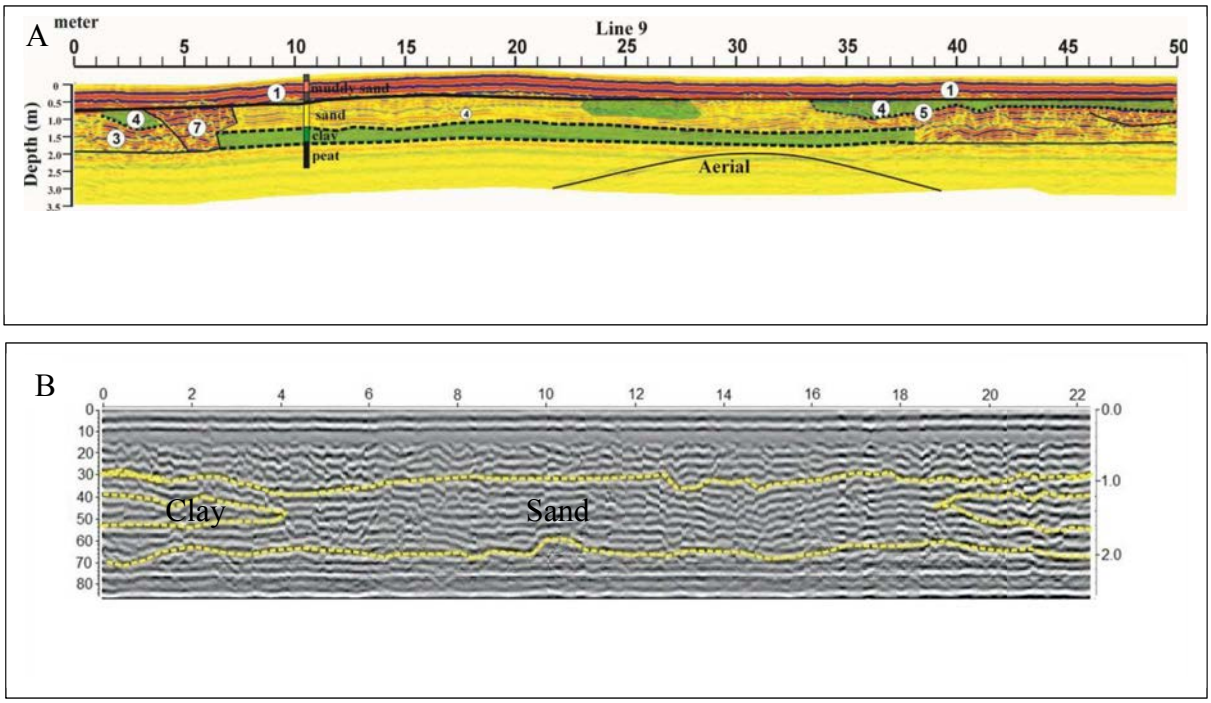

Figure 7.1 GPR result comparison between Tern and Hammer site (A) Profile 9 in Tern site and (B) Profile 73 in Hammer site.

7.2 Summary of key findings

The primary aim of this study was to develop and demonstrate the suitability of ground penetrating radar (GPR) in riverine research to identify the structural heterogeneity of both floodplain and in-stream channel sediments and analyse their impact on groundwater and surface water exchange flow and biogeochemical processes. The key workflow/conceptual model of the utility of GPR in this riverine research is shown in Figure 7.2. A new experimental approach has been developed, based on the determination of high resolution GPR surveys in the floodplain accompanied with longitudinal in stream surveys, in order to create a quasi-three-dimensional interpretation of the sub-surface that help to better understand the spatial distribution of heterogeneity in physical properties of the alluvial deposits. The subsurface lithology maintained at the River Tern study site is very complex and heterogeneous. Based on GPR profiles and core samples, quasi three-dimensional geological reconstruction of the Tern site helped to better understanding the radar facies of surficial sedimentary deposits as well as the spatial extent and geometry of the alluvial aquitard.

Low conductivity structures in the subsurface resulted in significantly attenuated GPR signals in floodplain and in-stream surveys at the Tern river site. The permeability distribution map (from GPR profiles) and derived three-dimensional model showed that low conductivity layers are distributed at different spatial locations with various thicknesses and extensions. These low conductivity structures have been interpreted as channel fill sediments. The results of GPR in riverine system and grain size analysis showed that the northern parts of the floodplain were rich in high conductivity strata, whereas, southern parts were dominated by low conductivity structures that in some places extended into the riverbed.

The geological information gained from GPR profiles confirmed that groundwater hydraulic heads observed in groundwater boreholes were controlled by low conductivity layers which

are distributed in the river Tern catchment as alluvial cap (channel fill sediment) covering Permo-Triassic sandstone.

At locations identified to be representative of the range of streambed hydrofacies (identified by GPR in investigated stream reach), a network of piezometers with multilevel pore samplers were designed to offer more insight into the groundwater and surface water exchanges flow patterns and biogeochemical processes at the sediment-water interface (Figure 7.2).

In-stream GPR surveys helped to delineate zones of contrasting sediment properties. Depth changes in hydraulic conductivity were observed. The presence of low-conductivity layers within the riverbed around the downstream and upstream piezometer clusters, as outlined in GPR surveys, caused prevailing pressure gradients in this region, driven by groundwater upwelling from the underlying sandstone bedrock. Peat and clay layers that dominate shallow lithology, especially in the downstream section, are likely to represent riverwards extensions of the low conductivity structures (alluvial aquitard) in the riparian zones. All measured vertical hydraulic gradients using riverbed piezometers were recorded as positive values during measurement campaigns, confirming widespread groundwater up-welling. Elevated VHG was observed in downstream piezometers where peat and clay structures were identified by GPR and core samples with low hydraulic conductivity values. This indicated that patterns of VHG in the riverbed were controlled by flow-confining deposits. The presence of low conductivity in this region may be inhibiting discharge of groundwater to the surface water (river). Above low conductivity lenses, the observed rather high flow velocity could be attributed to the surface water infiltration or horizontal flow patterns. The highest groundwater fluxes were observed at locations within high hydraulic conductivity regions (gravely sand area) (midstream area). These areas indicate the absence of low conductivity

structures, thus preferential discharge of groundwater as a result of enhanced connectivity to underlying aquifer is more likely.

Small-scale variability in riverbed physical properties have significantly influenced the fate of solutes (e.g., dissolved oxygen, dissolved organic carbon and nitrate) in upwelling groundwater flow paths. Significant reductions in nitrate and DO concentrations were recorded from pore-water within the boundaries of the low-conductivity riverbed strata. This reduction in nitrate and DO concentrations indicates that there was an increase in riverbed residence times due to the bulk low hydraulic conductivity. The anoxic conditions that arise after this depletion are highly conducive for reductive denitrification. Whereas, in the high-conductive region, preferential discharge from upwelling groundwater was associated with high nitrate and dissolved oxygen creating oxic conditions. Furthermore, there was a positive correlation between hydraulic conductivity and subsurface DO.

At the Hammer stream study site, which has investigated as a comparison for its general similar sediment properties but with substantially different distributions, grain size analysis of core samples revealed sand and clay particle were present. Clay was the dominant component at some of the core sampling sites. GPR provided distinct signal reflections due to strong dielectic contrasts between sand and clay. The prominent reflections were used to define the upper part of the infinite clay layers throughout the profiles. These clay layers form an aquitard in the study area and are characterised by low hydraulic conductivity. These low conductivity clay layers extend towards the river channel in part of the floodplain. Despite this, some permeable zones exist in the form of “conductive holes” which might be examples of preferential flow in the study reach. Variations in hydraulic conductivity with depth were observed. Upper layers recorded higher hydraulic conductivity values than lower layers. Relatively high hydraulic conductivity value was observed at the greatest depth in certain test sites. This is likely to be the lower clay layers being non-existent or interrupted, as illustrated

in riverbed cores and GPR profiles. Thus, the presence of low permeability clay structures which disperse within saturated region are likely to impact groundwater flow patterning along the bank and river corridor. The revealed impact of strongly heterogeneous physical streambed properties on hotspots of enhanced residence time and biogeochemical turnover highlights the value of GPR-based high-resolution streambed monitoring.

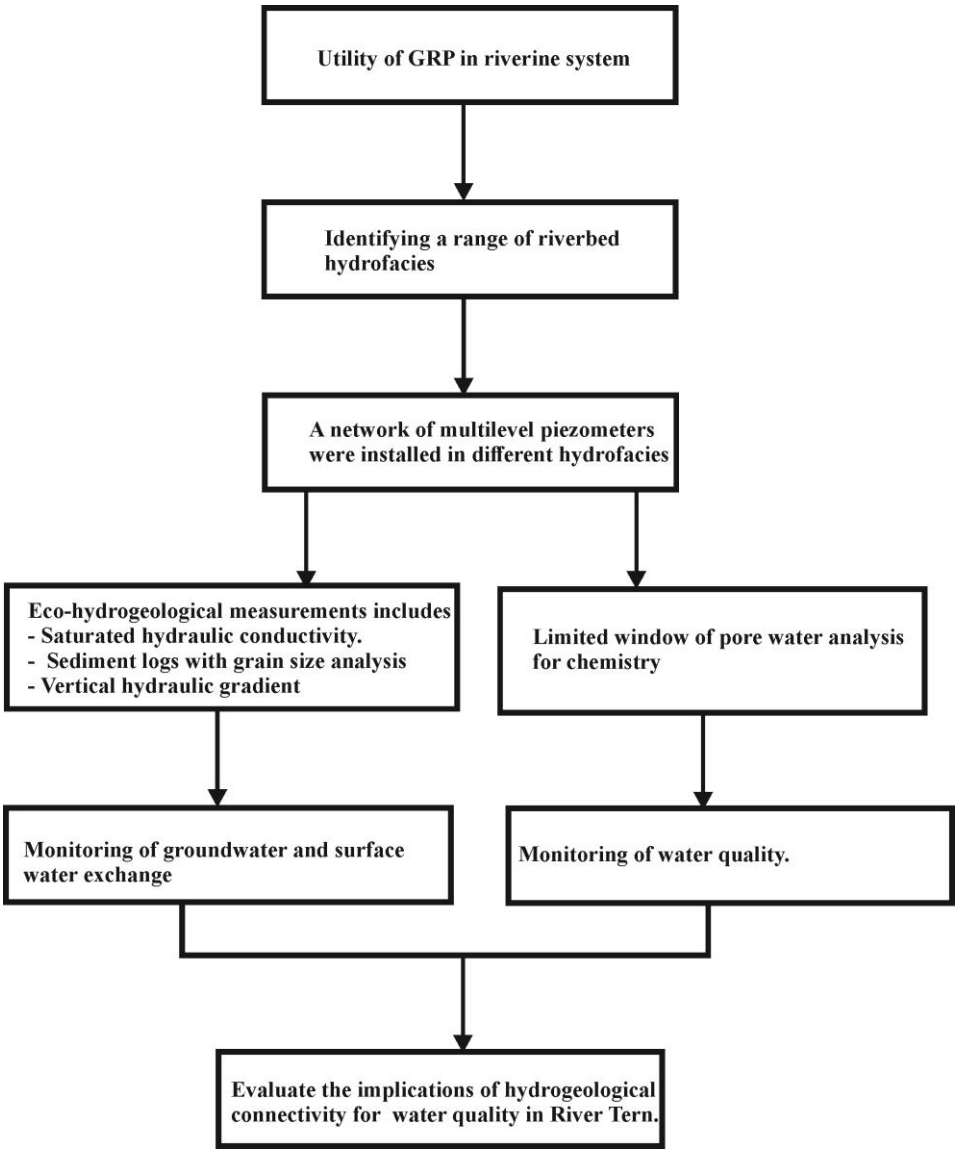

Figure 7.2 Key workflow shows the outcomes of the PhD research

7.3 Synthesis

This section synthesises the new understanding provided in the thesis to identify spatial patterns in riverbed physical properties as the main controls of groundwater and surface water exchange flow patterns and biogeochemical processes.

In this study, investigations using a combination of novel in-stream GPR with riparian surveys, in conjunction with point observations of local lithology from core logs, suggest that aquifer-to-river hydraulic connectivity, biogeochemical processes and residence times are controlled by near-river sediment heterogeneities. Hence, detailed knowledge of architecture and spatial distribution of sediments in the hyporheic zone is crucial for understanding the biotransformation and transport of discharging groundwater contaminants.

This study highlights that GPR is a suitable technology for efficiently identifying the spatial distributions of subsurface structures (and their spatial heterogeneity across different scales) (spatial distribution of high versus low permeability fields) that control water fluxes in river corridors, including the exchange between river and aquifer and biogeochemical processes. With the permeability field distribution, this study develops a suitable tool for identifying subsurface flow controls with impact on spatial patterns of groundwater and surface water exchange, including hot spots of groundwater upwelling into riverbed environments.

The application of GPR in two contrasting geological settings revealed contrasting patterns and dynamics of subsurface flow controls, resulting in very different residence time distribution in the riverbed. The resulting RTD evidently had significant impact on the transport and transformation of solutes such as DO and NO_3. The spatial patterning of the subsurface low conductivity structures differs heavily between sites. In lowland settings, the complexity of the geology which controls flow pathways and residence time distribution, for example, small scale variability in streambed physical properties; including hotspots, have substantial impact on biogeochemical processes.

Thus, this study contributes significant evidence of the relevance of small scale structural heterogeneity in lowland meandering subsurface environments, to the discussion of the importance of small-scale drivers and controls on hyporheic exchange flow patterns and biogeochemical cycling for larger scale assessments – at least for lowland rivers proven to be essential.

7.4 Limitations and outlook for future research

Each of the chapters represents significant contributions towards identifying streambed structural heterogeneity (very detailed geology) using GPR on groundwater and surface water exchange flow paths and biogeochemical processes. Extending observations and research beyond these two sites will lead to improved mechanistic process understanding of drivers and controls of exchange fluxes and biogeochemical cycling at groundwater – surface water interfaces on a wider spatial and interdisciplinary scale. Different geophysical methods in combination increase certainty and confidence in results. Moreover, collecting geophysical data with different configuration and therefore high resolution and depth penetration needs to be investigated for future hydrogeophysical research. This study focused on two river sites only. Investigations into the relationship between sediment structural heterogeneity to the transformations of the contaminants in other river sites with distinct geological characteristics are needed. One-dimensional vertical fluxes were measured through the riverbed in Tern site. Point-dilutions tracer test could be performed in piezometers to measure the contribution of horizontal flow patterns (Binley et al., 2013). Riverbed hydraulic conductivity and its anisotropy could also be examined using permeameter test (Conant, 2004) for a more robust analysis of hydraulic connectivity between aquifer and river. This study did not take into account the temporal variability of streambed sediments. Future research is needed to investigate temporal variability of streambed sediments. Limited window of analysis for chemistry provided a very important snapshot but further analysis of system dynamics in time

would be beneficial. Furthermore, total amounts of nitrate transport to the shallow riverbed in preferential groundwater discharge zone needs to be investigated under different conditions.

8 References

ADAMS, B., PEACH, D. & BLOOMFIELD, J. 2003. The LOCAR hydrogeological infrastructure in the tern catchment. Groundwater Systems and Water Quality Programme, Internal Report IR/03/180. British Geological Survey, Keyworth.

Alley, W. M., Healy, R. W., LaBaugh, J. W., Reilly, T. E., 2002. Flow and storage in groudwater systems. *Science* 296, 1985–1990.

AMBUS, P., MOSIER, A.R., CHRISTENSEN, S., 1992. Nitrogen turnover rates in a riparian fen determined by 15N dilution. Biol. Fertil. Soils 14, 230-236.

ANGERMANN, L., KRAUSE, S. & LEWANDOWSKI, J. 2012. Application of heat pulse injections for investigating shallow hyporheic flow in a lowland river. *Water Resources Research,* 48, W00P02, DOI: 10.1029/2012WR012564.

ANIBAS, C., BUIS, K., VERHOEVEN, R., MEIRE, P. & BATELAAN, O. 2011. A simple thermal mapping method for seasonal spatial patterns of groundwater–surface water interaction. *Journal of Hydrology,* 397**,** 93-104.

ANNAN, A. P. 2005. Electromagnetic principles of ground penetrating radar. *In:* JOL, H. M. (ed.) *Ground penetrating radar: theory and applications.* Amsterdam: Elsevier, 3-40.

ARRIGONI, A. S., POOLE, G. C., MERTES, L. A., O'DANIEL, S. J., WOESSNER, W. W. & THOMAS, S. A. 2008. Buffered, lagged, or cooled? Disentangling hyporheic influences on temperature cycles in stream channels. *Water Resources Research,* 44.

ASPRION, U. & AIGNER, T. 1999. Towards realistic aquifer models: three-dimensional georadar surveys of Quaternary gravel deltas (Singen Basin, SW Germany). *Sedimentary Geology,* 129**,** 281-297.

BAKER, M. A., DAHM, C. N. & VALETT, H. M. 1999. Acetate retention and metabolism in the hyporheic zone of a mountain stream. *Limnology and Oceanography,* 44, 1530-1539.

BAKER, M. A., DAHM, C. N. & VALETT, H. M. 2000. Anoxia, anaerobic metabolism and biogeochemistry of the stream water–groundwater groundwater interface. *In:* JONES, J. B., MULHOLLAND, P.J. (ed.) *Streams and Ground Waters.* Academic Press, New York.

BAKER, M.A., VERVIER, P., 2004. Hydrological variability, organic matter supply and denitrification in the Garonne River ecosystem. Freshw. Biol. 49, 181-190.

BANO, M., MARQUIS, G., NIVIÈRE, B., MAURIN, J. & CUSHING, M. 2000. Investigating alluvial and tectonic features with ground-penetrating radar and analyzing diffractions patterns. *Journal of Applied Geophysics,* 43**,** 33-41.

BARDINI, L., BOANO, F., CARDENAS, M. B., SAWYER, A. H., REVELLI, R. & RIDOLFI, L. 2013. Small-scale permeability heterogeneity has negligible effects on nutrient cycling in streambeds. *Geophysical Research Letters,* 40**,** 1118-1122.

BARONE, P., MATTEI, E. & PETTINELLI, E. 2013. Non-invasive archaeological exploration in stratigraphically complex rural settings: an example from Ferento (Viterbo, Italy). *Archaeological and Anthropological Sciences,* 5**,** 267-273.

BAXTER, C., HAUER, F. R. & WOESSNER, W. W. 2003. Measuring groundwater–stream water exchange: new techniques for installing minipiezometers and estimating hydraulic conductivity. *Transactions of the American Fisheries Society,* 132**,** 493-502.

BENCALA, K. E. 1993. A perspective on stream-catchment connections. *Journal of the North American Benthological Society***,** 44-47.

BERES, M., GREEN, A., HUGGENBERGER, P. & HORSTMEYER, H. 1995. Mapping the architecture of glaciofluvial sediments with three-dimensional georadar. *Geology,* 23**,** 1087.

BERES, M. & HAENI, F. 1991. Application of ground-penetrating-radar methods in Hydrogeologie Studies. *Ground Water,* 29**,** 375-386.

BERSEZIO, R., GIUDICI, M. & MELE, M. 2007. Combining sedimentological and geophysical data for high-resolution 3-D mapping of fluvial architectural elements in the Quaternary Po plain (Italy). *Sedimentary Geology,* 202**,** 230-248.

BEST, J., WOODWARD, J., ASHWORTH, P., SMITH, G. S. & SIMPSON, C. 2006. Bar-top hollows: A new element in the architecture of sandy braided rivers. *Sedimentary Geology,* 190**,** 241-255.

BINLEY, A., CASSIANI, G. & DEIANA, R. 2010. Hydrogeophysics: Opportunities and challenges. *Boll. Geofis. Teor. Appl.,* 51**,** 267-284.

BINLEY, A., HUBBARD, S. S., HUISMAN, J. A., REVIL, A., ROBINSON, D. A., SINGHA, K. & SLATER, L. D. 2015. The emergence of hydrogeophysics for improved understanding of subsurface processes over multiple scales. *Water Resources Research,* 51**,** 3837-3866.

BINLEY, A., ULLAH, S., HEATHWAITE, A. L., HEPPELL, C., BYRNE, P., LANSDOWN, K., TRIMMER, M. & ZHANG, H. 2013. Revealing the spatial variability of water fluxes at the groundwater-surface water interface. *Water Resources Research,* 49**,** 3978-3992.

BINLEY, A., WINSHIP, P., POKAR, M. & WEST, J. Cross borehole radar and resistivity tomography: a comparison of techniques in unsaturated sandstone. Symp. Applications of Geophysics to Engineering and Environmental Problems (SAGEEP), 2001.

BITTON, G., 1994. Role of microorganisms in biogeochemical cycles. Wastewater Microbiology, Third Edition, pp.75-105.

BITTON, G. & GERBA, C. P. 1994. Groundwater pollution microbiology. Malabar, USA: Krieger Publishing Company, 377pp.

BLASCHKE, A. P., STEINER, K. H., SCHMALFUSS, R., GUTKNECHT, D. & SENGSCHMITT, D. 2003. Clogging processes in hyporheic interstices of an impounded river, the Danube at Vienna, Austria. *International Review of Hydrobiology,* 88**,** 397-413.

BLOTT, S. J. & PYE, K. 2001. GRADISTAT: a grain size distribution and statistics package for the analysis of unconsolidated sediments. *Earth surface processes and Landforms,* 26**,** 1237-1248.

BOANO, F., CAMPOREALE, C., REVELLI, R. & RIDOLFI, L. 2006. Sinuosity-driven hyporheic exchange in meandering rivers. Geophysical Research Letters, 33, L18406, doi:10.1029/2006GL027630.

BOANO, F., REVELLI, R. & RIDOLFI, L. 2007. Bedform-induced hyporheic exchange with unsteady flows. *Advances in water resources,* 30**,** 148-156.

BOANO, F., REVELLI, R. & RIDOLFI, L. 2009. Quantifying the impact of groundwater discharge on the surface–subsurface exchange. *Hydrological processes,* 23**,** 2108-2116.

BOARDMAN, J., SHEPHEARD, M. L., WALKER, E. & FOSTER, I. D. 2009. Soil erosion and risk-assessment for on-and off-farm impacts: A test case using the Midhurst area, West Sussex, UK. *Journal of environmental management,* 90**,** 2578-2588.

BOARDMAN, J. & VANDAELE, K. 2016. Effect of the spatial organization of land use on muddy flooding from cultivated catchments and recommendations for the adoption of control measures. *Earth Surface Processes and Landforms,* 41, 336-343.

BOISSON, J., HEGGY, E., CLIFFORD, S. M., YOSHIKAWA, K., ANGLADE, A. & LOGNONNÉ, P. 2011. Radar sounding of temperate permafrost in Alaska: Analogy to the Martian midlatitude to high-latitude ice-rich terrains. *Journal of Geophysical Research: Planets,* 116, E11003, doi:10.1029/2010JE003768.

BOULTON, A. J., DATRY, T., KASAHARA, T., MUTZ, M. & STANFORD, J. A. 2010. Ecology and management of the hyporheic zone: stream–groundwater interactions of running waters and their floodplains. *Journal of the North American Benthological Society,* 29**,** 26-40.

BOULTON, A. J., FINDLAY, S., MARMONIER, P., STANLEY, E. H. & VALETT, H. M. 1998. The functional significance of the hyporheic zone in streams and rivers. *Annual Review of Ecology and Systematics***,** 29, 59-81.

BRADFORD, J. H., MCNAMARA, J. P., BOWDEN, W. & GOOSEFF, M. N. 2005. Measuring thaw depth beneath peat-lined arctic streams using ground-penetrating radar. *Hydrological Processes,* 19**,** 2689-2699.

BRIDGE, J. S., ALEXANDER, J., COLLIER, R. E., GAWTHORPE, R. L. & JARVIS, J. 1995. Ground-penetrating radar and coring used to study the large-scale structure of point-bar deposits in three dimensions. *Sedimentology,* 42**,** 839-852.

BRIGGS, M. A., LAUTZ, L. K. & HARE, D. K. 2014. Residence time control on hot moments of net nitrate production and uptake in the hyporheic zone. *Hydrological Processes,* 28**,** 3741-3751.

BRIGGS, M. A., LAUTZ, L. K., HARE, D. K. & GONZÁLEZ-PINZÓN, R. 2013. Relating hyporheic fluxes, residence times, and redox-sensitive biogeochemical processes upstream of beaver dams, Freshwater Science, 32,622-641.

BRISTOW, C., SKELLY, R. & ETHRIDGE, F. 1999. Crevasse splays from the rapidly aggrading, sand-bed, braided Niobrara River, Nebraska: effect of base-level rise. *Sedimentology,* 46**,** 1029-1048.

BRISTOW, C. S. & JOL, H. M. 2003. An introduction to ground penetrating radar (GPR) in sediments. *Geological Society, London, Special Publications,* 211**,** 1-7.

BROSTEN, T. R., BRADFORD, J. H., MCNAMARA, J. P., ZARNETSKE, J. P., GOOSEFF, M. N. & BOWDEN, W. B. 2006. Profiles of temporal thaw depths beneath two arctic stream types using ground-penetrating radar. *Permafrost and Periglacial Processes,* 17**,** 341-355.

BRUNKE, M. & GONSER, T. 1997. The ecological significance of exchange processes between rivers and groundwater. *Freshwater biology,* 37**,** 1-33.

BUFFINGTON, J. M. & MONTGOMERY, D. R. 1999. Effects of sediment supply on surface textures of gravel-bed rivers. *Water Resources Research,* 35**,** 3523-3530.

BURKHOLDER, B. K., GRANT, G. E., HAGGERTY, R., KHANGAONKAR, T. & WAMPLER, P. J. 2008. Influence of hyporheic flow and geomorphology on temperature of a large, gravel-bed river, Clackamas River, Oregon, USA. *Hydrological Processes,* 22**,** 941-953.

BURNETTE, M. C., GENEREUX, D. P. & BIRGAND, F. 2016. In-situ falling-head test for hydraulic conductivity: Evaluation in layered sediments of an analysis derived for homogenous sediments. *Journal of Hydrology,* 539**,** 319-329.

BURT, T.P., PINAY, G., SABATER, S., 2010. What we still need to know about the ecohydrology of riparian zones? Ecohydrology 3, 373-377.

BYRNE, P., BINLEY, A., HEATHWAITE, A., ULLAH, S., HEPPELL, C., LANSDOWN, K., ZHANG, H., TRIMMER, M. & KEENAN, P. 2014. Control of river stage on the reactive chemistry of the hyporheic zone. *Hydrological Processes,* 28**,** 4766-4779.

CARDENAS, M. B. 2008. Surface water-groundwater interface geomorphology leads to scaling of residence times. *Geophysical Research Letters,* 35, L08402, doi:10.1029/2008GL033753.

CARDENAS, M. B. & JIANG, X. W. 2010. Groundwater flow, transport, and residence times through topography-driven basins with exponentially decreasing permeability and porosity. Water Resources Research, 46, DOI: 10.1029/2010WR009370.

CARDENAS, M. B., WILSON, J. & ZLOTNIK, V. A. 2004. Impact of heterogeneity, bed forms, and stream curvature on subchannel hyporheic exchange. Water Resources Research, 40, W08307, doi:10.1029/2004WR003008.

CARDENAS, M. B. & WILSON, J. L. 2007. Dunes, turbulent eddies, and interfacial exchange with permeable sediments. *Water Resources Research*, 43, W08412. doi:10.1029/2006WR005787.

CARDENAS, M. B. & ZLOTNIK, V. A. 2003. Three-dimensional model of modern channel bend deposits. *Water Resources Research,* 39, 1141, doi:10.1029/2002WR001383.

CASSIDY, N. J. 2009. Electrical and magnetic properties of rocks, soils and fluids. In: Jol, H.M. (ed.), Ground penetrating radar: theory and applications, Elsevier: Amsterdam; 41-72.

CASSIDY, N. J. & JOL, H. 2009. Ground penetrating radar data processing, modelling and analysis. In: Jol, H.M. (ed.), Ground penetrating radar: theory and application, Elsevier: Amsterdam; 141-176.

CHAFIQ, M., GIBERT, J. & CLARET, C. 1999. Interactions among sediments, organic matter, and microbial activity in the hyporheic zone of an intermittent stream. *Canadian Journal of Fisheries and Aquatic Sciences*, 56**,** 487-495.

CHEN, X. 2000. Measurement of streambed hydraulic conductivity and its anisotropy. *Environmental Geology,* 39**,** 1317-1324.

CHEN, X. 2004. Streambed hydraulic conductivity for rivers in south-central Nebraska. *JAWRA Journal of the American Water Resources Association,* 40**,** 561-573.

CHEN, X. 2011. Depth-dependent hydraulic conductivity distribution patterns of a streambed. *Hydrological Processes,* 25**,** 278-287.

CHEN, X., DONG, W., OU, G., WANG, Z. & LIU, C. 2013. Gaining and losing stream reaches have opposite hydraulic conductivity distribution patterns. *Hydrology and Earth System Sciences,* 17**,** 2569.

CHENG, D.-H., CHEN, X.-H., HUO, A.-D., MIN, G. & WANG, W.-K. 2013. Influence of bedding orientation on the anisotropy of hydraulic conductivity in a well-sorted fluvial sediment. *International Journal of Sediment Research,* 28**,** 118-125.

CLARET, C. & BOULTON, A. J. 2009. Integrating hydraulic conductivity with biogeochemical gradients and microbial activity along river–groundwater exchange zones in a subtropical stream. *Hydrogeology Journal,* 17**,** 151-160.

CLIFFORD, J. & BINLEY, A. 2010. Geophysical characterization of riverbed hydrostratigraphy using electrical resistance tomography. *Near Surface Geophysics,* 8**,** 493-501.

COMAS, X., SLATER, L. & REEVE, A. 2004. Geophysical evidence for peat basin morphology and stratigraphic controls on vegetation observed in a Northern Peatland. *Journal of Hydrology,* 295**,** 173-184.

CONANT, B. 2004. Delineating and quantifying ground water discharge zones using streambed temperatures. *Ground Water,* 42**,** 243-257.

CONANT, B., CHERRY, J. A. & GILLHAM, R. W. 2004. A PCE groundwater plume discharging to a river: influence of the streambed and near-river zone on contaminant distributions. *Journal of Contaminant Hydrology,* 73**,** 249-279.

COVINO, T. 2017. Hydrologic connectivity as a framework for understanding biogeochemical flux through watersheds and along fluvial networks. *Geomorphology,* 277**,** 133-144.

CRISPELL, J. K. & ENDRENY, T. A. 2009. Hyporheic exchange flow around constructed in-channel structures and implications for restoration design. *Hydrological Processes,* 23**,** 1158-1168.

CROOK, N., BINLEY, A., KNIGHT, R., ROBINSON, D., ZARNETSKE, J. & HAGGERTY, R. 2008. Electrical resistivity imaging of the architecture of substream sediments. *Water Resources Research,* 44, 1-11.

CUTHBERT, M. O., MACKAY, R., DURAND, V., ALLER, M. F., GRESWELL, R. B. & RIVETT, M. O. 2010. Impacts of river bed gas on the hydraulic and thermal dynamics of the hyporheic zone. *Advances in Water Resources,* 33**,** 1347-1358.

D'ANGELO, D., WEBSTER, J., GREGORY, S. & MEYER, J. 1993. Transient storage in Appalachian and Cascade mountain streams as related to hydraulic characteristics. *Journal of the North American Benthological Society***,** 12, 223-235.

DAILY, W. & RAMIREZ, A. L. 2000. Electrical imaging of engineered hydraulic barriers. *Geophysics,* 65**,** 83-94.

DATRY, T., LAMOUROUX, N., THIVIN, G., DESCLOUX, S. & BAUDOIN, J. 2015. Estimation of sediment hydraulic conductivity in river reaches and its potential use to evaluate streambed clogging. *River Research and Applications,* 31**,** 880-891.

DAVIS, J. & ANNAN, A. 1989. Ground penetrating radar for high-resolution mapping of soil and rock stratigraphy. *Geophysical Prospecting,* 37**,** 531-551.

DIETRICH, W. E., KIRCHNER, J. W., IKEDA, H. & ISEYA, F. 1989. Sediment supply and the development of the coarse surface layer in gravel-bedded rivers. *Nature,* 340**,** 215-217.

DONG, W., CHEN, X., WANG, Z., OU, G. & LIU, C. 2012. Comparison of vertical hydraulic conductivity in a streambed-point bar system of a gaining stream. *Journal of Hydrology,* 450**,** 9-16.

DUDLEY-SOUTHERN, M. & BINLEY, A. 2015. Temporal responses of groundwater-surface water exchange to successive storm events. *Water Resources Research,* 51**,** 1112-1126.

DUFF, J. H. & TRISKA, A. F. J. 2000. Nitrogen biochemistry and surfacesubsurface exchange in streams. *In:* MULHOLLAND, J. B. J. A. P. J. (ed.) *Streams and Groundwater.* Academic Press, London, 197–220.

DUFF, J. H. & TRISKA, F. J. 1990. Denitrifications in sediments from the hyporheic zone adjacent to a small forested stream. *Canadian Journal of Fisheries and Aquatic Sciences,* 47**,** 1140-1147.

EC. 2000. Directive 2000/60/EC of the European Parliament and of the Council of 23 October 2000 establishing a framework for community action in the field of water policy. European Commission. Available: http://eur-lex.europa.eu/legal-content/EN/TXT/HTML/?uri=CELEX:32000L0060&from=en [Accessed 16 May 2017].

EKES, C. & HICKIN, E. J. 2001. Ground penetrating radar facies of the paraglacial Cheekye Fan, southwestern British Columbia, Canada. *Sedimentary Geology,* 143**,** 199-217.

ELLIOTT, A. H. & BROOKS, N. H. 1997a. Transfer of nonsorbing solutes to a streambed with bed forms: Laboratory experiments. *Water Resources Research,* 33**,** 137-151.

ELLIOTT, A. H. & BROOKS, N. H. 1997b. Transfer of nonsorbing solutes to a streambed with bed forms: Theory. *Water Resources Research,* 33**,** 123-136.

ELLIS, P. A. 2003. *The impact of urban groundwater upon surface water quality: Birmingham-River Tame study, UK.* Unpublished PhD thesis, School of Earth Sciences, University of Birmingham.

ENDRENY, T. & LAUTZ, L. 2012. Comment on 'Munz M, Krause S, Tecklenburg C, Binley A. Reducing monitoring gaps at the aquifer–river interface by modelling groundwater–surfacewater exchange flow patterns. Hydrological Processes. DOI: 10.1002/hyp. 8080'. *Hydrological Processes,* 26**,** 1586-1588.

ENDRENY, T., LAUTZ, L. & SIEGEL, D. 2011. Hyporheic flow path response to hydraulic jumps at river steps: Flume and hydrodynamic models. Water Resources Research, 47, W02517, doi:10.1029/2009WR008631.

FETTER, C. W. 1994. Applied Hydrogeology. Third Edition, Mc Millian College Publishing Company, New York.

FETTER, C. W. 2000. *Applied hydrogeology,* Prentice hall.

FINDLAY, S., 1995. Importance of surface-subsurface exchange in stream ecosystems: The hyporheic zone. Limnology and oceanography, 40, 159-164.

FINDLAY, S. & SOBCZAK, W. V. 1996. Variability in removal of dissolved organic carbon in hyporheic sediments. *Journal of the North American Benthological Society,* 15**,** 35-41.

FISHER, S. G., GRIMM, N. B., MARTÍ, E., HOLMES, R. M. & JONES JR, J. B. 1998. Material spiraling in stream corridors: a telescoping ecosystem model. *Ecosystems,* 1**,** 19-34.

FLECKENSTEIN, J. H., NISWONGER, R. G. & FOGG, G. E. 2006. River-aquifer interactions, geologic heterogeneity, and low-flow management. *Ground water,* 44**,** 837-852.

FLEWELLING, S. A., HERMAN, J. S., HORNBERGER, G. M. & MILLS, A. L. 2012. Travel time controls the magnitude of nitrate discharge in groundwater bypassing the riparian zone to a stream on Virginia's coastal plain. *Hydrological Processes,* 26**,** 1242-1253.

FOLK, R. L. 1980. *Petrology of sedimentary rocks,* Austin, Hemphill Publishing Company.

FOLK, R. L. & WARD, W. C. 1957. Brazos River bar: a study in the significance of grain size parameters. *Journal of Sedimentary Research,* 27, 3-26.

FOSTER, S. 2000. The Ninth Ineson Lecture Assessing and Controlling the Impacts of Agriculture on Groundwater—from Barley Barons to Beef Bans. *Quarterly Journal of Engineering Geology and Hydrogeology,* 33**,** 263-280.

FREEZE, R. A. & AND CHERRY, J. A. 1979. *Groundwater,* Englewood Cliffs, NJ: Prentice Hall, 604 pp.

FRIEDMAN, G. M. 1979. Differences in size distributions of populations of particles among sands of various origins: addendum to IAS Presidential Address. *Sedimentology,* 26**,** 859-862.

FROESE, D. G., SMITH, D. G. & CLEMENT, D. T. 2005. Characterizing large river history with shallow geophysics: Middle Yukon River, Yukon Territory and Alaska. *Geomorphology,* 67**,** 391-406.

FULLER, C. C. & HARVEY, J. W. 2000. Reactive uptake of trace metals in the hyporheic zone of a mining-contaminated stream, Pinal Creek, Arizona. *Environmental Science & Technology,* 34**,** 1150-1155.

GENEREUX, D. P., LEAHY, S., MITASOVA, H., KENNEDY, C. D. & CORBETT, D. R. 2008. Spatial and temporal variability of streambed hydraulic conductivity in West Bear Creek, North Carolina, USA. *Journal of Hydrology,* 358**,** 332-353.

GILMORE, T. E., GENEREUX, D. P., SOLOMON, D. K., SOLDER, J. E., KIMBALL, B. A., MITASOVA, H. & BIRGAND, F. 2016. Quantifying the fate of agricultural nitrogen in an unconfined aquifer: Stream-based observations at three measurement scales. *Water Resources Research,* 52**,** 1961-1983.

GÓMEZ-ORTIZ, D., MARTÍN-CRESPO, T., MARTÍN-VELÁZQUEZ, S., MARTÍNEZ-PAGÁN, P., HIGUERAS, H. & MANZANO, M. 2010. Application of ground penetrating radar (GPR) to delineate clay layers in wetlands. A case study in the Soto Grande and Soto Chico watercourses, Doñana (SW Spain). *Journal of Applied Geophysics,* 72**,** 107-113.

GOMEZ-VELEZ, J. D., KRAUSE, S. & WILSON, J. L. 2014. Effect of low-permeability layers on spatial patterns of hyporheic exchange and groundwater upwelling. *Water Resources Research,* 50**,** 5196-5215.

GOOSEFF, M. N., ANDERSON, J. K., WONDZELL, S. M., LANIER, J. & HAGGERTY, R. 2006. A modelling study of hyporheic exchange pattern and the sequence, size, and spacing of stream bedforms in mountain stream networks, Oregon, USA. *Hydrological Processes,* 20**,** 2443-2457.

GOOSEFF, M. N., WONDZELL, S. M., HAGGERTY, R. & ANDERSON, J. 2003. Comparing transient storage modeling and residence time distribution (RTD) analysis in geomorphically varied reaches in the Lookout Creek basin, Oregon, USA. *Advances in Water Resources,* 26**,** 925-937.

GOURRY, J.-C., VERMEERSCH, F., GARCIN, M. & GIOT, D. 2003. Contribution of geophysics to the study of alluvial deposits: a case study in the Val d'Avaray area of the River Loire, France. *Journal of Applied Geophysics,* 54**,** 35-49.

GREENWALD, M., J. 2007. *Hyporheic exchange and biogeochemical processing in Arctic Tundra stream.*, MSc. thesis, The University of Vermont.

GRIMALDI, C. & CHAPLOT, V. 2000. Nitrate depletion during within-stream transport: effects of exchange processes between streamwater, the hyporheic and riparian zones. *Water, Air, and Soil Pollution,* 124**,** 95-112.

HAGGERTY, R., WONDZELL, S. M. & JOHNSON, M. A. 2002. Power-law residence time distribution in the hyporheic zone of a 2nd-order mountain stream. *Geophysical Research Letters,* 29, 18-1.

HANNAH, D. M., MALCOLM, I. A. & BRADLEY, C. 2009. Seasonal hyporheic temperature dynamics over riffle bedforms. *Hydrological Processes,* 23**,** 2178-2194.

HARVEY, J. W. & BENCALA, K. E. 1993. The effect of streambed topography on surface-subsurface water exchange in mountain catchments. *Water Resources Research,* 29**,** 89-98.

HATCH, C. E., FISHER, A. T., RUEHL, C. R. & STEMLER, G. 2010. Spatial and temporal variations in streambed hydraulic conductivity quantified with time-series thermal methods. *Journal of Hydrology,* 389**,** 276-288.

HAZEN, A. 1911. Discussion—Dams on sand foundations: Transactions of American Society of Civil Engineers, v. 73, 199 pp.

HEDIN, L. O., VON FISCHER, J. C., OSTROM, N. E., KENNEDY, B. P., BROWN, M. G. & ROBERTSON, G. P. 1998. Thermodynamic constraints on nitrogentransformations and other biogeochemicalprocesses at soil–stream interfaces. *Ecology,* 79**,** 684-703.

HEINZ, J. & AIGNER, T. 2003b. Three-dimensional GPR analysis of various Quaternary gravel-bed braided river deposits (southwestern Germany). *Geological Society, London, Special Publications,* 211**,** 99-110.

HEPPELL, C., HEATHWAITE, A. L., BINLEY, A., BYRNE, P., ULLAH, S., LANSDOWN, K., KEENAN, P., TRIMMER, M. & ZHANG, H. 2014. Interpreting spatial patterns in redox and coupled water–nitrogen fluxes in the streambed of a gaining river reach. *Biogeochemistry,* 117**,** 491-509.

HETEREN, S. V., FITZGERALD, D. M., MCKINLAY, P. A. & BUYNEVICH, I. V. 1998. Radar facies of paraglacial barrier systems: coastal New England, USA. *Sedimentology,* 45**,** 181-200.

HICKIN, A.S., Kerr, B., BARCHYN, T.E. and PAULEN, R.C., 2009. Using ground-penetrating radar and capacitively coupled resistivity to investigate 3-D fluvial architecture and grain-size distribution of a gravel floodplain in northeast British Columbia, Canada. *Journal of Sedimentary Research*, 79, 457-477.

HILL, A. R. & CARDACI, M. 2004. Denitrification and organic carbon availability in riparian wetland soils and subsurface sediments. *Soil Science Society of America Journal,* 68**,** 320-325.

HOAG, R. S. & PRICE, J. S. 1997. The effects of matrix diffusion on solute transport and retardation in undisturbed peat in laboratory columns. *Journal of Contaminant Hydrology,* 28**,** 193-205.

HOLMES, R. M., FISHER, S. G. & GRIMM, N. B. 1994. Parafluvial nitrogen dynamics in a desert stream ecosystem. *Journal of the North American Benthological Society,* 13**,** 468-478.

HOLMES, R. M., JONES, J. B., FISHER, S. G. & GRIMM, N. B. 1996. Denitrification in a nitrogen-limited stream ecosystem. *Biogeochemistry,* 33**,** 125-146.

HUGGENBERGER, P. 1993. Radar facies: recognition of facies patterns and heterogeneities within Pleistocene Rhine gravels, NE Switzerland. *Geological Society, London, Special Publications,* 75**,** 163-176.

HUGGENBERGER, P., MEIER, E. & PUGIN, A. 1994. Ground-probing radar as a tool for heterogeneity estimation in gravel deposits: advances in data-processing and facies analysis. *Journal of Applied Geophysics,* 31**,** 171-184.

HUISINK, M. 2000a. Changing river styles in response to Weichselian climate changes in the Vecht valley, eastern Netherlands. *Sedimentary Geology,* 133**,** 115-134.

HUISINK, M. 2000b. Changing river styles in response to Weichselian climate changes in the Vecht valley, eastern Netherlands. *Sedimentary Geology,* 133**,** 115-134.

HUSBAND, C., CASSIDY, N. & STIMPSON, I. 2009. The geophysical investigation of lake water seepage in the regulated environment of the Bosherston Lily Ponds, South Wales, U.K. Part 1: Natural fracture related pathways. Near Surface Geophysics, 7, (5-6), 499-515.

Hvorslev, M. J., 1951. *Time lag and soil permeability in ground-water observations*. U.S. Corps of Engineers, Waterways Experiment Station, Bulletin 36. Mississippi.

HYUN, Y., KIM, H., LEE, S.-S. & LEE, K.-K. 2011. Characterizing streambed water fluxes using temperature and head data on multiple spatial scales in Munsan stream, South Korea. *Journal of Hydrology,* 402**,** 377-387.

JOL, H. M. & BRISTOW, C. S. 2003. GPR in sediments: advice on data collection, basic processing and interpretation, a good practice guide. *Geological Society, London, Special Publications,* 211**,** 9-27.

JOL, H. M. & SMITH, D. G. 1991. Ground penetrating radar of northern lacustrine deltas. *Canadian Journal of Earth Sciences,* 28**,** 1939-1947.

JOL, H. M. & SMITH, D. G. 1995. Ground penetrating radar surveys of peatlands for oilfield pipelines in Canada. *Journal of Applied Geophysics,* 34**,** 109-123.

JONES, J. B., FISHER, S. G. & GRIMM, N. B. 1995. Vertical hydrologic exchange and ecosystem metabolism in a Sonoran Desert stream. *Ecology,* 76**,** 942-952.

JONES, J. B. & HOLMES, R. M. 1996. Surface-subsurface interactions in stream ecosystems. *Trends in Ecology & Evolution,* 11**,** 239-242.

JONES, J. B., FISHER, S. G. & GRIMM, N. B. 1995. Nitrification in the hyporheic zone of a desert stream ecosystem. *Journal of the North American Benthological Society,* 14**,** 249-258.

KALBUS, E., REINSTORF, F. & SCHIRMER, M. 2006. Measuring methods for groundwater? surface water interactions: a review. *Hydrology and Earth System Sciences Discussions,* 10**,** 873-887.

KAPLAN, L. A. & NEWBOLD, J. D. 2000. Surface and subsurface dissolved organic carbon. *Streams and ground waters*. *In:* JONES, J. B., MULHOLLAND, P.J. (ed.) *Streams and Ground Waters.* Academic Press, New York, **,** 237-258.

KASAHARA, T. & HILL, A. R. 2006. Effects of riffle step restoration on hyporheic zone chemistry in N-rich lowland streams. *Canadian Journal of Fisheries and Aquatic Sciences,* 63**,** 120-133.

KASAHARA, T. & WONDZELL, S. M. 2003. Geomorphic controls on hyporheic exchange flow in mountain streams. *Water Resources Research,* 39, 3-14.

KÄSER, D. H., BINLEY, A., HEATHWAITE, A. L. & KRAUSE, S. 2009. Spatio-temporal variations of hyporheic flow in a riffle-step-pool sequence. *Hydrological Processes,* 23**,** 2138-2149.

KEERY, J., BINLEY, A., CROOK, N. & SMITH, J. W. 2007. Temporal and spatial variability of groundwater–surface water fluxes: development and application of an analytical method using temperature time series. *Journal of Hydrology,* 336**,** 1-16.

KELLY, S. E. & MURDOCH, L. C. 2003. Measuring the hydraulic conductivity of shallow submerged sediments. *Ground Water,* 41**,** 431-439.

KENNEDY, C. D., GENEREUX, D. P., CORBETT, D. R. & MITASOVA, H. 2009a. Relationships among groundwater age, denitrification, and the coupled groundwater and nitrogen fluxes through a streambed. *Water Resources Research,* 45, W09402, doi:10.1029/2008WR007400.

KENNEDY, C. D., GENEREUX, D. P., CORBETT, D. R. & MITASOVA, H. 2009b. Spatial and temporal dynamics of coupled groundwater and nitrogen fluxes through a streambed in an agricultural watershed. *Water Resources Research,* 45, W09401, doi:10.1029/2008WR007397.

KOSTIC, B. & AIGNER, T. 2007a. Sedimentary architecture and 3D ground-penetrating radar analysis of gravelly meandering river deposits (Neckar Valley, SW Germany). *Sedimentology,* 54**,** 789-808.

KOSTIC, B. & AIGNER, T. 2007b. Sedimentary architecture and 3D ground-penetrating radar analysis of gravelly meandering river deposits (Neckar Valley, SW Germany). *Sedimentology,* 54**,** 789-808.

KOSTIC, B., BECHT, A. & AIGNER, T. 2005. 3-D sedimentary architecture of a Quaternary gravel delta (SW-Germany): Implications for hydrostratigraphy. *Sedimentary Geology,* 181**,** 147-171.

KRAUSE, S., BLUME, T. & CASSIDY, N. 2012a. Application of fibre-optic DTS to identify streambed controls on aquifer-river exchange fluxes in lowland rivers. *Hydrol. Earth Syst. Sci,* 16**,** 1775-1792.

KRAUSE, S., BLUME, T. & CASSIDY, N. J. 2012b. Investigating patterns and controls of groundwater up-welling in a lowland river by combining Fibre-optic Distributed Temperature Sensing with observations of vertical hydraulic gradients. *Hydrology and Earth System Sciences,* 16**,** 1775-1792.

KRAUSE, S., HANNAH, D. & BLUME, T. 2011a. Heat transport patterns at pool-riffle sequences of an UK lowland stream. *Ecohydrology,* 4**,** 549-563.

KRAUSE, S., HANNAH, D., FLECKENSTEIN, J., HEPPELL, C., KAESER, D., PICKUP, R., PINAY, G., ROBERTSON, A. & WOOD, P. 2011b. Inter-disciplinary perspectives on processes in the hyporheic zone. *Ecohydrology,* 4**,** 481-499.

KRAUSE, S., HANNAH, D. M. & FLECKENSTEIN, J. H. 2009a. Hyporheic hydrology: interactions at the groundwater-surface water interface. *Hydrological Processes,* 23**,** 2103-2107.

KRAUSE, S., HEATHWAITE, L., BINLEY, A. & KEENAN, P. 2009b. Nitrate concentration changes at the groundwater-surface water interface of a small Cumbrian river. *Hydrological Processes,* 23**,** 2195-2211.

KRAUSE, S., TECKLENBURG, C., MUNZ, M. & NADEN, E. 2013. Streambed nitrogen cycling beyond the hyporheic zone: Flow controls on horizontal patterns and depth distribution of nitrate and dissolved oxygen in the upwelling groundwater of a lowland river. *Journal of Geophysical Research: Biogeosciences,* 118**,** 54-67.

LANDON, M. K., RUS, D. L. & HARVEY, F. E. 2001. Comparison of instream methods for measuring hydraulic conductivity in sandy streambeds. *Groundwater,* 39**,** 870-885.

LAUTZ, L. & FANELLI, R. 2008. Seasonal biogeochemical hotspots in the streambed around restoration structures. *Biogeochemistry,* 91**,** 85-104.

LAUTZ, L. K., KRANES, N. T. & SIEGEL, D. I. 2010. Heat tracing of heterogeneous hyporheic exchange adjacent to in-stream geomorphic features. *Hydrological Processes,* 24**,** 3074-3086.

LECLERC, R. F. & HICKIN, E. J. 1997. The internal structure of scrolled floodplain deposits based on ground-penetrating radar, North Thompson River, British Columbia. *Geomorphology,* 21**,** 17-38.

LEEK, R., WU, J. Q., WANG, L., HANRAHAN, T. P., BARBER, M. E. & QIU, H. 2009. Heterogeneous characteristics of streambed saturated hydraulic conductivity of the Touchet River, south eastern Washington, USA. *Hydrological Processes,* 23**,** 1236-1246.

LEJZEROWICZ, A., KOWALCZYK, S. & WYSOCKA, A. 2014. The usefulness of ground-penetrating radar images for the research of a large sand-bed braided river: case study from the Vistula River (central Poland). *Geologos,* 20, 35-47.

LEOPOLD, L. B., WOLMAN, M. G. & AND MILLER, J. P. 1964. *Fluvial processes in geomorphology,* San Francisco, California, W. H. Freeman and Company.

LISLE, T. E., ISEYA, F. & IKEDA, H. 1993. Response of a channel with alternate bars to a decrease in supply of mixed-size bed load: A flume experiment. *Water Resources Research,* 29**,** 3623-3629.

LUNT, I., BRIDGE, J. & TYE, R. 2004. A quantitative, three-dimensional depositional model of gravelly braided rivers. *Sedimentology,* 51**,** 377-414.

LUNT, I., HUBBARD, S. & RUBIN, Y. 2005. Soil moisture content estimation using ground-penetrating radar reflection data. *Journal of Hydrology,* 307**,** 254-269.

LYFORD, F. P., FLIGHT, L., STONE, J. R. & CLIFFORD, S. 1999. Distribution of trichloroethylene and geologic controls on contaminant pathways near the Royal River, McKin Superfund Site area, Gray, Maine. *US Geological Survey Water-Resources Investigations Report***,** 99-4125.

MALARD, F., TOCKNER, K., DOLE-OLIVIER, M. J. & WARD, J. 2002. A landscape perspective of surface–subsurface hydrological exchanges in river corridors. *Freshwater Biology,* 47**,** 621-640.

MALCOLM, I., SOULSBY, C., YOUNGSON, A. & PETRY, J. 2003. Heterogeneity in ground water–surface water interactions in the hyporheic zone of a salmonid spawning stream. *Hydrological Processes,* 17**,** 601-617.

MARZADRI, A., TONINA, D. & BELLIN, A. 2012. Morphodynamic controls on redox conditions and on nitrogen dynamics within the hyporheic zone: Application to gravel bed rivers with alternate-bar morphology. Journal of Geophysical Research: Biogeosciences, 117, G00N10, doi:10.1029/2012JG001966.

MCKNIGHT, U. S., FUNDER, S. G., RASMUSSEN, J. J., FINKEL, M., BINNING, P. J. & BJERG, P. L. 2010. An integrated model for assessing the risk of TCE groundwater contamination to human receptors and surface water ecosystems. *Ecological Engineering,* 36**,** 1126-1137.

MIALL, A. 1996. Sedimentary facies, basin analysis, and petroleum geology. Springer-Verlag, 582 pp.

MILOSEVIC, N., THOMSEN, N. I., JUHLER, R. K., ALBRECHTSEN, H.-J. & BJERG, P. L. 2012. Identification of discharge zones and quantification of contaminant mass discharges into a local stream from a landfill in a heterogeneous geologic setting. *Journal of Hydrology,* 446**,** 13-23.

MITCHUM, R., VAIL, P. & SANGREE, J. 1977. Stratigraphic interpretation of seismic reflection patterns in depositional sequences. In: Payton, C.E. (Ed.), Seismic Stratigraphy—Applications to Hydrocarbon Exploration. AAPG Mem. 16, 117– 123.

MORRICE, J. A., DAHM, C. N., VALETT, H. M., UNNIKRISHNA, P. V. & CAMPANA, M. E. 2000. Terminal electron accepting processes in the alluvial sediments of a headwater stream. *Journal of the North American Benthological Society,* 19**,** 593-608.

NADEN, E. 2011. *Characterisation of aquifer-to-river connectivity using hydrogeophysical methods for surface water protection.* Unpublished MSc. thesis, Keele University.

NAEGELI, M. W., HUGGENBERGER, P. & UEHLINGER, U. 1996. Ground penetrating radar for assessing sediment structures in the hyporheic zone of a prealpine river. *Journal of the North American Benthological Society***,** 15, 353-366.

NARANJO, R. C., NISWONGER, R. G. & DAVIS, C. J. 2015. Mixing effects on nitrogen and oxygen concentrations and the relationship to mean residence time in a hyporheic zone of a riffle-pool sequence. *Water Resources Research,* 51**,** 7202-7217.

NARANJO, R. C., NISWONGER, R. G., STONE, M., DAVIS, C. & MCKAY, A. 2012. The use of multiobjective calibration and regional sensitivity analysis in simulating hyporheic exchange, *Water Resource Research*, 48, W01538, doi:10.1029/2011WR011179.

NEAL, A. 2004. Ground-penetrating radar and its use in sedimentology: principles, problems and progress. *Earth-Science Reviews,* 66**,** 261-330.

NISWONGER, R. G. & FOGG, G. E. 2008. Influence of perched groundwater on base flow. Water resources research, 44, W03405, doi:10.1029/2007WR006160.

NOGARO, G. & MERMILLOD-BLONDIN, F. 2009. Stormwater sediment and bioturbation influences on hydraulic functioning, biogeochemical processes, and pollutant dynamics in laboratory infiltration systems. *Environmental Science & Technology,* 43**,** 3632-3638.

PACKMAN, A. I., MARION, A., ZARAMELLA, M., CHEN, C., GAILLARD, J.-F. & KEANE, D. T. 2006. Development of layered sediment structure and its effects on pore water transport and hyporheic exchange. *Water, Air, & Soil Pollution: Focus,* 6**,** 433-442.

PACKMAN, A. I. & SALEHIN, M. 2003. Relative roles of stream flow and sedimentary conditions in controlling hyporheic exchange. *Hydrobiologia*, 494, 291–297.

PACKMAN, A. I., SALEHIN, M. & ZARAMELLA, M. 2004. Hyporheic exchange with gravel beds: basic hydrodynamic interactions and bedform-induced advective flows. *Journal of Hydraulic Engineering,* 130**,** 647-656.

PALLANT, J. 2005. *SPSS Survival Manual, 2nd ed.,* New York, McGraw-Hill.

PAPATOLIOS, K. T. & LERNER, D. N. 1993. Defining a borehole capture zone in a complex sandstone aquifer: a modelling case study from Shropshire, UK. *Quarterly Journal of Engineering Geology and Hydrogeology,* 26**,** 193-204.

PINAY, G., CLÉMENT, J. C. & NAIMAN, R. J. 2002. Basic principles and ecological consequences of changing water regimes on nitrogen cycling in fluvial systems. *Environmental Management,* 30**,** 481-491.

PINAY, G., O'KEEFE, T. C., EDWARDS, R. T. & NAIMAN, R. J. 2009. Nitrate removal in the hyporheic zone of a salmon river in Alaska. *River Research and Applications,* 25**,** 367-375.

PINAY, G., PEIFFER, S., DE DREUZY, J.-R., KRAUSE, S., HANNAH, D. M., FLECKENSTEIN, J. H., SEBILO, M., BISHOP, K. & HUBERT-MOY, L. 2015. Upscaling nitrogen removal capacity from local hotspots to low stream orders' drainage basins. *Ecosystems,* 18**,** 1101-1120.

POETER, E. & GAYLORD, D. R. 1990. Influence of aquifer heterogeneity on contaminant transport at the Hanford Site. *Ground Water,* 28**,** 900-909.

POOLE, G. C., STANFORD, J. A., RUNNING, S. W., FRISSELL, C., WOESSNER, W. W. & ELLIS, B. K. 2004. A patch hierarchy approach to modeling surface and subsurface hydrology in complex flood-plain environments. *Earth Surface Processes and Landforms,* 29**,** 1259-1274.

PRETTY, J., HILDREW, A. & TRIMMER, M. 2006. Nutrient dynamics in relation to surface–subsurface hydrological exchange in a groundwater fed chalk stream. *Journal of Hydrology,* 330**,** 84-100.

REDDY, K, DELAUNE R.D. 2008. Biogeochemistry of wetlands: science and applications.

Boca Raton, USA: CRC Press.

REVELLI, R., BOANO, F., CAMPOREALE, C. & RIDOLFI, L. 2008. Intra-meander hyporheic flow in alluvial rivers. *Water Resources Research,* 44, W12428, doi:10.1029/2008WR007081.

REYNOLDS, J. M. 2011. *An introduction to applied and environmental geophysics*. John Wiley & Sons, 710 pp.

RIVETT, M., ELLIS, P., GRESWELL, R., WARD, R., ROCHE, R., CLEVERLY, M., WALKER, C., CONRAN, D., FITZGERALD, P. & WILLCOX, T. 2008a. Cost-effective mini drive-point piezometers and multilevel samplers for monitoring the hyporheic zone. *Quarterly Journal of Engineering Geology and Hydrogeology,* 41**,** 49-60.

RIVETT, M., SMITH, J., BUSS, S. & MORGAN, P. 2007. Nitrate occurrence and attenuation in the major aquifers of England and Wales. *Quarterly Journal of Engineering Geology and Hydrogeology,* 40**,** 335-352.

RIVETT, M. O., BUSS, S. R., MORGAN, P., SMITH, J. W. & BEMMENT, C. D. 2008b. Nitrate attenuation in groundwater: a review of biogeochemical controlling processes. *Water Research,* 42**,** 4215-4232.

ROBINSON, D., BINLEY, A., CROOK, N., DAY-LEWIS, F., FERRÉ, T., GRAUCH, V., KNIGHT, R., KNOLL, M., LAKSHMI, V. & MILLER, R. 2008. Advancing process-based watershed hydrological research using near-surface geophysics: A vision for, and review of, electrical and magnetic geophysical methods. *Hydrological Processes,* 22**,** 3604-3635.

ROQUE, A. J. & DIDIER, G. 2006. Calculating hydraulic conductivity of fine-grained soils to leachates using linear expressions. *Engineering geology,* 85**,** 147-157.

ROSENBERRY, D. O., LABAUGH, J. W. & HUNT, R. J. 2008. Use of monitoring wells, portable piezometers, and seepage meters to quantify flow between surface water and ground water. *Field techniques for estimating water fluxes between surface water and ground water. US Geological Survey Techniques and Methods***,** 4-D2.

ROSENBERRY, D. O. & PITLICK, J. 2009. Local-scale variability of seepage and hydraulic conductivity in a shallow gravel-bed river. *Hydrological processes,* 23**,** 3306-3318.

ROSENSHEIN, J. S. 1998. Hydrology of North America, Region 18, Alluvial valleys. *In:* BACK W., ROSENSHEIN J.S. & AND SEABER P.R. (eds.) *The Geology of North America.* Boulder, Colorado: Geological Society of North America, 165-176.

RYAN, R. J. & PACKMAN, A. I. 2006. Changes in streambed sediment characteristics and solute transport in the headwaters of Valley Creek, an urbanizing watershed. *Journal of Hydrology,* 323**,** 74-91.

SALEHIN, M., PACKMAN, A. I. & PARADIS, M. 2004. Hyporheic exchange with heterogeneous streambeds: Laboratory experiments and modeling. *Water Resources Research,* 40, W11504, doi:10.1029/2003WR002567.

SAMBROOK SMITH, G. H., ASHWORTH, P. J., BEST, J. L., WOODWARD, J. & SIMPSON, C. J. 2006. The sedimentology and alluvial architecture of the sandy braided South Saskatchewan River, Canada. *Sedimentology,* 53**,** 413-434.

SASS, O., FRIEDMANN, A., HASELWANTER, G. & WETZEL, K.-F. 2010. Investigating thickness and internal structure of alpine mires using conventional and geophysical techniques. *Catena,* 80**,** 195-203.

SAWYER, A. H. & CARDENAS, M. B. 2009. Hyporheic flow and residence time distributions in heterogeneous cross-bedded sediment. *Water Resources Research,* 45, w08406, doi:10.1029/2008WR007632.

SCHLOTZHAUER, S. M. & PRICE, J. S. 1999. Soil water flow dynamics in a managed cutover peat field, Quebec: Field and laboratory investigations. *Water Resources Research,* 35**,** 3675-3683.

SCHMIDT, C., MARTIENSSEN, M. & KALBUS, E. 2011. Influence of water flux and redox conditions on chlorobenzene concentrations in a contaminated streambed. *Hydrological Processes,* 25**,** 234-245.

SCHUENEMEYER, J. & DREW, L. 2011. *Statistics for earth and environmental scientists,* John Wiley & Sons, 407 pp.

SCOTT, J.T., McCARTHY, M.J., GARDNER, W.S., DOYLE, R.D., 2008. Denitrification, dissimilatory nitrate reduction to ammonium, and nitrogen fixation along a nitrate concentration gradient in a created freshwater wetland. Biogeochemistry 87, 99-111.

SEBOK, E., DUQUE, C., ENGESGAARD, P. & BOEGH, E. 2015. Spatial variability in streambed hydraulic conductivity of contrasting stream morphologies: channel bend and straight channel. *Hydrological Processes,* 29**,** 458-472.

SENSORS AND SOFTWARE. 1996. Technical Manual 21: PulseEKKO Basic Plotting and Editing. Sensors and Software.

Sensors and Software (2005) PulseEKKO PRO User's Guide. Sensors and Software, Ontario.

SGOURIDIS, F.A., HEPPELL, C.M., WHARTON, G., LANSDOWN, K. & TRIMMER M. 2011. Denitrification and dissimilatory nitrate reduction to ammonium (DNRA) in a temperate re-connected floodplain. *Water Research,* 45, 4909-4922.

SHEPLEY, M. & STREETLY, M. 2007. The estimation of 'natural'summer outflows from the Permo-Triassic Sandstone aquifer, UK. *Quarterly Journal of Engineering Geology and Hydrogeology,* 40**,** 213-227.

SLOWIK, M. 2012a. Changes of river bed pattern of a lowland river: effect of natural processes or anthropogenic intervention? *Geografiska Annaler: Series A, Physical Geography,* 94**,** 301-320.

SŁOWIK, M. 2012b. Influence of measurement conditions on depth range and resolution of GPR images: The example of lowland valley alluvial fill (the Obra River, Poland). *Journal of Applied Geophysics,* 85**,** 1-14.

SŁOWIK, M. 2013a. GPR and aerial imageries to identify the recent historical course of the Obra River and spatial extent of Obrzańskie Lake, altered by hydro-technical works. *Environmental Earth Sciences,* 70**,** 1277-1295.

SŁOWIK, M. 2013b. Transformation of a lowland river from a meandering and multi-channel pattern into an artificial canal: retracing a path of river channel changes (the Middle Obra River, W Poland). *Regional Environmental Change,* 13**,** 1287-1299.

SŁOWIK, M. 2014a. Analysis of fluvial, lacustrine and anthropogenic landforms by means of ground-penetrating radar (GPR): field experiment. *Near Surface Geophysics,* 12, 777-791.

SŁOWIK, M. 2014b. Holocene evolution of meander bends in lowland river valley formed in complex geological conditions (the Obra River, Poland). *Geografiska Annaler: Series A, Physical Geography,* 96**,** 61-81.

SŁOWIK, M. 2015. The influence of meander bend evolution on the formation of multiple cutoffs: findings inferred from floodplain architecture and bend geometry. *Earth Surface Processes and Landforms***,** 41, 626–641.

SMITH, J. 2005. Groundwater–surface water interactions in the hyporheic zone. Environment Agency Science report SC030155/SR1. Environment Agency, Bristol, UK.

SMITH, J., BONELL, M., GIBERT, J., MCDOWELL, W., SUDICKY, E., TURNER, J. & HARRIS, R. 2008. Groundwater–surface water interactions, nutrient fluxes and ecological response in river corridors: translating science into effective environmental management. *Hydrological Processes,* 22**,** 151-157.

SMITH, J. & LERNER, D. 2008. Geomorphologic control on pollutant retardation at the groundwater–surface water interface. *Hydrological processes,* 22**,** 4679-4694.

SOBCZAK, W. V., HEDIN, L. O. & KLUG, M. J. 1998. Relationships between bacterial productivity and organic carbon at a soil—stream interface. *Hydrobiologia,* 386**,** 45-53.

SONG, J., CHEN, X., CHENG, C., SUMMERSIDE, S. & WEN, F. 2007. Effects of hyporheic processes on streambed vertical hydraulic conductivity in three rivers of Nebraska. *Geophysical Research Letters*, 34, L07409, doi:10.1029/2007GL029254.

SONG, J., JIANG, W., XU, S., ZHANG, G., WANG, L., WEN, M., ZHANG, B., WANG, Y. & LONG, Y. 2016. Heterogeneity of hydraulic conductivity and Darcian flux in the submerged streambed and adjacent exposed stream bank of the Beiluo River, northwest China. *Hydrogeology Journal,* 24**,** 2049-2062.

SOPHOCLEOUS, M. 2002. Interactions between groundwater and surface water: the state of the science. *Hydrogeology Journal,* 10**,** 52-67.

STANFORD, J. & WARD, J. 1988. The hyporheic habitat of river ecosystems. *Nature*, 335, 64-66.

STANFORD, J. A. & WARD, J. 1993. An ecosystem perspective of alluvial rivers: connectivity and the hyporheic corridor. *Journal of the North American Benthological Society***,** 48-60.

STEEL, R. & THOMPSON, D. 1983. Structures and textures in Triassic braided stream conglomerates ('Bunter'pebble beds) in the Sherwood Sandstone Group, North Staffordshire, England. *Sedimentology*, 30**,** 341-367.

STELZER, R. S. & BARTSCH, L. A. 2012. Nitrate removal in deep sediments of a nitrogen-rich river network: A test of a conceptual model. *Journal of Geophysical Research: Biogeosciences,* 117.

STOREY, R., FULTHORPE, R. & WILLIAMS, D. 1999. Perspectives and predictions on the microbial ecology of the hyporheic zone. *Freshwater Biology,* 41**,** 119-130.

STOREY, R. G., WILLIAMS, D. D. & FULTHORPE, R. R. 2004. Nitrogen processing in the hyporheic zone of a pastoral stream. *Biogeochemistry,* 69**,** 285-313.

STREETLY, M. & SHEPLEY, M. 2005. Final Report, East Shropshire Permo-Triassic Sandstone Groundwater Modelling Project – Task 8. Environment Agency, Bristol.

STUBBINGTON, R., WOOD, P. J. & BOULTON, A. 2009. Low flow controls on benthic and hyporheic macroinvertebrate assemblages during supra-seasonal drought. *Hydrological Processes,* 23**,** 2252-2263.

THAMDRUP B, DALSGAARD T. 2008. Nitrogen cycling in sediments. John Wiley & Sons, Inc.; Tod SP, Schmid-Araya JM. Meiofauna versus macrofauna: secondary production of invertebrates in a lowland chalk stream. Limnol Oceanogr 2009;54:450–6.

THEIMER, B. D., NOBES, D. C. & WARNER, B. G. 1994. A study of the geoelectrical properties of peatlands and their influence on ground-penetrating radar surveying. *Geophysical prospecting,* 42**,** 179-209.

TONINA, D. & BUFFINGTON, J. M. 2007. Hyporheic exchange in gravel bed rivers with pool-riffle morphology: Laboratory experiments and three-dimensional modeling. *Water Resources Research,* 43, W01421, doi:10.1029/2005WR004328.

TONINA, D. & BUFFINGTON, J. M. 2009. Hyporheic exchange in mountain rivers I: Mechanics and environmental effects. *Geography Compass,* 3**,** 1063-1086.

TOPP, G. C., DAVIS, J. & ANNAN, A. P. 1980. Electromagnetic determination of soil water content: Measurements in coaxial transmission lines. *Water Resources Research,* 16**,** 574-582.

TRAN, A. P., WIAUX, F. & LAMBOT, S. Soil moisture estimation using full-wave inversion of near-and far-field ground-penetrating radar data: A comparative evaluation. Ground Penetrating Radar (GPR), 2012 14th International Conference on, 2012. IEEE, 296-300.

TRIMMER, M., GREY, J., HEPPELL, C.M., HILDREW, A.G., LANSDOWN, K., STAHL, H. and YVON-DUROCHER, G., 2012. River bed carbon and nitrogen cycling: State of play and some new directions. Science of the total environment, 434, 143-158.

TRISKA, F. J., KENNEDY, V. C., AVANZINO, R. J., ZELLWEGER, G. W. & BENCALA, K. E. 1989. Retention and Transport of Nutrients in a Third-Order Stream: Channel Processes. *Ecology,* 70**,** 1877-1892.

ULLAH, S., ZHANG, H., HEATHWAITE, A. L., HEPPELL, C., LANSDOWN, K., BINLEY, A. & TRIMMER, M. 2014. Influence of emergent vegetation on nitrate cycling in sediments of a groundwater-fed river. *Biogeochemistry,* 118**,** 121-134.

ULRIKSEN, C. P. F. 1982. Application of impulse radar to civil engineering. Ph.D. Thesis, Lund University of Technology, Lund, Sweden.

VALETT, H. M., FISHER, S. G., GRIMM, N. B. & CAMILL, P. 1994. Vertical hydrologic exchange and ecological stability of a desert stream ecosystem. *Ecology,* 75**,** 548-560.

VALETT, H. M., MORRICE, J. A. & DAHM, C. N. 1996. Parent lithology, surface-groundwater exchange and nitrate retention in headwater streams. *Limnology Oceanography,* 41**,** 333–345.

VAN OVERMEEREN, R. 1998. Radar facies of unconsolidated sediments in The Netherlands: A radar stratigraphy interpretation method for hydrogeology. *Journal of Applied Geophysics,* 40**,** 1-18.

VANDENBERGHE, J. & VAN OVERMEEREN, R. 1999. Ground penetrating radar images of selected fluvial deposits in the Netherlands. *Sedimentary Geology,* 128**,** 245-270.

VAUX, W. G. 1962. *Interchange of stream and intragravel water in a salmon spawning riffle*, US Department of Interior, Fish and Wildlife Service.

VERVIER, P., GIBERT, J., MARMONIER, P. & DOLE-OLIVIER, M.-J. 1992. A perspective on the permeability of the surface freshwater-groundwater ecotone. *Journal of the North American Benthological Society,* 11**,** 93-102.

VOKES, W. 2015. *Spatial and Temporal Variation of Nitrogen Concentrations in the Groundwater of a Clay and Sand Based Floodplain: the effect of Hydrology and Substrate.*, Unpublished MSc. thesis, School of Geography, Earth and Environmental Sciences, University of Birmingham.

WAKEFIELD, O. J., HOUGH, E. & PEATFIELD, A. W. 2015. Architectural analysis of a Triassic fluvial system: the Sherwood Sandstone of the East Midlands Shelf, UK. *Sedimentary Geology,* 327**,** 1-13.

WANG, L., JIANG, W., SONG, J., DOU, X., GUO, H., XU, S., ZHANG, G., WEN, M., LONG, Y. & LI, Q. 2017. Investigating spatial variability of vertical water fluxes through the streambed in distinctive stream morphologies using temperature and head data. *Hydrogeology Journal***,** 25, 1283–1299.

WARD, A. S., GOOSEFF, M. N. & SINGHA, K. 2010. Imaging hyporheic zone solute transport using electrical resistivity. *Hydrological Processes,* 24**,** 948-953.

WEATHERILL, J. 2015. *Investigating the natural attenuation and fate of a trichloroethene plume at the groundwater-surface water interface of a UK lowland river*, Unpublished PhD thesis, Keele University.

WEATHERILL, J., KRAUSE, S., VOYCE, K., DRIJFHOUT, F., LEVY, A. & CASSIDY, N. 2014. Nested monitoring approaches to delineate groundwater trichloroethene discharge to a UK lowland stream at multiple spatial scales. *Journal of Contaminant Hydrology,* 158**,** 38-54.

WHEATER, H. S. & PEACH, D. 2004. Developing interdisciplinary science for integrated catchment management: the UK lowland catchment research (LOCAR) programme. *International Journal of Water Resources Development,* 20**,** 369-385.

WHITE, D. S. 1993. Perspectives on defining and delineating hyporheic zones. *Journal of the North American Benthological Society***,** 12, 61-69.

WILLIAMS, D. D. & HYNES, H. 1974. The occurrence of benthos deep in the substratum of a stream. *Freshwater Biology,* 4**,** 233-256.

WOESSNER, W. W. 2000. Stream and fluvial plain ground water interactions: rescaling hydrogeologic thought. *Ground Water,* 38**,** 423-429.

WOJNAR, A., J. 2008. *Investigating riverbd hydraulic conductivity at several well fields along the great Miami River, southwestern Ohio.* MSc., Miami University, Oford, Ohio.

WONDZELL, S. M. & GOOSEFF, M. N. 2013. Geomorphic controls on hyporheic exchange across scales: watersheds to particles. *In:* SHRODER, J. E. I. C. & WOHL, E. E. (eds.) *Treatise on Geomorphology.* San Diego, CA, USA: Academic Press, 203–218.

WONDZELL, S. M. & SWANSON, F. J. 1996. Seasonal and storm dynamics of the hyporheic zone of a 4th-order mountain stream. I: Hydrologic processes. *Journal of the North American Benthological Society***,** 3-19.

WRIGHT, S., HOWATH, G., CLARKE, T. & AND ANSTRUTHER, S. 2013. Hammer Stream Farmer Participation Project Final Report for Natural England CSF. Natural England.

WROBLICKY, G. J., CAMPANA, M. E., VALETT, H. M. & DAHM, C. N. 1998. Seasonal variation in surface-subsurface water exchange and lateral hyporheic area of two stream-aquifer systems. *Water Resources Research,* 34**,** 317-328.

WU, G., SHU, L., LU, C. & CHEN, X. 2016. The heterogeneity of 3-D vertical hydraulic conductivity in a streambed. *Hydrology Research,* 47**,** 15-26.

ZARNETSKE, J. P., HAGGERTY, R., WONDZELL, S. M. & BAKER, M. A. 2011a. Dynamics of nitrate production and removal as a function of residence time in the hyporheic zone. *Journal of Geophysical Research,* 116, GO1025, doi:10.1029/2010JG001356.

ZARNETSKE, J. P., HAGGERTY, R., WONDZELL, S. M. & BAKER, M. A. 2011b. Labile dissolved organic carbon supply limits hyporheic denitrification. *Journal of Geophysical Research,* 116, G04036, doi:10.1029/2011JG001730.

ZUK, T. 2011. *Acquisition, 3-D display and interpretation of GPR data in fluvial sedimentology.* M.Phil. thesis, University of Birmingham.

9. Appendices

Appendix 1 NE-SW orientation profiles collected in the river Tern west bank site (profiles 94-14).

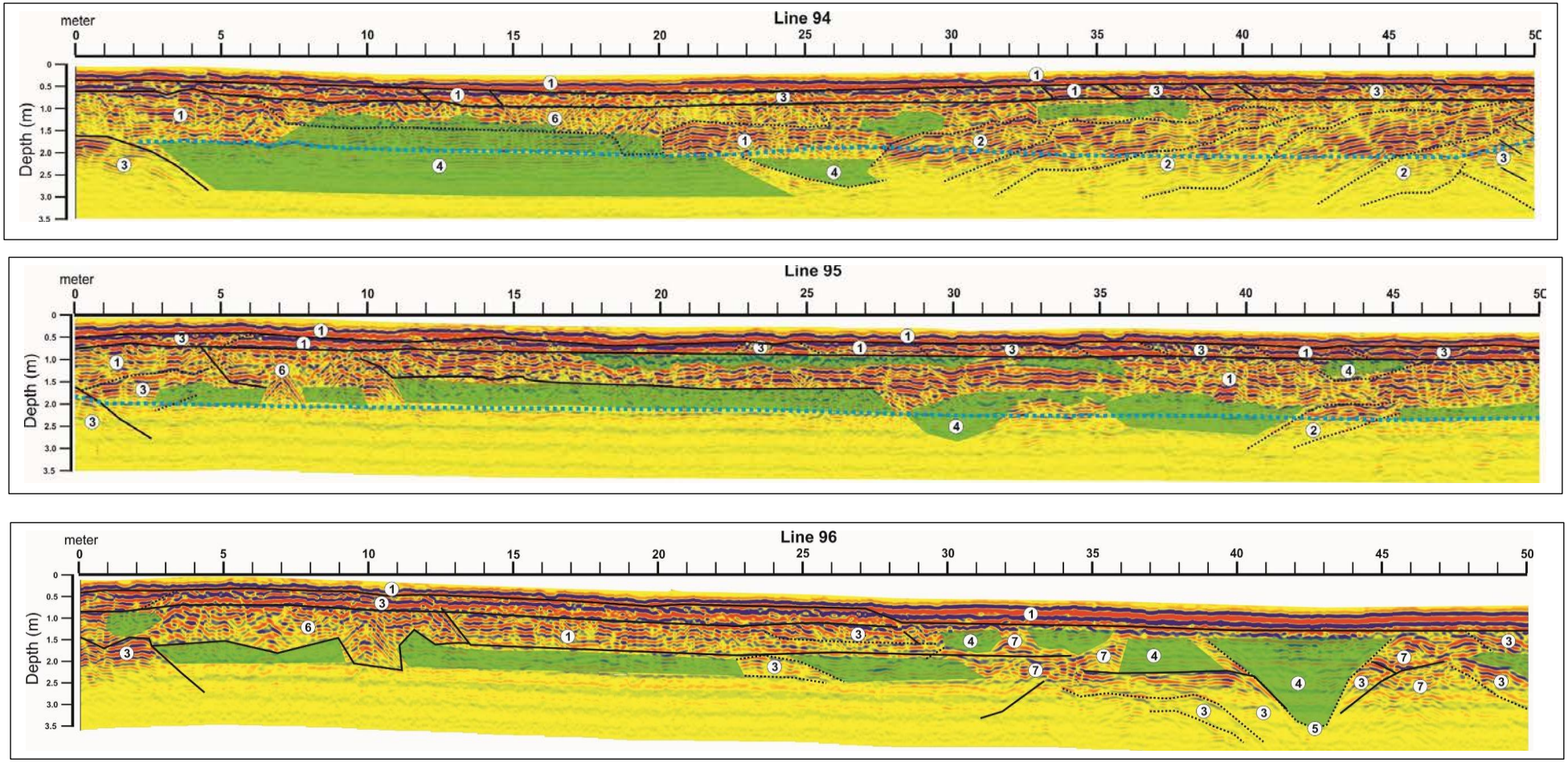

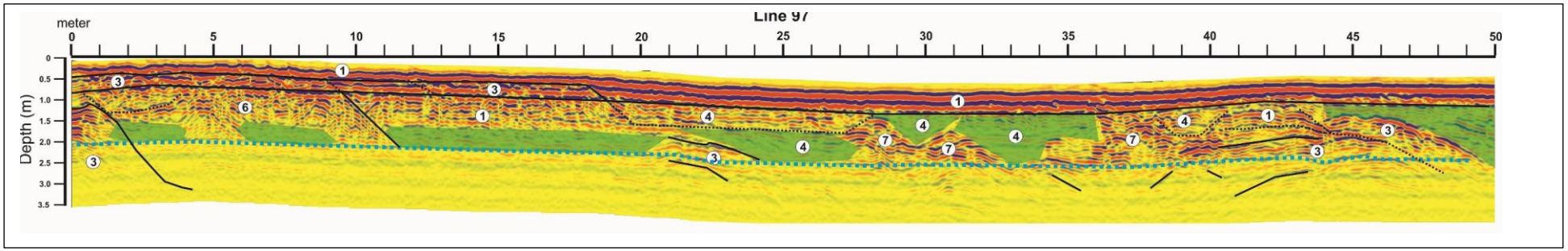
Line 97
meter
0 5 10 15 20 25 30 35 40 45 50
Depth (m)
0 0.5 1.0 1.5 2.0 2.5 3.0 3.5

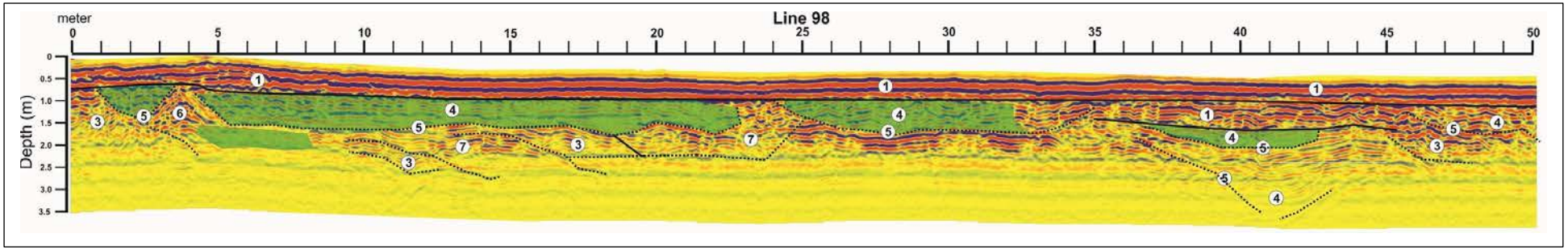
Line 98
meter
0 5 10 15 20 25 30 35 40 45 50
Depth (m)
0 0.5 1.0 1.5 2.0 2.5 3.0 3.5

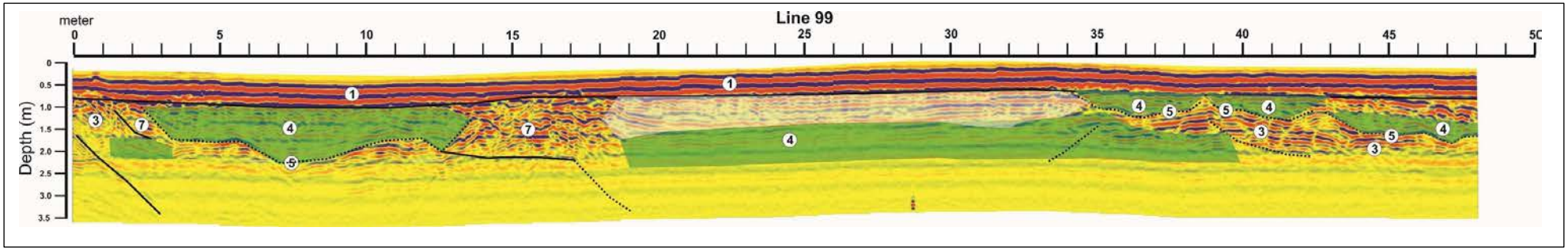
Line 99
meter
0 5 10 15 20 25 30 35 40 45 50
Depth (m)
0 0.5 1.0 1.5 2.0 2.5 3.0 3.5

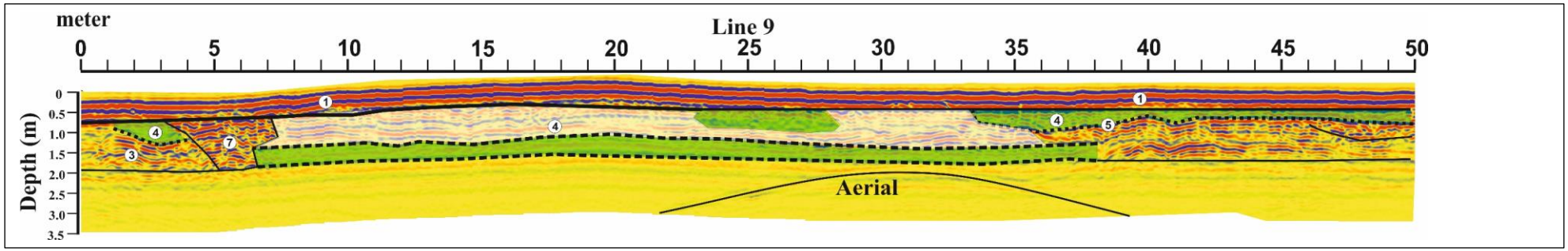
meter
Line 9
0 5 10 15 20 25 30 35 40 45 50
Depth (m)
0 0.5 1.0 1.5 2.0 2.5 3.0 3.5
Aerial

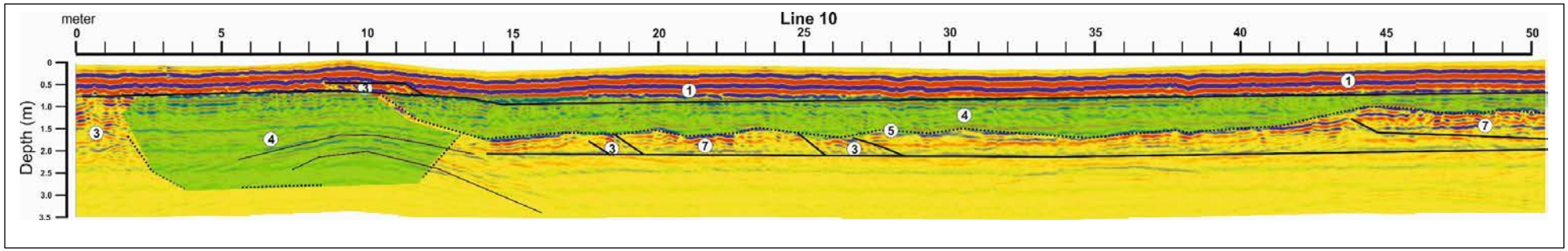
meter
Line 10
0 5 10 15 20 25 30 35 40 45 50
Depth (m)
0 0.5 1.0 1.5 2.0 2.5 3.0 3.5

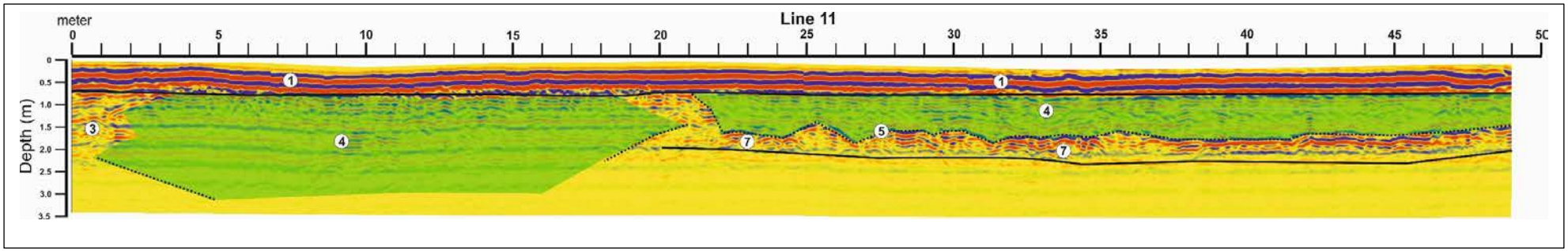
meter
Line 11
0 5 10 15 20 25 30 35 40 45
Depth (m)
0 0.5 1.0 1.5 2.0 2.5 3.0 3.5

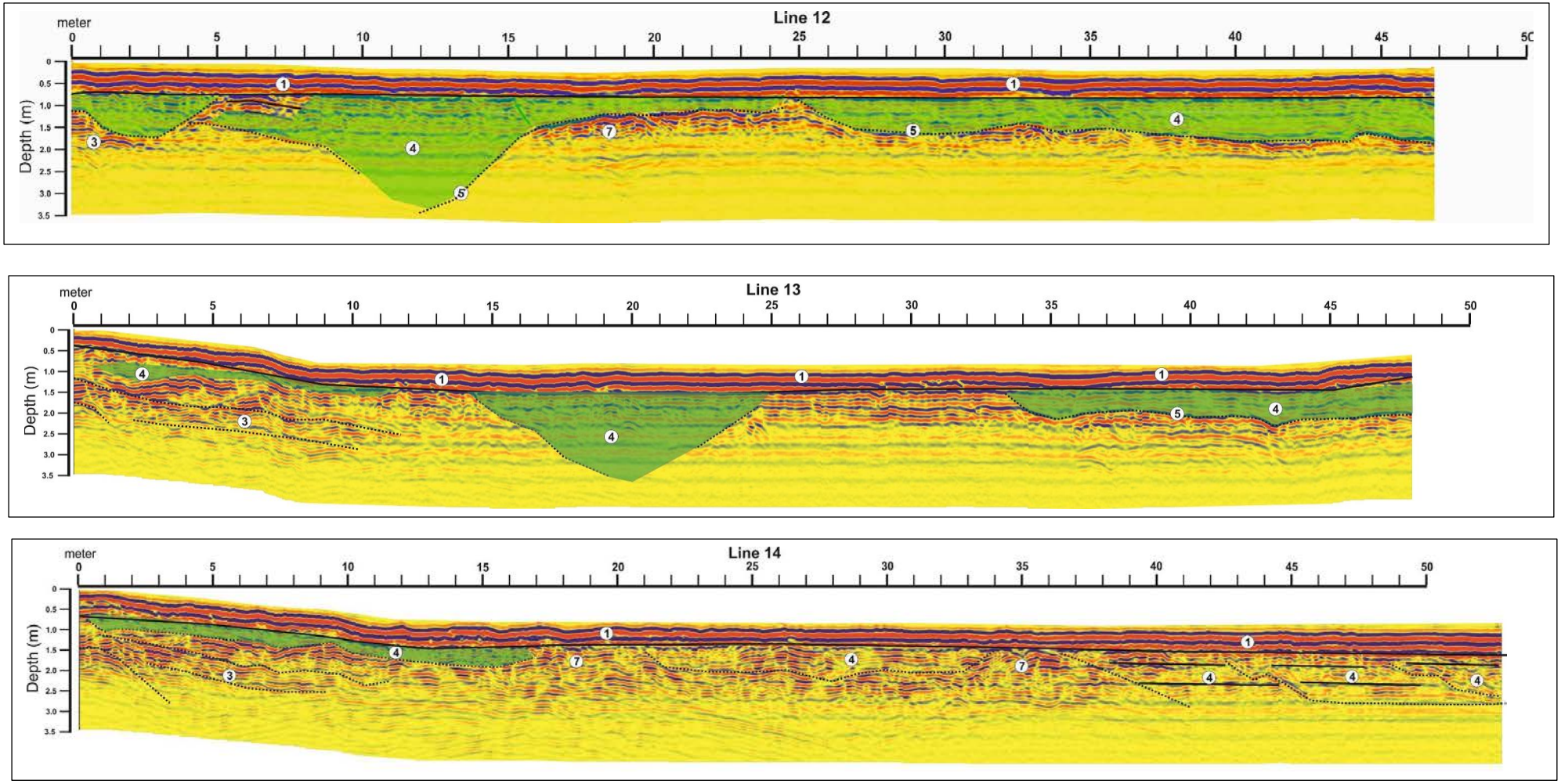
Line 12
meter
0
5
10
15
20
25
30
35
40
45
Depth (m)
0
0.5
1.0
1.5
2.0
2.5
3.0
3.5
1
3
4
5
7
Line 13
meter
0
5
10
15
20
25
30
35
40
45
50
Depth (m)
0
0.5
1.0
1.5
2.0
2.5
3.0
3.5
1
3
4
5
Line 14
meter
0
5
10
15
20
25
30
35
40
45
50
Depth (m)
0
0.5
1.0
1.5
2.0
2.5
3.0
3.5
1
3
4
7

Appendix 2 NW-SE orientation profiles collected in the river Tern west bank site, longer profiles (profiles 15-20).

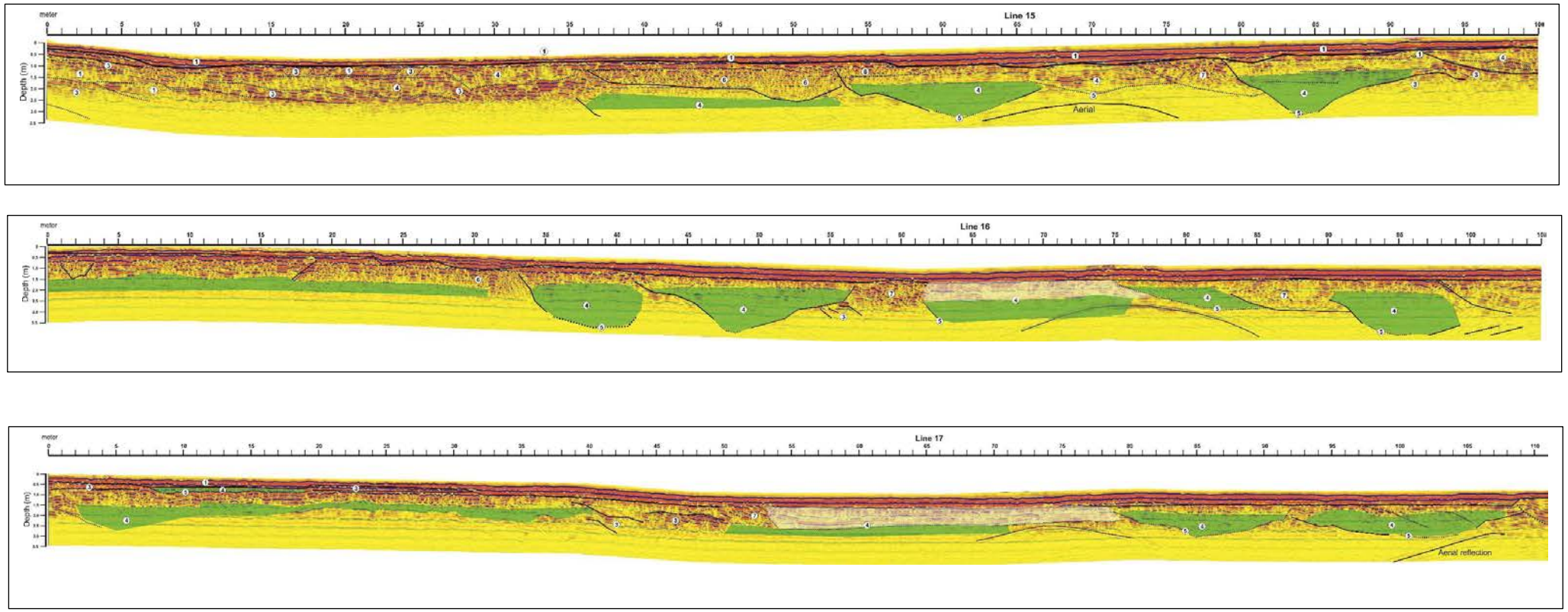

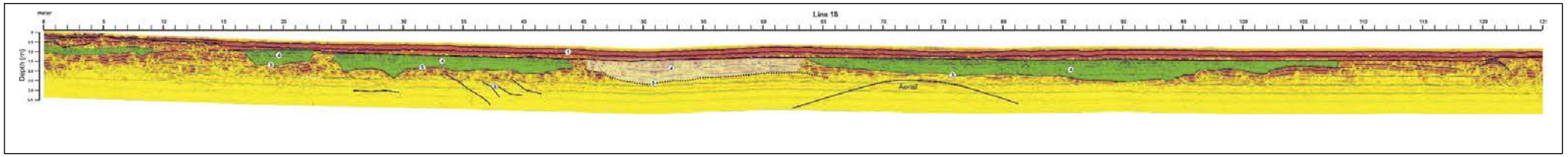
Line 18
meter
Depth (m)
Aerial

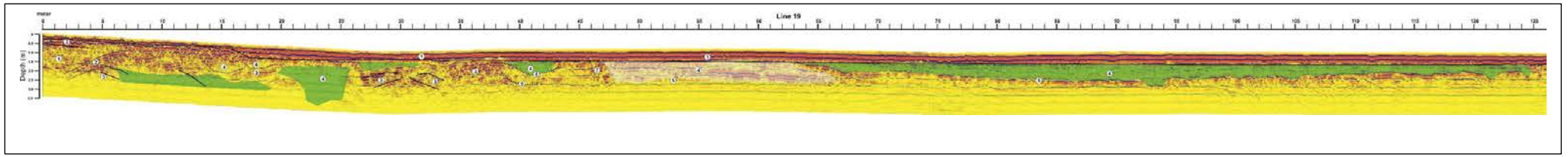
Line 19
meter
Depth (m)

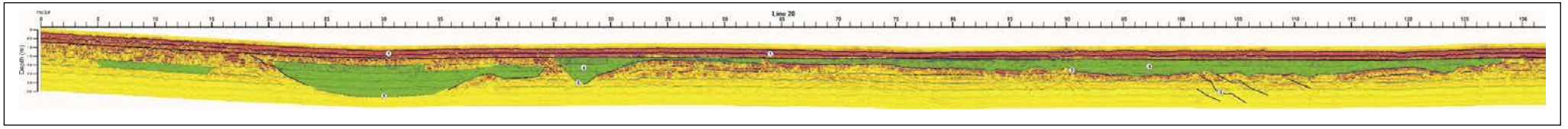
Line 20
meter
Depth (m)

Appendix 3 Locations details of all mini-piezometers used in this study (see chapter 4 and 5).

	Easting	Northing	Elevation
Name	(m)	(m)	m (AOD)
P1	363340.013	328865.517	58.200
P2	363338.335	328865.216	58.400
P3	363339.66	328863.258	58.450
P4	363337.308	328859.852	58.432
P5	363336.130	328859.393	58.321
P6	363337.053	328857.391	58.370
P7	363340.517	328835.939	57.900
P8	363341.044	328836.879	57.908
P9	363339.783	328836.437	57.826
P10	363341.588	328829.375	57.705
P11	363340.436	328828.699	57.810
P12	363340.415	328830.292	57.700
P13	363359.350	328818.469	58.391
P14	363360.399	328816.833	58.315
P15	363363.564	328817.709	57.988
P16	363366.489	328813.593	58.389
P17	363367.523	328809.693	58.407
P18	363372.503	328799.178	58.425

Appendix 4 GRADISTAT printout for the floodplain core samples (Hammer stream, UK), (A) Floodplain core 1 (B) Floodplain core 2. (C) Floodplain core 3. (D) Floodplain core 4.

A

SAMPLE STATISTICS

SAMPLE IDENTITY: **Floodplain core 1** ANALYST & DATE: R. Dara, 20/09/2016

SAMPLE TYPE: Bimodal, Poorly Sorted TEXTURAL GROUP: Muddy Sand

SEDIMENT NAME: Very Coarse Silty Fine Sand

	µm	ϕ
MODE 1:	152.5	2.737
MODE 2:	76.50	3.731
MODE 3:		
D_{10}:	7.036	2.594
MEDIAN or D_{50}:	64.66	3.951
D_{90}:	165.6	7.151
(D_{90} / D_{10}):	23.54	2.757
(D_{90} - D_{10}):	158.6	4.557
(D_{75} / D_{25}):	8.520	2.089
(D_{75} - D_{25}):	123.4	3.091

GRAIN SIZE DISTRIBUTION

GRAVEL:	0.0%	COARSE SAND:	0.4%
SAND:	51.3%	MEDIUM SAND:	2.2%
MUD:	48.7%	FINE SAND:	32.3%
		V FINE SAND:	16.4%
V COARSE GRAVEL:	0.0%	V COARSE SILT:	12.3%
COARSE GRAVEL:	0.0%	COARSE SILT:	12.3%
MEDIUM GRAVEL:	0.0%	MEDIUM SILT:	12.3%
FINE GRAVEL:	0.0%	FINE SILT:	11.9%
V FINE GRAVEL:	0.0%	V FINE SILT:	0.0%
V COARSE SAND:	0.0%	CLAY:	0.0%

	METHOD OF MOMENTS			FOLK & WARD METHOD		
	Arithmetic µm	Geometric µm	Logarithmic ϕ	Geometric µm	Logarithmic ϕ	Description
MEAN ($\bar{x}$):	87.27	45.76	4.450	46.23	4.435	Very Coarse Silt
SORTING (σ):	70.30	2.920	1.546	3.380	1.757	Poorly Sorted
SKEWNESS (Sk):	2.328	0.161	-0.161	-0.398	0.398	Very Fine Skewed
KURTOSIS (K):	14.52	1.304	1.304	0.669	0.669	Very Platykurtic

B

SAMPLE STATISTICS

SAMPLE IDENTITY: **Floodplain core 2**

ANALYST & DATE: R. Dara, 20/09/2016

SAMPLE TYPE: Bimodal, Poorly Sorted

TEXTURAL GROUP: Muddy Sand

SEDIMENT NAME: Coarse Silty Fine Sand

	µm	ϕ
MODE 1:	152.5	2.737
MODE 2:	76.50	3.731
MODE 3:		
D_{10}:	8.858	2.545
MEDIAN or D_{50}:	80.02	3.644
D_{90}:	171.4	6.819
(D_{90} / D_{10}):	19.35	2.680
(D_{90} - D_{10}):	162.5	4.274
(D_{75} / D_{25}):	5.075	1.851
(D_{75} - D_{25}):	118.9	2.343

GRAIN SIZE DISTRIBUTION

GRAVEL:	0.0%	COARSE SAND:	0.9%
SAND:	65.4%	MEDIUM SAND:	4.0%
MUD:	34.6%	FINE SAND:	37.5%
		V FINE SAND:	23.0%
V COARSE GRAVEL:	0.0%	V COARSE SILT:	8.7%
COARSE GRAVEL:	0.0%	COARSE SILT:	8.7%
MEDIUM GRAVEL:	0.0%	MEDIUM SILT:	8.7%
FINE GRAVEL:	0.0%	FINE SILT:	8.4%
V FINE GRAVEL:	0.0%	V FINE SILT:	0.0%
V COARSE SAND:	0.0%	CLAY:	0.0%

	METHOD OF MOMENTS			FOLK & WARD METHOD		
	Arithmetic	Geometric	Logarithmic	Geometric	Logarithmic	Description
	µm	µm	ϕ	µm	ϕ	
MEAN ($\bar{x}$):	104.1	61.23	4.030	56.94	4.134	Very Coarse Silt
SORTING (σ):	81.63	2.842	1.507	3.075	1.621	Poorly Sorted
SKEWNESS (Sk):	2.538	-0.275	0.275	-0.473	0.473	Very Fine Skewed
KURTOSIS (K):	14.62	1.588	1.588	0.860	0.860	Platykurtic

C

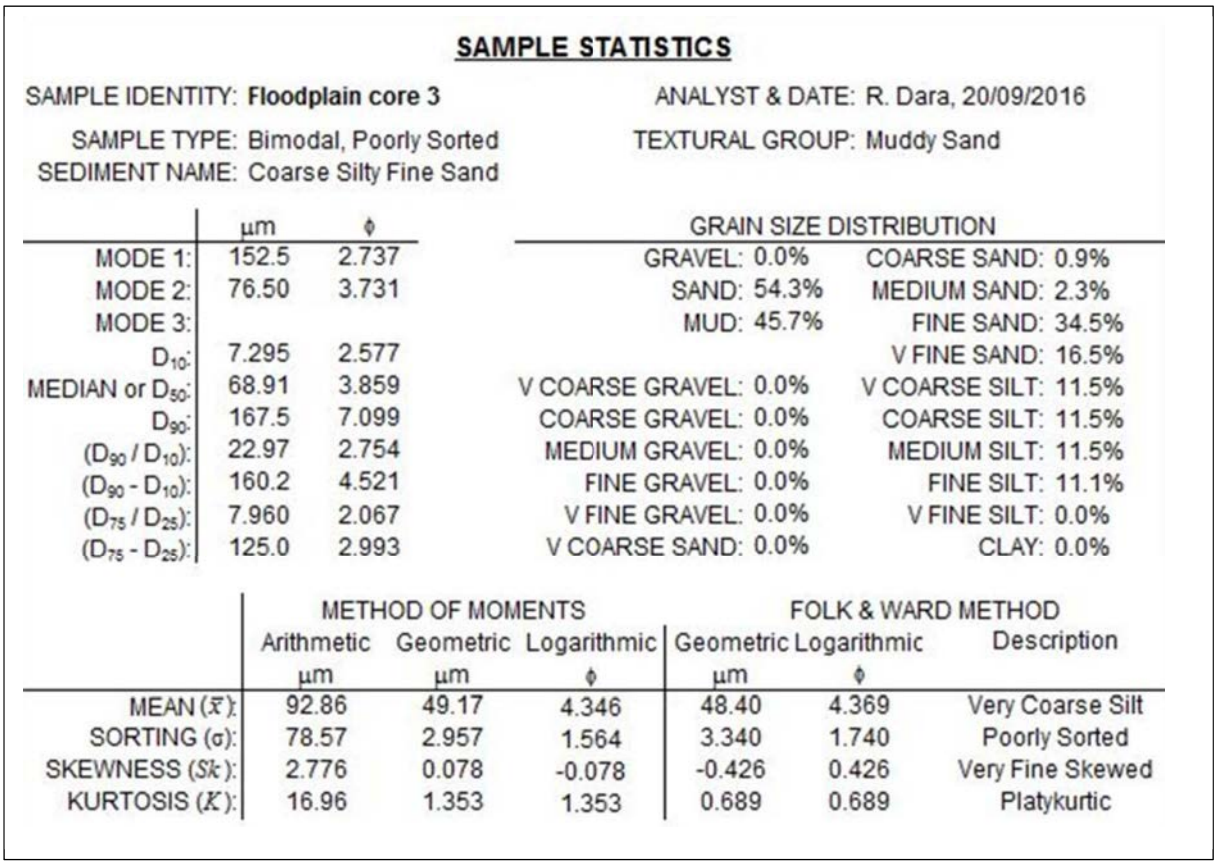

SAMPLE STATISTICS

SAMPLE IDENTITY: **Floodplain core 3**
ANALYST & DATE: R. Dara, 20/09/2016

SAMPLE TYPE: Bimodal, Poorly Sorted
TEXTURAL GROUP: Muddy Sand

SEDIMENT NAME: Coarse Silty Fine Sand

	µm	ϕ
MODE 1:	152.5	2.737
MODE 2:	76.50	3.731
MODE 3:		
D_{10}:	7.295	2.577
MEDIAN or D_{50}:	68.91	3.859
D_{90}:	167.5	7.099
(D_{90} / D_{10}):	22.97	2.754
(D_{90} - D_{10}):	160.2	4.521
(D_{75} / D_{25}):	7.960	2.067
(D_{75} - D_{25}):	125.0	2.993

GRAIN SIZE DISTRIBUTION

GRAVEL:	0.0%	COARSE SAND:	0.9%
SAND:	54.3%	MEDIUM SAND:	2.3%
MUD:	45.7%	FINE SAND:	34.5%
		V FINE SAND:	16.5%
V COARSE GRAVEL:	0.0%	V COARSE SILT:	11.5%
COARSE GRAVEL:	0.0%	COARSE SILT:	11.5%
MEDIUM GRAVEL:	0.0%	MEDIUM SILT:	11.5%
FINE GRAVEL:	0.0%	FINE SILT:	11.1%
V FINE GRAVEL:	0.0%	V FINE SILT:	0.0%
V COARSE SAND:	0.0%	CLAY:	0.0%

	METHOD OF MOMENTS			FOLK & WARD METHOD		
	Arithmetic	Geometric	Logarithmic	Geometric	Logarithmic	Description
	µm	µm	ϕ	µm	ϕ	
MEAN ($\bar{x}$):	92.86	49.17	4.346	48.40	4.369	Very Coarse Silt
SORTING (σ):	78.57	2.957	1.564	3.340	1.740	Poorly Sorted
SKEWNESS (Sk):	2.776	0.078	-0.078	-0.426	0.426	Very Fine Skewed
KURTOSIS (K):	16.96	1.353	1.353	0.689	0.689	Platykurtic

D

SAMPLE STATISTICS

SAMPLE IDENTITY: **Floodplain core 4** ANALYST & DATE: R. Dara, 20/09/2016

SAMPLE TYPE: Bimodal, Poorly Sorted TEXTURAL GROUP: Sandy Mud

SEDIMENT NAME: Very Fine Sandy Medium Silt

	µm	ϕ
MODE 1:	76.50	3.731
MODE 2:	152.5	2.737
MODE 3:		
D_{10}:	6.178	2.719
MEDIAN or D_{50}:	35.15	4.830
D_{90}:	151.9	7.339
(D_{90} / D_{10}):	24.59	2.699
(D_{90} - D_{10}):	145.7	4.620
(D_{75} / D_{25}):	6.727	1.754
(D_{75} - D_{25}):	67.91	2.750

GRAIN SIZE DISTRIBUTION

GRAVEL:	0.0%	COARSE SAND:	0.4%
SAND:	36.8%	MEDIUM SAND:	1.7%
MUD:	63.2%	FINE SAND:	17.0%
		V FINE SAND:	17.7%
V COARSE GRAVEL:	0.0%	V COARSE SILT:	15.9%
COARSE GRAVEL:	0.0%	COARSE SILT:	15.9%
MEDIUM GRAVEL:	0.0%	MEDIUM SILT:	15.9%
FINE GRAVEL:	0.0%	FINE SILT:	15.4%
V FINE GRAVEL:	0.0%	V FINE SILT:	0.0%
V COARSE SAND:	0.0%	CLAY:	0.0%

	METHOD OF MOMENTS			FOLK & WARD METHOD		
	Arithmetic	Geometric	Logarithmic	Geometric	Logarithmic	Description
	µm	µm	ϕ	µm	ϕ	
MEAN ($\bar{x}$):	67.98	32.54	4.941	33.52	4.899	Very Coarse Silt
SORTING (σ):	63.15	2.667	1.415	3.447	1.785	Poorly Sorted
SKEWNESS (Sk):	3.443	0.797	-0.797	-0.080	0.080	Symmetrical
KURTOSIS (K):	23.05	2.007	2.007	0.758	0.758	Platykurtic

Appendix 5 GRADISTAT printout for the riverbed core samples (Hammer stream, UK), (A) Riverbed core 1 (B) Riverbed core 2. (C) Riverbed core 3. (D) Riverbed core 4. (E) Riverbed core 5.

A

SAMPLE STATISTICS

SAMPLE IDENTITY: **Riverbed core 1** ANALYST & DATE: R.Dara, 20/09/2016

SAMPLE TYPE: Polymodal, Poorly Sorted TEXTURAL GROUP: Muddy Sand

SEDIMENT NAME: Very Coarse Silty Fine Sand

	μm	ϕ
MODE 1:	152.5	2.737
MODE 2:	302.5	1.747
MODE 3:	605.0	0.747
D_{10}:	24.21	0.895
MEDIAN or D_{50}:	167.5	2.577
D_{90}:	537.8	5.368
(D_{90} / D_{10}):	22.21	5.998
(D_{90} - D_{10}):	513.6	4.473
(D_{75} / D_{25}):	2.385	1.738
(D_{75} - D_{25}):	178.8	1.254

GRAIN SIZE DISTRIBUTION

GRAVEL:	0.0%	COARSE SAND:	12.6%
SAND:	84.7%	MEDIUM SAND:	30.5%
MUD:	15.3%	FINE SAND:	35.0%
		V FINE SAND:	6.6%
V COARSE GRAVEL:	0.0%	V COARSE SILT:	3.8%
COARSE GRAVEL:	0.0%	COARSE SILT:	3.8%
MEDIUM GRAVEL:	0.0%	MEDIUM SILT:	3.8%
FINE GRAVEL:	0.0%	FINE SILT:	3.7%
V FINE GRAVEL:	0.0%	V FINE SILT:	0.0%
V COARSE SAND:	0.0%	CLAY:	0.0%

	METHOD OF MOMENTS			FOLK & WARD METHOD		
	Arithmetic	Geometric	Logarithmic	Geometric	Logarithmic	Description
	μm	μm	ϕ	μm	ϕ	
MEAN ($\bar{x}$):	232.1	149.1	2.745	155.2	2.687	Fine Sand
SORTING (σ):	170.0	2.973	1.572	2.830	1.501	Poorly Sorted
SKEWNESS (Sk):	1.022	-1.009	1.009	-0.254	0.254	Fine Skewed
KURTOSIS (K):	3.276	3.125	3.125	1.952	1.952	Very Leptokurtic

B

SAMPLE STATISTICS

SAMPLE IDENTITY: **Riverbed core 2** ANALYST & DATE: R. Dara, 20/09/2016

SAMPLE TYPE: Trimodal, Poorly Sorted TEXTURAL GROUP: Sand

SEDIMENT NAME: Poorly Sorted Fine Sand

	µm	ϕ
MODE 1:	152.5	2.737
MODE 2:	302.5	1.747
MODE 3:	76.50	3.731
D_{10}:	64.98	1.560
MEDIAN or D_{50}:	164.4	2.605
D_{90}:	339.1	3.944
(D_{90} / D_{10}):	5.218	2.528
(D_{90} - D_{10}):	274.1	2.384
(D_{75} / D_{25}):	2.168	1.625
(D_{75} - D_{25}):	156.1	1.116

GRAIN SIZE DISTRIBUTION

GRAVEL:	0.0%	COARSE SAND:	5.6%
SAND:	90.7%	MEDIUM SAND:	33.4%
MUD:	9.3%	FINE SAND:	44.0%
		V FINE SAND:	7.6%
V COARSE GRAVEL:	0.0%	V COARSE SILT:	2.3%
COARSE GRAVEL:	0.0%	COARSE SILT:	2.3%
MEDIUM GRAVEL:	0.0%	MEDIUM SILT:	2.3%
FINE GRAVEL:	0.0%	FINE SILT:	2.3%
V FINE GRAVEL:	0.0%	V FINE SILT:	0.0%
V COARSE SAND:	0.0%	CLAY:	0.0%

	METHOD OF MOMENTS			FOLK & WARD METHOD		
	Arithmetic	Geometric	Logarithmic	Geometric	Logarithmic	Description
	µm	µm	ϕ	µm	ϕ	
MEAN ($\bar{x}$):	211.3	156.9	2.672	165.2	2.598	Fine Sand
SORTING (σ):	131.8	2.404	1.266	2.318	1.213	Poorly Sorted
SKEWNESS (Sk):	1.264	-1.379	1.379	-0.155	0.155	Fine Skewed
KURTOSIS (K):	4.977	4.777	4.777	1.796	1.796	Very Leptokurtic

C

SAMPLE STATISTICS

SAMPLE IDENTITY: **Riverbed core 3** ANALYST & DATE: R. Dara, 20/09/2016

SAMPLE TYPE: Trimodal, Poorly Sorted TEXTURAL GROUP: Muddy Sand

SEDIMENT NAME: Very Coarse Silty Medium Sand

	µm	ϕ
MODE 1:	302.5	1.747
MODE 2:	152.5	2.737
MODE 3:	605.0	0.747
D_{10}:	15.16	0.881
MEDIAN or D_{50}:	271.0	1.884
D_{90}:	543.0	6.044
(D_{90} / D_{10}):	35.82	6.860
(D_{90} - D_{10}):	527.8	5.163
(D_{75} / D_{25}):	2.504	1.818
(D_{75} - D_{25}):	195.4	1.324

GRAIN SIZE DISTRIBUTION

GRAVEL:	0.0%	COARSE SAND:	13.1%
SAND:	79.4%	MEDIUM SAND:	48.0%
MUD:	20.6%	FINE SAND:	15.6%
		V FINE SAND:	2.7%
V COARSE GRAVEL:	0.0%	V COARSE SILT:	5.2%
COARSE GRAVEL:	0.0%	COARSE SILT:	5.2%
MEDIUM GRAVEL:	0.0%	MEDIUM SILT:	5.2%
FINE GRAVEL:	0.0%	FINE SILT:	5.0%
V FINE GRAVEL:	0.0%	V FINE SILT:	0.0%
V COARSE SAND:	0.0%	CLAY:	0.0%

	METHOD OF MOMENTS			FOLK & WARD METHOD		
	Arithmetic	Geometric	Logarithmic	Geometric	Logarithmic	Description
	µm	µm	ϕ	µm	ϕ	
MEAN ($\bar{x}$):	257.0	154.0	2.699	147.0	2.766	Fine Sand
SORTING (σ):	172.4	3.445	1.785	3.479	1.799	Poorly Sorted
SKEWNESS (Sk):	0.568	-1.044	1.044	-0.704	0.704	Very Fine Skewed
KURTOSIS (K):	2.809	2.585	2.585	1.955	1.955	Very Leptokurtic

D

SAMPLE STATISTICS

SAMPLE IDENTITY: **Riverbed core 4** ANALYST & DATE: R. Dara, 20/09/2016

SAMPLE TYPE: Trimodal, Poorly Sorted TEXTURAL GROUP: Sand

SEDIMENT NAME: Poorly Sorted Medium Sand

	µm	ϕ
MODE 1:	302.5	1.747
MODE 2:	605.0	0.747
MODE 3:	152.5	2.737
D_{10}:	125.8	0.732
MEDIAN or D_{50}:	288.3	1.794
D_{90}:	602.3	2.990
(D_{90} / D_{10}):	4.786	4.088
(D_{90} - D_{10}):	476.4	2.259
(D_{75} / D_{25}):	2.110	1.703
(D_{75} - D_{25}):	181.8	1.077

GRAIN SIZE DISTRIBUTION

GRAVEL:	0.0%	COARSE SAND:	21.3%
SAND:	94.6%	MEDIUM SAND:	48.3%
MUD:	5.4%	FINE SAND:	20.7%
		V FINE SAND:	4.2%
V COARSE GRAVEL:	0.0%	V COARSE SILT:	1.4%
COARSE GRAVEL:	0.0%	COARSE SILT:	1.4%
MEDIUM GRAVEL:	0.0%	MEDIUM SILT:	1.4%
FINE GRAVEL:	0.0%	FINE SILT:	1.3%
V FINE GRAVEL:	0.0%	V FINE SILT:	0.0%
V COARSE SAND:	0.0%	CLAY:	0.0%

	METHOD OF MOMENTS			FOLK & WARD METHOD		
	Arithmetic	Geometric	Logarithmic	Geometric	Logarithmic	Description
	µm	µm	ϕ	µm	ϕ	
MEAN ($\bar{x}$):	311.8	241.3	2.051	280.2	1.836	Medium Sand
SORTING (σ):	173.6	2.307	1.206	2.065	1.046	Poorly Sorted
SKEWNESS (Sk):	0.539	-1.734	1.734	-0.209	0.209	Fine Skewed
KURTOSIS (K):	2.379	6.523	6.523	1.394	1.394	Leptokurtic

E

SAMPLE STATISTICS

SAMPLE IDENTITY: **Riverbed core 5** ANALYST & DATE: R. Dara, 20/09/2016

SAMPLE TYPE: Trimodal, Poorly Sorted TEXTURAL GROUP: Muddy Sand

SEDIMENT NAME: Coarse Silty Medium Sand

	µm	ϕ
MODE 1:	302.5	1.747
MODE 2:	152.5	2.737
MODE 3:	605.0	0.747
D_{10}:	24.98	0.935
MEDIAN or D_{50}:	271.4	1.882
D_{90}:	523.1	5.323
(D_{90} / D_{10}):	20.94	5.694
(D_{90} - D_{10}):	498.1	4.388
(D_{75} / D_{25}):	2.250	1.718
(D_{75} - D_{25}):	179.4	1.170

GRAIN SIZE DISTRIBUTION

GRAVEL:	0.0%	COARSE SAND:	11.5%
SAND:	85.0%	MEDIUM SAND:	50.3%
MUD:	15.0%	FINE SAND:	21.4%
		V FINE SAND:	1.9%
V COARSE GRAVEL:	0.0%	V COARSE SILT:	3.8%
COARSE GRAVEL:	0.0%	COARSE SILT:	3.8%
MEDIUM GRAVEL:	0.0%	MEDIUM SILT:	3.8%
FINE GRAVEL:	0.0%	FINE SILT:	3.7%
V FINE GRAVEL:	0.0%	V FINE SILT:	0.0%
V COARSE SAND:	0.0%	CLAY:	0.0%

	METHOD OF MOMENTS			FOLK & WARD METHOD		
	Arithmetic	Geometric	Logarithmic	Geometric	Logarithmic	Description
	µm	µm	ϕ	µm	ϕ	
MEAN ($\bar{x}$):	260.6	174.8	2.516	192.1	2.380	Fine Sand
SORTING (σ):	159.3	2.990	1.580	2.720	1.443	Poorly Sorted
SKEWNESS (Sk):	0.639	-1.371	1.371	-0.646	0.646	Very Fine Skewed
KURTOSIS (K):	3.211	3.678	3.678	2.078	2.078	Very Leptokurtic

Appendix 6 More GPR profiles of the floodplain Hammer stream.

Profile 80

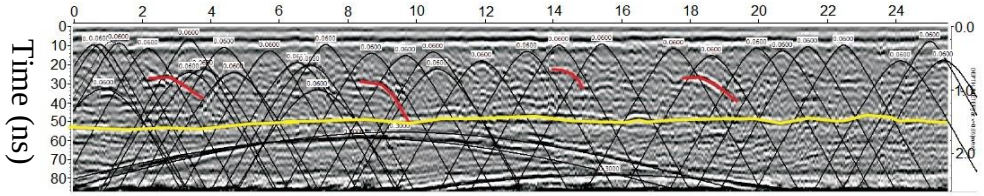

Profile 81

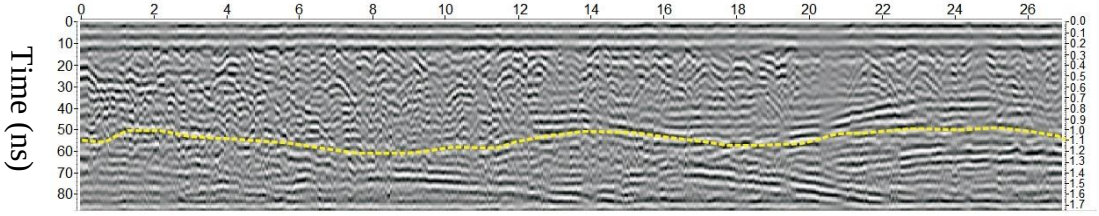

Profile 82